Parasites, Hosts and Diseases

Volume 64 • Number 4 • October 2026

CONTENTS

Invited Review

291 Functional roles of extracellular vesicles in *Trichomonas vaginalis*
Seow-Chin Ong, Hong-Wei Luo, Jhen-Wei Syu, Cheng-Hsun Chiu, Petrus Tang

Mini Review

299 Host genetic regulation of immune tolerance and disease persistence in human echinococcosis
Emad Shamsan, Liu Chuanchuan, Fan Haining

Original Articles

310 Functional characterization of CsGTP5, a sodium-independent glucose transporter-related protein in *Clonorchis sinensis*
Seok Ho Cha, Wang-Jong Lee, Jadidan Hada Syahada, Fadhila Fitriana, Muhammad Fajri Rokhmad, Hyun-Young Sim, Zijian Wu, Bo Wang, Jin-Hee Han

320 Salivary *Plasmodium falciparum* histidine-rich protein 2 levels are poor predictors of parasite density and clinical malaria status in patients with acute uncomplicated malaria in Chulaimbo, western Kenya
Ruth Awuor Omingo, Cyrus Ayieko, Patrick Ogola Onyango, Ben Okeyo Sati, Vane Kwamboka Omwenga, Sidney Ogolla

329 Rapid detection of viable *Acanthamoeba* spp. trophozoites and cysts in water treatment processes using propidium monoazide coupled with real-time PCR
Eun-Sook Lee, Ji-Yeon Lee, Young-Ae Baek, Seok-Ju Cho

337 Zoonotic and prey-derived protozoa in Tibetan fox (*Vulpes ferrilata*) and other wild canids: Implications for public health in the eastern Tibetan Plateau
Xueying Deng, Chuizhao Xue, Qilu Chen, Qingqiu Zuo, Mengqing Li, Xiaoxue Peng, Peng Li, Xu Wang

350 Morphological and molecular identification of hard ticks using mitochondrial 16S and 12S rDNA in Korea
Choon-Mee Kim, Seon Gyeong Kim, You Mi Lee, Jun-Won Seo, Da Young Kim, Na Ra Yun, Dong-Min Kim

Brief Communications

360 Infection status of zoonotic intestinal helminths in striped field mice from Jeollabuk-do, Korea
Woon-Mok Sohn, Byoung-Kuk Na, Cheon-Hyeon Kim

366 *Toxoplasma gondii* GRA16 enhances the inhibitory effects of standard DNA-damaging chemotherapeutics in liver, pancreatic, and colorectal cancer cells
Seung-Hwan Seo, Ji-Eun Lee, Eun-Ji Cho, Eun-Hee Shin

374 Occurrence and preliminary molecular characterization of *Sarcocystis* spp. in wild Korean roe deer from Jeju Island, Korea
Da-Ye Nam, Sunmin Kim, Jinho Jang, YoungMin Yun, Jae-Hoon Kim, Ji-Youl Jung

Case Reports

379 Molecular and pathological characterization of a *Dirofilaria* sp. infection in a little egret (*Egretta garzetta*)
Eunjeong Go, You-Jeong Lee, Da-Ye Nam, Beoul Kim, Hyo-Min Woo, Min-Goo Seo, Dayoung Choi, Jae-Hoon Kim, Jinho Jang, YoungMin Yun, Ji-Youl Jung

385 Isolation and whole-genome characterization of *Coxiella burnetii* from an acute Q fever patient in Korea
Yejin Choi, Dayoung Kim, Yeon-Joo Choi, Sun-Woo Choi, Da-Eun Jeong, Jeong Yoon Lee, Nam-Hyuk Cho, Kwang-Jun Lee, Dong-Min Kim, Won-Jong Jang, Jun-Gu Kang

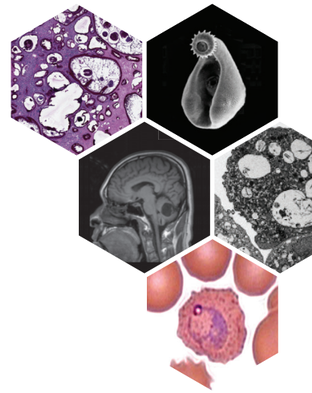
391 Wound myiasis caused by *Lucilia* spp. (Diptera: Calliphoridae) in a dog and a cat in Korea
Subin Lee, Joohyung Kim, Kihwan Yang, Seongjun Choe, Seung-Hun Lee

http://parahostdis.org

The Korean Society for Parasitology and Tropical Medicine

Parasites, Hosts and Diseases

Parasites, Hosts and Diseases



pISSN 2982-5164 eISSN 2982-6799

Volume 64 • Number 4 • October 2026

Volume 64 • Number 4 • October 2026



http://parahostdis.org

The Korean Society for Parasitology and Tropical Medicine

Parasites, Hosts and Diseases

pISSN 2982-5164
eISSN 2982-6799

Volume 64 • Number 4 • October 2026

Parasites, Hosts and Diseases (Parasites Hosts Dis, PHD) is a peer-reviewed, open-access journal published quarterly on the last day of January, April, July, and October. Established in 1963 as *The Korean Journal of Parasitology*, the journal transitioned to an online-only publication starting with Vol. 53 in 2015, and adopted its current title in 2023. As the official publication of The Korean Society for Parasitology and Tropical Medicine, PHD is dedicated to advancing knowledge on human and animal parasites, disease vectors, host-parasite interactions, zoonoses, and tropical medicine. The journal publishes original articles, review articles, case reports, brief communications, letters to the editor, and book reviews.

Abstracting and Indexing Services

A part of articles, metadata, or full text is available from KoreaMed (1963–), CrossRef metadata (1963–), Korea Citation Index (2002–), Science Citation Index Expanded (2008–), MedLine (1993–), PubMed Central (1998–), PubMed (1993–), Scopus (1977–), and EMBASE (2023–).

Open Access

PHD is an open access journal. All contents of the journal are available immediately upon publication without embargo period (https://parahostdis.org/). All articles are distributed under the terms of the Creative Commons Attribution Non-Commercial License (https://creativecommons.org/licenses/by-nc/4.0/) which permits unrestricted non-commercial use, distribution, and reproduction in any medium, provided the original work is properly cited.

Publisher The Korean Society for Parasitology and Tropical Medicine
Editor-in-Chief Myeong Heon Shin, MD, PhD

Editorial Office The Korean Society for Parasitology and Tropical Medicine
Department of Tropical Medicine, Yonsei University College of Medicine, Yonsei-ro 50-1, Seodaemun-gu, Seoul 03722 Korea
Tel: +82-2-2228-1844 E-mail: support@parahostdis.org

Publishing Office M2PI
#805, 26 Sangwon 1-gil, Seongdong-gu, Seoul 04779, Korea
Tel: +82-2-6966-4930 Fax: +82-2-6966-4945 E-mail: support@m2-pi.com

This journal was supported by the Korea Association of Health Promotion, National Research Foundation of Korea (NRF) grant and the Korean Federation of Science and Technology Societies (KOFST) grant funded by the Korean Government.

ⓒ Korean Society for Parasitology and Tropical Medicine
ⓒ It is identical to Creative Commons Non-Commercial License.

Parasites, Hosts and Diseases

pISSN 2982-5164
eISSN 2982-6799

Volume 64 • Number 4 • October 2026

Editorial Board

Editor-in-Chief: Myeong Heon Shin

Section Editors: Hak Sun Yu, Soon-Jung Park, Eun-Hee Shin, Hyun Hee Kong, Dongmi Kwak, Byoung-Kuk Na

Editorial Board

Pornpimon Angkasekwinai *Thailand*
Jong-Yil Chai
Soumyananda Chakraborti *India*
Minkyoung Cho
Seongjun Choe
Min-Ho Choi
Ki Back Chu
Mary Jane Cruz-Flores *Philippines*
Dr Muh Fauzi *Indonesia*
Hector H. Garcia *Peru*
Youn Kyoung Goo
Eun-Tae Han
Jin-Hee Han
Yeonchul Hong
Dr Thi Thi Htoon *South Africa*
Bong-Kwang Jung
Shin Ae Kang
Hyoung-Pyo Kim
Jong-Hyun Kim
Ju Yeong Kim
Juri Kim
Min Jae Kim
Sung Hye Kim
Seung-Hun Lee
Feng Lu *China*
Ernest Mazigo *Tanzania*
Humphrey Deogratias Mazigo *Tanzani*
Eun-Kyung Moom
Yukifumi Nawa *Japan*
Choosak Nithikathkul *Thailand*
Tomoyoshi Nozaki *Japan*
Fu-Shi Quan
Min-Goo Seo
Sang Phil Shin
Seobo Sim
Woon-Mok Sohn
Xi Sun *China*
Urusa Thaenkham *Thailand*
Zhao-Shou Yang *China*
Chaoqun Yao *USA*
Seon-Ju Yeo
Won Gi Yoo

Manuscript Editor: Jae Hwa Chang

Staff of The Korean Society for Parasitology and Tropical Medicine (2026-2027)

President	Eun-Teak Han
Vice-President	Hak-Sun Yu
Secretary-Treasurer	Jin-Hee Han
Secretary for Academic Affairs	Joo Hwan No
Secretary for International Cooperation	Bong-Kwang Jung
Secretary for Planning Publicitiy	Ju Yeong Kim

© 2026 The Korean Society for Parasitology and Tropical Medicine

Parasites, Hosts and Diseases

pISSN 2982-5164
eISSN 2982-6799

Volume 64 • Number 4 • October 2026

Contents

Invited Review

291 Functional roles of extracellular vesicles in *Trichomonas vaginalis*
Seow-Chin Ong, Hong-Wei Luo, Jhen-Wei Syu, Cheng-Hsun Chiu, Petrus Tang

Mini Review

299 Host genetic regulation of immune tolerance and disease persistence in human echinococcosis
Emad Shamsan, Liu Chuanchuan, Fan Haining

Original Articles

310 Functional characterization of CsGTP5, a sodium-independent glucose transporter-related protein in *Clonorchis sinensis*
Seok Ho Cha, Wang-Jong Lee, Jadidan Hada Syahada, Fadhila Fitriana, Muhammad Fajri Rokhmad, Hyun-Young Sim, Zijian Wu, Bo Wang, Jin-Hee Han

320 Salivary *Plasmodium falciparum* histidine-rich protein 2 levels are poor predictors of parasite density and clinical malaria status in patients with acute uncomplicated malaria in Chulaimbo, western Kenya
Ruth Awuor Omingo, Cyrus Ayieko, Patrick Ogola Onyango, Ben Okeyo Sati, Vane Kwamboka Omwenga, Sidney Ogolla

329 Rapid detection of viable *Acanthamoeba* spp. trophozoites and cysts in water treatment processes using propidium monoazide coupled with real-time PCR
Eun-Sook Lee, Ji-Yeon Lee, Young-Ae Baek, Seok-Ju Cho

337 Zoonotic and prey-derived protozoa in Tibetan fox (*Vulpes ferrilata*) and other wild canids: Implications for public health in the eastern Tibetan Plateau
Xueying Deng, Chuizhao Xue, Qilu Chen, Qingqiu Zuo, Mengqing Li, Xiaoxue Peng, Peng Li, Xu Wang

350 Morphological and molecular identification of hard ticks using mitochondrial 16S and 12S rDNA in Korea
Choon-Mee Kim, Seon Gyeong Kim, You Mi Lee, Jun-Won Seo, Da Young Kim, Na Ra Yun, Dong-Min Kim

Brief Communications

360 Infection status of zoonotic intestinal helminths in striped field mice from Jeollabuk-do, Korea
Woon-Mok Sohn, Byoung-Kuk Na, Cheon-Hyeon Kim

366 *Toxoplasma gondii* GRA16 enhances the inhibitory effects of standard DNA-damaging chemotherapeutics in liver, pancreatic, and colorectal cancer cells
Seung-Hwan Seo, Ji-Eun Lee, Eun-Ji Cho, Eun-Hee Shin

374 Occurrence and preliminary molecular characterization of *Sarcocystis* spp. in wild Korean roe deer from Jeju Island, Korea
Da-Ye Nam, Sunmin Kim, Jinho Jang, YoungMin Yun, Jae-Hoon Kim, Ji-Youl Jung

© 2026 The Korean Society for Parasitology and Tropical Medicine

Parasites, Hosts and Diseases

pISSN 2982-5164
eISSN 2982-6799

Volume 64 • Number 4 • October 2026

Case Reports

379 Molecular and pathological characterization of a *Dirofilaria* sp. infection in a little egret (*Egretta garzetta*)
Eunjeong Go, You-Jeong Lee, Da-Ye Nam, Beoul Kim, Hyo-Min Woo, Min-Goo Seo, Dayoung Choi, Jae-Hoon Kim, Jinho Jang, YoungMin Yun, Ji-Youl Jung

385 Isolation and whole-genome characterization of *Coxiella burnetii* from an acute Q fever patient in Korea
Yejin Choi, Dayoung Kim, Yeon-Joo Choi, Sun-Woo Choi, Da-Eun Jeong, Jeong Yoon Lee, Nam-Hyuk Cho, Kwang-Jun Lee, Dong-Min Kim, Won-Jong Jang, Jun-Gu Kang

391 Wound myiasis caused by *Lucilia* spp. (Diptera: Calliphoridae) in a dog and a cat in Korea
Subin Lee, Joohyung Kim, Kihwan Yang, Seongjun Choe, Seung-Hun Lee

© 2026 The Korean Society for Parasitology and Tropical Medicine

Invited Review

Parasites Hosts Dis 2026;64(4):291-298
https://doi.org/10.3347/PHD.26039

Parasites, Hosts and Diseases

pISSN 2982-5164 • eISSN 2982-6799

Functional roles of extracellular vesicles in *Trichomonas vaginalis*

Seow-Chin Ong[1], Hong-Wei Luo[2], Jhen-Wei Syu[2], Cheng-Hsun Chiu[3], Petrus Tang[1,3,4,*]

[1]Department of Parasitology, College of Medicine, Chang Gung University, Taoyuan City, Taiwan; [2]Graduate Institute of Biomedical Sciences, Chang Gung University, Taoyuan City, Taiwan; [3]Molecular Infectious Disease Research Center, Chang Gung Memorial Hospital, Linkou Branch, Taoyuan City, Taiwan; [4]Molecular Medicine Research Center, Chang Gung University, Taoyuan City, Taiwan

Extracellular vesicles (EVs) secreted by *Trichomonas vaginalis* are now recognized as important mediators of host-parasite communication and play crucial roles in the development of trichomoniasis. These membrane-enclosed vesicles, which include exosomes and microvesicles, carry a diverse array of cargo, including proteins, lipids, and nucleic acids, as well as virulence-associated components such as adhesion molecules, proteases, and tRNA-derived small RNAs. Functionally, EVs enhance parasite attachment to vaginal epithelial cells, facilitate colonization, and contribute to host tissue damage. They also influence host immune responses, exhibiting both pro-inflammatory and immunosuppressive activities. Furthermore, the composition of EVs can be modulated by endosymbionts such as *Trichomonasvirus*, thereby influencing host-pathogen interactions. In addition, EVs mediate parasite-parasite communication, thereby promoting parasite adaptation and survival. This review summarizes current knowledge on the composition and functional roles of *T. vaginalis* EVs, highlighting their involvement in adhesion, immune modulation, and infection, as well as their potential utility as diagnostic biomarkers and therapeutic targets.

Keywords: *Trichomonas vaginalis*, extracellular vesicles, exosome, *Trichomonasvirus*, pathogenesis, adherence

Introduction

Trichomonas vaginalis is a single-celled protozoan parasite that causes trichomoniasis in humans. This parasite is an extracellular pathogen that primarily infects host tissues by adhering to urogenital epithelial cells [1]. This cytoadherence to vaginal and prostate epithelium is enhanced by the secretion of extracellular vesicles (EVs), including exosome-like vesicles. Notably, *T. vaginalis* was among the early protozoan parasites reported to release small EVs, or exosomes, capable of altering the physical and biochemical properties of host cells, thereby facilitating host-parasite interactions [2].

The International Society for Extracellular Vesicles recommends the use of the umbrella term "EVs" to describe all membrane-derived vesicles [3]. EVs are generally categorized into 3 main groups based on their size and biogenesis: exosomes, microvesicles, and apoptotic bodies. Exosomes are small (30–150 nm), lipid bilayer vesicles with a characteristic cup-shaped morphology, formed through the inward budding of endosomal membranes to generate intraluminal vesicles within multivesicular bodies. Upon fusion of multivesicular bodies with the plasma membrane, the intraluminal vesicles are released into the extracellular space as exosomes. Their biogenesis may occur via endosomal sorting complexes required for transport (ESCRT)-dependent or ESCRT-independent pathways, and they carry diverse molecular cargo for intercellular communication. Microvesicles (50–1,000 nm), in contrast, originate from outward budding of the plasma membrane, a process often

Received: April 29, 2026 Accepted: June 8, 2026
*Correspondence: petang@mail.cgu.edu.tw

© 2026 The Korean Society for Parasitology and Tropical Medicine
This is an open-access article distributed under the terms of the Creative Commons Attribution Non-Commercial License (http://creativecommons.org/licenses/by-nc/4.0/) which permits unrestricted non-commercial use, distribution, and reproduction in any medium, provided the original work is properly cited.

Citation
Ong SC, Luo HW, Syu JW, Chiu CH, Tang P. Functional roles of extracellular vesicles in *Trichomonas vaginalis*. Parasites Hosts Dis 2026;64(4):291-298.

triggered by increased intracellular Ca^{2+} levels, which activate cytoskeletal remodeling and phospholipid redistribution. In contrast, apoptotic bodies (1–5 μm) are larger vesicles formed during programmed cell death (apoptosis), encapsulating cellular components as cells undergo fragmentation.

Generally, *T. vaginalis* releases 2 types of EVs: small EVs (exosomes, 30–150 nm) generated within endosomal multivesicular bodies [2,4-7], and microvesicles (50–1,000 nm) or larger vesicles (>200 nm) that bud directly from the flagellar membrane of the parasite [8-10]. *T. vaginalis* EVs (TvEVs) are internalized by host cells predominantly through caveolae-mediated and lipid raft-mediated endocytosis, a process mediated by host cell cholesterol and caveolin-1. This uptake mechanism is facilitated by interactions with heparan sulfate proteoglycans on the host cell surface, leading to increased production of pro-inflammatory cytokines, enhanced parasite adherence, and modulation of host cell metabolism [11]. Fig. 1 illustrates the biogenesis of TvEVs and biomolecular cargo of exosome, along with the characterization of exosomes by transmission electron microscope.

Collectively, TvEVs function as intercellular messengers, delivering a diverse cargo that consists of conserved eukaryotic EV components and parasite-specific molecules. These specific molecules include virulence-associated factors such as adhesins, proteases (e.g., GP63-like proteins), tetraspanins, and regulatory small RNAs. Subsequently, these EVs promote parasite adherence, modulate host immune responses, and influence inflammatory processes to support parasite survival and colonization. In this review, we focus on the key roles and functions of EVs in *T. vaginalis* (Fig. 2), with Table 1 [2,4-15]summarizing the major studies on TvEVs published from 2013 to the present.

Key Roles on EV of *T. vaginalis*

Pathogenesis and adherence

T. vaginalis releases exosomes, small EV that can fuse with host cells. Adherence of the parasite to epithelial cells represents the initial step in host infection [1]. Studies have shown that exosome enhances the parasite's ability to attach to host cells, serving as a key mechanism during the early stages of colonization.

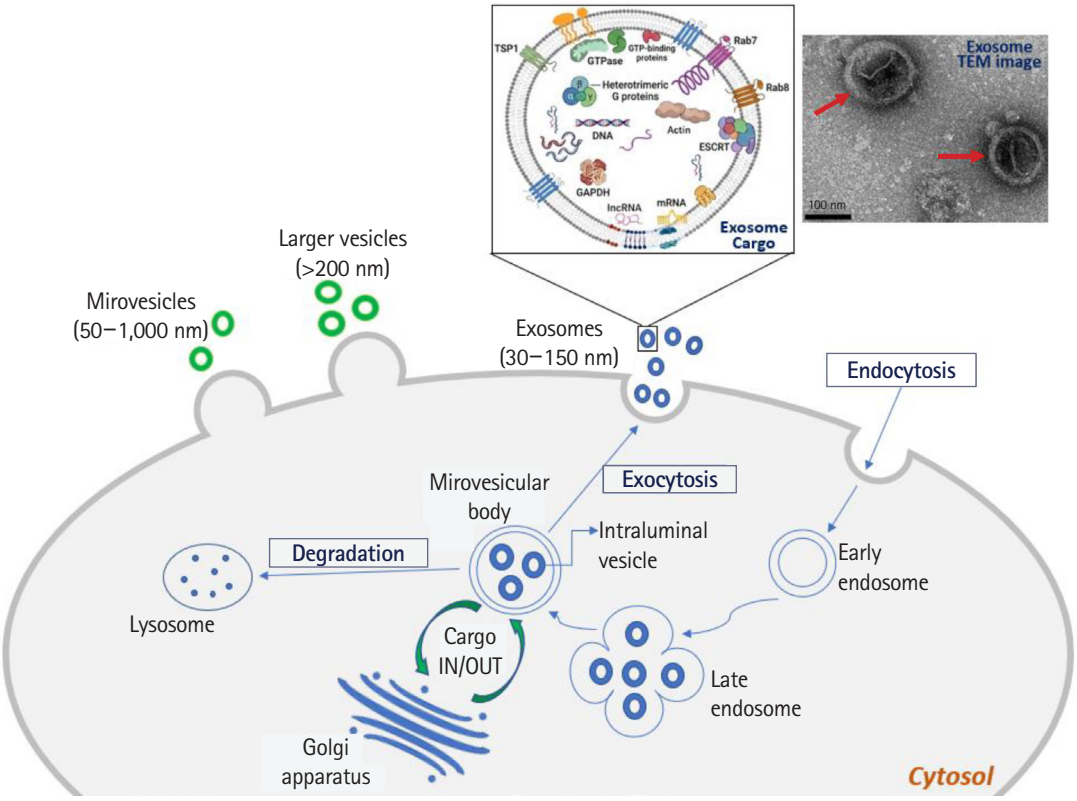


Fig. 1. Biogenesis and protein cargo of *Trichomonas vaginalis* extracellular vesicles. Microvesicles and larger vesicles are produced by outward budding of the plasma membrane, whereas exosomes are formed through the endosomal pathway and released following fusion of the multivesicular bodies with the plasma membrane. Exosomes carry diverse bioactive cargo, including proteins, lipids, and nucleic acids, as well as a range of common proteins, highlighting their role in mediating intercellular communication. The transmission electron microscope (TEM) image (red arrows) shows exosomes with the characteristic cup-shaped morphology, observed by TEM (JEOL JEM-2100Plus) following negative staining with 1% uranyl acetate, as described in our previous study [7]. These vesicles have a diameter of approximately 100–150 nm, consistent with the size range of exosome. Scale bar=100 nm.

https://doi.org/10.3347/PHD.26039

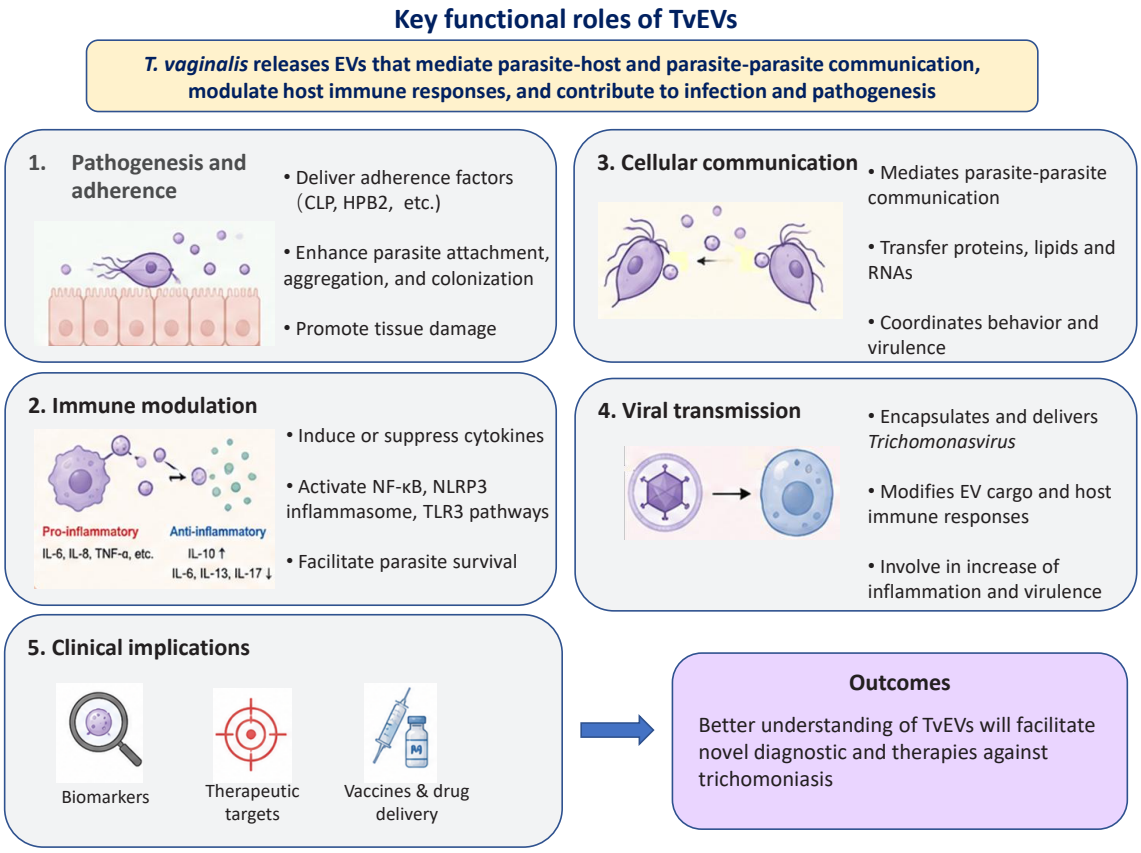


Fig. 2. Schematic representation illustrating the major physiological functions and clinical applications of extracellular vesicles (EVs) released by *Trichomonas vaginalis* (TvEVs).

Table 1. Key literature supporting major studies on TvEVs

Reference	TV strain	EV type	EV isolation method	Protein analysis	Biomolecular cargo content	In vitro/in vivo (animal) experiments	RNA analysis and viral experiments	Research applications
Twu et al. (2013) [2]	B7RC2 (ATCC 50167)	Exosome	UC with sucrose gradient	215 proteins detected by MudPIT-based mass spectrometry	Small RNAs, TSPs, Alix, Rabs, HSP70, BspA, TcTP, GP63-like	Immunolocalization of parasite with human cervical Ect cells Annexin V-FITC in PKH-67	mRNA analysis by Agilent 2000 Bioanalyzer	Immunomodulation Increase parasite adhesion to host cells
Olmos-Ortiz et al. (2017) [4]	GT-21	Exosome-like vesicles	UC	Not reported	Not reported	Nitric oxide dosage and cytokine expression in murine macrophages Cytokine expression in vivo after EVs stimulation in mice	Not reported	Immunomodulation
Nievas et al. (2018) [8]	B7RC2 (PA) and Jt wild type	MV-like structures	UC	LC–MS/MS	TSP, RAB proteins, ARF, endoplasmin, GP63-like, BspA, P270, CPs, metallopeptidases	Immunolocalization anti-HA tag antibody PKH67	Not reported	Interaction of MVs and LVs with parasites and host cells
Rai et al. (2019) [11]	B7RC2	EV	UC	Not reported	Not reported	Cell uptake with EVs CFSE-labeled and R18 labeled	Not reported	Involved in host-parasite and parasite-parasite interaction

(Continued on the next page)

Table 1. Continued

Reference	TV strain	EV type	EV isolation method	Protein analysis	Biomolecular cargo content	In vitro/in vivo (animal) experiments	RNA analysis and viral experiments	Research applications
Artuyants et al. (2020) [9]	B7RC2	EV	UC	Not reported	Not reported	sEVs derived from TVV+ parasite stimulates a proinflammatory response in human HaCaT cells	Analysis of small RNA in EVs cargo RNA sequencing	Revealed a preferential RNA cargo in EVs, which might be involved in parasite-host communication
Govender et al. (2020) [5]	Isolate 347V+, 347V-, B7RC2, UR1, OC7, OC8	sEV	Total exosome isolation reagent	171 proteins detected by TMT peptide labeling	Zinc ion binding and transferase activity proteins	EVs stimulation NF-kB activity in endocervical cells EVs stimulation of cytokines in PBMC Endocervical cells and PBMC viability	TVVs modulate small RNA cargo in EVs	Suppression of the immune response
Ong et al. (2022) [15]	ATCC 30236, 30238, 50148, 50143, PRA-98 and T1	sEV	UC with 30% sucrose	LC–MS/MS	TSP1, TSP6 & TSP8, TVV capsid proteins	Not reported	Identification of TVV subspecies by RT-PCR, RNA sequencing and NGS	Encapsulation of TVV particles
Rada et al. (2022) [6]	TV79-49c1+ and TV79-49c1–	sEV	UC with 5%–50% OptiPrep	1633 proteins detected by label-free quantitative mass spectrometry	TSP1, Rab small GTPases, HSP70, TSG101, BspA, calpains, GP63-like metallopeptidases, small regulatory ts-RNA	sEVs derived from TVV+ parasite stimulates a proinflammatory response in human HaCaT cells	TVVs modulate small RNA cargo in EVs RNA sequencing	Encapsulation of TVV particles
Salas et al. (2023) [10]	G3, B7RC2, and CDC1132	MVs (cytoneme structure) and exosomes	UC	LC–MS/MS	VPS32, Rab proteins, BspA, cathepsin L-like cysteine peptidase, GP63-like metallopeptidases, peptidase T-like	Parasites were seeded onto human prostate BPH-1 cells to quantify binding to the host cells	Not reported	Increase parasite adhesion to host cells
Molgora et al. (2023) [12]	B7RC2	EV	UC	Not reported	Not reported	Delivering parasites into the murine urogenital tract via transurethral catheterization	Not reported	Increase the adherence of TV to host cell monolayers in vitro Increased survival of the parasite in murine
Ong et al. (2024) [7]	ATCC 30236, 30238, 50148, 50143, PRA-98, and T1	Exosome	UC with 30% sucrose	Total of 1207 exosomal-specific proteins detected by LC–MS/MS	TSP1, ribosomal proteins, Rabs, heterotrimeric G proteins, actin, VPS32, GP63-like	Not reported	Not reported	Established a reference core exosome proteome of TV
Kochanowsky et al. (2024) [13]	B7RC2 and G3	EV	Total exosome isolation reagent	303 proteins detected by MS/MS	TSPs, small Rab & Ras GTPases, VSPs, HPB, CLP	Co-infection with EVs in mouse	RNA sequencing	Identify TvEVs as a mediator of parasite-parasite communication
Huang et al. (2025) [14]	ATCC 30236 and ATCC 50143	EV	Total exosome isolation reagent	LC–MS/MS	Adhesins, cysteine proteases	Mice were inoculated intravaginally with TvEVs Co-incubation of labeled EV with THP-1 macrophages and human Ect cells	RNA sequencing	Investigate the molecular mechanisms driving inflammation induced by TvEVs Involved in host-parasite interaction

TvEVs, *Trichomonas vaginalis* extracellular vesicles; TV, *Trichomonas vaginalis*; EV, extracellular vesicles; UC, ultracentrifugation; MV, microvesicles; ARF, ADP ribosylation factor; LV, large vesicles; sEV, small extracellular vesicles; TVV, *Trichomonasvirus*; TMT, Tandem-Mass-Tag; PBMC, peripheral blood mononuclear cells; HPB, heteropolysaccharide binding proteins; CLP, cadherin-like protein.

https://doi.org/10.3347/PHD.26039

Notably, co-inoculation of *T. vaginalis* with exosomes derived from highly adherent strains significantly increases parasite attachment to vaginal and prostate epithelial cells [2]. In addition, the parasite can lyse host epithelial cells, leading to inflammation and tissue damage, further underscoring the role of exosomes in promoting pathogenicity.

Exosomes are also thought to deliver bioactive molecules into host cells, altering the expression of adhesion-related factors and thereby facilitating parasite attachment. Adhesion is further enhanced when both parasites and host cells are pre-exposed to exosomes, suggesting that these vesicles help coordinate host-parasite interactions. Moreover, Molgora et al. [12] demonstrated that parasite-derived EVs enhance *T. vaginalis* adherence to host cell monolayers in vitro [2] and are associated with improved parasite survival in a murine model. These findings provide the first in vivo evidence that TvEVs contribute to host-parasite interactions and support earlier in vitro findings that TvEVs facilitate parasite colonization within the host [2,11].

Evidence suggests that the molecules involved in parasite-parasite aggregation may also mediate parasite-host binding, with exosomes potentially depositing adhesion ligands onto host cell surfaces. Notably, exosomes derived from a highly adherent *T. vaginalis* strain (B7RC2) can transfer a high-adhesion phenotype to a less adherent strain (G3), significantly enhancing their survival, aggregation, and attachment to host cells. Acting as mediators of parasite-parasite communication, EVs transfer virulence-associated proteins, such as cadherin-like protein (CLP), that improve the adhesive capacity of recipient parasites [10]. Salas et al. [10] revealed that *T. vaginalis* coordinates behavior via cytonemes and EVs, with EVs influencing the formation of communication structures in neighboring parasites. In addition, Kochanowsky et al. [13] reported that TvEVs upregulate heteropolysaccharide binding protein (HPB2) expression and facilitate the transfer of adherence factors between parasites, thereby increasing overall virulence. However, it remains unclear whether these effects are driven by molecules on the exosome surface or by cargo delivered into the host cells.

In addition to exosomes, the parasite also produces ectosomes, larger vesicles that bud directly from the plasma membrane, which are released in greater amounts during host-cell contact. This observation suggests that ectosomes may likewise contribute to host-parasite interactions and play a role in disease pathogenesis [8].

Immune modulation

The immunomodulatory roles of exosomes derived from *T. vaginalis* have been extensively studied, with evidence demonstrating that they can exert both pro-inflammatory and anti-inflammatory effects in vitro and in vivo. The internalization of exosomes by ectocervical cells induces IL-6 secretion and modest IL-8 release. Conversely, exosomes that fuse with host cells may also deliver regulatory molecules that suppress IL-8 secretion from ectocervical cells, thereby limiting neutrophil recruitment to infection sites [2]. In addition, Nievas et al. [8] reported that *T. vaginalis* releases microvesicles and larger vesicles in the presence of HeLa cells, supporting a role for parasite-derived EVs in modulating host cell interactions.

Further evidence from Olmos-Ortiz et al. [4] showed that pretreatment with these vesicles in a murine model enhances IL-10 production and suppresses pro-inflammatory cytokines, including IL-6, IL-13, and IL-17, in RAW264.7 macrophages, indicating an anti-inflammatory effect. Furthermore, Govender et al. [5] showed that these vesicles activate NF-κB signaling, promoting parasite adherence and persistence, modulating host cell pathways, and inducing metabolic changes in macrophages.

More recently, Huang et al. [14] reported that TvEVs trigger pro-inflammatory cytokine production through the TLR3-dependent signaling pathway, activating NF-κB/NLRP3 in human THP-1 macrophages and PI3K/NF-κB signaling in epithelial cells. Collectively, these findings highlight the dual role of TvEVs in supporting parasite survival and pathogenesis.

Cellular communication

Exosomes can fuse with host cells and deliver their cargo, thereby altering the host cellular environment. These vesicles act as key mediators of both parasite-parasite and parasite-host communication. Twu et al. [2] demonstrated that exosomes carry a diverse range of molecules, including proteins, RNA, cytoskeletal components, membrane proteins, and adherence factors involved in metabolism, binding, and virulence. These vesicles also contain parasite-specific factors, such as BspA-like proteins and GP63-like metalloproteases, which are likely to be involved in the pathogenicity of trichomoniasis.

Previous studies have identified 3 tetraspanins (TvTSP1, TvTSP6, and TvTSP8) on the surface of *T. vaginalis* [15,16], supporting its ability to secrete exosomes, as tetraspanins are widely recognized as classical markers of small EVs. Twu et al. [2] further showed that exosomes enriched in TvTSP1 enhance parasite adherence to host cells, indicating that tetrasp-

anins play an important role in virulence. In addition, Salas et al. [10] reported that TvTSPs are involved in multiple aspects of cell biology and physiology by regulating both intracellular and intercellular processes. TvTSPs are critical membrane organizers that contribute to parasite survival, infection, and intercellular communication within the human urogenital tract. Research indicates that TvTSPs function as key virulence factors in the parasite's biology, facilitating adhesion to host cells, promoting cellular aggregation, and inducing inflammatory responses [17].

Proteomic analysis of *T. vaginalis* exosomes has revealed that approximately 73% of their protein content is orthologous to proteins found in mammalian exosomes. Twu et al. [2] reported that a member of the ESCRT-III component, VPS32, plays a central role in EV biogenesis and cargo sorting, and its overexpression has been shown to enhance EV secretion, as well as host cell binding and uptake. Salas et al. [18] demonstrated that VPS32 also promotes parasite adherence to prostate epithelial cells, which contributes to pathogenesis. Furthermore, proteomic studies of exosomes have been performed by Rada et al. [6], Twu et al. [2], Govender et al. [5], which identified 1633, 215, and 171 proteins, respectively. In comparison, our study on core exosome proteome [7] has discovered a total of 72 common exosomal-specific proteins across 6 *T. vaginalis* isolates. Among these, 16 core exosomal-specific proteins consistently found when comparing with 3 previous studies on *T. vaginalis* exosomes. These core proteins include tetraspanins (TvTSP1), VPS32, Rab proteins, and heterotrimeric G proteins [7].

Additionally, TvEVs contain small RNAs ranging from 25 to 200 nucleotides, accounting for approximately 55% of the total RNA content and predominantly consisting of tRNA-derived fragments. Among these, 5′ tRNA halves are the most abundant species [9]. Given that *T. vaginalis* lacks canonical microRNA genes, these RNA fragments are likely to play important roles in gene regulation and parasite communication [19]. However, their enrichment may result from stress conditions such as serum starvation during EV isolation, highlighting the need for further studies to clarify their functional significance.

Viral transmission

T. vaginalis is an extracellular parasite that damages host tissues through both mechanical interactions and a range of virulence factors. This parasite can harbor a double-stranded RNA virus endosymbiont, *Trichomonasvirus* (TVV), which belongs to the family *Pseudototiviridae* and specifically infects *T. vaginalis* without causing lethal effects to its host parasite [20]. The TVV genome is non-segmented, approximately 4.5–5.5 kilobase pairs in length, and encodes 2 overlapping open reading frames corresponding to the capsid protein (CP) and the RNA-dependent RNA polymerase (RdRp) [21]. Infection with TVV has been shown to enhance the expression of cysteine proteases and P270, thereby promoting the ability of *T. vaginalis* to degrade hemoglobin, fibronectin, collagen IV, and components of the host epithelial basement membrane [22].

Both exosomes and microvesicles transport proteins and RNA, and may also encapsulate TVV virions [8]. These EVs can be internalized by host cells, thereby enhancing parasite adherence and contributing to infection and pathogenesis [2,13,14]. Accordingly, it has been proposed that TVV infection may alter the composition of EVs released by the parasite, or that the virus itself could be delivered to host cells via EVs to induce an antiviral immune response.

Recent studies have highlighted the clinical relevance of TVV and exosomes in *T. vaginalis* infections [5,7,15]. Notably, TVV can be released into the extracellular environment together with host-derived proteins and RNA via exosomes. For example, exosomes from TVV-positive parasites have been associated with decreased secretion of pro-inflammatory cytokines such as IL-8, IL-6, and TNF-α by mononuclear leukocytes, as well as reduced activation of NF-κB, IL-8, and RANTES signaling pathways in endocervical epithelial cells [5]. Govender et al. [5] reported that exosomes from virus-positive *T. vaginalis* exert immunosuppressive effects; however, these findings contrast with those of Rada et al. [6]. Rada et al. [6] provided the first evidence that TVV particles can be packaged into exosomes and released by *T. vaginalis*. Exosomes from TVV-positive isolates have been shown to induce stronger pro-inflammatory responses in HaCaT epithelial cells compared with those from TVV-negative isolates. In addition, exosomes released by *T. vaginalis* may facilitate the transfer of TVV to host cells, although the underlying mechanisms remain unclear. The presence of TVV appears to modify the molecular cargo of these vesicles, thereby enhancing their capacity to stimulate host immune responses [6].

Although the clinical identification and epidemiological studies have characterized different TVV types, research on how TVV infection regulates host immune responses remains limited, and the classification of TVV types remains unresolved. Further investigation is required to clarify how these viral components contribute to inflammatory pathogenesis in trichomoniasis.

https://doi.org/10.3347/PHD.26039

Diagnostic and therapeutic potential

Proteomic analyses of TvEVs have identified numerous proteins, including the GP63 protease, BspA family proteins, and the surface immunogen P270, which may serve as potential biomarkers for trichomoniasis diagnosis and for elucidating disease pathogenesis. In addition, these vesicles carry tRNA-derived small RNAs (tsRNAs), whose expression profiles reflect the physiological and pathological states of the originating cells. As EV-associated tsRNAs change dynamically during infection and disease progression, they serve as promising molecular biomarkers for characterizing specific disease states, monitoring infection dynamics, and evaluating therapeutic responses. In *T. vaginalis*, EV-derived tsRNAs may also indicate parasite physiology and TVV burden, providing a potential tool for tracking infection progression and clinical outcomes of trichomoniasis [6].

Future studies should explore strategies to target key adherence factors, such as CLP or HPB2, delivered by EVs to disrupt parasite communication or enable targeted drug delivery to infection sites. TvEVs have also been shown to modulate host cytokine profiles, highlighting their potential as targets for therapeutic interventions to mitigate excessive inflammatory responses during infection. A deeper understanding of EV-mediated host immune modulation and infection establishment will improve target specificity and therapeutic efficacy, and may also support the development of vaccines and immunotherapies.

Conclusion

Studies on TvEVs consistently indicate that they function as central mediators of both parasite-host and parasite-parasite communication, playing complex roles in disease pathogenesis. Functionally, TvEVs enhance parasite adherence to host epithelial cells by delivering adhesion-related molecules and altering host cell surface properties. Moreover, they can either promote pro-inflammatory responses or suppress host immune defenses, thereby facilitating parasite survival and infection. The presence of the endosymbiotic TVV further modifies EV composition, enhances host inflammatory responses, and may contribute to more severe disease outcomes.

In summary, evidence from both in vivo and in vitro studies supports that TvEVs are not merely byproducts of cellular processes but active contributors to virulence and disease progression. They integrate multiple mechanisms, including virulence factor delivery, immune modulation, and intercellular communication, to promote infection establishment and persistence. A deeper understanding of their biogenesis, cargo selection, and functional roles will be crucial for the future development of novel diagnostic markers and effective therapeutic strategies for trichomoniasis.

Author contributions

Conceptualization: Ong SC. Data curation: Luo HW, Syu JW. Formal analysis: Luo HW, Syu JW. Supervision: Tang P. Validation: Luo HW, Syu JW, Chiu CH. Writing – original draft: Ong SC. Writing – review & editing: Ong SC, Tang P.

Conflict of interest

The authors have no conflicts of interest to declare.

Funding

This work was supported by grants from the National Science and Technology Council of Taiwan (NSTC 108-2923-B-182-001-MY3 and NSTC 113-2320-B-182-017-MY3) awarded to Tang P. Ong SC is supported by an NSTC Postdoctoral Fellowship (NSTC 114-2811-B-182-015).

ORCID

Seow-Chin Ong, https://orcid.org/0000-0002-6436-3199
Hong-Wei Luo, https://orcid.org/0009-0008-0479-6006
Jhen-Wei Syu, https://orcid.org/0009-0005-9311-6372
Cheng-Hsun Chiu, https://orcid.org/0000-0003-4324-7743
Petrus Tang, https://orcid.org/0000-0002-2779-0116

References

1. Ryan CM, de Miguel N, Johnson PJ. *Trichomonas vaginalis*: current understanding of host-parasite interactions. Essays Biochem 2011;51:161-75. https://doi.org/10.1042/bse0510161
2. Twu O, de Miguel N, Lustig G, et al. *Trichomonas vaginalis* exosomes deliver cargo to host cells and mediate host : parasite interactions. PLoS Pathog 2013;9:e1003482. https://doi.org/10.1371/journal.ppat.1003482
3. Théry C, Witwer KW, Aikawa E, et al. Minimal information for studies of extracellular vesicles 2018 (MISEV2018): a position statement of the International Society for Extracellular Vesicles and update of the MISEV2014 guidelines. J Extracell Vesicles 2018;7:1535750. https://doi.org/10.1080/20013078.2018.1535750
4. Olmos-Ortiz LM, Barajas-Mendiola MA, Barrios-Rodiles M, et al. *Trichomonas vaginalis* exosome-like vesicles modify the cytokine profile and reduce inflammation in parasite-infected mice. Parasite Immunol 2017;39:https://doi.org/10.1111/pim.12426
5. Govender Y, Chan T, Yamamoto HS, Budnik B, Fichorova RN. The

role of small extracellular vesicles in viral-protozoan symbiosis: lessons from *Trichomonasvirus* in an isogenic host parasite model. Front Cell Infect Microbiol 2020;10:591172. https://doi.org/10.3389/fcimb.2020.591172

6. Rada P, Hrdý I, Zdrha A, et al. Double-stranded RNA viruses are released from *Trichomonas vaginalis* inside small extracellular vesicles and modulate the exosomal cargo. Front Microbiol 2022;13:893692. https://doi.org/10.3389/fmicb.2022.893692
7. Ong SC, Luo HW, Cheng WH, et al. The core exosome proteome of *Trichomonas vaginalis*. J Microbiol Immunol Infect 2024;57:246-56. https://doi.org/10.1016/j.jmii.2024.02.003
8. Nievas YR, Coceres VM, Midlej V, et al. Membrane-shed vesicles from the parasite *Trichomonas vaginalis*: characterization and their association with cell interaction. Cell Mol Life Sci 2018;75:2211-26. https://doi.org/10.1007/s00018-017-2726-3
9. Artuyants A, Campos TL, Rai AK, et al. Extracellular vesicles produced by the protozoan parasite *Trichomonas vaginalis* contain a preferential cargo of tRNA-derived small RNAs. Int J Parasitol 2020;50:1145-55. https://doi.org/10.1016/j.ijpara.2020.07.003
10. Salas N, Blasco Pedreros M, Dos Santos Melo T, et al. Role of cytoneme structures and extracellular vesicles in *Trichomonas vaginalis* parasite-parasite communication. Elife 2023;12:e86067. https://doi.org/10.7554/eLife.86067
11. Rai AK, Johnson PJ. *Trichomonas vaginalis* extracellular vesicles are internalized by host cells using proteoglycans and caveolin-dependent endocytosis. Proc Natl Acad Sci USA 2019;116:21354-60. https://doi.org/10.1073/pnas.1912356116
12. Molgora BM, Mukherjee SK, Baumel-Alterzon S, et al. *Trichomonas vaginalis* adherence phenotypes and extracellular vesicles impact parasite survival in a novel in vivo model of pathogenesis. PLoS Negl Trop Dis 2023;17:e0011693. https://doi.org/10.1371/journal.pntd.0011693
13. Kochanowsky JA, Mira PM, Elikaee S, et al. *Trichomonas vaginalis* extracellular vesicles upregulate and directly transfer adherence factors promoting host cell colonization. Proc Natl Acad Sci USA 2024;121:e2401159121. https://doi.org/10.1073/pnas.2401159121
14. Huang CY, Chiu SF, Chu LJ, et al. *Trichomonas vaginalis* extracellular vesicles activate the NLRP3 inflammasome and TLR3-mediated inflammatory cascades in host cells. PLoS Pathog 2025;21:e1013216. https://doi.org/10.1371/journal.ppat.1013216
15. Ong SC, Cheng WH, Ku FM, et al. Identification of endosymbiotic virus in small extracellular vesicles derived from *Trichomonas vaginalis*. Genes (Basel) 2022;13:531. https://doi.org/10.3390/genes13030531
16. de Miguel N, Lustig G, Twu O, et al. Proteome analysis of the surface of *Trichomonas vaginalis* reveals novel proteins and strain-dependent differential expression. Mol Cell Proteomics 2010;9:1554-66. https://doi.org/10.1074/mcp.M000022-MCP201
17. Coceres VM, Alonso AM, Nievas YR, et al. The C-terminal tail of tetraspanin proteins regulates their intracellular distribution in the parasite *Trichomonas vaginalis*. Cell Microbiol 2015;17:1217-29. https://doi.org/10.1111/cmi.12431
18. Salas N, Coceres VM, Melo TDS, et al. VPS32, a member of the ESCRT complex, modulates adherence to host cells in the parasite *Trichomonas vaginalis* by affecting biogenesis and cargo sorting of released extracellular vesicles. Cell Mol Life Sci 2021;79:11. https://doi.org/10.1007/s00018-021-04083-3
19. Wang ZS, Zhou HC, Wei CY, et al. Global survey of miRNAs and tRNA-derived small RNAs from the human parasitic protist *Trichomonas vaginalis*. Parasit Vectors 2021;14:87. https://doi.org/10.1186/s13071-020-04570-9
20. Goodman RP, Ghabrial SA, Fichorova RN, Nibert ML. *Trichomonasvirus*: a new genus of protozoan viruses in the family Totiviridae. Arch Virol 2011;156:171-9. https://doi.org/10.1007/s00705-010-0832-8
21. Wang AL, Wang CC. The double-stranded RNA in *Trichomonas vaginalis* may originate from virus-like particles. Proc Natl Acad Sci USA 1986;83:7956-60. https://doi.org/10.1073/pnas.83.20.7956
22. Luo HW, Ong SC, Syu JW, et al. Viral load dependent cellular heterogeneity in *Trichomonas vaginalis* at the single cell level. iScience 2025;29:114260. https://doi.org/10.1016/j.isci.2025.114260

Mini Review

Parasites Hosts Dis 2026;64(4):299-309
https://doi.org/10.3347/PHD.26012

Parasites, Hosts and Diseases

pISSN 2982-5164 • eISSN 2982-6799

Host genetic regulation of immune tolerance and disease persistence in human echinococcosis

Emad Shamsan[1,2], Liu Chuanchuan[1,3,*], Fan Haining[1,3,*]

[1]College of Clinical Medicine, Qinghai University, Xining, China; [2]College of Medical Science, Taiz University, Taiz, Yemen; [3]Qinghai University Affiliated Hospital, Xining, China

Human echinococcosis, caused by *Echinococcus* spp., remains a significant public health concern in endemic regions and manifests primarily as cystic echinococcosis (CE) and alveolar echinococcosis (AE), both characterized by chronic infection and heterogeneous clinical outcomes. This review synthesizes current evidence on host genetic determinants that influence immune responses, susceptibility, and disease persistence in CE and AE. Available studies indicate that polymorphisms in genes encoding key immunoregulatory cytokines, particularly IL10 and TGFB1, are associated with an anti-inflammatory immune profile that favors parasite persistence through enhanced regulatory activity and suppression of protective effector responses. Cytokine pathways involving IL-4, IL-13, and IFN-γ further modulate the balance between Th2-mediated and Th1-mediated immune responses, thereby influencing infection outcomes. In addition, innate immune pathways, including Toll-like receptor signaling, affect early parasite recognition and downstream immune responses, although direct human genetic evidence for Toll-like receptor polymorphisms in CE and AE remains limited. Human leukocyte antigen class II polymorphisms may also contribute to inter-individual differences in antigen presentation and CE susceptibility, although reported associations remain population-specific and require further validation. Collectively, these findings support a mechanistic framework in which host immunogenetic variation shapes the balance between immune activation and tolerance and may influence disease trajectory. Integration of genetic markers with clinical and imaging data may improve risk stratification and support the development of more targeted therapeutic strategies. Future research should prioritize large-scale, multicenter studies, standardized phenotyping, and functional validation to clarify the clinical relevance of identified variants.

Keywords: Echinococcosis, host genetics, polymorphism, immune tolerance, human leukocyte antigen, Toll-like receptors

Introduction

Echinococcus infection and its life cycle

Echinococcosis is a zoonotic parasitic disease caused by cestodes of the genus *Echinococcus*, primarily *Echinococcus granulosus* and *Echinococcus multilocularis*, which are responsible for cystic echinococcosis (CE) and alveolar echinococcosis (AE), respectively [1,2]. The parasite life cycle involves 2 hosts: a definitive host, typically canids such as dogs and foxes, and an intermediate host, including livestock and humans. Infection occurs when intermediate hosts ingest parasite eggs shed in the feces of definitive hosts. Following ingestion, larvae penetrate the intestinal wall and develop into hydatid cysts, predominantly in the liver and lungs, leading to progressive tissue damage and clinical disease [2].

Received: February 8, 2026 Accepted: June 2, 2026
*Correspondence: lc, 18797331470@139.com; fh, fanhaining@medmail.com.cn
© 2026 The Korean Society for Parasitology and Tropical Medicine
This is an open-access article distributed under the terms of the Creative Commons Attribution Non-Commercial License (http://creativecommons.org/licenses/by-nc/4.0/) which permits unrestricted non-commercial use, distribution, and reproduction in any medium, provided the original work is properly cited.

Citation
Shamsan E, Chuanchuan L, Haining F. Host genetic regulation of immune tolerance and disease persistence in human echinococcosis. Parasites Hosts Dis 2026;64(4):299-309.

Epidemiology and global burden

Echinococcosis remains a significant global health concern, particularly in pastoral and resource-limited regions. CE is widely distributed across South America, the Mediterranean basin, Eastern Europe, Africa, and Asia, whereas AE is more prevalent in the Northern Hemisphere, including parts of China, Central Europe, and Russia [3]. Despite the implementation of control strategies such as dog deworming, livestock inspection, and public health education, the disease persists in endemic regions and continues to pose major challenges [4]. The global burden of echinococcosis is substantial, with estimates indicating approximately one million disability-adjusted life years lost annually, alongside considerable economic losses in both human health and livestock production [5]. These impacts are exacerbated by delayed diagnosis, limited access to healthcare, and the complexity of treatment in advanced cases.

Pathogenesis and clinical manifestations

In humans, echinococcosis manifests primarily as CE or AE, which differ markedly in their biological behavior and clinical progression. CE is characterized by the formation of fluid-filled hydatid cysts, most commonly in the liver and lungs, although other organs may also be affected [6]. These cysts typically grow slowly and may remain asymptomatic for years, but can cause clinical symptoms such as abdominal pain, nausea, or organ dysfunction due to mass effect. Cyst rupture may result in severe allergic reactions or secondary dissemination [7]. In contrast, AE exhibits a more aggressive and infiltrative growth pattern, resembling a malignant tumor. The parasite forms irregular, invasive lesions in the liver that can spread to adjacent tissues and distant organs. Clinical manifestations include jaundice, weight loss, and hepatic dysfunction, and the disease is often fatal if left untreated [3,8].

Diagnostic and therapeutic overview

Diagnosis of echinococcosis relies primarily on imaging techniques, including ultrasound, computed tomography, and magnetic resonance imaging, supported by serological assays such as ELISA and indirect hemagglutination tests [9,10]. Molecular methods, including PCR-based detection, provide additional specificity in complex or ambiguous cases [11]. Management strategies depend on disease stage and include surgical intervention, antiparasitic chemotherapy such as albendazole, active surveillance in selected cases, and percutaneous techniques such as PAIR. PAIR refers to puncture, aspiration, injection of a scolicidal agent, and re-aspiration, and is mainly used for selected uncomplicated CE cysts [12-15]. However, treatment outcomes remain variable, particularly in AE, where complete cure is often difficult to achieve.

The Importance of Studying Genetic Determinants of Susceptibility to Echinococcus

Understanding the genetic determinants of host susceptibility to *Echinococcus* infection is critical for elucidating the mechanisms underlying parasite persistence and disease progression. Host genetic variation, particularly in genes regulating cytokine production and immune responses, plays a pivotal role in shaping infection outcomes by influencing the balance between protective immunity and immune tolerance. Identifying these genetic factors provides a foundation for the development of targeted therapeutic strategies and improved diagnostic approaches. Furthermore, integrating genetic information into clinical practice may enable personalized medicine, allowing treatment strategies to be tailored according to individual immune and genetic profiles. As summarized in Fig. 1, investigating host genetic susceptibility not only advances our understanding of host–parasite interactions but also supports the development of more precise and effective interventions.

This review is based on a targeted literature survey of published studies relevant to host genetic and immunological factors in echinococcosis. Relevant articles were identified through major scientific databases and selected based on their relevance to CE and AE, host immune responses, and genetic susceptibility. Both clinical and experimental studies were included to provide a comprehensive overview of the topic. No formal systematic review protocol was applied.

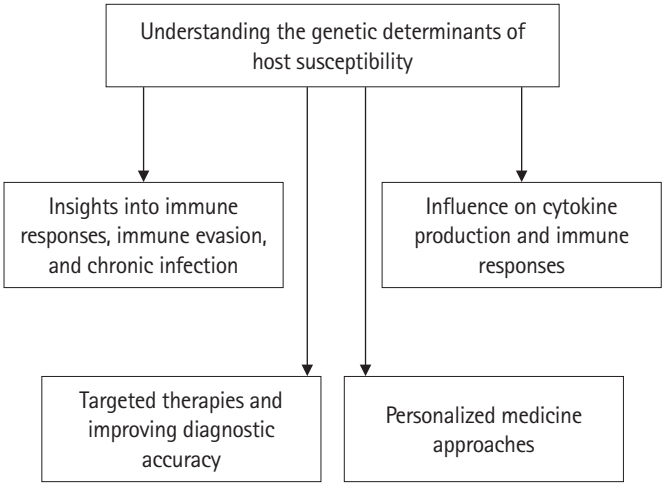


Fig. 1. Schematic summary of the importance of studying genetic determinants of susceptibility to *Echinococcus* infection.

https://doi.org/10.3347/PHD.26012

Host Immune Response to *Echinococcus* Infection

Mechanisms of immune response against Echinococcus

The host immune response to *Echinococcus* infection involves coordinated interactions between innate and adaptive immune systems. Following infection, parasite-derived antigens are recognized by host immune cells, initiating a cascade of immunological responses that determine infection outcome.

Innate immune response to Echinococcus

The innate immune system constitutes the first line of defense against *Echinococcus*. Innate immune cells, including macrophages, dendritic cells, and neutrophils, express pattern-recognition receptors such as Toll-like receptors (TLRs), which recognize pathogen-associated molecular patterns. In cystic and alveolar echinococcosis, TLR2 and TLR4 have been implicated in immune regulation, although their precise roles remain incompletely characterized. TLR signaling can activate MyD88-dependent pathways involving NF-κB and mitogen-activated protein kinases, thereby promoting pro-inflammatory cytokine production. Activated macrophages may also produce nitric oxide, which contributes to preventing the dissemination of hydatid cyst layers [16]. Evidence from helminth infection models further suggests that parasite-derived excretory–secretory products can modulate innate immune responses, including alterations in co-stimulatory molecule expression and cytokine production, thereby contributing to immune evasion strategies [17].

Adaptive immune response to Echinococcus

Adaptive immune responses play an important role in controlling Echinococcus multilocularis infection. In a chronic murine model of alveolar echinococcosis, PD-L1 blockade reduced parasite burden, increased $CD4^+$ and $CD8^+$ effector T cells, decreased regulatory T cells, and restored dendritic cells and Kupffer cells/macrophages. These findings indicate that PD-L1 signaling regulates coordinated innate and adaptive immune responses and influences parasite control and tissue [18]. In addition, both cellular and humoral immune components are involved in responses to parasite-derived antigens. Studies have demonstrated that exposure to hydatid cyst antigens induces the production of pro-inflammatory cytokines, such as IFN-γ and TNF-α, as well as parasite-specific IgG antibodies, highlighting the role of antigen-specific immune responses in host defense [19]. Fig. 2 summarizes the principal immune mechanisms involved in host responses to *Echinococcus* infection.

Mechanisms of immune evasion by Echinococcus

Echinococcus species have evolved multiple sophisticated strategies to evade host immune defenses, enabling long-term survival and chronic infection.

Modulation of host immune response

Echinococcus infection is associated with the activation of immunosuppressive pathways that promote immune tolerance. In patients with AE, increased expression of the Tim-3/Galectin-9 pathway was associated with elevated IL-10 and TGF-β expression, altered $CD8^+$ T-cell activity, and reduced cytotoxic T-lymphocyte responses. These immunoregulatory changes may impair parasite clearance and contribute to persistent infection [20]. In addition, parasite-derived antigens and ES products can modulate immune-cell responses in ex vivo and in vitro settings. These effects may involve peripheral blood mononuclear cells, dendritic cells, and $CD4^+$ T-cell subsets, and may be reflected by reduced protoscolex-killing activity and nitric oxide production, impaired dendritic-cell function, suppression of Th1 development, and induction of $CD4^+CD25^{+-}$ $Foxp3^+$ regulatory T cells, thereby contributing to immune evasion and chronic infection [21,22].

Antigenic diversity and immune interference

Rather than classical antigenic switching, *Echinococcus* exhibits antigenic diversity across different cyst compartments and host tissues. In *E. granulosus*, antigens from the laminated layer (LL), protoscoleces, and hydatid cyst fluid have been shown to display immunogenically distinct protein profiles, with the LL containing prominent immunogenic proteins [23].

Induction of regulatory T cells

A key immune evasion mechanism involves the expansion of Tregs, which suppress protective immune responses. Studies demonstrate increased $Foxp3^+$ Treg activity and associated cytokines (IL-10 and TGF-β), contributing to a tolerogenic environment that favors parasite survival [24-26].

Macrophage polarization and immune regulation

Parasite-driven immune responses are often associated with a shift toward Th2-type immunity, characterized by cytokines such as IL-4 and IL-13. These cytokines promote the polarization of macrophages toward an alternatively activated phenotype, which exhibits reduced microbicidal activity, including decreased nitric oxide production, thereby facilitating parasite persistence [27].

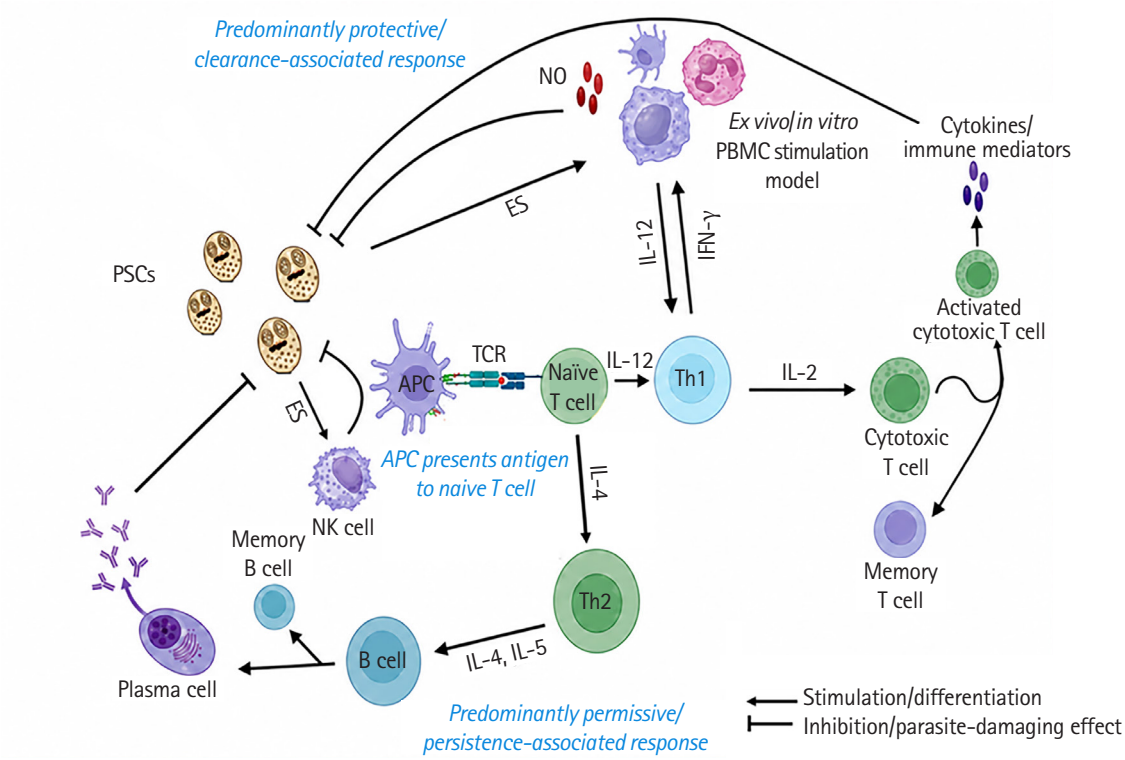


Fig. 2. Immune responses to *Echinococcus* protoscoleces (PSCs). PSC-derived excretory-secretory (ES) products are recognized by antigen-presenting cells (APCs), which present parasite antigens to naïve T cells and promote Th1/Th2 differentiation. IL-12 and IL-4 indicate cytokine signals that promote Th1 and Th2 differentiation, respectively. Th1-associated responses, including IFN-γ production, immune-cell activation, and nitric oxide (NO) production, are generally considered protective and may contribute to parasite clearance. Th2-associated humoral responses involving IL-4, IL-5, B-cell activation, plasma-cell differentiation, and antibody production may contribute to parasite recognition or containment, whereas Th1-associated IFN-γ/NO responses are more directly associated with parasite clearance. Peripheral blood mononuclear cells (PBMCs)-related interactions shown in the figure represent ex vivo/in vitro PBMC stimulation models and do not imply in vivo localization of PSCs in peripheral blood. TCR, T-cell receptor; NK, natural killer.

Physical and molecular barriers

The hydatid cyst contains parasite-derived molecules that play key roles in host–parasite interactions. These components exhibit antigenic diversity and bioactive properties that contribute to immune modulation and parasite survival within the host [28]. Fig. 3 provides a schematic overview of the principal immune evasion mechanisms of *Echinococcus*.

Genetic Determinants of Host Susceptibility

Overview of host genetic factors influencing susceptibility

Host genetic factors play an important role in determining susceptibility to parasitic infections, including *E. granulosus* and *E. multilocularis*. Variations in genes involved in immune regulation can influence how effectively the host recognizes, responds to, and controls infection [29].

In particular, genetic variations such as cytokine gene polymorphisms and other immune-related factors have been implicated in shaping host–parasite interactions and infection susceptibility [29]. These variations may influence immune regulation and contribute to differences in infection outcomes [29].

Beyond host genetic influences, helminth infections are also characterized by strong parasite-driven immunomodulation. Parasites such as *E. granulosus* can manipulate host immune pathways, promoting regulatory and anti-inflammatory responses that support chronic infection, while excessive inflammatory responses may contribute to host tissue damage despite limiting parasite survival [30-32].

Key case studies and research findings

IL-10: immunoregulation and disease persistence

IL-10 is a key anti-inflammatory cytokine that suppresses pro-inflammatory responses and promotes immune toler-

https://doi.org/10.3347/PHD.26012

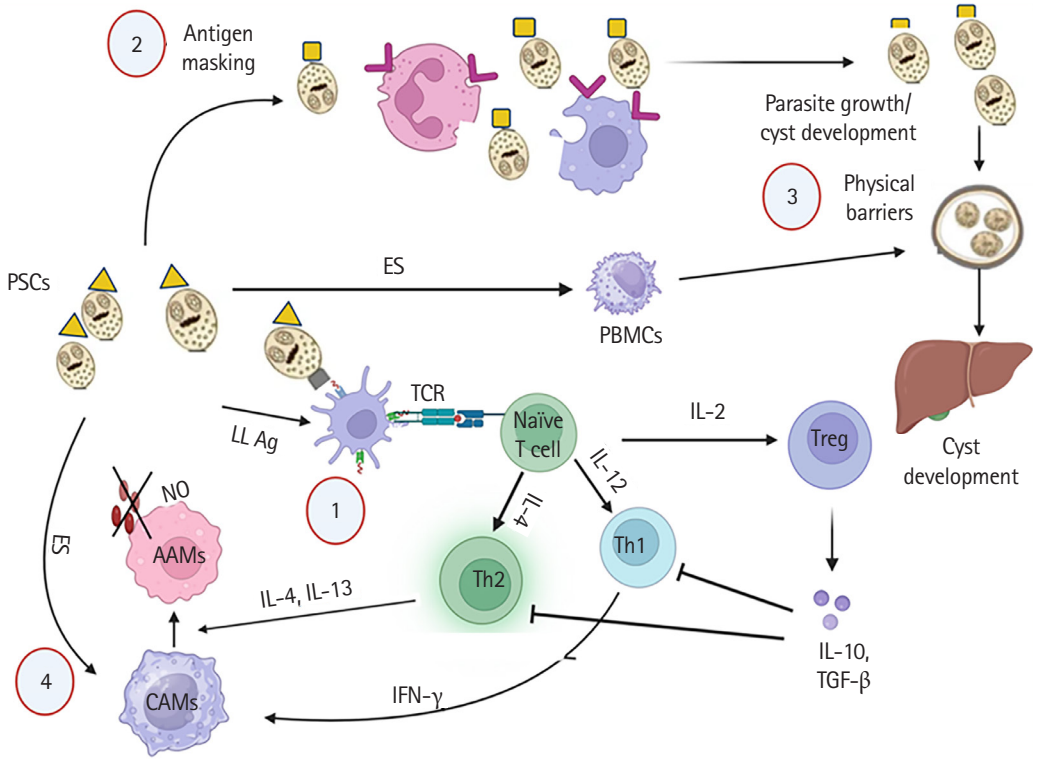


Fig. 3. Mechanisms of immune evasion by *Echinococcus* spp. The figure summarizes 4 major immune-evasion mechanisms: (1) laminated layer antigens (LL Ag) may impair dendritic-cell maturation and promote Th2/Treg-skewed responses associated with IL-10 and TGF-β production; (2) antigen masking reduces immune recognition; (3) cyst barriers restrict immune-cell access and support cyst development; and (4) parasite-derived excretory-secretory (ES) products promote alternative macrophage activation, reduce nitric oxide (NO) production, and impair parasite clearance. ES products may also modulate peripheral blood mononuclear cell responses in ex vivo/in vitro stimulation models; this does not imply that protoscoleces (PSCs) are normally present in peripheral blood. Treg, regulatory T cell; AAMs, alternatively activated macrophages; CAMs, classically activated macrophages.

ance. In CE, elevated IL-10 levels have been associated with chronic infection and parasite persistence, particularly in patients with active cystic disease [33,34]. Functional studies indicate that IL-10, together with IL-4, impairs parasite killing by reducing nitric oxide production and suppressing Th1-mediated immunity [22], while parasite-derived factors from *E. granulosus* may further enhance regulatory immune responses [21]. At the genetic level, the IL10 rs1800896 variant has been identified in an exploratory genomic screening study related to *E. granulosus* susceptibility in an endemic population [35]. However, this evidence is based on a small cohort and lacks case-control validation.

TGFB1: immune tolerance and parasite survival

TGF-β1 is a multifunctional cytokine involved in immune suppression, immune tolerance, and tissue remodeling. In CE and AE, increased TGF-β expression has been associated with parasite persistence, immune tolerance, and tissue remodeling or fibrosis, supporting its potential role in chronic infection [36-38]. TGFB1 rs1800469 was also reported as a high-frequency candidate variant in the same exploratory *E. granulosus*–related study [35]. However, this evidence remains preliminary and lacks validation in independent cohorts. Overall, TGFB1 should be regarded as a biologically plausible candidate gene involved in immune tolerance and tissue remodeling in CE and AE, although its genetic association with susceptibility remains preliminary and requires validation in larger, independent cohorts.

IL-4 and IL-13: Th2 polarization and immune deviation

IL-4 and IL-13 are key mediators of Th2 immune responses, promoting humoral immunity and IgE production. These cytokines play a central role in helminth infections by driving Th2 polarization and modulating host immune responses [39,40]. In *E. multilocularis* infections, parasite-derived antigens have been shown to induce IL-4 and IL-13 production, contributing to a Th2-skewed immune environment. This Th2 deviation may counterbalance Th1-associated protective re-

sponses and contribute to conditions that favor parasite persistence [40].

IFNG: Th1-mediated protective immunity

IFN-γ is a key cytokine in Th1-mediated immune responses and plays a central role in macrophage activation and parasite clearance. In CE, parasite-derived antigens have been shown to induce IFN-γ production by $CD4^+$ and $CD8^+$ T cells, supporting Th1-mediated immunity [41]. Genetic polymorphisms in IFNG are known to influence cytokine production and host resistance in infectious diseases. IFNG rs2779249 was reported as a high-frequency candidate variant in an exploratory hydatidosis study related to *E. granulosus*; however, no direct validated association with disease susceptibility has yet been established [35]. Overall, IFNG represents a biologically plausible candidate gene in CE, although current genetic evidence remains limited and requires further validation.

TLR2 and TLR4: innate immune recognition and regulation

TLRs, particularly TLR2 and TLR4, play important roles in innate immune recognition and early host responses to *Echinococcus* infection. In CE, hydatid cyst-derived antigens from *E. granulosus* have been shown to modulate TLR2 and TLR4 expression in peripheral blood mononuclear cells, suggesting that the parasite may interfere with innate immune activation and downstream cytokine responses [42]. In AE, experimental murine studies have also implicated TLR signaling in immune regulation; for example, TLR2 expression has been associated with IL-10 production during *E. multilocularis* infection, indicating a possible role in promoting regulatory or tolerogenic immune responses [43]. Overall, current evidence supports the involvement of TLR2 and TLR4 signaling in immune modulation during CE and AE. However, direct human genetic evidence linking specific TLR polymorphisms to susceptibility or disease progression in CE or AE remains limited. Therefore, TLR2 and TLR4 should currently be interpreted as biologically plausible candidate pathways rather than validated genetic risk markers in echinococcosis.

HLA genes: antigen presentation and genetic susceptibility

Human leukocyte antigen (HLA) class II molecules are central to antigen presentation and the activation of adaptive immune responses by presenting peptide antigens to T cells. The high polymorphism of HLA genes results in substantial inter-individual variability in the repertoire of peptides that can be presented, thereby influencing immune recognition and response to pathogens [44].

Several case-control studies have investigated the association between HLA class II polymorphisms and susceptibility to CE. Specific alleles, including HLA-DRB1*07, HLA-DQB1*09, and HLA-DQB1*02, have been associated with an increased risk of CE in children, while HLA-DQB1*02 and HLA-DRB1*03 have been reported more frequently in patients with suppuration-complicated cysts [45]. In contrast, a reduced frequency of HLA-DRB1*03 has been observed in patients compared to healthy controls, suggesting a potential protective role against infection [46].

These findings collectively indicate that HLA genetic variation may influence host susceptibility to CE by modulating antigen presentation and subsequent T-cell–mediated immune responses. However, the reported associations remain heterogeneous and may vary across populations, highlighting the need for larger, multicenter studies to better clarify the role of HLA class II polymorphisms in the natural history of *E. granulosus* infection.

Integrated perspective on host genetic regulation

Recent studies highlight the critical role of host–parasite cross-talk mechanisms involving TLR signaling, apoptosis, and inflammasome activation in both CE and AE, with these pathways contributing to immune modulation and disease progression [16]. In addition, exploratory genetic studies have identified associations between polymorphisms in immune-related genes—such as IL10, IL17A, IFNG, FOXP3, TGFB1, and VDR—and susceptibility to *E. granulosus* infection. These findings suggest that genetic variability in immune regulatory pathways may modulate host responses; however, most evidence is derived from small-scale studies and should be considered preliminary [35]. Furthermore, the immunological landscape of hepatic AE has been increasingly characterized in recent years, with bibliometric analyses identifying major research trends, hotspots, and emerging themes related to host–parasite immune interactions, diagnosis, and treatment strategies. This growing body of research reflects increasing interest in AE immunology and may help guide future investigations in the field [47]. Because many reported genetic associations are derived from small-scale, exploratory, or population-specific studies, the variants summarized in Table 1 should be interpreted as candidate susceptibility markers rather than validated clinical predictors [35,44-46]. Table 1 summarizes specific gene functions, proposed immunological roles, disease context where available, and evidence summaries for reported candidate associations [35,44-46]. Table 2 summarizes immune-regulatory pathways and host–parasite

https://doi.org/10.3347/PHD.26012

interaction mechanisms in echinococcosis, with disease context and evidence type specified where available [21,33,34,37,38,42,43].

Genetic influences on immune modulation and disease persistence

Accumulating evidence suggests that host immunogenetic variation may contribute to inter-individual differences in immune responses and susceptibility in echinococcosis, although current genetic evidence remains limited and is derived mainly from exploratory *E. granulosus*/CE-related studies. Polymorphisms in immunoregulatory genes, including IL10 rs1800896 and TGFB1 rs1800469, have been reported as candidate variants in an exploratory genomic analysis, but their functional relevance requires further validation [35]. Functional and tissue-based evidence indicates that IL-4- and IL-10-associated responses can reduce Th1-related parasite-killing mechanisms, whereas IL-10- and TGF-β-associated immune regulation may contribute to parasite persistence in CE [22,36]. In AE, longitudinal immune profiling has shown that antigen-specific IFN-γ responses increase after cure, supporting the association between stronger Th1-type responses

Table 1. Candidate host genetic susceptibility factors in echinococcosis with disease context where available

Gene/locus	Variant/allele	Disease context	Functional role	Evidence summary	References
IL10	rs1800896	CE-related exploratory evidence	Immune regulatory cytokine	Candidate variant; requires validation	[35]
TGFB1	rs1800469	CE-related exploratory evidence	Immune regulation and fibrosis	Candidate variant; preliminary evidence	[35]
IL17A	rs2275913	CE-related exploratory evidence	Th17 immune response	Candidate variant; requires validation	[35]
IFNG	rs2779249	CE-related exploratory evidence	Th1 cytokine response	Candidate variant; association unconfirmed	[35]
FOXP3	rs11568821	CE-related exploratory evidence	Regulatory T-cell function	Candidate variant; limited validation	[35]
HLA-DRB1/HLA-DQB1	HLA-DRB1*07, HLA-DQB1*02, HLA-DQB1*09	CE	Antigen presentation	Reported increased-risk alleles in pediatric CE	[45]
HLA-DRB1	HLA-DRB1*03	CE	Antigen presentation	Possible protective association	[46]
HLA class II (general)	HLA variants and haplotypes	General HLA biology; not echinococcosis-specific	Peptide-presentation diversity	Mechanistic rationale only	[44]

CE, cystic echinococcosis; HLA, human leukocyte antigen.

Table 2. Immune regulation and host–parasite interaction mechanisms in echinococcosis with disease context where available

Pathway/molecule	Disease context	Observed effect	Immunological role	Evidence type	References
TLR2/TLR4	CE	Downregulation or modulation by parasite antigens	Innate immune recognition and immune evasion	Functional in vitro study	[42]
TLR2/TLR4 + cytokines	AE	Altered expression linked with IL-10, IFN-γ, IL-5 changes	Regulation of innate–adaptive immune signaling	Murine infection model	[43]
IL-10	CE	Elevated or infection-associated expression in CE patients	Anti-inflammatory immune regulation	Clinical cytokine profiling	[33]
IFN-γ	CE	Increased in hepatic CE patients; Th1-type cytokines more evident in inactive cysts	Th1-associated immune response and possible parasite control	Clinical cytokine profiling	[33,34]
TGF-β–Smad pathway	CE and AE	Activated/upregulated in experimental CE and AE models	Immune tolerance, altered T/NK-cell responses, and AE-associated fibrosis	Mouse studies and human AE tissue analysis	[37,38]
$FOXP3^+$ T cells	CE	Induction of $CD4^+CD25^+Foxp3^+$ Tregs	DC impairment, Treg induction, and immune evasion	In vitro BMDC–T-cell co-culture study	[21]
Th1/Th2 balance	CE	Th2 dominance in active cysts; Th1/Th17 in inactive stages	Regulation of infection progression and parasite persistence	Human clinical studies	[34]

CE, cystic echinococcosis; AE, alveolar echinococcosis; NK, natural killer; Treg, regulatory T cell.

and improved disease control [48]. Innate immune pathways further contribute to this balance. In AE, an experimental murine study showed that *E. multilocularis* infection is associated with altered TLR2 and TLR4 expression and changes in cytokines such as IL-10, IFN-γ, and IL-5, with TLR2 expression positively correlated with IL-10 production, suggesting a possible role in immune tolerance [43]. In parallel, host genetic background modulates adaptive immune responses. The HLA-B8, DR3, DQ2 haplotype has been associated with altered cytokine production profiles, including increased IL-10 secretion and modulation of Th1/Th2 responses, which may contribute to disease severity and clinical course in AE [49]. Despite these advances, some available evidence is derived from small-scale or population-specific studies, including recent exploratory genomic analyses [35]. Consequently, the functional significance and clinical applicability of many candidate variants remain to be fully established. Future studies integrating large-scale genomics with functional immunological approaches and standardized clinical phenotyping will be essential to clarify the mechanistic links between host genetics, immune modulation, and disease outcomes.

Future research directions in understanding genetic susceptibility to *Echinococcus* infection

Understanding the genetic determinants of host susceptibility to CE and AE remains a critical research priority. To date, most available evidence is derived from candidate gene studies and small-scale association analyses, which provide limited insight into the complex genetic architecture underlying disease susceptibility. Recent exploratory genomic investigations in endemic populations have identified polymorphisms in immune-related genes, including IL10, IL17A, IFNG, FOXP3, and TGFB1, suggesting potential genetic contributions to host susceptibility. However, these findings are based on relatively small cohorts and require validation in larger, well-designed studies [35]. In this context, genome-wide approaches, particularly genome-wide association studies, represent a promising strategy for identifying novel susceptibility loci in an unbiased manner. Although the genome-wide association study approach has been widely applied to other infectious and complex diseases, its application to CE and AE remains limited. In addition to host genetic variation, gene–environment interactions are likely to play a significant role in shaping susceptibility to echinococcosis. Environmental and epidemiological factors, such as geographic distribution, parasite genotype diversity, host nutritional status, and co-infections, may interact with genetic predisposition to influence disease progression and severity. Integrative approaches combining genomic, environmental, and epidemiological data are therefore essential for a more comprehensive understanding of disease heterogeneity. Furthermore, advances in molecular and genomic technologies offer new opportunities for improving diagnosis and disease monitoring. The detection of *E. granulosus* cell-free DNA and the characterization of parasite genotypes in clinical samples highlight the potential of molecular tools to complement conventional diagnostic methods. Such approaches may contribute to improved diagnostic sensitivity and enable better tracking of transmission dynamics, although further refinement and validation are required before routine clinical application [50]. Finally, future research should prioritize the integration of large-scale genomics, functional immunology, and standardized clinical phenotyping. Linking genetic variants to specific immune pathways, such as cytokine regulation, innate immune signaling, and antigen presentation, will be essential to bridge the gap between genetic susceptibility and disease pathogenesis. These efforts may ultimately support the development of personalized diagnostic and therapeutic strategies for echinococcosis.

Conclusion

This review highlights the emerging role of host genetic factors in shaping susceptibility and immune responses in CE and AE. Available evidence suggests that variants in immunoregulatory and immune-response genes, including IL10, TGFB1, IFNG, FOXP3, IL17A, and HLA loci, may contribute to inter-individual differences in host–parasite interactions and disease progression. However, most reported associations are derived from small-scale, exploratory, or population-specific studies, particularly in *E. granulosus*–related settings, and require validation in larger, well-characterized cohorts. In addition, although cytokine regulation, TLR signaling, and Th1/Th2/Treg balance are biologically relevant to CE and AE pathogenesis, direct human genetic evidence for several candidate pathways remains limited. Advancing this field will require integrative approaches combining large-scale genomics, functional immunology, standardized clinical phenotyping, and disease-specific analysis of CE and AE. Such efforts may clarify the mechanistic links between genetic variation and immune regulation and support the development of improved diagnostic, prognostic, and targeted disease-management strategies in endemic regions.

https://doi.org/10.3347/PHD.26012

Author contributions

Conceptualization: Shamsan E, Chuanchuan L, Haining F. Data curation: Shamsan E. Formal analysis: Shamsan E, Chuanchuan L. Funding acquisition: Haining F. Investigation: Shamsan E. Methodology: Shamsan E, Chuanchuan L, Haining F. Project administration: Haining F, Chuanchuan L. Resources: Haining F. Software: Shamsan E, Chuanchuan L. Supervision: Chuanchuan L, Haining F. Validation: Shamsan E, Chuanchuan L. Visualization: Shamsan E. Writing – original draft: Shamsan E. Writing – review & editing: Chuanchuan L, Haining F.

Conflict of interest

The authors have no conflicts of interest to declare.

Funding

This work was supported by the National Clinical Key Specialty Construction Project of Hepatobiliary Surgery (Hydatidosis) at Qinghai University Affiliated Hospital (Qinghai [2023]-125) and the Qinghai Scholar Program (2025-qhxz-fhn).

ORCID

Emad Shamsan, https://orcid.org/0009-0000-1184-2607
Liu Chuanchuan, https://orcid.org/0000-0002-8885-2368
Fan Haining, https://orcid.org/0000-0001-5313-5732

References

1. Grezzi L, González C, Díaz Á, Casaravilla C. The acute inflammatory potential of particles from the *Echinococcus granulosus* laminated layer is moderated by its calcium inositol hexakisphosphate component. Parasite Immunol 2024;46:e13040. https://doi.org/10.1111/pim.13040
2. Craig PS, Rogan MT, Campos-Ponce M. Echinococcosis: disease, detection and transmission. Parasitology 2003;127 Suppl:S5-20.
3. Moro P, Schantz PM. Echinococcosis: a review. Int J Infect Dis 2009;13:125-33. https://doi.org/10.1016/j.ijid.2008.03.037
4. Budke CM, Deplazes P, Torgerson PR. Global socioeconomic impact of cystic echinococcosis. Emerg Infect Dis 2006;12:296-303. https://doi.org/10.3201/eid1202.050499
5. Nedjim SA, Bencherki Y, Daghdagh Y, et al. Diagnosis and multidisciplinary management of a large primary retroperitoneal hydatid cyst: report of a sporadic case. Afr J Urol 2024;30:29. https://doi.org/10.1186/s12301-024-00431-4
6. Siyadatpanah A, Brunetti E, Emami Zeydi A, Moghadam YD, Agudelo Higuita NI. Cerebral cystic echinococcosis. Case Rep Infect Dis 2020;2020:1754231. https://doi.org/10.1155/2020/1754231
7. Hogea MO, Ciomaga BF, Muntean MM, et al. Cystic echinococcosis in the early 2020s: a review. Trop Med Infect Dis 2024;9:36. https://doi.org/10.3390/tropicalmed9020036
8. Craig PS, Hegglin D, Lightowlers MW, Torgerson PR, Wang Q. Echinococcosis: control and prevention. Adv Parasitol 2017;96:55-158. https://doi.org/10.1016/bs.apar.2016.09.002
9. Erganis S, Sarzhanov F, Al FD, Cağlar K. Comparison of methods in the serologic diagnosis of cystic echinococcosis. Acta Parasitol 2024;69:1122-31. https://doi.org/10.1007/s11686-024-00840-z
10. Kronenberg PA, Deibel A, Gottstein B, et al. Serological assays for alveolar and cystic echinococcosis: a comparative multi-test study in Switzerland and Kyrgyzstan. Pathogens 2022;11:518. https://doi.org/10.3390/pathogens11050518
11. Grimm J, Krickl J, Beck A, et al. Establishing and evaluation of a polymerase chain reaction for the detection of *Echinococcus multilocularis* in human tissue. PLoS Negl Trop Dis 2021;15:e0009155. https://doi.org/10.1371/journal.pntd.0009155
12. Mönnink GLE, Stijnis C, van Delden OM, Spijker R, Grobusch MP. Percutaneous versus surgical interventions for hepatic cystic echinococcosis: a systematic review and meta-analysis. Cardiovasc Intervent Radiol 2021;44:1689-96. https://doi.org/10.1007/s00270-021-02911-4
13. Akhan O, Erdoğan E, Ciftci TT, et al. Comparison of the long-term results of puncture, aspiration, injection and re-aspiration (PAIR) and catheterization techniques for the percutaneous treatment of CE1 and CE3a liver hydatid cysts: a prospective randomized trial. Cardiovasc Intervent Radiol 2020;43:1034-40. https://doi.org/10.1007/s00270-020-02477-7
14. Hemphill A, Stadelmann B, Rufener R, et al. Treatment of echinococcosis: albendazole and mebendazole: what else? Parasite 2014;21:70. https://doi.org/10.1051/parasite/2014073
15. Stojkovic M, Rosenberger KD, Steudle F, Junghanss T. Watch and wait management of inactive cystic echinococcosis: does the path to inactivity matter: analysis of a prospective patient cohort. PLoS Negl Trop Dis 2016;10:e0005243. https://doi.org/10.1371/journal.pntd.0005243
16. Bakhtiar NM, Spotin A, Mahami-Oskouei M, Ahmadpour E, Rostami A. Recent advances on innate immune pathways related to host-parasite cross-talk in cystic and alveolar echinococcosis. Parasit Vectors 2020;13:232. https://doi.org/10.1186/s13071-020-04103-4
17. Bakshi M, Hebert D, Gulbronson C, et al. *Ostertagia ostertagi* mediates early host immune responses via macrophage and toll-like receptor pathways. Infect Immun 2021;89:e00017-21. https://doi.org/10.1128/IAI.00017-21
18. Jebbawi F, Bellanger AP, Lunström-Stadelmann B, et al. Innate and adaptive immune responses following PD-L1 blockade in treating

chronic murine alveolar echinococcosis. Parasite Immunol 2021;43:e12834. https://doi.org/10.1111/pim.12834
19. Vatankhah A, Ghaffari SMR, Vatankhah RG, et al. Characterization of cellular and humoral immune responses to alkaline phosphatase from fertile hydatid cysts in the human peripheral blood. J Cell Physiol 2019;234:2765-77. https://doi.org/10.1002/jcp.27092
20. Zhao H, Ma Y, Tian F, et al. Expression of Tim-3/Galectin-9 pathway and CD8+T cells and related factors in patients with cystic echinococcosis. Exp Parasitol 2023;254:108623. https://doi.org/10.1016/j.exppara.2023.108623
21. Wang Y, Zhou H, Shen Y, et al. Impairment of dendritic cell function and induction of CD4(+)CD25(+)Foxp3(+) T cells by excretory-secretory products: a potential mechanism of immune evasion adopted by *Echinococcus granulosus*. BMC Immunol 2015;16:44. https://doi.org/10.1186/s12865-015-0110-3
22. Amri M, Mezioug D, Touil-Boukoffa C. Involvement of IL-10 and IL-4 in evasion strategies of *Echinococcus granulosus* to host immune response. Eur Cytokine Netw 2009;20:63-8. https://doi.org/10.1684/ecn.2009.0154
23. Amni F, Hajizadeh M, Elmi T, et al. Different manifestation of *Echinococcus granulosus* immunogenic antigens in the liver and lungs of intermediate host. Comp Immunol Microbiol Infect Dis 2021;74:101573. https://doi.org/10.1016/j.cimid.2020.101573
24. Gottstein B, Soboslay P, Ortona E, et al. Immunology of alveolar and cystic echinococcosis (AE and CE). Adv Parasitol 2017;96:1-54. https://doi.org/10.1016/bs.apar.2016.09.005
25. Wang J, Cardoso R, Marreros N, et al. Foxp3(+) T regulatory cells as a potential target for immunotherapy against primary infection with *Echinococcus multilocularis* eggs. Infect Immun 2018;86:e00542-18. https://doi.org/10.1128/IAI.00542-18
26. Yarahmadov T, Wang J, Sanchez-Taltavull D, et al. Primary infection by *E. multilocularis* induces distinct patterns of cross talk between hepatic natural killer T cells and regulatory T cells in mice. Infect Immun 2022;90:e0017422. https://doi.org/10.1128/iai.00174-22
27. Peón AN, Ledesma-Soto Y, Terrazas LI. Regulation of immunity by *Taeniids*: lessons from animal models and in vitro studies. Parasite Immunol 2016;38:124-35. https://doi.org/10.1111/pim.12289
28. Ahn CS, Kim JG, Han X, Kang I, Kong Y. Comparison of *Echinococcus multilocularis* and *Echinococcus granulosus* hydatid fluid proteome provides molecular strategies for specialized host-parasite interactions. Oncotarget 2017;8:97009-24. https://doi.org/10.18632/oncotarget.20761
29. Ye C, Zhang L, Tang L, et al. Host genetic backgrounds: the key to determining parasite-host adaptation. Front Cell Infect Microbiol 2023;13:1228206. https://doi.org/10.3389/fcimb.2023.1228206
30. Siracusano A, Delunardo F, Teggi A, Ortona E. Host-parasite relationship in cystic echinococcosis: an evolving story. Clin Dev Immunol 2012;2012:639362. https://doi.org/10.1155/2012/639362
31. Zakeri A, Hansen EP, Andersen SD, Williams AR, Nejsum P. Immunomodulation by helminths: intracellular pathways and extracellular vesicles. Front Immunol 2018;9:2349. https://doi.org/10.3389/fimmu.2018.02349
32. Legorreta-Herrera M, Rodriguez-Sosa M, Satoskar AR. Editorial: regulation of the host's immune system by parasitic infections and its implications. Front Cell Infect Microbiol 2022;12:1118692. https://doi.org/10.3389/fcimb.2022.1118692
33. Beyhan YE, Albayrak C, Guven I. IL-4, IL-10, TNF-α and IFN-γ cytokine levels in patients with cystic echinococcosis and fascioliasis. Iran J Public Health 2022;51:1339-47. https://doi.org/10.18502/ijph.v51i6.9679
34. Yasen A, Li W, Aini A, et al. Th1/Th2/Th17 cytokine profile in hepatic cystic echinococcosis patients with different cyst stages. Parasite Immunol 2021;43:e12839. https://doi.org/10.1111/pim.12839
35. Jaramillo-Valverde L, Garcia-Paitan MY, Landeo D, Santivañez SJ, Cacacabelos R. Exploratory study on genetic variants related to hydatidosis susceptibility and albendazole pharmacogenetics in the Cusco region in Peru. Front Biosci (Schol Ed) 2025;17:40566. https://doi.org/10.31083/FBS40566
36. De Biase D, Prisco F, Pepe P, et al. Evaluation of the local immune response to hydatid cysts in sheep liver. Vet Sci 2023;10:315. https://doi.org/10.3390/vetsci10050315
37. Yin S, Chen X, Zhang J, et al. The effect of *Echinococcus granulosus* on spleen cells and TGF-β expression in the peripheral blood of BALB/c mice. Parasite Immunol 2017;39:https://doi.org/10.1111/pim.12415
38. Wang J, Zhang C, Wei X, et al. TGF-β and TGF-β/Smad signaling in the interactions between *Echinococcus multilocularis* and its hosts. PLoS One 2013;8:e55379. https://doi.org/10.1371/journal.pone.0055379
39. Wang M, Qiao F, Li Z, et al. Impact of *Echinococcus granulosus* antigens on monocyte development and dendritic cell differentiation. Iran J Immunol 2023;20:348-58. https://doi.org/10.22034/iji.2023.98163.2557
40. Aumüller E, Schramm G, Gronow A, et al. *Echinococcus multilocularis* metacestode extract triggers human basophils to release interleukin-4. Parasite Immunol 2004;26:387-95. https://doi.org/10.1111/j.0141-9838.2004.00724.x
41. Yang J, Zhao Y, Fu Y, et al. Recombinant antigen P29 of *Echinococcus granulosus* induces Th1, Tc1, and Th17 cell immune responses in sheep. Front Immunol 2023;14:1243204. https://doi.org/10.3389/fimmu.2023.1243204
42. Soleymani N, Taran F, Nazemshirazi M, et al. Dysregulation of ovine toll-like receptors 2 and 4 expression by hydatid cyst-derived antigens. Iran J Parasitol 2021;16:219-28. https://doi.org/10.18502/ijpa.

v16i2.6271

43. Apaer S, Tuxun T, Ma HZ, et al. Expression of toll-like receptor 2, 4 and related cytokines in intraperitoneally inoculated Balb/C mice with *Echinococcus multilocularis*. Int J Clin Exp Pathol 2017;10:7947-55.
44. Karnaukhov V, Paes W, Woodhouse IB, et al. HLA variants have different preferences to present proteins with specific molecular functions which are complemented in frequent haplotypes. Front Immunol 2022;13:1067463. https://doi.org/10.3389/fimmu.2022.1067463
45. Lukmanova GI, Gumerov AA, Elicheva ZM, Lukmanova LI. Distribution of HLA specificity frequencies in patients with cystic echinococcosis. Med Parazitol (Mosk) 2011;14-6.
46. Madih AN, Ravari MS, Yousefi M, et al. HLA class II profile in patients with different stages of cystic echinococcosis according to the WHO ultrasound imaging classification. Parasitol Res 2024;123:330. https://doi.org/10.1007/s00436-024-08353-4
47. Tulading A, Wu J, Zhang YF, et al. Immunological landscape of hepatic alveolar echinococcosis: a bibliometric analysis. World J Hepatol 2025;17:102001. https://doi.org/10.4254/wjh.v17.i2.102001
48. Grüner B, Peters L, Hillenbrand A, et al. *Echinococcus multilocularis* specific antibody, systemic cytokine, and chemokine levels, as well as antigen-specific cellular responses in patients with progressive, stable, and cured alveolar echinococcosis: a 10-year follow-up. PLoS Negl Trop Dis 2022;16:e0010099. https://doi.org/10.1371/journal.pntd.0010099
49. Godot V, Harraga S, Beurton I, et al. Resistance/susceptibility to *Echinococcus multilocularis* infection and cytokine profile in humans. II. Influence of the HLA B8, DR3, DQ2 haplotype. Clin Exp Immunol 2000;121:491-8. https://doi.org/10.1046/j.1365-2249.2000.01309.x
50. Moradi M, Meamar AR, Akhlaghi L, Roozbehani M, Razmjou E. Detection and genetic characterization of *Echinococcus granulosus* mitochondrial DNA in serum and formalin-fixed paraffin embedded cyst tissue samples of cystic echinococcosis patients. PLoS One 2019;14:e0224501. https://doi.org/10.1371/journal.pone.0224501

Original Article

Parasites Hosts Dis 2026;64(4):310-319
https://doi.org/10.3347/PHD.26060

Parasites, Hosts and Diseases

pISSN 2982-5164 • eISSN 2982-6799

Functional characterization of CsGTP5, a sodium-independent glucose transporter-related protein in *Clonorchis sinensis*

Seok Ho Cha[1], Wang-Jong Lee[2], Jadidan Hada Syahada[2], Fadhila Fitriana[2], Muhammad Fajri Rokhmad[2], Hyun-Young Sim[2], Zijian Wu[2], Bo Wang[3], Jin-Hee Han[2,*]

[1]Department of Parasitology and Tropical Medicine, Inha University School of Medicine, Incheon, Korea; [2]Department of Tropical Medicine, School of Medicine, Kangwon National University, Chuncheon, Korea; [3]Department of Clinical Laboratory, The First Affiliated Hospital of Anhui Medical University, Hefei, China

Glucose acquisition is essential for the long-term survival of adult *Clonorchis sinensis* within the host bile duct. Although several glucose transporter-related proteins have been identified in *C. sinensis*, the molecular and functional properties of facilitative glucose transport proteins, including the protein designated as glucose transporter protein 5 (CsGTP5) in this study, have not been characterized. In this study, CsGTP5 was cloned from adult *C. sinensis* and functionally analyzed using the *Xenopus laevis* oocyte expression system. The CsGTP5 open reading frame comprised 1,575 bp and encoded a 524-amino-acid protein with 12 predicted transmembrane domains, consistent with the topology of facilitative glucose transporter-like proteins. CsGTP5-expressing oocytes showed significantly increased uptake of [^{3}H] deoxy-D-glucose compared with water-injected control oocytes, whereas no significant uptake was observed for other tested substrates, including arginine, α-ketoglutarate, p-aminohippurate, taurocholate, and tetraethylammonium. CsGTP5-mediated [^{3}H] deoxy-D-glucose uptake increased in a time-dependent manner and was not affected by replacement of extracellular Na^+ with Li^+ or choline, indicating sodium-independent transport. Uptake was saturable, with an apparent *Km* of 4.0 mM and a *Vmax* of 300.0 pmol/oocyte/h. Competition assays showed that deoxy-D-glucose and glucose strongly inhibited CsGTP5-mediated uptake, whereas other monosaccharides had little effect. Molecular docking analysis further supported the predicted glucose-recognition capacity of CsGTP5. These findings demonstrate that CsGTP5 mediates sodium-independent deoxy-D-glucose uptake in a heterologous oocyte expression system and provide a basis for further investigation of its physiological role in *C. sinensis*.

Keywords: *Clonorchis sinensis*, CsGTP5, glucose transporter, deoxy-D-glucose uptake, *Xenopus laevis* oocyte

Introduction

The adult stage of *Clonorchis sinensis* resides for prolonged periods in the intrahepatic bile ducts of mammalian hosts, where it must continuously acquire nutrients from a restricted and specialized host environment [1]. Infection with *C. sinensis*, known as clonorchiasis, is a food-borne trematode disease caused mainly by the consumption of raw or inadequately cooked freshwater fish [1]. Clonorchiasis remains endemic in East Asia, including Korea, China, Taiwan, northern Vietnam, and the Russian Far East [1,2]. Chronic infection is clinically important because it is associated with hepatobiliary disorders such as cholangitis, biliary fibrosis, and cholangiocarcinoma [1]. The long-term survival of adult worms within the biliary tract suggests that efficient nutrient uptake systems are essen-

Received: July 5, 2026 Accepted: July 15, 2026
*Correspondence: han.han@kangwon.ac.kr

© 2026 The Korean Society for Parasitology and Tropical Medicine

This is an open-access article distributed under the terms of the Creative Commons Attribution Non-Commercial License (http://creativecommons.org/licenses/by-nc/4.0/) which permits unrestricted non-commercial use, distribution, and reproduction in any medium, provided the original work is properly cited.

Citation
Cha SH, Lee WJ, Syahada JH, Fitriana F, Rokhmad MF, Sim HY, Wu Z, Wang B, Han JH. Functional characterization of CsGTP5, a sodium-independent glucose transporter-related protein in *Clonorchis sinensis*. Parasites Hosts Dis 2026;64(4):310-319.

tial for parasite maintenance, growth, and reproduction [3,4].

Glucose is a major carbon and energy source for parasitic flatworms [5]. In trematodes, host-derived glucose supports glycolytic energy production and provides metabolic intermediates required for diverse physiological processes [5,6]. Because hydrophilic carbohydrates do not readily diffuse across lipid bilayers, their cellular uptake depends largely on membrane transport proteins [7]. Facilitative glucose transporters typically contain 12 transmembrane domains and mediate sodium-independent glucose transport across biological membranes [8]. In schistosomes, glucose transporters have been identified and functionally characterized, demonstrating their importance in parasite glucose acquisition and energy metabolism [9,10]. These findings indicate that membrane-associated carbohydrate transport systems play an important role in the adaptation of trematodes to their host environment.

In *C. sinensis*, several nutrient and metabolite transporters have been investigated in recent years. Glucose transporter (CsGLUT) was previously cloned and functionally characterized as a glucose transporter [11]. More recently, multiple glucose transporter-related proteins and a sodium/glucose co-transporter were identified and analyzed in *C. sinensis* [3,12]. In addition, other transporter families, including a bile acid-related transporter and a choline transporter, have been functionally characterized in this parasite [13-16]. These studies indicate that *C. sinensis* possesses diverse membrane transport systems for acquiring nutrients and metabolites from the host environment. However, the presence of multiple glucose transporter isoforms also suggests potential functional diversity within this transporter family and leaves unresolved whether each predicted isoform is functionally active [17]. Individual transporters may differ in substrate preference, transport efficiency, ion dependence, tissue distribution, and physiological role rather than serving as redundant components of a single glucose uptake pathway. Therefore, additional transporter candidates require direct functional validation to clarify how *C. sinensis* coordinates glucose acquisition through distinct membrane transport systems [18,19].

Sequence similarity and predicted membrane topology can suggest that a protein belongs to a glucose transporter-related family, but these features alone are insufficient to define its actual transport function [20,21]. Experimental analysis is required to determine whether a candidate protein mediates glucose uptake, whether transport is sodium-dependent or sodium-independent, and whether it exhibits selectivity for glucose over other carbohydrates or metabolites. Such functional characterization is particularly important for newly identified transporter isoforms whose biological roles have not yet been established.

An additional glucose transporter candidate from *C. sinensis* was identified and designated glucose transporter protein 5 (CsGTP5). Although previous studies have demonstrated the presence of multiple glucose transporter-related proteins in *C. sinensis*, the molecular and functional properties of CsGTP5 have not yet been defined. Thus, it remained unclear whether CsGTP5 represents an active glucose transporter-related protein and whether its transport properties are similar to or distinct from those of previously characterized *C. sinensis* glucose transporters. Therefore, the present study aimed to characterize CsGTP5 and to clarify its potential contribution to glucose acquisition in *C. sinensis*. By focusing on CsGTP5, this study addresses a remaining gap in the current understanding of glucose transport systems in liver flukes.

Methods

Ethics statement

All animal experiments involving mice were approved by the Institutional Animal Care and Use Committee of Inha University (approval No. INHA161208-460), which is accredited by the Association for Assessment and Accreditation of Laboratory Animal Care International. Procedures involving *Xenopus laevis* frogs were approved by the Inha University Committee on Animal Resources (approval No. INHA250701-977).

Chemicals

Radiolabeled compounds, including [^{3}H] deoxy-D-glucose (32.5 Ci/mmol), [^{3}H] arginine (50.5 Ci/mmol), [^{14}C] α-ketoglutaric acid (54.8 mCi/mmol), [^{14}C] p-aminohippurate (52.7 mCi/mmol), [^{3}H] taurocholic acid (15.5 Ci/mmol), and [^{14}C] tetraethylammonium (3.5 mCi/mmol), were purchased from Perkin-Elmer Life Sciences. All other chemicals and reagents were purchased commercially and were of analytical grade.

Preparation of *C. sinensis* adult worms

Adult *C. sinensis* worms were prepared as described previously [11,12]. Briefly, metacercariae were isolated from naturally infected freshwater fish, including *Pseudorasbora parva* and *Gnathopogon coreanus*, after artificial gastric digestion. Fifty metacercariae were orally administered to each 5–6-week-old male FVB/NJ mouse (Central Lab Animal). Infection was confirmed by detecting eggs in fecal samples using the formalin–ether sedimentation method 6 weeks after infection. Adult worms were recovered from the bile ducts and liver approximately 8 weeks after infection.

Cloning and assembly of CsGTP5 cDNA

Total RNA was isolated from adult *C. sinensis* worms using TRI Reagent (Sigma), according to the manufacturer's instructions. First-strand cDNA was synthesized from 1 μg of total RNA using Moloney murine leukemia virus reverse transcriptase (Promega), 10 mM dNTPs, and 2.5 μM oligo-dT primers in a total reaction volume of 30 μl. Reverse transcription was performed at 42°C for 30 min, followed by enzyme inactivation at 99°C for 5 min.

The full-length CsGTP5 cDNA was generated by overlap extension PCR using gene-specific primers designed from the predicted CsGTP5 sequence. Primer sequences are listed in Supplementary Table S1. Two overlapping fragments were first amplified using Ex Taq DNA polymerase (Takara), purified using a Gel Extraction Kit (GeneAll Biotechnology), subcloned into the pTOP TA V2 vector (Enzynomics), and sequenced by Macrogen (Supplementary Fig. S1A).

For final assembly, the 2 overlapping fragments were used as templates for overlap extension PCR using LA Taq DNA polymerase (Takara). The assembled PCR product was subcloned into a TA cloning vector and verified by sequencing using an ABI Prism 3730 sequencer (Macrogen) (Supplementary Fig. S1B). After sequence confirmation, the CsGTP5 insert was subcloned into the pBluescript SK II (-) vector and used as a template for cRNA synthesis.

Sequence analysis and molecular docking

The reference amino acid sequence of CsGTP5 was retrieved from the NCBI protein database under accession number KAG5452059.1. The open reading frame of CsGTP5 was identified from the assembled full-length cDNA sequence and compared with the reference sequence. The deduced amino acid sequence was used to calculate the predicted molecular mass using ExPASy ProtParam (https://www.expasy.org/resources/protparam). Putative transmembrane domains and membrane topology were predicted using TMHMM version 2.0 (https://services.healthtech.dtu.dk/services/TMHMM-2.0/). Putative N-glycosylation sites were predicted using the NetNGlyc 1.0 server (https://services.healthtech.dtu.dk/services/NetNGlyc-1.0/). Candidate N-glycosylation motifs were further evaluated based on the N-X-S/T consensus sequence, where X represents any amino acid except proline, and interpreted together with the predicted membrane topology.

Multiple sequence alignment of CsGTP5 with other glucose transporter-related proteins was performed using ClustalW version 2.1 (https://www.genome.jp/tools-bin/clustalw). Phylogenetic analysis was conducted using MEGA11 version 11.0.8 (https://megasoftware.net/). The phylogenetic tree was constructed using the neighbor-joining method, and branch reliability was evaluated by bootstrap analysis with 1,000 replicates.

Three-dimensional structural models of CsGTP proteins were retrieved and modified from AlphaFold protein structure database (https://alphafold.ebi.ac.uk/). The predicted model of CsGTP5 was visualized and examined using UCSF ChimeraX version 1.8 (https://www.cgl.ucsf.edu/chimerax/) to assess its overall architecture, membrane-spanning regions, and putative substrate-binding cavity.

Molecular docking analysis was performed to examine the predicted interaction between glucose and CsGTP proteins. The predicted structures of CsGTP1–5 were used as receptor models, and glucose was used as the ligand. Receptor and ligand files were prepared in PDBQT format, and docking simulations were carried out using AutoDock Vina version 1.2.7 (https://vina.scripps.edu/). The docking grid was positioned to include the putative central substrate-binding cavity of each CsGTP protein. Predicted docking poses and interacting residues were visualized using UCSF ChimeraX. Docking scores were reported as predicted binding energies in kcal/mol and were interpreted as relative in silico docking scores rather than experimental binding affinities.

cRNA synthesis and *X. laevis* oocyte injection

The *X. laevis* oocyte expression system was used as described previously [12], with modifications for CsGTP5 expression. This system was selected because it is a well-established platform for membrane transporter assays and allows direct measurement of cRNA-dependent radiolabeled substrate uptake. The CsGTP5 coding sequence cloned into pBluescript SK II (-) was linearized by complete digestion with EcoRI. Capped cRNA was synthesized using the mMESSAGE mMACHINE T7 kit (Thermo Fisher Scientific), according to the manufacturer's protocol.

Stage V–VI oocytes were prepared from ovarian tissue by collagenase treatment. Briefly, ovarian tissue was treated with 0.2% collagenase A in OR II solution at room temperature for 1–2 h, and defolliculated oocytes were selected for microinjection. Approximately 50 ng of CsGTP5 cRNA in 50 nl was injected into each oocyte. Control oocytes were injected with the same volume of distilled water. Injected oocytes were maintained at 18°C in Barth's solution supplemented with 50 μg/ml gentamicin and 2 mM sodium pyruvate. Uptake assays were performed 2–3 days after injection.

https://doi.org/10.3347/PHD.26060

Transport assays

Transport activity was assessed in CsGTP5-expressing and water-injected control oocytes using radiolabeled substrates. Uptake assays were performed in ND96 solution containing 96 mM NaCl, 2 mM KCl, 2 mM $CaCl_2$, 1 mM $MgCl_2$, and 5 mM HEPES (pH 7.4). For substrate screening, oocytes were incubated with radiolabeled deoxy-D-glucose, arginine, α-ketoglutarate, p-aminohippurate, taurocholate, or tetraethylammonium for 1 h at 22°C–25°C. Standard deoxy-D-glucose uptake assays were performed using 300 nM [^{3}H] deoxy-D-glucose.

Expression time-dependent uptake was measured at 1, 2, and 3 days after CsGTP5 cRNA injection. Incubation time-dependent uptake was assessed by incubating oocytes with 300 nM [^{3}H] deoxy-D-glucose for 10, 20, 30, 60, 90, and 120 min. To examine sodium dependence, NaCl in ND96 solution was replaced with an equivalent concentration of either LiCl or choline chloride, and uptake was measured after 1 h of incubation.

After incubation, oocytes were rapidly washed with ice-cold ND96 solution to remove extracellular radioactivity. Each oocyte was lysed in 10% sodium dodecyl sulfate and mixed with Ultima Gold AB scintillation cocktail (PerkinElmer). Radioactivity was measured using a MicroBeta 2 β-counter (PerkinElmer).

Efflux assay

Efflux assays were performed to examine whether CsGTP5-mediated deoxy-D-glucose transport was trans-stimulated by extracellular glucose. CsGTP5-expressing oocytes were preloaded with 300 nM [^{3}H] deoxy-D-glucose for 90 min. After preloading, oocytes were washed and transferred to ND96 solution without glucose or to ND96 solution containing unlabeled glucose at 0.3 or 3 mM, corresponding to 1,000-fold and 10,000-fold excess concentrations relative to [^{3}H] deoxy-D-glucose, respectively. After 60 min of incubation, radioactivity released into the medium and radioactivity remaining in the oocytes were measured. Efflux was expressed as the percentage of radioactivity released during the 60 min incubation relative to the amount of [^{3}H] deoxy-D-glucose preloaded into the oocytes.

Kinetic and competition analyses

The concentration dependence of CsGTP5-mediated deoxy-D-glucose uptake was determined by incubating CsGTP5-expressing and water-injected control oocytes with variable concentrations of deoxy-D-glucose for 1 h at 22°C–25°C. CsGTP5-mediated net uptake was calculated by subtracting uptake values in water-injected control oocytes from those in CsGTP5-expressing oocytes. Kinetic parameters were estimated using the Michaelis–Menten equation: $v = Vmax \times [S]/(Km+[S])$, where v is the uptake rate, [S] is the substrate concentration, *Km* is the Michaelis constant, and *Vmax* is the maximum uptake rate. Curve fitting was performed using the MULTI program with an iterative nonlinear least-squares method based on the damping Gauss–Newton algorithm [22].

For substrate competition assays, CsGTP5-expressing and water-injected control oocytes were incubated with 300 nM [^{3}H] deoxy-D-glucose in the absence or presence of 3 mM unlabeled deoxy-D-glucose, glucose, galactose, mannose, fructose, or 3-O-methylglucose. Results were expressed as a percentage of [^{3}H] deoxy-D-glucose uptake measured in CsGTP5-expressing oocytes in the absence of unlabeled monosaccharides.

Statistical analysis

Data are presented as the mean ± SE. Statistical analyses were performed using GraphPad Prism version 8 (GraphPad Software). Comparisons between 2 groups were performed using Student *t*-test. For comparisons among multiple groups, one-way analysis of variance followed by an appropriate post hoc test was used when applicable. Differences were considered statistically significant at $^*P < 0.05$ and highly significant at $^{**}P < 0.01$. The number of oocytes analyzed in each experiment is indicated in each figure legend.

Results

Molecular and structural features of CsGTP5

The open reading frame of CsGTP5 cDNA comprised 1,575 base pairs and encoded a protein of 524 amino acid residues, with a predicted molecular mass of 57.02 kDa. Topology analysis of the deduced amino acid sequence predicted 12 putative transmembrane domains, a characteristic feature of facilitative glucose transporter-related proteins (Fig. 1A). Both the N- and C-termini were predicted to face the intracellular side of the plasma membrane (Fig. 1A, B).

Motif analysis identified 3 putative N-glycosylation motifs in CsGTP5. Based on the predicted membrane topology, 2 of these sites, located at residues 41 and 51, were positioned in the first extracellular loop between transmembrane domains 1 and 2, whereas the third site, located at residue 420, was predicted to lie within a transmembrane domain and is therefore

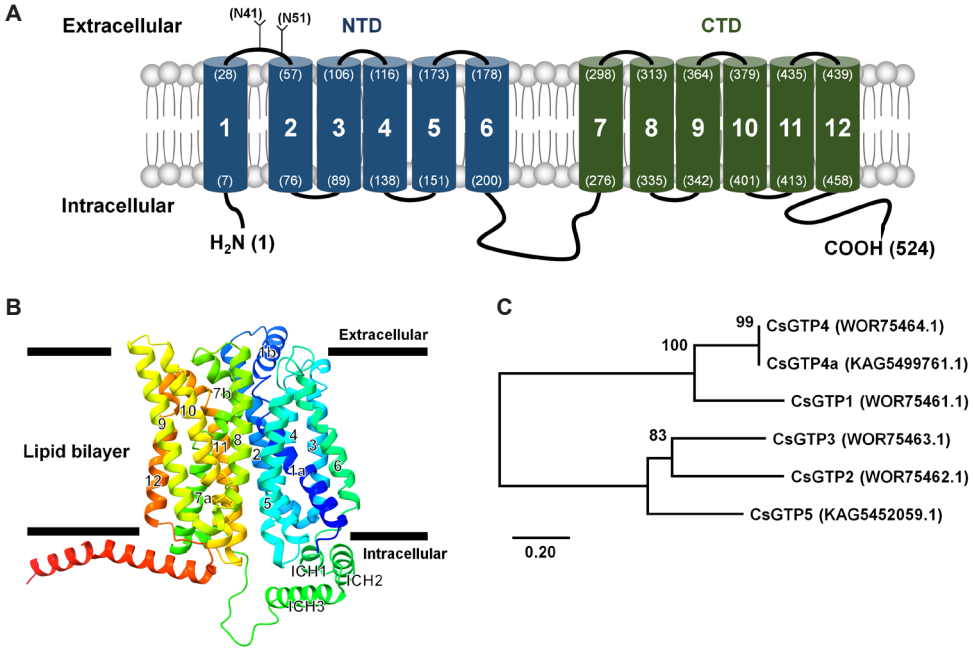


Fig. 1. Predicted structural features and phylogenetic relationship of CsGTP5. (A) Predicted membrane topology of full-length CsGTP5. CsGTP5 consists of 524 amino acids and contains 12 putative transmembrane domains. The predicted residue positions of the transmembrane domains are indicated in parentheses. NTD, N-terminal domain; CTD, C-terminal domain. (B) Predicted 3-dimensional structure of CsGTP5 generated using AlphaFold and visualized with UCSF ChimeraX. (C) Phylogenetic tree of CsGTP5 and selected glucose transporter-related proteins from *Clonorchis sinensis*. NCBI accession numbers are shown in parentheses.

unlikely to be glycosylated (Supplementary Fig. S2). Phylogenetic analysis showed that CsGTP5 clustered with other glucose transporter-related proteins from *C. sinensis*, supporting its classification as a member of the CsGTP family (Fig. 1C).

Functional characterization of CsGTP5-mediated deoxy-D-glucose uptake

To evaluate the substrate transport profile of CsGTP5, the uptake of several radiolabeled compounds was measured in *X. laevis* oocytes expressing CsGTP5. Among the substrates examined, only [^{3}H] deoxy-D-glucose showed significantly increased uptake in CsGTP5-expressing oocytes. The uptake of [^{3}H] deoxy-D-glucose in CsGTP5-expressing oocytes was 12.7±3.9 pmol/oocyte/h, approximately 3.5-fold higher than that in water-injected control oocytes, which showed an uptake level of 3.6±1.5 pmol/oocyte/h (Fig. 2). In contrast, no significant uptake of [^{3}H] arginine, [^{14}C] α-ketoglutarate, [^{14}C] p-aminohippurate, [^{3}H] taurocholate, or [^{14}C] tetraethylammonium was observed in CsGTP5-expressing oocytes (Fig. 2). These results indicate that CsGTP5 preferentially mediates deoxy-D-glucose uptake among the tested substrates.

The transport properties of CsGTP5-mediated [^{3}H] deoxy-D-glucose uptake were further examined in oocytes. Uptake increased in an expression time-dependent manner from 1 to 3 days after cRNA injection (Fig. 3A). In addition, [^{3}H] deoxy-D-glucose uptake increased with incubation time over the 10–120 min period (Fig. 3B). These findings support the functional expression of CsGTP5 in the oocyte membrane and its role in mediating deoxy-D-glucose uptake.

To determine whether CsGTP5-mediated transport was dependent on extracellular sodium ions, Na^+ in the uptake buffer was replaced with an equivalent concentration of either Li^+ or choline. Replacement of Na^+ did not significantly affect [^{3}H] deoxy-D-glucose uptake during the 1 h incubation period (Fig. 3C). These results suggest that CsGTP5-mediated deoxy-D-glucose uptake is not dependent on extracellular Na^+.

We next examined whether CsGTP5-mediated deoxy-D-glucose transport was trans-stimulated by extracellular glucose. The addition of unlabeled glucose at 0.3 or 3 mM, corresponding to 1,000-fold and 10,000-fold excess concentrations relative to [^{3}H] deoxy-D-glucose, did not significantly increase the efflux of preloaded [^{3}H] deoxy-D-glucose from CsGTP5-expressing oocytes (Fig. 3D). This result suggests that extracellular glucose did not significantly stimulate CsGTP5-mediated [^{3}H] deoxy-D-glucose efflux under the experimental conditions tested.

https://doi.org/10.3347/PHD.26060

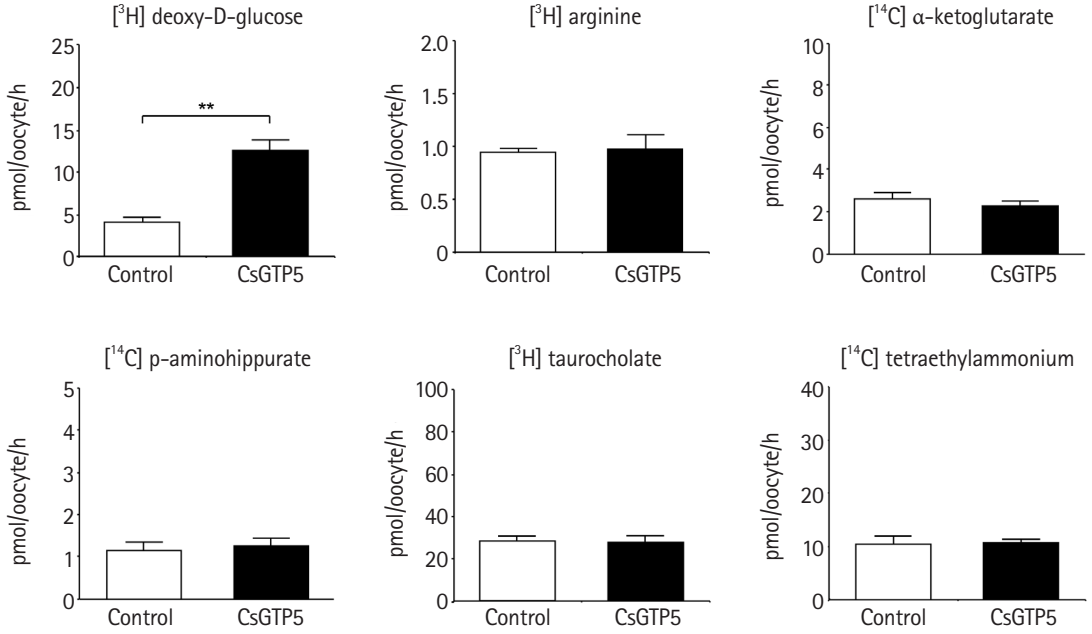


Fig. 2. Substrate uptake profile of CsGTP5 expressed in *Xenopus laevis* oocytes. Uptake of selected radiolabeled compounds was measured in water-injected control oocytes and CsGTP5-expressing oocytes for 1 h. The substrate concentrations were as follows: [^{3}H] deoxy-D-glucose, 300 nM; [^{3}H] arginine, 100 nM; [^{14}C] α-ketoglutarate, 5 μM; [^{14}C] p-aminohippurate, 10 μM; [^{3}H] taurocholate, 200 nM; and [^{14}C] tetraethylammonium, 10 μM. Data are presented as the mean±SE (n=6–8). $^{**}P$<0.01 by Student t-test.

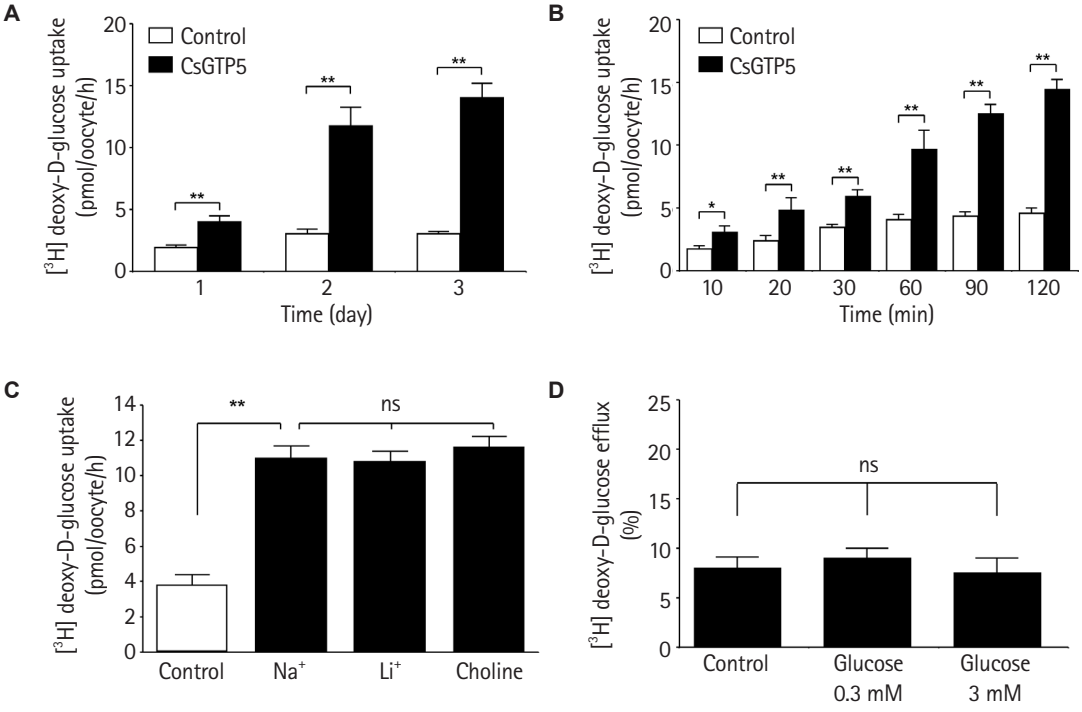


Fig. 3. Transport properties of CsGTP5-mediated [^{3}H] deoxy-D-glucose uptake. (A) Expression time-dependent uptake of [^{3}H] deoxy-D-glucose at 1, 2, and 3 days after CsGTP5 cRNA injection. (B) Incubation time-dependent uptake of [^{3}H] deoxy-D-glucose over 10–120 min. (C) Effect of extracellular cation replacement on CsGTP5-mediated [^{3}H] deoxy-D-glucose uptake. Extracellular Na^+ was replaced with choline or Li^+. (D) Efflux of preloaded [^{3}H] deoxy-D-glucose from CsGTP5-expressing oocytes. Oocytes were preloaded with 300 nM [^{3}H] deoxy-D-glucose for 90 min and incubated with or without unlabeled glucose at 0.3 or 3 mM for 60 min. Data are presented as the mean±SE (n=6–8). $^{**}P$<0.01. ns, not significant.

Glucose transport properties of CsGTP5

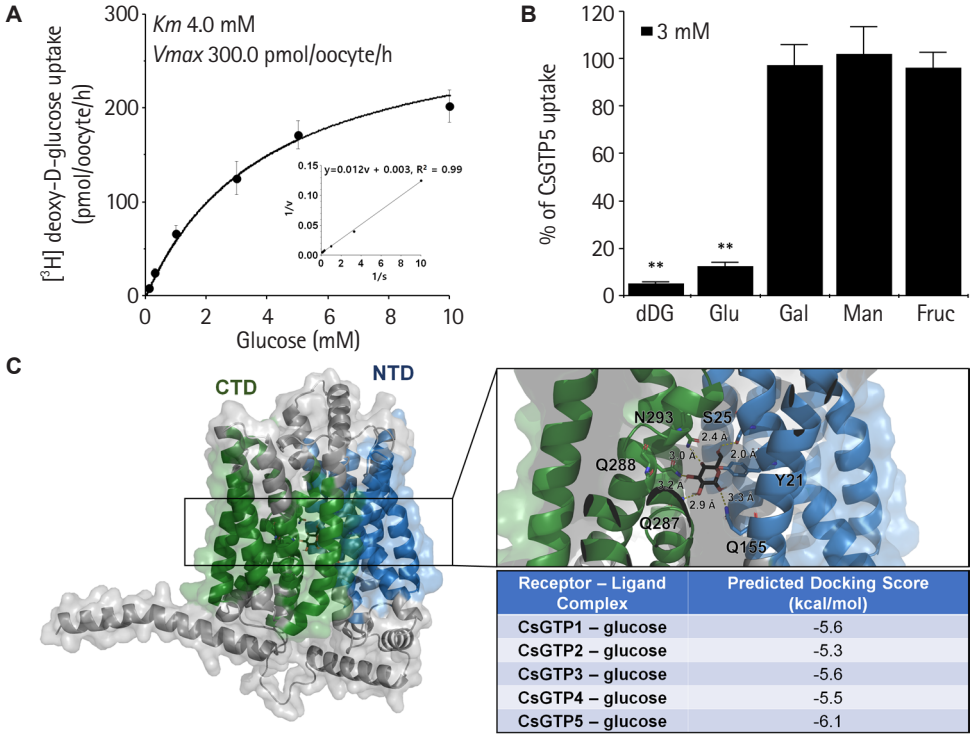
The concentration dependence of CsGTP5-mediated [^{3}H] deoxy-D-glucose uptake was analyzed to determine its kinetic properties. Uptake displayed saturable kinetics and was well fitted to the Michaelis–Menten equation (Fig. 4A). Nonlinear regression analysis yielded an apparent *Km* value of 4.0 mM and a *Vmax* value of 300.0 pmol/oocyte/h. These kinetic properties indicate that CsGTP5 mediates carrier-dependent deoxy-D-glucose uptake.

To investigate the substrate selectivity of CsGTP5, competition assays were performed using unlabeled monosaccharides. The addition of 3 mM unlabeled deoxy-D-glucose or glucose strongly inhibited CsGTP5-mediated [^{3}H] deoxy-D-glucose uptake (Fig. 4B). In contrast, galactose, mannose, and fructose did not show significant inhibitory effects. These results suggest that CsGTP5 preferentially recognizes deoxy-D-glucose and glucose over the other monosaccharides tested.

To further examine the structural plausibility of glucose recognition by CsGTP5, molecular docking analysis was performed using AutoDock Vina. Glucose was predicted to bind within the putative substrate-binding cavity of CsGTP5, where it formed predicted interactions with residues including Y21, S25, Q155, Q287, Q288, and N293 (Fig. 4C). Comparative docking analysis of CsGTP1–5 showed predicted docking scores ranging from -5.3 to -6.1 kcal/mol. Among the 5 CsGTP proteins, CsGTP5 showed the lowest, but only slightly more favorable predicted docking score for glucose (Fig. 4C). However, the differences among CsGTP docking scores were small, and these values should be interpreted as relative in silico predictions rather than experimental binding affinities.

Discussion

This study functionally characterized CsGTP5 as an additional glucose transporter-related protein derived from adult *C. sinensis*. Previous studies have reported several glucose transport systems in *C. sinensis*, including CsGLUT, CsGTP1–4, and



Receptor – Ligand Complex	Predicted Docking Score (kcal/mol)
CsGTP1 – glucose	-5.6
CsGTP2 – glucose	-5.3
CsGTP3 – glucose	-5.6
CsGTP4 – glucose	-5.5
CsGTP5 – glucose	-6.1

Fig. 4. Glucose transport properties and predicted glucose-binding features of CsGTP5. (A) Concentration-dependent uptake of [^{3}H] deoxy-D-glucose mediated by CsGTP5. The inset shows Lineweaver–Burk analysis. V, velocity; S, concentration of deoxy-D-glucose. Data are presented as the mean±SE (*n*=6–8). (B) Effects of unlabeled monosaccharides on CsGTP5-mediated [^{3}H] deoxy-D-glucose uptake. Oocytes were incubated with 300 nM [^{3}H] deoxy-D-glucose in the absence or presence of 3 mM unlabeled monosaccharides. dDG, deoxy-D-glucose; Glu, glucose; Gal, galactose; Man, mannose; Fruc, fructose. Data are presented as the mean±SE (*n*=6–8). Statistical comparisons were performed against the no-competitor control. Connecting lines indicate the post hoc comparisons shown. $^{**}P<0.01$. (C) Predicted glucose-binding pose in CsGTP5 and comparative AutoDock Vina docking scores for CsGTP1–5. CTD, C-terminal domain; NTD, N-terminal domain. Docking scores are shown as predicted binding energies in kcal/mol.

https://doi.org/10.3347/PHD.26060

CsSGLT [3,11,12]. The identification of CsGTP5 expands this transporter repertoire and supports the idea that glucose transporter-related proteins in *C. sinensis* may be functionally diverse rather than representing a single uniform glucose uptake pathway.

The predicted structure of CsGTP5 is consistent with that of facilitative glucose transporter-like proteins. CsGTP5 contains 12 putative transmembrane domains, a typical feature of major facilitator superfamily transporters, including members of the SLC2/GLUT family [7,8]. In addition, both the N-terminus and C-terminus were predicted to face the intracellular side of the membrane, further supporting its classification as a glucose transporter-related membrane protein [23-25]. The predicted extracellular N-glycosylation motifs may contribute to membrane localization, stability, or functional maturation, as reported for several mammalian GLUT proteins [26,27]. However, because glycosylation was not experimentally examined in this study, this remains a structural prediction.

Functionally, CsGTP5 shares several properties with previously characterized *C. sinensis* glucose transporters. CsGTP5-mediated deoxy-D-glucose uptake was sodium-independent and saturable, which is consistent with facilitative glucose transport rather than sodium-coupled glucose transport [7,28]. Similar sodium-independent and saturable uptake has been reported for CsGLUT and CsGTP4 [11,12]. These similarities suggest that CsGTP5 belongs to the facilitative glucose transporter-like group of *C. sinensis* transporters [3].

At the same time, CsGTP5 appears to possess distinct transport characteristics. Its apparent *Km* value suggests moderate affinity for deoxy-D-glucose, and its inhibition profile indicates selective recognition of deoxy-D-glucose and glucose rather than broad monosaccharide transport. This restricted substrate preference differs from CsGTP4, which has been reported to respond to glucose and galactose [12]. These differences suggest that CsGTP proteins may not be functionally redundant, but instead may differ in substrate preference, affinity, and physiological role [17,29].

The absence of detectable glucose-stimulated efflux under the tested conditions further indicates that CsGTP5 did not show measurable exchange-like efflux activity in this assay. In some facilitative transporters, extracellular substrate can stimulate the efflux of preloaded intracellular substrate through exchange-like transport [30,31]. In the present study, extracellular glucose did not induce detectable efflux of preloaded [^{3}H] deoxy-D-glucose from CsGTP5-expressing oocytes under the tested conditions, suggesting that measurable exchange-like efflux activity was not observed in this assay. However, because the present assay measured cumulative efflux over 60 min and did not include higher extracellular glucose concentrations or shorter time-course measurements, these results do not fully exclude the possibility of rapid or concentration-dependent trans-stimulation. Further experiments will be required to clarify whether CsGTP5 exhibits exchange-like transport properties.

Molecular docking analysis provided structural support for the glucose-recognition capacity of CsGTP5. Glucose was predicted to bind within the putative substrate-binding cavity of CsGTP5, and CsGTP5 showed the lowest, although only slightly more favorable, predicted docking score among CsGTP1–5. However, the docking scores among CsGTP proteins were relatively close, and docking analysis cannot directly demonstrate binding affinity or transport activity [32]. Therefore, the docking results should be interpreted as supportive and comparative in silico evidence that complements the functional uptake data.

Adult *C. sinensis* survives for prolonged periods in the host bile duct and depends on host-derived nutrients for growth, survival, and reproduction [2]. The presence of multiple glucose transporter-related proteins suggests potential functional diversity among transporter candidates involved in glucose acquisition. In this context, CsGTP5 may represent a functional glucose transporter-related candidate, as demonstrated by sodium-independent deoxy-D-glucose uptake in the heterologous oocyte expression system. However, because the present study was based on heterologous expression and did not include tissue localization, developmental expression, loss-of-function analysis, or parasite-based transport assays, the native physiological contribution of CsGTP5 to glucose uptake in adult worms remains to be determined. Although parasite nutrient transporters may be considered potential targets for future antiparasitic strategies, the physiological and therapeutic relevance of CsGTP5 will require further validation through tissue localization, developmental expression analysis, loss-of-function studies, and inhibitor-based transport assays [9,14].

In conclusion, CsGTP5 is a sodium-independent glucose transporter-related protein that mediates deoxy-D-glucose uptake. Its structural features, saturable transport kinetics, glucose-sensitive inhibition profile, and predicted glucose-binding capacity support its role as a facilitative glucose transporter-like protein. These findings provide additional evidence that glucose transporter-related proteins in *C. sinensis* may possess distinct transport properties within this transporter family.

Author contributions

Conceptualization: Cha SH, Han JH. Data curation: Cha SH, Lee WJ, Han JH. Formal analysis: Cha SH, Lee WJ, Syahada JH, Fitriana F, Rokhmad MF, Sim HY, Wu Z, Wang B, Han JH. Funding acquisition: Cha SH, Han JH. Investigation: Lee WJ, Syahada JH, Fitriana F, Rokhmad MF, Sim HY, Wu Z, Wang B. Methodology: Cha SH, Lee WJ, Han JH. Project administration: Cha SH, Han JH. Resources: Cha SH, Wang B, Han JH. Software: Cha SH, Wang B, Han JH. Supervision: Cha SH, Han JH. Validation: Cha SH, Wang B, Han JH. Visualization: Cha SH, Lee WJ, Syahada JH, Fitriana F, Rokhmad MF, Sim HY, Wu Z, Han JH. Writing – original draft: Cha SH, Lee WJ, Han JH. Writing – review & editing: Cha SH, Han JH.

Conflict of interest

Jin-Hee Han serves as an editor of Parasites, Hosts and Diseases but had no involvement in the decision to publish this article. No other potential conflicts of interest relevant to this study were reported.

Funding

This work was supported by the Inha Research Grant (SHC) and the National Research Foundation of Korea (NRF) funded by the Ministry of Science and ICT (MSIT) (RS-2025-16069701) (JHH).

Acknowledgments

Adult *X. laevis* was obtained from the Korean *Xenopus* Resource Center for Research.

Supplementary information

Supplementary material is available with this article at https://doi.org/10.3347/PHD.26060.

ORCID

Seok Ho Cha, https://orcid.org/0000-0002-0005-8320
Wang-Jong Lee, https://orcid.org/0000-0003-2152-8915
Jadidan Hada Syahada, https://orcid.org/0009-0005-8078-5948
Fadhila Fitriana, https://orcid.org/0009-0006-6668-7724
Muhammad Fajri Rokhmad, https://orcid.org/0000-0003-1176-691X
Hyun-Young Sim, https://orcid.org/0009-0001-5327-5847
Zijian Wu, https://orcid.org/0009-0007-4128-4715
Bo Wang, https://orcid.org/0009-0002-9602-6610
Jin-Hee Han, https://orcid.org/0000-0003-0836-6675

References

1. Qian MB, Keiser J, Utzinger J, Zhou XN. Clonorchiasis and opisthorchiasis: epidemiology, transmission, clinical features, morbidity, diagnosis, treatment, and control. Clin Microbiol Rev 2024;37:e0000923. https://doi.org/10.1128/cmr.00009-23
2. Tang ZL, Huang Y, Yu XB. Current status and perspectives of *Clonorchis sinensis* and clonorchiasis: epidemiology, pathogenesis, omics, prevention and control. Infect Dis Poverty 2016;5:71. https://doi.org/10.1186/s40249-016-0166-1
3. Dai F, Lee SO, Song JH, et al. Glucose transporters and sodium glucose co-transporters cooperatively import glucose into energy-demanding organs in carcinogenic liver fluke *Clonorchis sinensis*. PLoS Negl Trop Dis 2024;18:e0012315. https://doi.org/10.1371/journal.pntd.0012315
4. Wang X, Chen W, Huang Y, et al. The draft genome of the carcinogenic human liver fluke *Clonorchis sinensis*. Genome Biol 2011;12:R107. https://doi.org/10.1186/gb-2011-12-10-r107
5. You H, Stephenson RJ, Gobert GN, McManus DP. Revisiting glucose uptake and metabolism in schistosomes: new molecular insights for improved schistosomiasis therapies. Front Genet 2014;5:176. https://doi.org/10.3389/fgene.2014.00176
6. Skelly PJ, Tielens AG, Shoemaker CB. Glucose transport and metabolism in mammalian-stage schistosomes. Parasitol Today 1998;14:402-6. https://doi.org/10.1016/s0169-4758(98)01319-2
7. Mueckler M, Thorens B. The SLC2 (GLUT) family of membrane transporters. Mol Aspects Med 2013;34:121-38. https://doi.org/10.1016/j.mam.2012.07.001
8. Holman GD. Structure, function and regulation of mammalian glucose transporters of the SLC2 family. Pflugers Arch 2020;472:1155-75. https://doi.org/10.1007/s00424-020-02411-3
9. Krautz-Peterson G, Simoes M, Faghiri Z, et al. Suppressing glucose transporter gene expression in schistosomes impairs parasite feeding and decreases survival in the mammalian host. PLoS Pathog 2010;6:e1000932. https://doi.org/10.1371/journal.ppat.1000932
10. McKenzie M, Kirk RS, Walker AJ. Glucose uptake in the human pathogen *Schistosoma mansoni* is regulated through Akt/protein kinase B signaling. J Infect Dis 2018;218:152-64. https://doi.org/10.1093/infdis/jix654
11. Ahn SK, Cho PY, Na BK, et al. Molecular cloning and functional characterization of a glucose transporter (CsGLUT) in *Clonorchis sinensis*. Parasitol Res 2016;115:347-54. https://doi.org/10.1007/s00436-015-4754-y
12. Jun H, Mazigo E, Lee WJ, et al. Functional characterization of glucose transporter 4 involved in glucose uptake in *Clonorchis sinensis*. Parasites Hosts Dis 2024;62:450-60. https://doi.org/10.3347/PHD.24051

13. Lu Y, Yoo WG, Dai F, et al. Characterization of a novel organic solute transporter homologue from *Clonorchis sinensis*. PLoS Negl Trop Dis 2018;12:e0006459. https://doi.org/10.1371/journal.pntd.0006459
14. Dai F, Yoo WG, Lu Y, et al. Sodium-bile acid co-transporter is crucial for survival of a carcinogenic liver fluke *Clonorchis sinensis* in the bile. PLoS Negl Trop Dis 2020;14:e0008952. https://doi.org/10.1371/journal.pntd.0008952
15. Won JY, Louis JM, Roh ES, Cha SH, Han JH. Functional characterization of *Clonorchis sinensis* choline transporter. Parasites Hosts Dis 2023;61:428-38. https://doi.org/10.3347/PHD.23082
16. Lee WJ, Kim SJ, Lee WK, Han JH, Cha SH. *Clonorchis sinensis* dopamine transporter (CsDAT) facilitates dopamine uptake. Parasites Hosts Dis 2025;63:215-27. https://doi.org/10.3347/PHD.25040
17. Uldry M, Thorens B. The SLC2 family of facilitated hexose and polyol transporters. Pflugers Arch 2004;447:480-9. https://doi.org/10.1007/s00424-003-1085-0
18. Morrissey KM, Stocker SL, Wittwer MB, Xu L, Giacomini KM. Renal transporters in drug development. Annu Rev Pharmacol Toxicol 2013;53:503-29. https://doi.org/10.1146/annurev-pharmtox-011112-140317
19. Barghash A, Helms V. Transferring functional annotations of membrane transporters on the basis of sequence similarity and sequence motifs. BMC Bioinformatics 2013;14:343. https://doi.org/10.1186/1471-2105-14-343
20. Quistgaard EM, Low C, Guettou F, Nordlund P. Understanding transport by the major facilitator superfamily (MFS): structures pave the way. Nat Rev Mol Cell Biol 2016;17:123-32. https://doi.org/10.1038/nrm.2015.25
21. Drew D, North RA, Nagarathinam K, Tanabe M. Structures and general transport mechanisms by the major facilitator superfamily (MFS). Chem Rev 2021;121:5289-335. https://doi.org/10.1021/acs.chemrev.0c00983
22. Yamaoka K, Tanigawara Y, Nakagawa T, Uno T. A pharmacokinetic analysis program (multi) for microcomputer. J Pharmacobiodyn 1981;4:879-85. https://doi.org/10.1248/bpb1978.4.879
23. Mueckler M, Caruso C, Baldwin SA, et al. Sequence and structure of a human glucose transporter. Science 1985;229:941-5. https://doi.org/10.1126/science.3839598
24. Deng D, Xu C, Sun P. Crystal structure of the human glucose transporter GLUT1. Nature 2014;510(7503):121-5. https://doi.org/10.1038/nature13306
25. Deng D, Sun P, Yan C, et al. Molecular basis of ligand recognition and transport by glucose transporters. Nature 2015;526:391-6. https://doi.org/10.1038/nature14655
26. Breitling J, Aebi M. N-linked protein glycosylation in the endoplasmic reticulum. Cold Spring Harb Perspect Biol 2013;5:a013359. https://doi.org/10.1101/cshperspect.a013359
27. Asano T, Takata K, Katagiri H, et al. The role of N-glycosylation in the targeting and stability of GLUT1 glucose transporter. FEBS Lett 1993;324:258-61. https://doi.org/10.1016/0014-5793(93)80129-i
28. Gyimesi G, Pujol-Gimenez J, Kanai Y, Hediger MA. Sodium-coupled glucose transport, the SLC5 family, and therapeutically relevant inhibitors: from molecular discovery to clinical application. Pflugers Arch 2020;472:1177-206. https://doi.org/10.1007/s00424-020-02433-x
29. Burant CF, Bell GI. Mammalian facilitative glucose transporters: evidence for similar substrate recognition sites in functionally monomeric proteins. Biochemistry 1992;31:10414-20. https://doi.org/10.1021/bi00157a032
30. Carruthers A, DeZutter J, Ganguly A, Devaskar SU. Will the original glucose transporter isoform please stand up! Am J Physiol Endocrinol Metab 2009;297:E836-48. https://doi.org/10.1152/ajpendo.00496.2009
31. Vollers SS, Carruthers A. Sequence determinants of GLUT1-mediated accelerated-exchange transport: analysis by homology-scanning mutagenesis. J Biol Chem 2012;287:42533-44. https://doi.org/10.1074/jbc.M112.369587
32. Warren GL, Andrews CW, Capelli AM, et al. A critical assessment of docking programs and scoring functions. J Med Chem 2006;49:5912-31. https://doi.org/10.1021/jm050362n

Original Article

Parasites Hosts Dis 2026;64(4):320-328
https://doi.org/10.3347/PHD.26001

Parasites, Hosts and Diseases

pISSN 2982-5164 • eISSN 2982-6799

Salivary *Plasmodium falciparum* histidine-rich protein 2 levels are poor predictors of parasite density and clinical malaria status in patients with acute uncomplicated malaria in Chulaimbo, western Kenya

Ruth Awuor Omingo[1,*], Cyrus Ayieko[1], Patrick Ogola Onyango[1], Ben Okeyo Sati[1], Vane Kwamboka Omwenga[1], Sidney Ogolla[2]

[1]Department of Zoology, Maseno University, Maseno, Kenya; [2]Kenya Medical Research Institute, Center for Global Health Research, Kisumu, Kenya

Malaria is the leading cause of death and economic burden worldwide. Current diagnostic methods rely on microscopy and blood-based rapid diagnostic tests. A common rapid diagnostic test target is *Plasmodium falciparum* histidine-rich protein 2 (PfHRP2), a parasite protein released into the host's blood during *Plasmodium* infection; it has also been detected in saliva, although results have been inconsistent. This pilot study quantified plasma and salivary PfHRP2 antigen levels and assessed their associations with age, parasite density, and clinical malaria status in a malaria-endemic region of western Kenya with high transmission. This pilot study enrolled 34 patients with acute uncomplicated malaria. Paired blood and saliva samples were collected at enrolment, with repeat sampling 4 weeks after treatment. *P. falciparum* infection was confirmed by light microscopy, and PfHRP2 concentrations were measured using an enzyme-linked immunosorbent assay. Data were analyzed in R version 4.5.2. Spearman's rank correlation and robust linear regression were used to examine the relationship between plasma and salivary *P. falciparum* antigen levels in individuals with acute malaria and to assess whether PfHRP2 concentrations in either matrix predicted parasite density, clinical malaria status, and age. Salivary PfHRP2 levels did not significantly predict parasite density or age (χ^2=0.54, *P*=0.76). By contrast, plasma PfHRP2 levels strongly predicted both parasite density and age (*P*=0.034). Plasma and salivary PfHRP2 concentrations were not significantly correlated (ρ=-0.327, *P*=0.059). Nevertheless, routine measurement of salivary PfHRP2 using more sensitive methods may improve diagnosis and guide treatment management.

Keywords: Rapid diagnostic test, malaria, microscopy, enzyme-linked immunosorbent assay, saliva

Introduction

Malaria remains a major public health concern and a leading cause of morbidity and mortality in the tropics [1]. An estimated 247 million malaria cases occurred worldwide in 2021 across 84 malaria-endemic countries, up from 245 million in 2020; countries in the World Health Organization African Region accounted for most of this increase [2]. In 2021, more than 40% of global investment in malaria was channeled through the Global Fund to Fight AIDS, Tuberculosis and Malaria. Countries and partners raised a total of 15.9 billion US dollars, the largest replenishment in the fund's history [2]. However, malaria elimination efforts continue to face setbacks associated with the coronavirus disease 2019 pandemic and treatment and

Received: December 31, 2025 Accepted: June 25, 2026
*Correspondence: omingoruth49@gmail.com

© 2026 The Korean Society for Parasitology and Tropical Medicine

This is an open-access article distributed under the terms of the Creative Commons Attribution Non-Commercial License (http://creativecommons.org/licenses/by-nc/4.0/) which permits unrestricted non-commercial use, distribution, and reproduction in any medium, provided the original work is properly cited.

Citation
Omingo RA, Ayieko C, Onyango PO, Sati BO, Omwenga VK, Ogolla S. Salivary *Plasmodium falciparum* histidine-rich protein 2 levels are poor predictors of parasite density and clinical malaria status in patients with acute uncomplicated malaria in Chulaimbo, western Kenya. Parasites Hosts Dis 2026;64(4):320-328.

control campaigns, among other challenges. Improved malaria diagnosis is therefore urgently needed to reduce malaria-related deaths and economic burden. Timely, accurate diagnosis followed by effective treatment is the primary strategy for malaria treatment [3].

Microscopy measures peripheral parasitemia and remains the gold standard for malaria diagnosis [4], although it has limitations [5] and is less reliable at low parasite levels [6]. Malaria rapid diagnostic tests (RDTs) detect *Plasmodium*-specific proteins, such as *Plasmodium falciparum* histidine-rich protein 2 (PfHRP2), in infected blood [7]. PfHRP2-based tests have demonstrated accuracy in detecting *P. falciparum* infection [8]. However, both methods require blood collection, which is labor-intensive and time-consuming and requires considerable expertise and trained healthcare workers [9]. These invasive procedures also cause discomfort and pain [10]. Saliva has shown considerable potential as a noninvasive specimen for detecting malaria antigens, although findings have been mixed [11]. Among children with malaria in Accra, Ghana, detection of PfHRP2 in whole saliva had a sensitivity of 43% and a specificity of 53% [12]. Another study using a blood-based RDT detected *P. falciparum* lactate dehydrogenase (PfLDH) with sensitivities of 77.9% in whole saliva and 96.7% in saliva supernatant [4]. A study in Lagos State reported sensitivities for PfHRP2 detection of 96.7% in blood and 12.7% in saliva [13]. Most studies of saliva for malaria diagnosis have been qualitative and have not quantified salivary antigens, making it difficult to determine whether low sensitivity reflects low antigen concentrations. The only study to quantify salivary PfHRP2 levels also found a good correlation between blood and salivary levels [11]. However, that study was conducted in an area of low malaria endemicity and included relatively few participants. Whether similar patterns occur in a malaria-endemic region therefore requires investigation. The utility of salivary PfHRP2 levels as a proxy for *Plasmodium* infection also needs to be evaluated. This pilot study detected and quantified PfHRP2 antigens in blood and saliva and examined their relationships with age, parasite density, and clinical malaria status in a highly malaria-endemic area of western Kenya.

Methods

Ethical statement

The School of Graduate Studies at Maseno University authorized this study. Ethical approval was obtained from the Maseno University Ethical Review Committee (MSU/DRPI/MUERC/00816/19). Participants' rights to informed consent, privacy, and confidentiality were upheld throughout and after the study. Consent for participants younger than 18 years was sought from their parents or guardians. This observational study did not pose a potential for harm, damage, or injury; accordingly, a trained, qualified phlebotomist collected the blood samples. Participants received no compensation, but the study findings benefited the wider community.

Study site

The study was conducted at Chulaimbo Sub-County Hospital in Kisumu County, a malaria-endemic area of western Kenya [14]. Residents receive approximately 100–300 infectious mosquito bites annually, and *P. falciparum* causes 97% of malaria infections [15]. According to the 2020 Kenya Malaria Indicator Survey, malaria prevalence among children aged 6 months to 14 years in Kisumu County was approximately 15.6%–19%. The hospital's catchment area is 1,131 m above sea level and receives 1,200–1,300 mm of rainfall annually. Humidity ranges from 50 to 68 g/m^3, and temperatures range from 20°C to 35°C [14]. In 2021, the population of the Chulaimbo Hospital catchment area was approximately 21,452. The hospital predominantly serves the rural population of North West Kisumu ward, whose economic activities include small-scale farming and business [14].

Study population and sample size determination

The study combined cross-sectional and longitudinal designs. Patients presenting to Chulaimbo Sub-County Hospital in Kisumu West Sub-County, Kenya, with symptoms of uncomplicated malaria were enrolled after consent was obtained. Blood and saliva were collected at enrollment and again from the same participants 4 weeks after treatment. Suspected clinical malaria was defined according to Kenya Ministry of Health guidelines.

The sample size for this pilot study was based on the statistical power needed to detect a moderate-to-strong correlation between systemic and oral malaria antigens. With a two-sided significance level (α) of 0.05 and target power (1–β) of 80%, the minimum sample size (n) was calculated using the formula for correlation coefficients:

$$n=\left(\frac{Z_\alpha+Z_\beta}{C}\right)^2+3$$

where n is the minimum sample size required to detect the target effect size; Z_α is the standard normal critical value for a 95% confidence interval (1.96); Z_β is the standard normal value for 80% statistical power (0.841); and C is Fisher's Z-transformation of the target correlation coefficient ($r=0.465$).

Calculation:

$$C=0.5\times\ln\left(\frac{1+0.465}{1-0.465}\right)\approx 0.503$$

$$n=\left(\frac{1.96+0.841}{0.503}\right)^2+3\approx 34$$

A minimum of 34 patients (28 children and 6 adults) was therefore required to provide sufficient power to detect a moderate-to-strong diagnostic relationship between plasma and salivary PfHRP2 levels. This sample size permitted quantitative evaluation of antigen levels and assessment of their diagnostic utility in a highly malaria-endemic area of western Kenya.

Inclusion and exclusion criteria

Patients were eligible if they were at least 1 year old, had malaria symptoms, and had microscopically confirmed *P. falciparum* infection. Informed consent was also required: adults consented for themselves, and parents or guardians consented on behalf of children. Patients were excluded if they were not Kisumu County residents, had symptoms of an illness other than malaria, or had symptoms of severe malaria. Blood and saliva were collected from 34 participants (28 children and 6 adults) to quantify *P. falciparum* antigens. Matched blood and saliva samples from each participant were processed at Chulaimbo Sub-County Hospital. Hemoglobin concentrations were measured using the HemoCue method.

Blood sample collection and processing

A trained phlebotomist collected approximately 1 ml of whole blood from each participant by finger prick into EDTA-treated anticoagulant tubes. Samples were labeled immediately, placed in a cool box, and transported to the laboratory within 2 h of collection. At the laboratory, blood samples were centrifuged at 2,600 × g for 15 min (Eppendorf). Supernatants were transferred to fresh 2 ml tubes and stored at -20°C for batch analysis. Malaria was diagnosed by both light microscopy and RDTs, as shown in Fig. 1.

Saliva sample collection and processing

Saliva was collected from each participant with confirmed *P. falciparum* infection as previously described [11]. Approximately 3 ml was collected into sterile cryovial tubes, immediately placed in a cool box maintained at 4°C, and transported to the laboratory within 2 h. On arrival, samples were centrifuged at 2,600 × g and 4°C for 15 min, as previously described [11]. After collection, the following protease inhibitors were added to the saliva: aprotinin (Sigma-Aldrich, lot A1153; 0.9 µl, 6.12 units/ml), sodium orthovanadate (Sigma-Aldrich, S6508; 3 µl at 400 mM, pH 10 in water), and phenylmethylsulfonyl fluoride (My Biosphere, catalog No. 545833; 10 µl at 10 mg/ml in isopropyl alcohol). Samples were then stored at -20°C for batch analysis.

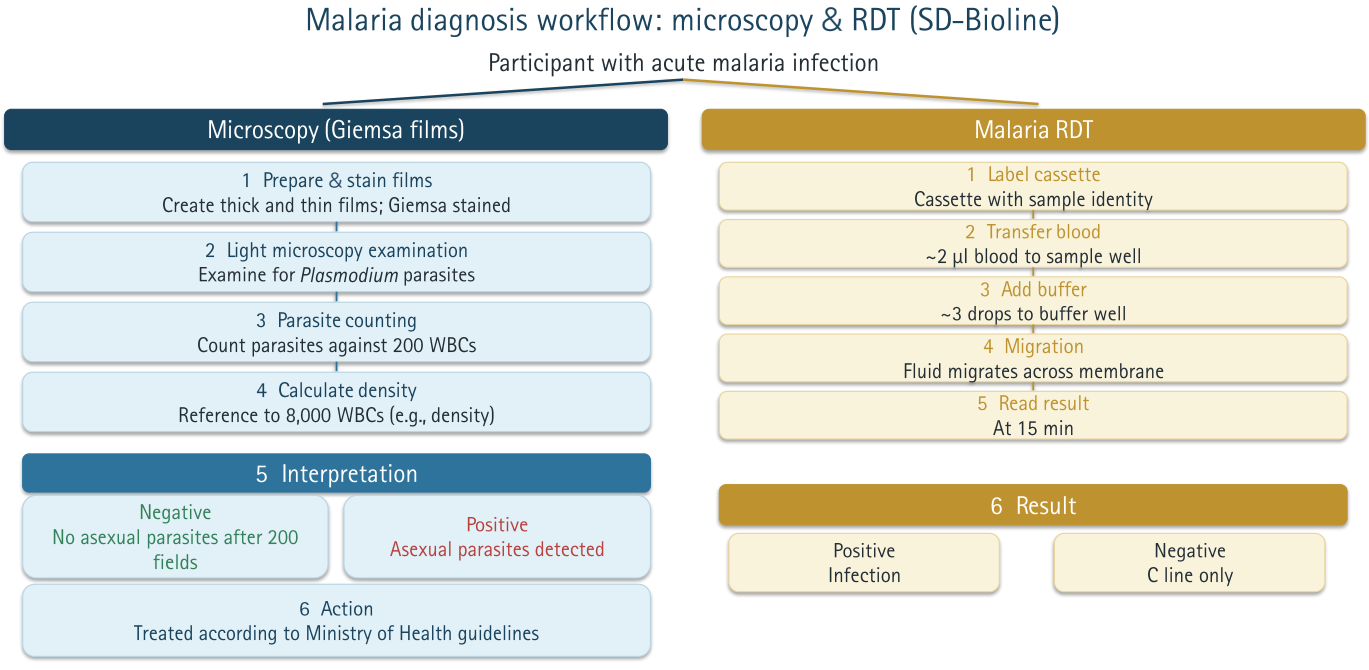


Fig. 1. Malaria diagnosis by microscopy and rapid diagnostic test (RDT).

https://doi.org/10.3347/PHD.26001

Detection of histidine-rich protein 2 in blood and saliva using a sandwich ELISA

PfHRP2 levels in saliva and blood were quantified using a sandwich ELISA, following a previously described method [11] with minor modifications. Immulon 4 HBX microtiter plates were coated with a PfHRP2 capture antibody (MyBioSource, catalog No. MBS532523) diluted in phosphate-buffered saline (PBS) to a final concentration of 0.1625 μg/ml, then incubated overnight at 4°C. The wells were washed 3 times with PBS containing 0.05% Tween-20 (PBS-T) and blocked for 1 h at room temperature with 4% (w/v) nonfat dry milk powder (Sigma-Aldrich) in PBS. After blocking, the plates were washed 3 times with PBS-T. Standards were prepared by diluting recombinant PfHRP2 in blocking buffer to an initial concentration of 5 ng/μl, followed by 1:1 serial dilutions in the same buffer for a total of 8 dilution steps. Standards, samples, and blanks were added in duplicate, and the plates were sealed with adhesive film and incubated for 1 h at room temperature. The plates were then emptied and washed 5 times with PBS-T. Biotinylated PfHRP2 detection antibody (MyBioSource, catalog No. 6120632), diluted in blocking buffer to a final concentration of 125 ng/ml, was added, followed by incubation for 1 h at room temperature. The plates were washed 5 times with PBS-T, and peroxidase-labeled streptavidin (0.8 μg/ml; Thermo Fisher Scientific, catalog No. 21126) was added. After incubation for 30 min at room temperature with gentle agitation, the plates were washed 5 times with PBS-T. A chemiluminescent substrate (Thermo Fisher Scientific, catalog No. 37070) was then added, and the plates were incubated for 25 min at room temperature. Luminescence was measured immediately at 460/20 nm in relative light units using a Synergy HTX multimode reader (Agilent Technologies/BioTek). Sample PfHRP2 concentrations were extrapolated from a standard curve generated from known recombinant PfHRP2 concentrations.

Data management and analysis

Data were analyzed in R version 4.5.2. *P. falciparum* antigen levels in saliva and blood were measured using a highly sensitive multimode ELISA reader. To address the inherent right-skewness of biomarker concentrations, all antigen levels (plasma and salivary PfHRP2) and parasite density values were $\log_{10}$-transformed before analysis, stabilizing variance across measurement scales. Robust linear regression related $\log_{10}$-transformed antigen levels to parasite density, clinical malaria status, and age. Logistic regression was used to model clinical malaria as a binary outcome (1 = clinical malaria, 0 = post-treatment follow-up). Clinical malaria was defined according to Kenya Ministry of Health guidelines for suspected uncomplicated malaria: an axillary temperature >37.0°C plus at least 1 of chills, headache, or severe malaise, together with microscopic confirmation of *P. falciparum* monoinfection. Spearman's rank correlation was used to assess the correlation between blood and salivary PfHRP2 levels. Chi-square tests assessed associations between categorical variables, including salivary PfHRP2 detectability (detectable versus nondeductible) and clinical malaria status. A two-sided $P < 0.05$ was considered statistically significant for all tests.

Results

Demographic characteristics of study participants

Table 1 presents participant demographics and laboratory findings during acute uncomplicated malaria and 4 weeks after treatment. Thirty-four participants (28 children and 6 adults) who presented to Chulaimbo Hospital with clinical malaria symptoms were enrolled after consent was obtained. Most participants were female (18/34, 53%). Mean weight (range) was 18.7 (11–28.8) kg in children and 59.9 (51.8–75.8) kg in adults. At enrollment, median age (interquartile range) was 6.6 (4.4) years in children and 26.4 (11.2) years in adults. Median parasite density (interquartile range) was higher in children, at 20,000 (21,400), than in adults, at 6,230 (9,370) (Table 1).

Relationships of histidine-rich protein 2 levels with *Plasmodium* parasite density and age

To evaluate salivary PfHRP2 as a proxy for *Plasmodium* infection, robust linear regression was used to examine the relationships of ELISA-measured PfHRP2 levels with blood smear parasite density and age. Salivary PfHRP2 levels did not significantly predict parasite density or age in individuals with acute malaria ($\chi^2 = 0.54$, $P = 0.76$). The negative coefficients for log parasite density ($\beta = -0.1384$, $t = -0.7314$) and age ($\beta = -0.0037$, $t = -0.3939$) further suggested an inverse, although nonsignificant, relationship between systemic parasite load across ages and salivary antigen concentration (Table 2). By contrast, plasma PfHRP2 levels strongly predicted parasite density and age in patients with acute malaria ($P = 0.034$), with a positive coefficient for log parasite density ($\beta = 0.2211$, $t = 1.2470$) and a negative coefficient for age ($\beta = -0.0435$, $t = -4.919$) (Table 2).

Relationship between clinical malaria and antigen levels

Robust linear regression was used to assess the relationship between clinical malaria and antigen levels. Plasma PfHRP2 showed a strong positive trend in predicting clinical malaria status (odds ratio, 8.73; 95% confidence interval, 0.620–623.42), whereas salivary PfHRP2 had a low odds ratio (0.23; 95% confidence interval, 0.003–3.99) (Table 3).

Correlation between salivary and blood histidine-rich protein 2 levels in individuals with acute malaria

The correlation between plasma and salivary PfHRP2 levels in individuals with acute malaria was assessed to determine whether saliva could serve as a non-invasive diagnostic alternative to plasma. Salivary PfHRP2 did not show a positive linear relationship with either systemic antigen levels ($\rho = -0.327$, $P = 0.059$) (Fig. 2) or total parasite burden ($\rho = -0.246$, $P = 0.161$) (Table 4).

Discussion

Table 1 presents participant demographics and laboratory findings during acute uncomplicated malaria and 4 weeks after treatment. Microscopy provided estimates of total parasite burden with greater precision and sensitivity. This overall assessment indicated high parasite density after treatment, particularly in children (Table 1). This finding may reflect markers associated with resistance to artemisinin combination therapy within a genetically heterogeneous parasite population [16], together with lower population immunity to clear parasites, DNA, and malaria antigens [17]. A subpopulation of dormant parasites is also the most likely explanation for delayed parasite clearance. During artemisinin-induced dormancy, a subset of asexual parasites temporarily enters a state of arrested growth and metabolic inactivity, allowing survival during artemisinin treatment [18]. These dormant parasites may be killed slowly by partner drugs while contributing to persistent parasite detection after treatment.

The utility of salivary PfHRP2 levels as a proxy for *Plasmodium* infection was evaluated using ELISA measurements. Relationships with blood smear parasite density, clinical malaria, and age were examined. The bivariate correlation between log plasma PfHRP2 concentration and log parasite density (Table 2),

Table 1. Age and clinical characteristics of study participants

	Children ($n = 28$)			Adults ($n = 6$)		
	Acute	Post-treatment	*P*-value[a]	Acute	Post-treatment	*P*-value[a]
Age (year)	6.6 (4.4)	6.6 (4.4)	1.000	26.4 (11.2)	26.4 (11.2)	1.000
Hemoglobin (g/dl)	11.1 (2.4)	11.9 (1.3)	0.236	14.9 (1.2)	15.2 (0.7)	0.317
Parasite density (/μl)	20,000 (21,400)	13,200 (0)	< 0.001	6,230 (9,370)	0 (0)	0.068
Temperature (°C)	38.4 (1.0)	36.4 (0.5)	< 0.001	36.4 (1.6)	35.7 (0.4)	0.109

Values are presented as median (interquartile range).
[a]Calculated using the Wilcoxon signed-rank test.

Table 2. Robust linear regression analysis of factors influencing plasma and salivary histidine-rich protein 2 concentrations (n=34)

Predictor variable	Predicted variable	Coefficient (β)	Standard error	*t*-value
Plasma PfHRP2[a]	$\log_{10}$(parasite density)	0.2211	0.1773	1.2470
	Age (year)	-0.0435	0.0088	-4.9199
Salivary PfHRP2[b]	$\log_{10}$(parasite density)	-0.1384	0.1893	-0.7314
	Age (year)	-0.0037	0.0094	-0.3939

PfHRP2, *Plasmodium falciparum* histidine-rich protein 2.
[a]Model statistics: P=0.034; residual standard error, 0.4034 on 31 degrees of freedom; scale estimate, 0.403; [b]Model statistics: residual standard error, 0.5998 on 31 degrees of freedom; Wald test, χ^2=0.54, 2 degrees of freedom, P=0.76.

Table 3. Logistic regression analysis predicting clinical malaria status

Predictor	Odds ratio	95% CI (lower bound)	95% CI (upper bound)
$\log_{10}$(plasma PfHRP2)	8.7339	0.6203	623.428
$\log_{10}$(salivary PfHRP2)	0.2362	0.0038	3.993
Age (year)	0.8776	0.6971	0.9853

Plasma PfHRP2 shows a strong positive trend in predicting clinical malaria status, whereas salivary PfHRP2 shows poor predictive utility (OR<1).
CI, confidence interval; PfHRP2, *Plasmodium falciparum* histidine-rich protein 2.

https://doi.org/10.3347/PHD.26001

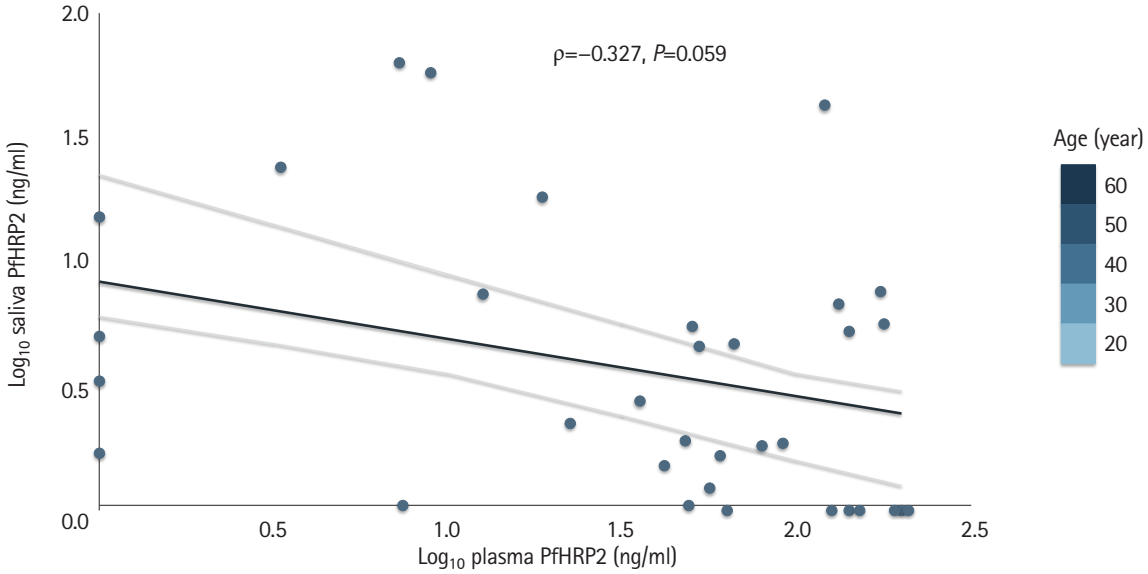


Fig. 2. Correlation between salivary and plasma histidine-rich protein 2 levels in children and adults with acute malaria. The plot shows the relationship between log-transformed plasma and salivary *Plasmodium falciparum* histidine-rich protein 2 (PfHRP2) concentrations in 34 patients with acute malaria. The analysis indicated a marginal inverse correlation (ρ=−0.327, *P*=0.059), shown by the negative slope of the regression line and the shaded 95% confidence interval. This downward trend suggests that higher plasma antigen levels do not correspond to higher salivary concentrations; the divergence between the 2 compartments approaches statistical significance. The age color gradient indicates that this pattern persists across the demographic range, from children to adults. This negative association supports the hypothesis that complex biological barriers in the oral cavity, including antigen degradation by salivary proteases or a saturation effect at the blood–saliva barrier, may decouple salivary PfHRP2 levels from systemic parasite burden.

Table 4. Spearman's rank correlation analysis of salivary histidine-rich protein 2 (*n*=34)

Correlation pair	Spearman's rho (ρ)	*P*-value
Plasma PfHRP2 vs. salivary PfHRP2	-0.3272	0.0589
Parasite density vs. salivary PfHRP2	-0.2459	0.1610

A negative ρ indicates a trend toward an inverse relationship.
PfHRP2, *Plasmodium falciparum* histidine-rich protein 2.

together with the positive relationship between plasma PfHRP2 and clinical malaria (Table 3), indicates a significant association between elevated plasma levels and symptomatic illness. These findings agree with those of Manning et al. [19] in Papua New Guinea and Martiáñez-Vendrell [20]. However, salivary PfHRP2 levels did not predict parasite density in individuals with acute malaria. The odds ratio for salivary PfHRP2 was also lower than that for plasma PfHRP2, suggesting that the salivary test produced a markedly weaker signal than blood-based measurements despite confirmed clinical malaria. This may primarily reflect the lower ELISA detection limit for antigens in saliva than in plasma observed in the results above. Protein transport into saliva depends on molecular mass, ionization, and salivary ph. Molecules may be diluted to different extents during transfer from plasma to saliva [11]. *P. falciparum* antigens also differ in stability between saliva and plasma. Salivary proteases may break down PfHRP2 [21], further reducing the sensitivity of salivary malaria-antigen detection. Saliva clarity varies among individuals even when patients are asked to provide unstimulated drool. Obtaining clear samples was particularly difficult in dehydrated children. Taken together, the findings indicate substantial decoupling of systemic and oral biomarkers. Plasma PfHRP2 remains a gold-standard indicator of malaria infection, whereas salivary PfHRP2 appears subject to distinct biological constraints. The lack of a strong predictive relationship suggests that standard salivary ELISA cannot yet directly replace blood-based testing without accounting for oral clearance or degradation. Future research should therefore prioritize substantially more sensitive salivary diagnostic tools or robust standardization methods that correct for oral matrix effects.

Age significantly predicted median plasma PfHRP2 levels but not salivary levels. Its highly significant contribution indicated that younger patients tended to have much higher systemic antigen levels. This finding is consistent with the high-transmission setting of western Kenya, where older individuals develop partial immunity and clear antigens more efficiently [22]. Previous studies similarly reported that parasite density declines with age [23], peaking in young children and decreasing thereafter [24]. Malaria antigen levels also increase

with parasite density [25]. Median PfHRP2 levels were therefore expected to be higher in children than in adults in both plasma and saliva, but this pattern was observed only in plasma. Direct age-stratified studies of salivary PfHRP2 are scarce, and most data come from small cohorts. For example, a 2012 pilot study reported levels <200 pg/ml in adolescents aged 13–15 years and up to 1,167 pg/ml in adults aged 23–57 years [11]. Research on plasma PfHRP2 nevertheless provides a robust explanation, because transfer into saliva depends on the plasma load. The longer PfHRP2 half-life in semi-immune adults results in antigen accumulation owing to mature immune modulation and renal/hepatic function [26]. Children, however, clear the antigen more rapidly through innate responses [27].

This study examined the relationship between plasma and salivary PfHRP2 levels in patients with malaria to determine whether saliva could replace plasma as a diagnostic specimen. The negative correlation suggests that detectable salivary levels tend to decrease as systemic antigen concentrations increase, with the relationship approaching statistical significance. Parasite density likewise showed a weak, nonsignificant negative correlation with salivary PfHRP2. Together, these findings provide empirical evidence of decoupling between salivary antigen levels and systemic parasite biomass. This divergence may reflect low assay sensitivity and inhibitors in saliva [21]. PfHRP2 is also less stable in saliva than in plasma. Compared with plasma, saliva contains proteases that may break down the enzymes [11], potentially reducing salivary *P. falciparum* antigen levels. In this study, however, the ELISA protocol was optimized for the salivary matrix by using a highly sensitive multimode reader capable of detecting luminescence. This significantly improved sensitivity, quantification, and overall reliability compared with standard colorimetric methods. Protease inhibitors were also added to saliva to reduce protease activity. When added immediately after collection, these inhibitors suppress enzymatic activity by binding competitively or reversibly to proteolytic enzymes' active sites, arresting catalysis and preserving antigen integrity. To further preserve sample integrity, saliva was collected by passive drooling. Samples were collected consistently during the morning to minimize circadian effects on flow rate. Participants were also instructed to refrain from eating, drinking, or performing oral hygiene for 30–60 min before collection to reduce matrix effects and contamination. Samples were collected at 4°C and transported to the laboratory within 2 h for processing to limit post collection variability. Nevertheless, variation in sample clarity, particularly in dehydrated children despite requests for unstimulated drool, may have affected antigen detection and consistency. This may explain the lack of correlation between plasma and salivary antigen levels in individuals with acute malaria. Fig. 2 illustrates the negative relationship between log-transformed plasma and salivary PfHRP2 concentrations in the 34 patients with acute malaria. The age color gradient indicates that this pattern persisted across the demographic range, from children to adults. This negative association supports the hypothesis that complex biological barriers in the oral cavity, such as antigen degradation by salivary proteases [11], may decouple salivary PfHRP2 levels from systemic parasite burden. Future studies should standardize saliva-collection protocols and ensure appropriate processing before analysis to improve salivary data.

In contrast to these findings, a study in Msambweni, Kwale County, found a slight positive linear relationship between blood and salivary PfLDH levels [28]. That study included 175 participants, compared with 34 in the present study, which may explain the slight positive relationship between plasma and salivary antigen levels. Future studies should increase the sample size to improve statistical power and detect subtle correlations, because larger cohorts have shown better proportionality for antigens such as PfLDH [21]. Differences between the target antigens, PfLDH and PfHRP2, may also reflect fundamental differences in their biochemical properties, secretion patterns, and behaviour in fluids such as saliva. PfHRP2 persists for weeks after treatment because of slow clearance, with a plasma half-life of approximately 7–14 days [11]. This persistence reflects cumulative parasite biomass rather than active infection. Salivary concentrations, however, are typically low (e.g., 17–1,167 pg/ml), and detection often correlates poorly with concurrent blood parasitemia. Salivary PfHRP2 may therefore primarily reflect accumulated or historical biomass rather than real-time active replication, consistent with its role as an indicator of exposure intensity or cumulative burden in low-density or post-treatment settings rather than acute parasitemia. PfLDH is a soluble glycolytic enzyme produced by viable parasites and is rapidly cleared from circulation after parasite death, making it a better marker of active infection in saliva [21]. In larger cohorts, PfLDH also appears to be more proportional to blood parasitemia, although this relationship remains weak. This may reflect differences in molecular size, approximately 140 kDa [21]. Both antigens, however, present challenges for salivary detection, including potential degradation by proteases, inhibitors, and matrix effects.

Saliva is a promising diagnostic fluid for malaria when pro-

https://doi.org/10.3347/PHD.26001

tein degradation and matrix effects are reduced, but the present study found no statistically significant relationship between median plasma and salivary PfHRP2 levels under the experimental conditions used. A more appropriate approach to malaria diagnosis would combine a test kit sufficiently sensitive to detect low salivary antigen levels with standardized sample collection and processing. Investigating other malaria antigens present in both plasma and saliva may yield different results and could form the basis of future work.

This study found no statistically significant association between plasma and salivary PfHRP2 levels in individuals with acute malaria. Nevertheless, routine measurement of salivary PfHRP2 using more sensitive methods may provide clinicians and researchers with a more robust, real-time dataset that could improve diagnosis and guide treatment management.

Data availability

The data are available from the authors upon request.

Author contributions

Conceptualization: Omingo RA, Ayieko C. Data curation: Omingo RA, Ayieko C, Onyango PO. Formal analysis: Omingo RA, Ayieko C, Onyango PO. Funding acquisition: Ayieko C. Investigation: Omingo RA, Ayieko C, Onyango PO. Methodology: Omingo RA, Ayieko C, Onyango PO. Project administration: Ayieko C. Resources: Omingo RA, Ayieko C, Onyango PO, Sati BO, Omwenga VK, Ogolla S. Software: Omingo RA, Ayieko C, Onyango PO, Sati BO. Supervision: Ayieko C, Onyango PO, Ogolla S. Validation: Ayieko C, Onyango PO, Sati BO, Omwenga VK, Ogolla S. Visualization: Omingo RA, Ayieko C. Writing – original draft: Omingo RA. Writing – review & editing: Ayieko C.

Conflict of interest

The authors have no conflicts of interest to declare.

Funding

This study was funded by the Wellcome Trust through an HRCS Postdoctoral Grant (reference 209329/Z/17/Z).

Acknowledgments

The authors thank the study participants, guardians, and parents who provided samples. We are grateful to the Kenya Medical Research Institute-Kisian for permitting sample processing and storage at its facility. We also thank Mr. Ben Okeyo Sati, Boniface Ariera, Kevin Waomba, and Emilly Koech for helping collect samples at Chulaimbo Sub-County Hospital. Gertrude Wekesa and Regina Njeri of the International Livestock Research Institute provided guidance on sample analysis by ELISA at their facility. We thank Mr. Philip N. Ochien'g, Walter Odipo, Barnabas Muya, Joab Pira, and Julius Adundo, laboratory technicians in the Department of Zoology at Maseno University, for their technical assistance and guidance during the laboratory experiments.

ORCID

Ruth Awuor Omingo, https://orcid.org/0009-0008-6725-241X
Cyrus Ayieko, https://orcid.org/0000-0003-1673-225X
Patrick Ogola Onyango, https://orcid.org/0000-0002-5227-9571
Ben Okeyo Sati, https://orcid.org/0009-0008-8603-8064
Vane Kwamboka Omwenga, https://orcid.org/0009-0004-6227-0054
Sidney Ogolla, https://orcid.org/0000-0003-1570-6164

References

1. Okoyo C, Githinji E, Muia RW, et al. Assessment of malaria infection among pregnant women and children below five years of age attending rural health facilities of Kenya: a cross-sectional survey in two counties of Kenya. PLoS One 2021;16:e0257276. https://doi.org/10.1371/journal.pone.0257276
2. World Health Organization. World malaria report. World Health Organization; 2022.
3. Otambo WO, Olumeh JO, Ochwedo KO, et al. Health care provider practices in diagnosis and treatment of malaria in rural communities in Kisumu County, Kenya. Malar J 2022;21:129. https://doi.org/10.1186/s12936-022-04156-z
4. Nantavisai K. Malaria detection using non-blood samples. Songklanakarin J Sci Technol 2014;36:633-41.
5. Kifude CM, Rajasekariah HG, Sullivan DJ Jr, et al. Enzyme-linked immunosorbent assay for detection of *Plasmodium falciparum* histidine-rich protein 2 in blood, plasma, and serum. Clin Vaccine Immunol 2008;15:1012-8. https://doi.org/10.1128/CVI.00385-07
6. Berzosa P, de Lucio A, Romay-Barja M, et al. Comparison of three diagnostic methods (microscopy, RDT, and PCR) for the detection of malaria parasites in representative samples from Equatorial Guinea. Malar J 2018;17:333. https://doi.org/10.1186/s12936-018-2481-4
7. Amoah LE, Abankwa J, Oppong A. *Plasmodium falciparum* histidine rich protein-2 diversity and the implications for PfHRP 2: based malaria rapid diagnostic tests in Ghana. Malar J 2016;15:101. https://doi.org/10.1186/s12936-016-1159-z
8. Ly AB, Tall A, Perry R, et al. Use of HRP-2-based rapid diagnostic test for *Plasmodium falciparum* malaria: assessing accuracy and

cost-effectiveness in the villages of Dielmo and Ndiop, Senegal. Malar J 2010;9:153. https://doi.org/10.1186/1475-2875-9-153
9. Tangpukdee N, Duangdee C, Wilairatana P, Krudsood S. Malaria diagnosis: a brief review. Korean J Parasitol 2009;47:93-102. https://doi.org/10.3347/kjp.2009.47.2.93
10. Owusu EDA, Campillo A, Daily J, Ding XC. Acceptance and perceived value of non-invasive malaria diagnostic tests in malaria-endemic countries. Malar J 2021;20:379. https://doi.org/10.1186/s12936-021-03911-y
11. Fung AO, Damoiseaux R, Grundeen S, et al. Quantitative detection of PfHRP2 in saliva of malaria patients in the Philippines. Malar J 2012;11:175. https://doi.org/10.1186/1475-2875-11-175
12. Wilson NO, Adjei AA, Anderson W, Baidoo S, Stiles JK. Detection of *Plasmodium falciparum* histidine-rich protein II in saliva of malaria patients. Am J Trop Med Hyg 2008;78:733-5.
13. Elendu JA, Oyibo W. Performance of HRP2 based malaria rapid diagnostic test (SD-Bioline) in whole blood and saliva in patient's in Lagos State. Int J Innov Appl Sci 2014;9:642-7.
14. Kishoyian G, Njagi ENM, Orinda GO, et al. Efficacy of artemisinin-lumefantrine for treatment of uncomplicated malaria after more than a decade of its use in Kenya. Epidemiol Infect 2021;149:e27. https://doi.org/10.1017/S0950268820003167
15. Shah MM, Krystosik AR, Ndenga BA, et al. Malaria smear positivity among Kenyan children peaks at intermediate temperatures as predicted by ecological models. Parasit Vectors 2019;12:288. https://doi.org/10.1186/s13071-019-3547-z
16. Brhane BG, Fola AA, Nigussie H, et al. Rising prevalence of *Plasmodium falciparum* Artemisinin partial resistance mutations in Ethiopia. Commun Med (Lond) 2025;5:297. https://doi.org/10.1038/s43856-025-01008-0
17. Ntuku H, Whittemore B, Dausab L, et al. Post-treatment duration of positivity for standard and ultra-sensitive *Plasmodium falciparum* antigen-based rapid diagnostic tests, a cohort study from a low-endemic setting in Namibia. EBioMedicine 2025;111:105489. https://doi.org/10.1016/j.ebiom.2024.105489
18. Goodwin J, Kajubi R, Wang K, et al. Persistent and multiclonal malaria parasite dynamics despite extended artemether-lumefantrine treatment in children. Nat Commun 2024;15:3817. https://doi.org/10.1038/s41467-024-48210-7
19. Manning L, Laman M, Stanisic D, et al. Plasma *Plasmodium falciparum* histidine-rich protein-2 concentrations do not reflect severity of malaria in Papua new guinean children. Clin Infect Dis 2011;52:440-6. https://doi.org/10.1093/cid/ciq105
20. Martiáñez-Vendrell X, Jiménez A, Vásquez A, et al. Quantification of malaria antigens PfHRP2 and pLDH by quantitative suspension array technology in whole blood, dried blood spot and plasma. Malar J 2020;19:12. https://doi.org/10.1186/s12936-019-3083-5
21. Nambati EA, Kiarie WC, Kimani F, et al. Unclear association between levels of *Plasmodium falciparum* lactate dehydrogenase (PfLDH) in saliva of malaria patients and blood parasitaemia: diagnostic implications? Malar J 2018;17:9. https://doi.org/10.1186/s12936-017-2151-y
22. Martiáñez-Vendrell X, Skjefte M, Sikka R, Gupta H. Factors affecting the performance of HRP2-based malaria rapid diagnostic tests. Trop Med Infect Dis 2022;7:265. https://doi.org/10.3390/tropicalmed7100265
23. Hendriksen IC, White LJ, Veenemans J, et al. Defining falciparum-malaria-attributable severe febrile illness in moderate-to-high transmission settings on the basis of plasma PfHRP2 concentration. J Infect Dis 2013;207:351-61. https://doi.org/10.1093/infdis/jis675
24. Koepfli C, Robinson LJ, Rarau P, et al. Blood-stage parasitaemia and age determine *Plasmodium falciparum* and *P. vivax* gametocytaemia in Papua New Guinea. PLoS One 2015;10:e0126747. https://doi.org/10.1371/journal.pone.0126747
25. Dondorp AM, Desakorn V, Pongtavornpinyo W, et al. Estimation of the total parasite biomass in acute falciparum malaria from plasma PfHRP2. PLoS Med 2005;2:e204. https://doi.org/10.1371/journal.pmed.0020204
26. Michael OS, Orimadegun AE, Falade CO. Persistence of *Plasmodium falciparum* HRP2 antigen after effective antimalarial therapy. Ann Ib Postgrad Med 2021;19:15-21.
27. Hendriksen IC, Mwanga-Amumpaire J, von Seidlein L, et al. Diagnosing severe falciparum malaria in parasitaemic African children: a prospective evaluation of plasma PfHRP2 measurement. PLoS Med 2012;9:e1001297. https://doi.org/10.1371/journal.pmed.1001297
28. Adu-Gyasi D, Asante KP, Newton S, et al. Malaria parasite density estimated with white blood cells count reference value agrees with density estimated with absolute in children less than 5 years in Central Ghana. Malar Res Treat 2015;2015:923674. https://doi.org/10.1155/2015/923674

Original Article

Parasites Hosts Dis 2026;64(4):329-336
https://doi.org/10.3347/PHD.26034

Parasites, Hosts and Diseases

pISSN 2982-5164 • eISSN 2982-6799

Rapid detection of viable *Acanthamoeba* spp. trophozoites and cysts in water treatment processes using propidium monoazide coupled with real-time PCR

Eun-Sook Lee*, Ji-Yeon Lee, Young-Ae Baek, Seok-Ju Cho

Seoul Water Institute, Seoul, Korea

Acanthamoeba spp. are known to cause human diseases such as granulomatous amoebic encephalitis and keratitis. These protozoa can persist in aquatic environments for extended periods and exhibit resistance to disinfectants used in water treatment, posing a significant threat to public health. Traditional culture and molecular methods have limitations in the rapid detection of viable *Acanthamoeba* in water. Therefore, we optimized real-time PCR (qPCR) combined with propidium monoazide (PMA) and evaluated the applicability of PMA-qPCR for the rapid detection of viable *Acanthamoeba* throughout the tap water production process. Using a PMA concentration of 50 μM, we successfully differentiated viable from non-viable cells and selected a 180-bp fragment of the 18S rRNA gene to enhance qPCR efficiency while minimizing amplification from non-viable cells. Application of PMA-qPCR to samples collected from each stage of the water treatment process, from raw water to purified water, enabled the detection of viable *Acanthamoeba* in samples with turbidity levels between 0.03 and 13.7 nephelometric turbidity units. These results demonstrate that PMA-qPCR is a suitable tool for monitoring pathogenic *Acanthamoeba* in drinking water supplies and enabling prompt responses to potential waterborne contamination events.

Keywords: *Acanthamoeba*, propidium monoazide, real-time PCR, water treatment process

Introduction

Acanthamoeba spp. are free-living amoebae that are widely distributed in natural environments, including water, and cause diseases such as granulomatous amoebic encephalitis, cutaneous acanthamoebiosis, and keratitis in humans [1]. *Acanthamoeba* has a 2-stage life cycle alternating between trophozoite and cyst forms. The cyst, characterized by a double-layered cell wall composed of cellulose, exhibits strong environmental resistance and prolonged survival, thereby maintaining pathogenic potential [2,3]. In particular, it can survive several stages of physical and chemical purification processes for tap water production, and its resistance to disinfectants such as chlorine and ozone can threaten a safe water supply [2-4]. In addition to its own pathogenicity, *Acanthamoeba* can act as a reservoir for various pathogens. Many pathogens, such as *Legionella*, *Mycobacteria*, and other emerging pathogens, can proliferate within *Acanthamoeba* while remaining protected during disinfectant and water treatment processes, which can play a role in spreading these pathogens [5-7]. Moreover, it is known that the virulence and drug resistance of pathogenic bacteria grown in *Acanthamoeba* increase compared to those that are not [8,9]. Therefore, to protect public health and

Received: April 10, 2026 Accepted: June 23, 2026
*Correspondence: leuns21@seoul.go.kr

© 2026 The Korean Society for Parasitology and Tropical Medicine
This is an open-access article distributed under the terms of the Creative Commons Attribution Non-Commercial License (http://creativecommons.org/licenses/by-nc/4.0/) which permits unrestricted non-commercial use, distribution, and reproduction in any medium, provided the original work is properly cited.

Citation
Lee ES, Lee JY, Baek YA, Cho SJ. Rapid detection of viable *Acanthamoeba* spp. trophozoites and cysts in water treatment processes using propidium monoazide coupled with real-time PCR. Parasites Hosts Dis 2026;64(4):329-336.

strengthen the safety of tap water, it is necessary to monitor *Acanthamoeba* during both the water purification and tap water supply processes.

In general, cultivation has been applied to detect and quantify *Acanthamoeba* in water. However, the method is complex as it involves several steps, including sample dilution, preparation of medium for seeding bacteria, sample inoculation, culture, and result reading [10,11]. In addition, damaged *Acanthamoeba* cells are difficult to culture, and the analysis is time-consuming because of the 5-day to 7-day incubation period. Moreover, a high level of expertise is required to examine the cultures under a microscope [10,11].

Real-time PCR (qPCR), which has been widely used recently, is a rapid and sensitive method that is effective in quantifying *Acanthamoeba* present in water. However, qPCR cannot distinguish between viable and non-viable of *Acanthamoeba*, so it may underestimate the efficiency of the water purification process [12]. This limitation can be overcome by combining qPCR with a nucleic acid intercalating dye such as propidium monoazide (PMA). This dye penetrates into cells with damaged cell membranes and irreversibly binds to DNA via photoactivation, ultimately preventing amplification by PCR [13-15]. There have been very few qPCR studies using PMA dye for the quantification of *Acanthamoeba*, but since those studies were not conducted on environmental water, their applicability to actual field samples has not been evaluated [16,17].

Therefore, in this study, we optimized the PMA-qPCR method to quantify the viability of pathogenic *Acanthamoeba*, including both trophozoites and cysts, in water. In addition, we evaluated the applicability of PMA-qPCR to quickly monitor viable *Acanthamoeba* in the tap water supply process. Ultimately, PMA-qPCR is intended to be applied for rapid responses to infections caused by *Acanthamoeba* in water-related incidents and for evaluating the safety of water treatment processes.

Methods

Ethics statement

Not applicable.

Microorganisms

The *Acanthamoeba* strains used in this study were *A. culbertsoni* (ATCC 30171) and *A. polyphaga* (ATCC 30461). The trophozoites were grown in proteose yeast glucose medium (20 g/L proteose peptone, 2 g/L yeast extract, 0.1 M glucose, 4 mM $MgSO_4$, 0.4 mM $CaCl_2$, 3.4 mM sodium citrate, 0.05 mM $Fe(NH_4)_2(SO_4)_2$, 2.5 mM Na_2HPO_4, and 2.5 mM KH_2PO_4; Sigma-Aldrich) at 27℃ for 3 days [18]. The trophozoites were harvested by centrifugation at 200 × g for 8 min and the resulting pellet was washed twice with sterile Page's amoeba saline (2.05 mM NaCl, 0.016 mM $MgSO_4 \cdot 7H_2O$, 0.036 mM $CaCl_2$, 1 mM KH_2PO_4, and 1 mM Na_2HPO_4; Sigma-Aldrich) [16]. For encystation of *Acanthamoeba*, the pellet was then re-suspended in encystment medium (0.1 M KCl, 0.02 M Tris-HCl, 8 mM $MgSO_4$, 0.4 mM $CaCl_2$, 1 mM $NaHCO_3$; Sigma-Aldrich). This suspension was incubated at 25℃ for 10 days [11]. The cysts were harvested by centrifugation and stored at room temperature. The trophozoites and cysts were observed by light microscopy (Carl Zeiss).

Preparation of viable and non-viable cells

To evaluate the ability of PMA-qPCR to quantify viable *Acanthamoeba*, viable and non-viable cells were prepared. Viable cells were obtained by culturing the amoebae on non-nutrient agar (Oxoid) plates with 200 μl of *Escherichia coli* (ATCC 11775) suspension at 30℃ for 5 days [16]. Non-viable cells were prepared the cell suspension by heating at 100°C for 5 min using a standard laboratory heat block. The heated cells were then cultured on non-nutrient agar plates with *E. coli* and examined daily by microscopy throughout the incubation period to confirm the absence of viable cells. The densities of viable and non-viable cells were adjusted to approximately 10^4–10^8 cells/ml.

PMA treatment

PMA (Biotum) was dissolved in 20% dimethyl sulfoxide (Sigma-Aldrich) to prepare a 20 mM stock solution. Given the limited research on PMA and amoebae, the concentration range was determined by referring to previous studies [12-17]. To evaluate the optimal PMA concentration, 500 μl samples containing either viable or non-viable *Acanthamoeba* (trophozoites of *A. culbertsoni* and *A. polyphaga* or cysts of *A. culbertsoni*) were treated with PMA at final concentrations of 0, 25, 50, 100, 150, and 200 μM. Furthermore, to assess whether the optimal PMA concentration varied with the initial target cell density, the samples were divided into low (10^2–10^3 copies per reaction) and high (10^4–10^5 copies per reaction) density groups prior to PMA treatment. The PMA-treated samples were incubated in the dark for 5 min with occasional mixing and then exposed on ice to a 650 W halogen lamp at a distance of 20 cm for 5 min [13,14,19].

Samples

A total of 72 samples were collected and analyzed from each stage of the treatment process (raw water, sedimentation, sand filtration, ozonation, activated carbon filtration, and final puri-

https://doi.org/10.3347/PHD.26034

fication) in water purification plant A, which produces tap water from the Han River in Seoul, Korea (Fig. 1). To evaluate the seasonal characteristics of the samples, they were collected every month from December 2023 to November 2024. Each sample (2.5 L) was collected in a sterile sample bag, and 2 L of it was centrifuged at 4,000 × g for 15 min. After several stages of centrifugation, the final 1 ml concentrate was transferred to a 1.5-ml microcentrifuge tube and centrifuged at 12,000 × g for 5 min. The pellet was then re-suspended in 1 ml of sterile phosphate-buffered saline (PBS; pH 7.4, Sigma-Aldrich) and the resuspension was divided into 3 aliquots of 250 µl. Each of the first 2 samples was adjusted with sterile PBS to a final volume of 500 µl and used for PMA-qPCR and qPCR analysis. The remaining sample was spiked with 250 µl of viable *A. culbertsoni* trophozoites and analyzed together to evaluate the applicability of PMA-qPCR for field samples. All samples were simultaneously analyzed for turbidity, expressed as nephelometric turbidity units (NTU, Hach), total organic carbon (Ionics), and residual chlorine (except for raw water, Hach), following the Korean standard method for water examination [20].

DNA extraction

PMA treated samples were washed with PBS and centrifuged at 12,000 rpm for 3 min. The total genomic DNA from the samples was extracted by the FastDNA SPIN Kit for Soil (MP Biomedicals) according to the manufacturer's manual.

qPCR

qPCR was performed using a CFX Opus Real-Time PCR system (Bio-Rad). Primers and probes of 2 different sizes targeting the 18S rRNA gene were used to quantify *Acanthamoeba*. To assess the analytical efficiency of the PMA-qPCR assay in relation to amplicon size, 2 primer sets (yielding 180 bp and 420 bp amplicons) were applied to both viable and non-viable *A. culbertsoni* trophozoites (Table 1) [21,22]. The qPCR mixture using a probe contained 12.5 µl of iQ Supermix (Bio-Rad), 0.2 µM of each forward and reverse primer, 0.1 µM of probe, 2 µl of extracted or standard DNA, and PCR-grade water in a 25-µl total volume. The qPCR mixture without a probe contained 12.5 µl of iQ SYBR Green Supermix (Bio-Rad), 0.2 µM of each forward and reverse primer, 2 µl of extracted or standard DNA, and PCR-grade water in a 25-µl total volume. The qPCR protocols were applied according to the respective references. A standard curve was generated using 10-fold serial dilutions of plasmid DNA containing the 18S rRNA gene of *A. culbertsoni* (cloning by Macrogen), which served as a quantitative reference for subsequent qPCR assays. Through this comparative evaluation, the optimal primer sets for the *Acanthamoeba* PMA-qPCR assay were selected.

Statistical analysis

All experiments were performed at least in duplicate, and the qPCR results were expressed as gene copy numbers calculated from a standard curve. The gene copy number data were log-transformed prior to statistical analysis. Statistical analyses were performed using Excel 2021 (Microsoft), and significance was evaluated using *t*-tests. Paired *t*-tests were conducted to compare the PMA-qPCR and qPCR results, as well as the spiked and detected copy numbers in the samples. Differences were considered statistically significant at $P < 0.05$.

Table 1. Primers and probe used for propidium monoazide–real-time PCR

Size (bp)	Sequence (5'→3')	Reference
180	F: CCCAGATCGTTTACCGTGAA	[21]
	R: TAAATATTAATGCCCCCAACTATCC	
	FAM-CTGCCACCGAATACATTAGCATGG-BHQ1	
420–470	F: GGCCCAGATCGTTTACCGTGAA	[22]
	R: TCTCACAAGCTGCTAGGGAGTCA	

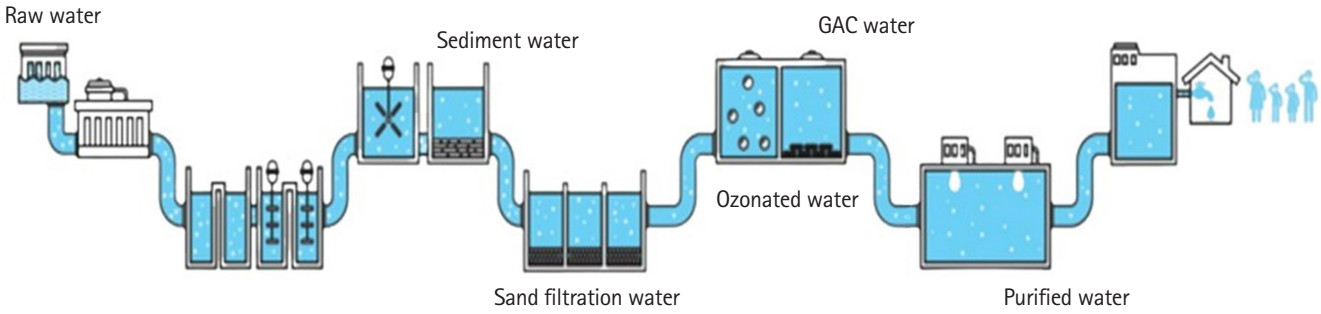


Fig. 1. Sampling points at each stage of water purification plant A.

Results

Optimization of PMA-qPCR

To optimization PMA-qPCR conditions for selective detection of viable *Acanthamoeba* cells, the effects of amplicon length, PMA concentration, and target cell density were evaluated (Figs. 2-4). First, the influence of amplicon length on PMA-qPCR analysis was assessed using primers generating 180 bp and 420 bp amplicons. With the 180 bp primer, treatment with 50 μM PMA resulted in a copy number difference of more than 4.0 log between viable and non-viable cells; however, complete prevention of amplification from non-viable cells required at least 200 μM PMA (Fig. 2A). In contrast, the 420 bp primer completely inhibited amplification from non-viable cell at 50 μM PMA (Fig. 2B). Nevertheless, the PCR efficiency of 420 bp assay (86.2 ± 7.8%) was lower than that of the 180 bp assay (101.7 ± 3.0%) (Table 2). Therefore, the 180 bp primer set was selected for subsequent analyses because it provided higher PCR efficiency while maintaining effective prevention of amplification from non-viable cells (< 1% amplification) following PMA treatment.

In the absence of PMA treatment, some non-viable trophozoites were detected by qPCR (Fig. 3A, B). Treatment with 25 μM PMA reduced the average copy number by 0.3 log compared with the untreated control; however, non-viable trophozoites were not completely excluded. In contrast, no non-viable trophozoites were detected at PMA concentrations of 50 μM or higher. Similarly, non-viable cysts were undetectable following treatment with ≥ 50 μM PMA. These results demonstrate that PMA effectively penetrates non-viable trophozoites and cysts, thereby inhibiting the amplification of their DNA.

PMA-qPCR analysis revealed that the exclusion efficiency of non-viable cells was dependent on the initial target cell density.

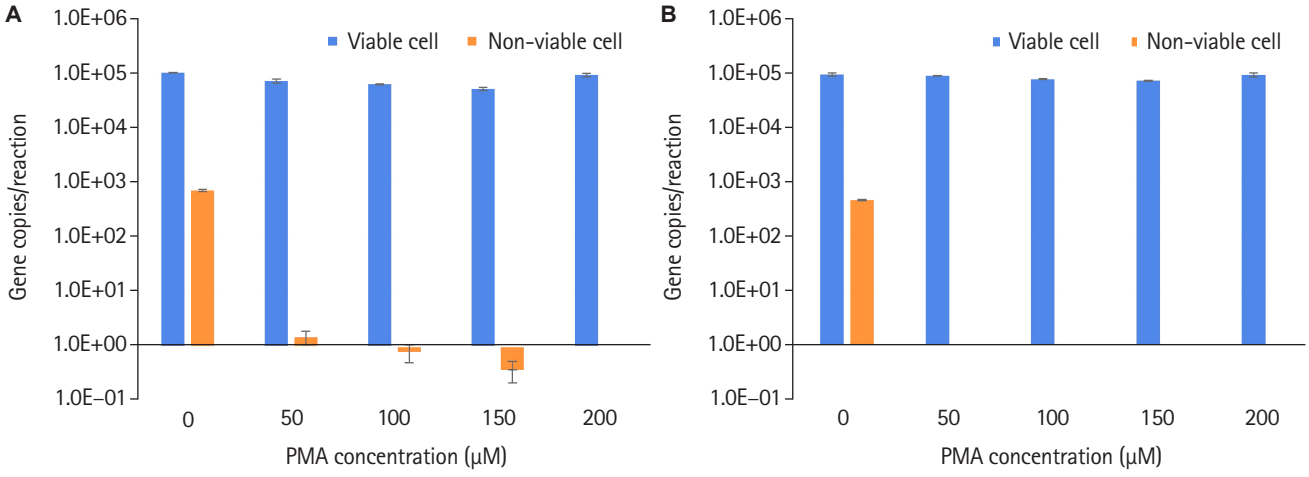


Fig. 2. Effect of amplicon size on the propidium monoazide (PMA) concentration required to inhibit amplification of non-viable *Acanthamoeba culbertsoni*. (A) 180 bp and (B) 420 bp. Error bars represent standard deviations from 2 independent replicates.

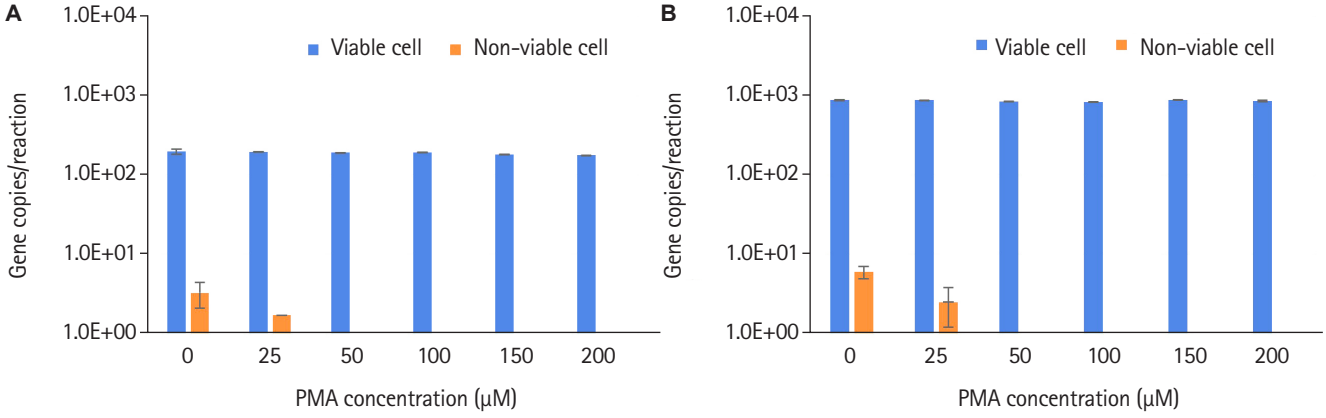


Fig. 3. Effect of propidium monoazide (PMA) concentration on the detection of viable and non-viable *Acanthamoeba culbertsoni* (A) trophozoites and (B) cysts. Error bars represent standard deviations from 2 independent replicates.

https://doi.org/10.3347/PHD.26034

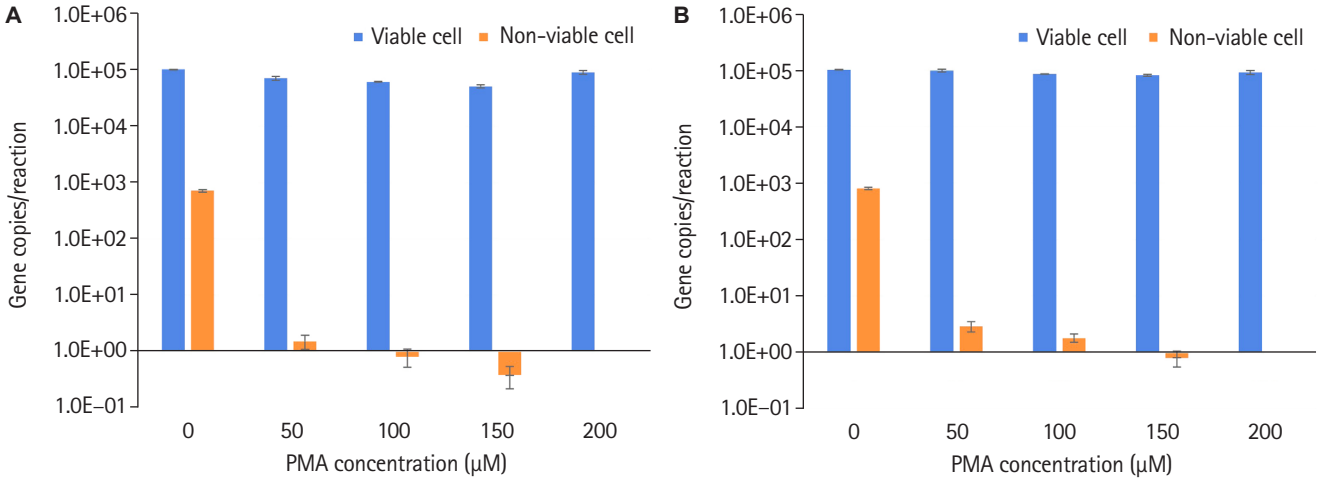


Fig. 4. PMA concentration required for the selective detection of viable *Acanthamoeba* trophozoites at high target copy numbers (10^4–10^5 copies per reaction). (A) *A. culbertsoni* and (B) *A. polyphaga*. Error bars represent standard deviations from 2 independent replicates.

Table 2. Analytical efficiency of propidium monoazide–real-time PCR using primers with different target sizes

Size (bp)	Efficiency (%)				
	1[a]	2	3	Average	SD
180	101.4	98.8	104.8	101.7	3.0
420–470	80.7	91.7	87.3	86.2	7.8

[a]Replicate number.

At lower cell densities (10^2–10^3 copies per reaction), non-viable cells were excluded from detection at 50 μM PMA (Fig. 3). However, at higher cell densities (10^4–10^5 copies per reaction), complete inhibition of non-viable cell detection was achieved only at 200 μM PMA (Fig. 4A, B). Comparable results were obtained for both *A. culbertsoni* and *A. polyphaga*, indicating that the PMA concentration required for the effective exclusion of non-viable cells increases with target cell density.

Applicability of PMA-qPCR in environmental samples

A total of 72 samples were collected from various treatment processes at water purification plant A. Water quality parameters varied across samples, with turbidity ranging from 0.03 to 28.7 NTU, pH from 6.9 to 8.7, total organic carbon from 0.3 to 3.4 mg/L, and residual chlorine from 0.00 to 0.62 mg/L (Table 3). Upon applying the PMA-qPCR method to these environmental samples, the spiked positive control was detected in 71 samples. The copy numbers of the detected positive control showed no statistically significant difference compared to the initial spiked amount ($P > 0.05$). However, the spiked positive control failed to be detected in one raw water sample collected in July. This sample, collected during a period of heavy rainfall, exhibited a turbidity of 28.7 NTU, which was the highest among all analyzed samples; in comparison, the turbidity of the remaining 71 samples ranged from 0.03 to 13.7 NTU.

Consequently, the 71 samples deemed suitable for PMA-qPCR application were analyzed for *Acanthamoeba*. According to the qPCR and PMA-qPCR results for each treatment stage (Fig. 5), the proportion of viable *Acanthamoeba* in raw water was 40.2%, indicating that approximately 60% of the detected population was in a non-viable state. In sedimented water, viable *Acanthamoeba* decreased by more than 50% compared to raw water, and no viable *Acanthamoeba* were detected in the final purified water (Fig. 5). Conventional qPCR detected total *Acanthamoeba* DNA at an average of 452 copies/L in raw water and 10 copies/L in purified water. In contrast, PMA-qPCR, through the selective amplification of viable *Acanthamoeba*, yielded an average of 182 copies/L in raw water. This value further declined during the treatment process, rendering the target undetectable after the activated carbon filtration stage (Fig. 5).

Discussion

Our results demonstrated that the performance of PMA-qPCR is influenced by both the *Acanthamoeba* density and the target amplicon length. When primers and probes targeting a 180 bp amplicon were applied, complete prevention of non-viable cell detection was achieved at a PMA concentration of 200 μM for an initial density of approximately 10^5 gene copies/reaction (Fig. 4). Conversely, at lower initial densities (10^2–10^3 gene copies/reaction), non-viable cells were successfully excluded from detection using 50 μM PMA (Fig. 3). Moreover, when using amplicons longer than 400 bp, preven-

Table 3. Measurement results of water quality parameters in process water at water purification plant A

Sample type	Turbidity (NTU)	pH	TOC (mg/L)	Residual chlorine (mg/L)
Raw water	7.1 (1.8–28.7)	7.8 (7.1–8.7)	2.0 (1.6–3.4)	-
Sediment water	0.49 (0.24–0.78)	7.2 (6.9–7.5)	1.0 (0.3–1.6)	0.31 (0.16–0.62)
Sand filtration water	0.05 (0.03–0.13)	7.3 (7.0–7.6)	0.9 (0.3–1.2)	0.32 (0.12–0.59)
Ozonated water	0.16 (0.06–0.77)	7.2 (6.9–7.6)	0.9 (0.3–1.4)	0.20 (0.00–0.60)
GAC water	0.09 (0.04–0.14)	7.2 (6.9–7.5)	0.7 (0.3–1.2)	0.04 (0.01–0.07)
Purified water	0.05 (0.04–0.09)	7.1 (6.9–7.3)	0.6 (0.3–0.8)	0.52 (0.34–0.62)

Values are presented as average (range).
NTU, nephelometric turbidity units; TOC, total organic carbon; GAC, granular activated carbon.

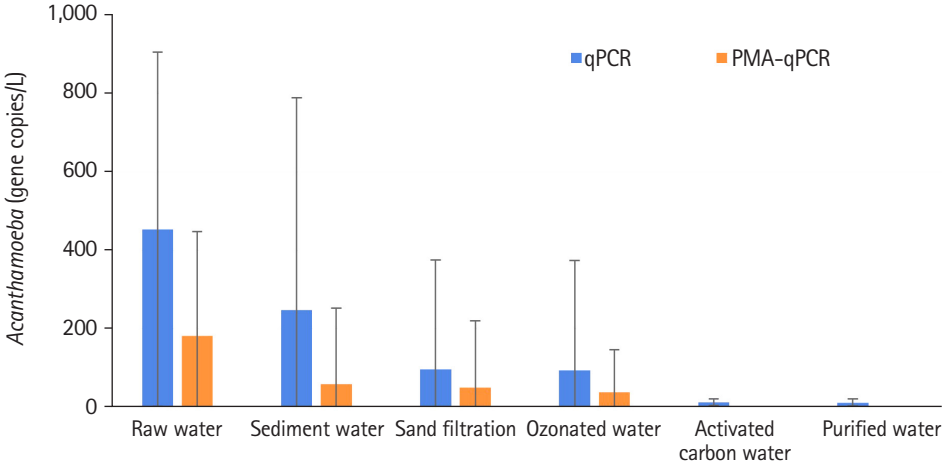


Fig. 5. Distribution of *Acanthamoeba* DNA across water treatment stages determined by real-time PCR (qPCR) and propidium monoazide (PMA)-qPCR. Error bars indicate standard deviations from 71 environmental samples analyzed in duplicate.

tion of non-viable cell detection was achieved at 50 μM PMA, even at high initial densities (10^5 gene copies/reaction). Previous studies have typically employed a PMA concentration of 200 μM, likely because they focused on the diagnosis and treatment of *Acanthamoeba*-related keratitis, where relatively high densities (≥ 10^5 cells/ml) were expected [16,17]. In contrast, the present study targeted environmental water samples, in which *Acanthamoeba* densities in raw water from the Han River were typically below 10^3 gene copies/L (Fig. 5). Given these relatively low densities, a PMA concentration of 50 μM was selected. Under these conditions, 50 μM PMA was sufficient to prevent the detection of non-viable trophozoites and cysts without affecting the detection of viable *Acanthamoeba*.

Furthermore, as the target amplicon size increased, the PMA concentration required to completely eliminate amplification from non-viable cells decreased from 200 to 50 μM. Several studies have reported that longer PCR amplicons are more effective at excluding signals from non-viable cells, likely because the probability of PMA binding to DNA increases with amplicon length [12,23-25]. However, amplicons longer than 400 bp were associated with reduced PCR efficiency. Therefore, selecting an optimal target amplicon size that minimizes amplification from non-viable cells while maintaining high PCR efficiency is crucial for successful PMA-qPCR analysis. Based on these findings, when analyzing samples with high densities of *Acanthamoeba* (e.g., clinical keratitis samples or heavily contaminated water), it may be more appropriate not only to increase the PMA concentration but also to design primers and probe targeting amplicons in the range of 200–300 bp.

The PMA-qPCR method successfully detected viable *Acanthamoeba* across the 71 environmental samples collected at various stages of the water treatment process, thereby demonstrating its utility as a rapid, culture-independent detection approach. These findings highlight that, due to the presence of non-viable *Acanthamoeba* in process water, conventional gene-based qPCR may overestimate microbial densities, whereas PMA-qPCR provides a more accurate assessment by selectively detecting viable cells. As the treatment progressed,

https://doi.org/10.3347/PHD.26034

the density of viable *Acanthamoeba* cells gradually decreased (Fig. 5). Notably, during the sedimentation stage following coagulation, the number of viable cells decreased by more than 50% on average compared to the raw water, indicating that this process is highly efficient at removing *Acanthamoeba*. After the granular activated carbon filtration stage, viable *Acanthamoeba* were no longer detected, confirming that the current treatment process is effective in eliminating these pathogenic amoebae. In contrast, samples not treated with PMA showed the presence of non-viable *Acanthamoeba*, further reinforcing the high utility of the PMA-qPCR method for viable cell selection.

The PMA-qPCR method was successfully applied to all samples throughout the treatment process; however, it failed for a single raw water sample with a turbidity of 28.7 NTU. This limitation was likely due to the high turbidity caused by heavy rainfall, which introduced suspended solids and other interfering substances into the sample, thereby reducing light transmission and diminishing the efficiency of PMA treatment [16,19,26]. Turbidity can negatively affect PMA activation not only by scattering and absorbing light but also by altering dye availability through interactions with organic matter [19]. Previous studies have reported that high levels of suspended solids or sludge matrices can substantially reduce the effectiveness of PMA-qPCR, requiring assay optimization to maintain reliable discrimination between viable and non-viable cells [23,27]. Based on these results, the PMA-qPCR method is applicable to environmental water samples with turbidity levels of up to 13.7 NTU. For samples exceeding this threshold, further research is needed to improve PMA treatment efficiency. Potential strategies include reducing sample volume, applying pre-dilution to lower turbidity, or exploring alternative light sources with stronger penetration capacity [19,26]. However, dilution must be carefully considered, as it may compromise detection in samples with low densities of target microorganisms [26]. For instance, as observed in our study where the average density of viable *Acanthamoeba* was only 182 copies/L, dilution of the sample could increase the risk of false-negative results. The findings of this study were obtained from a single water treatment plant located on the Han River, and conditions may differ in other source waters or treatment plants employing different processes. In addition, non-viable *Acanthamoeba* cells used for PMA-qPCR optimization were generated by heat treatment, which provided a practical and reproducible approach for preparing non-viable control cells. However, heat-induced cell damage may differ from that caused by chemical disinfectants commonly used in water treatment processes, such as chlorine and ozone. Future studies incorporating chlorine- or ozone-inactivated *Acanthamoeba* cells would help to better reflect real-world water treatment conditions and further validate the applicability of PMA-qPCR for assessing *Acanthamoeba* viability in drinking water systems.

In conclusion, the PMA-qPCR method was validated as an effective technique for detecting the viable trophozoites and cysts of pathogenic *Acanthamoeba* in environmental water. Unlike conventional culture methods, this approach significantly reduces analysis time to a few hours, enabling the rapid detection of viable *Acanthamoeba*. Therefore, this method can be utilized to evaluate the efficiency of water treatment processes aimed at removing *Acanthamoeba* and to monitor safety during the water supply distribution. Ultimately, it is expected to contribute to the safe and hygienic management of tap water, ensuring protection against pathogenic microorganisms and thereby mitigating public health risks.

Author contributions

Conceptualization: Lee ES. Investigation: Lee ES, Lee JY. Methodology: Lee ES, Lee JY, Baek YA, Cho SJ. Validation: Lee ES, Baek YA, Cho SJ. Writing - original draft: Lee ES. Writing - review & editing: Lee JY, Baek YA, Cho SJ.

Conflict of interest

The authors have no conflicts of interest to declare.

ORCID

Eun-Sook Lee, https://orcid.org/0000-0003-3516-4649
Ji-Yeon Lee, https://orcid.org/0009-0006-6394-3104
Young-Ae Baek, https://orcid.org/0000-0003-4189-7689
Seok-Ju Cho, https://orcid.org/0000-0003-1008-5215

References

1. Marciano-Cabral F, Cabral G. *Acanthamoeba* spp. as agents of disease in humans. Clin Microbiol Rev 2003;16:273-307. https://doi.org/10.1128/cmr.16.2.273-307.2003
2. Muchesa P, Mwamba O, Barnar TG, Bartie C. Detection of free-living amoebae using amoebal enrichment in a wastewater treatment plant of Gauteng Province, South Africa. BioMed Res Int 2014;2014:575297. https://doi.org/10.1155/2014/575297
3. Dupuy M, Berne F, Herbelin P, et al. Sensitivity of free-living amoeba trophozoites and cysts to water disinfectants. Int J Hyg Environ Health 2014;217:335-9. https://doi.org/10.1016/j.ijheh.2013.07.007
4. Loret JF, Greub G. Free-living amoebae: biological by-passes in wa-

ter treatment. Int J Hyg Environ Health 2010;213:167-75. https://doi.org/10.1016/j.ijheh.2010.03.004
5. Horn M, Wagner M. Bacterial endosymbionts of free-living amoebae. J Eukaryot Microbiol 2004;51:509-14. https://doi.org/10.1111/j.1550-7408.2004.tb00278.x
6. Pagnier I, Merchat M, La Scola B. Potentially pathogenic amoeba-associated microorganisms in cooling towers and their control. Future Microbiol 2009;4:615-29. https://doi.org/10.2217/fmb.09.25
7. Steinert M, Birkness K, White E, Fields B, Quinn F. *Mycobacterium avium* bacilli grow saprozoically in coculture with *Acanthamoeba polyphaga* and survive within cyst walls. Appl Environ Microbiol 1998;64:2256-61. https://doi.org/10.1128/AEM.64.6.2256-2261.1998
8. Barker J, Brown MR, Collier PJ, Farrell I, Gilbert P. Relationship between *Legionella pneumophila* and *Acanthamoeba polyphaga*: physiological status and susceptibility to chemical inactivation. Appl Environ Microbiol 1992;58:2420-5. https://doi.org/10.1128/aem.58.8.2420-2425.1992
9. Cirillo JD, Falkow S, Tompkins LS, Bermudez LE. Interaction of *Mycobacterium avium* with environmental amoebae enhances virulence. Infect Immun 1997;65:3759-67. https://doi.org/10.1128/iai.65.9.3759-3767.1997
10. Beattie TK, Seal DV, Tomlinson A, McFadyen AK, Grimason AM. Determination of amoebicidal activities of multipurpose contact lens solutions by using a most probable number enumeration technique. J Clin Microbiol 2003;41:2992-3000. https://doi.org/10.1128/JCM.41.7.2992-3000.2003
11. Rivière D, Szczebara FM, Berjeaud J, Frère J, Héchard Y. Development of a real-time PCR assay for quantification of *Acanthamoeba* trophozoites and cysts. J Microbiol Methods 2006;64:78-83. https://doi.org/10.1016/j.mimet.2005.04.008
12. Chang B, Taguri T, Sugiyama K, et al. Comparison of ethidium monoazide and propidium monoazide for the selective detection of viable *Legionella* cells. Jpn J Infect Dis 2010;63:119-23. https://doi.org/10.7883/yoken.63.119
13. Nocker A, Cheung CY, Camper AK. Comparison of propidium monoazide with ethidium monoazide for differentiation of live vs. dead bacteria by selective removal of DNA from dead cells. J Microbiol Methods 2006;67:310-20. https://doi.org/10.1016/j.mimet.2006.04.015
14. Nocker A, Mazza A, Masson L, Camper AK, Brousseau R. Selective detection of live bacteria combining propidium monoazide sample treatment with microarray technology. J Microbiol Methods 2009;76:253-61. https://doi.org/10.1016/j.mimet.2008.11.004
15. Kralik P, Nocker A, Pavlik I. *Mycobacterium avium* subsp. *paratuberculosis* viability determination using F57 quantitative PCR in combination with propidium monoazide treatment. Int J Food Microbiol 2010;141 Suppl 1:S80-6. https://doi.org/10.1016/j.ijfoodmicro.2010.03.018
16. Fittipaldi M, Rodriguez NJP, Adrados B, et al. Discrimination of viable *Acanthamoeba castellani* trophozoites and cysts by propidium monoazide real-time polymerase chain reaction. J Eukaryot Microbiol 2011;58:359-64. https://doi.org/10.1111/j.1550-7408.2011.00557.x
17. Veugen JMJ, Savelkoul PHM, Nuijts RMMA, Dickman MM, Wolffs PFG. Enhancing *Acanthamoeba* diagnostics: rapid detection of viable *Acanthamoeba* trophozoites and cysts using viability PCR assay. Microbiol Spectr 2025;13:e0181124. https://doi.org/10.1128/spectrum.01811-24
18. Visvesvara GS, Balamuth W. Comparative studies on related free-living and pathogenic amebae with special reference to *Acanthamoeba*. J Protozool 1975;22:245-56. https://doi.org/10.1111/j.1550-7408.1975.tb05860.x
19. Fittipaldi M, Nocker A, Codony F. Progress in understanding preferential detection of live cells using viability dyes in combination with DNA amplification. J Microbiol Methods 2012;91:276-89. https://doi.org/10.1016/j.mimet.2012.08.007
20. Ministry of Environment. Korean standard method for the examination of water. Ministry of Environment; 2013.
21. Quarnstrom Y, Visvesvara GS, Sriram R, da Silva AJ. Multiplex real-time PCR assay for simultaneous detection of *Acanthamoeba* spp., *Balamuthia mandrillaris*, and *Naegleria fowleri*. J Clin Microbiol 2006;44:3589-95. https://doi.org/10.1128/jcm.00875-06
22. Schroeder JM, Booton GC, Hay J, et al. Use of subgenic 18S ribosomal DNA PCR and sequencing for genus and genotype identification of *Acanthamoebae* from humans with keratitis and from sewage sludge. J Clin Microbiol 2001;39:1903-11. https://doi.org/10.1128/jcm.39.5.1903-1911.2001
23. Luo JF, Lin WT, Guo Y. Method to detect only viable cells in microbial ecology. Appl Microbiol Biotechnol 2010;86:377-84. https://doi.org/10.1007/s00253-009-2373-1
24. Contreras PJ, Urrutia H, Sossa K, Nocker A. Effect of PCR amplicon length on suppressing signals from membrane-compromised cells by propidium monoazide treatment. J Microbiol Methods 2011;87:89-95. https://doi.org/10.1016/j.mimet.2011.07.016
25. Soejima T, Iida K, Qin T, et al. Method to detect only live bacteria during PCR amplification. J Clin Microbiol 2008;46:2305-13. https://doi.org/10.1128/jcm.02171-07
26. Yuan Y, Zheng G, Lin M, Mustapha A. Detection of viable *Escherichia coli* in environmental water using combined propidium monoazide staining and quantitative PCR. Water Res 2018;145:398-407. https://doi.org/10.1016/j.watres.2018.08.044
27. Bae S, Wuertz S. Discrimination of viable and dead fecal *Bacteroidales* bacteria by quantitative PCR with propidium monoazide. Appl Environ Microbiol 2009;75:2940-4. https://doi.org/10.1128/AEM.01333-08

Original Article

Parasites Hosts Dis 2026;64(4):337-349
https://doi.org/10.3347/PHD.26037

Parasites, Hosts and Diseases

pISSN 2982-5164 • eISSN 2982-6799

Zoonotic and prey-derived protozoa in Tibetan fox (*Vulpes ferrilata*) and other wild canids: Implications for public health in the eastern Tibetan Plateau

Xueying Deng[1], Chuizhao Xue[2,3,4,5], Qilu Chen[6,7], Qingqiu Zuo[2,3,4,5], Mengqing Li[2,3,4,5], Xiaoxue Peng[8], Peng Li[1,*], Xu Wang[2,3,4,5,*]

[1]Chengdu Center for Disease Control and Prevention (Chengdu Institute of Health Supervision), Chengdu, China; [2]National Key Laboratory of Intelligent Tracking and Forecasting for Infectious Diseases, National Institute of Parasitic Diseases, Chinese Center for Disease Control and Prevention (Chinese Center for Tropical Diseases Research), Shanghai, China; [3]Key Laboratory on Parasite and Vector Biology, National Health Commission of the People's Republic of China, Shanghai, China; [4]World Health Organization Collaborating Centre for Tropical Diseases, Shanghai, China; [5]National Center for International Research on Tropical Diseases, Ministry of Science and Technology, Shanghai, China; [6]Anhui Provincial Center for Diseases Control and Prevention, Hefei, China; [7]Anhui Provincial Academy of Preventive Medicine, Hefei, China; [8]Chongqing Three Gorges Medical College, Chongqing, China

Enteric protozoan infections—cryptosporidiosis, giardiasis, microsporidiosis, and coccidiosis—constitute a significant global burden on human and animal health. Yet comprehensive parasitological surveys of wildlife in the eastern Tibetan Plateau, where anthropogenic, livestock, and wildlife activities extensively intersect, remain deficient. We collected 359 fecal specimens from wild carnivores across 98 random quadrats and employed molecular techniques for host identification and protozoan screening. Seven carnivore species were identified, with Tibetan fox (*Vulpes ferrilata*) predominating. Intestinal protozoa were exclusively recovered from *Vulpes* species, yielding a prevalence of 19.37% (68/351; 95% CI, 15.24%–23.51%). *Eimeria falciformis* (7.41%, 26/351) and *Eimeria banffensis* (7.12%, 25/351) were the most frequently detected, followed by *Enterocytozoon bieneusi* (3.70%, 13/351). *Cryptosporidium* was confirmed in one *V. ferrilata*, and *Giardia intestinalis* in 2 samples (*V. ferrilata* and *Vulpes vulpes*). This investigation furnishes the first molecular evidence that wild carnivores, especially *V. ferrilata*, harbor zoonotic protozoa including *G. intestinalis* assemblage AII and *E. bieneusi* genotypes PigEBITS5 and a D-like variant. The concurrent detection of *Cryptosporidium* yak genotype and *E. bieneusi* subgroup 1i in foxes, pikas, yaks, and sheep implies potential interspecies transmission at the wildlife–livestock interface. These findings fill knowledge gaps in regional parasite diversity and emphasize the need for enhanced surveillance of wildlife-borne protozoa under a One Health framework, thereby providing scientific evidence for zoonotic risk assessment and public health planning.

Keywords: Protozoa, Tibetan Plateau, Carnivores, *Cryptosporidium*, *Giardia intestinalis*, *Enterocytozoon bieneusi*

Introduction

Protozoa comprise a highly diverse group of single-celled eukaryotic microorganisms, many of which are pathogenic and exhibit a global distribution. Diseases caused by these protozoa are especially prevalent in tropical and subtropical regions due to conducive environmental conditions and socioeconomic factors [1]. Zoonotic protozoan infections pose serious threats to human health worldwide. Notable examples include cryptosporidiosis, giardiasis, and microsporidiosis, which can lead to

Received: April 20, 2026 Accepted: June 22, 2026
*Correspondence: pl, 441739496@qq.com; xw, wangxu@nipd.chinacdc.cn

© 2026 The Korean Society for Parasitology and Tropical Medicine
This is an open-access article distributed under the terms of the Creative Commons Attribution Non-Commercial License (http://creativecommons.org/licenses/by-nc/4.0/) which permits unrestricted non-commercial use, distribution, and reproduction in any medium, provided the original work is properly cited.

Citation
Deng X, Xue C, Chen Q, Zuo Q, Li M, Peng X, Li P, Wang X. Zoonotic and prey-derived protozoa in Tibetan fox (*Vulpes ferrilata*) and other wild canids: Implications for public health in the eastern Tibetan Plateau. Parasites Hosts Dis 2026;64(4):337-349.

chronic diarrhea, severe emaciation, and elevated mortality among immunocompromised individuals. In children, these infections are associated with growth retardation and impaired cognitive development [2]. In China, intestinal protozoan diseases have emerged as a significant public health challenge, predominantly caused by such pathogens as *Cryptosporidium* spp. and *Giardia intestinalis* [3]. With the expansion of animal husbandry and increased human encroachment into wildlife habitats, the risk of pathogens carried by wildlife contaminating water sources or the food chain and transmitting to humans and livestock has risen significantly [4]. Studies conducted in the Americas and Europe have confirmed that wild canids such as coyotes (*Canis latrans*) and red foxes (*Vulpes vulpes*) serve as reservoirs for various zoonotic protozoa, including *Cryptosporidium* spp. and *G. intestinalis*. Some detected strains show high genetic homology with those found in human clinical cases, suggesting possible cross-species transmission and shared infection sources [5]. Additionally, other protozoan species such as *Enterocytozoon bieneusi* and *Eimeria* spp. are highly prevalent in wildlife populations. These pathogens can be widely disseminated into the environment through fecal excretion, thereby posing continued risks to human and animal health [6]. These findings collectively indicate that wildlife-origin protozoa may increasingly spill over into human populations through ecological interfaces, thereby creating multifaceted and evolving public health concerns. Understanding the transmission dynamics and host range of these protozoans is critical for assessing emerging zoonotic risks and developing effective control strategies.

The eastern Tibetan Plateau, a global biodiversity hotspot, sustains a unique ecosystem with extensive overlap between wildlife habitats and human activities. Dominated by pastoral economies, this region exposes herders and livestock (e.g., yaks and sheep) to wildlife-inhabited areas, amplifying risks of cross-species pathogen transmission. Previous investigations revealed that the area's complex topography and climatic diversity support rich carnivore communities, including canids like the Tibetan fox (*Vulpes ferrilata*), red fox, and wolf (*Canis lupus*), alongside rare species such as the Tibetan brown bear (*Ursus arctos pruinosus*) and snow leopard (*Panthera uncia*). These animals harbor diverse parasites, including helminths transmissible to humans or livestock [7]. Since wildlife and domestic animals in this region share grazing routes and water sources, a "bridge" for bidirectional pathogen transmission may form [8]. However, current parasite surveillance systems primarily focus on humans and livestock, resulting in fragmented data on wildlife parasites, which hinders the assessment of their role as hosts and their zoonotic potential.

This study utilizes molecular methods to systematically characterize the species composition of wild carnivores in the eastern Tibetan Plateau, along with the genetic characteristics, prevalence, and public health risks of high-priority zoonotic protozoa (*Cryptosporidium* spp. and *G. intestinalis*) and highly prevalent protozoa with cross-species transmission potential (*Eimeria* spp. and *E. bieneusi*). The research aims to fill the gap in baseline parasitological data for this region, provide a scientific basis for assessing zoonotic disease risks, and offer theoretical support for formulating One Health-oriented prevention and control strategies.

Methods

Ethics statement

Ethical approval was not applicable because this study involved only the collection of fecal samples from free-ranging wild carnivores, with no direct contact with or disturbance to the animals.

Sample collection and processing

This study was conducted in November 2021 and November 2023 in the border region of Sichuan, Xizang, and Qinghai provinces on the eastern Tibetan Plateau, with Shiqu County, Sichuan Province serving as the primary sampling area (Fig. 1). Using a randomized sampling design, 98 environmental quadrats measuring 50 m × 200 m were established. Within each quadrat, all visible fecal samples of wild carnivores were systematically collected using disposable sampling forceps, transferred to 50 ml centrifuge tubes, and preserved with 95% ethanol. Samples were transported to the laboratory and stored at -80°C in an ultra-low temperature freezer for at least 1 week to inactivate potential pathogens. After initial morphological screening, weathered or fragmented samples were excluded, resulting in 436 intact samples retained for subsequent analysis.

DNA extraction and host identification

Genomic DNA was extracted from fecal samples using the QIAamp Fast DNA Stool Mini Kit (Qiagen). Host species were identified by amplifying the vertebrate-specific 16S rRNA gene fragment using universal primers (V-16S). Primer sequences are listed in Table 1 [9-13]. The PCR mixture (25 μl) consisted of 1 μl each of forward and reverse primers, 12 μl of Ex Taq PCR Premix (RR902A, Takara), 0.5 μl of bovine serum albumin (Takara), 2 μl of template DNA, and RNase-free water (Takara) to

https://doi.org/10.3347/PHD.26037

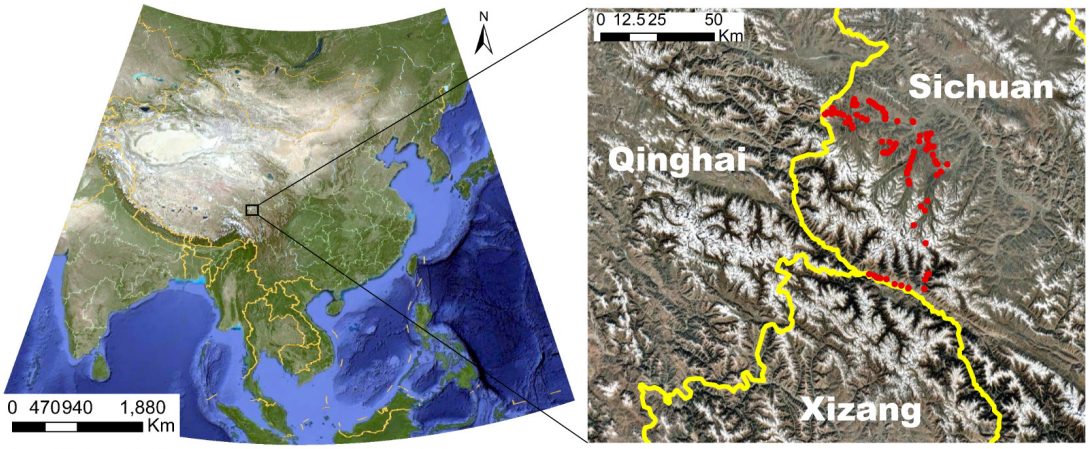


Fig. 1. Study area. The red points represent the coordinate points of the sample quadrats and the yellow lines represent the provincial boundaries.

Table 1. Sequences of the host and protozoan primers and annealing temperature of PCR in this study

Primers	Classification	Primer names	Target genes	Primer sequences (from 5'→3')	Product length (bp)	Annealing temperature (°C)	References
Universal primers for host recognition	Vertebrate	V-16S	16S ribosomal RNA (*16S rRNA*)	F: GAGAAGACCCTATGGAGC R: ATAGAAACCGACCTGGAT	380	55	[9]
Specific primers for parasite detection	*Cryptosporidium*	CRY	Small subunit ribosomal RNA (*SSU rRNA*)	F1: TTCTAGAGCTAATACATGCG R1: CCCATTTCCTTCGAAACAGGA	~1,325	55	[10]
				F2: GGAAGGGTTGTATTTATTAGATAAAG R2: AAGGAGTAAGGAACAACCTCCA	830	55	
	Giardia intestinalis	GITS	Triosephosphate isomerase (*TPI*)	F1: AAATIATGCCTGCTCGTCG R1: CAAACCTTITCCGCAAACC	605	50	[11]
				F2: CCCTTCATCGGIGGTAACTT R2: GTGGCCACCACICCCGTGCC	530	50	
	Enterocytozoon bieneusi	EB	Internal transcribed spacer 1 (*ITS1*)	F1: GGTCATAGGGATGAAGAG R1: TTCGAGTTCTTTCGCGCTC	410	57	[12]
				F2: GCTCTGAATATCTATGGCT R2: ATCGCCGACGGATCCAAGTG	392	55	
	Eimeria	ESSU	*SSU rRNA*	F1: TACCCAATGAAAACAGTTT R1: CAGGAGAAGCCAAGGTAGG	636	53.6	[13]
				F2: CCTTCCGCGCTTCGCTGCGT R2: CGTCTTCAAACCCCCTACTG	294	66.5	

adjust the final volume. Amplification conditions were as follows: initial denaturation at 94°C for 5 min; 35 cycles of denaturation at 94°C for 30 sec, annealing at 55°C for 30 sec, and extension at 72°C for 30 sec; followed by a final extension at 72°C for 10 min. PCR products were stored at 4°C. PCR products were visualized by 1% agarose gel electrophoresis (120 V, 30 min), and positive products were sent to Sangon Biotech for molecular cloning (10 clones per sample) and sequencing. Host and prey species were identified by comparing the sequencing results with the NCBI database (https://blast.ncbi.nlm.nih.gov/Blast.cgi). The percent coverage and percent identity of the BLAST hits were above 99%.

Intestinal protozoan detection

Protozoa were detected using specific primers targeting the small subunit rRNA (*SSU rRNA*) gene for *Cryptosporidium* spp. and *Eimeria* spp., the triosephosphate isomerase (*TPI*) gene for *G. intestinalis*, and the internal transcribed spacer 1 (*ITS1*) region for *E. bieneusi* (Table 1) [9-13]. The reaction systems were consistent with those used for the host identification. The amplification conditions of each protozoan are listed in Table 1 [9-13], for example, for the detection of *Cryptosporidium* spp., a nested PCR approach was employed: the first round used primers CRY-F1/R1 (amplicon size: ~1,325 bp), and the second round used CRY-F2/R2 (about 830 bp), both with an annealing

temperature of 55°C. PCR products were purified and subjected to molecular cloning (5 clones per sample) when overlapping peaks were observed in sequencing chromatograms. Otherwise, products were directly sequenced by Sangon Biotech. Species or genotypes were determined by comparing obtained sequences with reference sequences in the NCBI database.

Phylogenetic analysis

Sequences were assembled and edited using DNAStar 7.0 (DNASTAR). Multiple sequence alignment and editing were performed using the ClustalW algorithm alongside reference sequences retrieved from GenBank. Haplotypes were identified using DnaSP version 6.12. The optimal nucleotide substitution model was selected with jModelTest 2.1.10 under the Akaike Information Criterion. The *TVM+I+G*, *TIM3+I+G*, *TrN+I+G*, and *TPM1uf+G* models were applied for phylogenetic analyses of *Cryptosporidium* sp., *G. intestinalis*, *Eimeria* spp., and *E. bieneusi*, respectively. Bayesian inference trees were constructed using MrBayes 3.2.4, running Markov Chain Monte Carlo simulations for 1,000,000 generations with sampling every 1,000 generations. The first 25% of samples were discarded as burn-in before summarizing the tree topology. Final trees were visualized and annotated using iTOL v7.2.1 (https://itol.embl.de/itol.cgi).

Statistics and visualization

Data on host identification and protozoan detection were compiled and analyzed using R version 4.3.2 (https://www.r-project.org). Differences in detection rates among groups were assessed using chi-square tests. Data were visualized using the Hiplot Pro platform (Shanghai Tengyun Biotechnology, https://hiplot.com.cn/).

Results

Host identification

A total of 436 wild carnivore fecal samples were collected from the eastern Tibetan Plateau. Host species were successfully identified for 359 samples (82.34%) via 16S rRNA gene sequencing, representing 7 carnivore species across 4 families: Canidae (354/359, 98.61%), Mustelidae (3/359, 0.84%), Ursidae (1/359, 0.28%), and Felidae (1/359, 0.28%). The Tibetan fox (*V. ferrilata*) was the predominant species (307/359, 85.52%), followed by the red fox (*V. vulpes*; 44/359, 12.26%) and the wolf (*C. lupus*; 3/359, 0.84%). Mustelid samples included 2 Asian badgers (*Meles leucurus*) and one mountain weasel (*Mustela altaica*). Single samples were identified for the Tibetan brown bear (*U. arctos pruinosus*) and leopard cat (*Prionailurus bengalensis*).

Protozoan haplotype identification

Eight distinct protozoan haplotypes were identified from 359 samples. *Cryptosporidium* was confirmed in *V. ferrilata* feces (haplotype CHSQ.C.36.7, 100% identical to sequence KF971356 from GenBank). *Giardia intestinalis* (haplotype CHSQ.G.13.9, 99.09% similarity to MN844148) was detected in both *V. ferrilata* and *V. vulpes*. *Eimeria banffensis* (CHSQ.E.25.5, 100% match to PP594267) occurred in both *Vulpes* species, while *Eimeria falciformis* (CHSQ.E.23.8, 100% match to MH752019) and a novel *Eimeria* sp. (CHSQ.E.25.4, 99.25% similarity to OP352330) were only detected in *V. ferrilata*. Three *E. bieneusi* haplotypes (CHSQ.E.4.8, CHSQ.E.8.3, and CHSQ.E.4.2) were identified solely in *V. ferrilata* (Table 2). All sequences were deposited in GenBank under accession numbers PX249759, PX262650, PX249765–PX249767, and PX262653–PX262655.

Phylogenetic analysis

Phylogenetic analysis revealed that the only *Cryptosporidium* sp. strain detected in *V. ferrilata* samples (CHSQ.C.36.7), together with isolates from yak (*Bos grunniens*) in Qinghai (GenBank accession No. KF971356) and plateau pika (*Ochotona curzoniae*) in Sichuan (PV523163), formed a distinct clade (100% bootstrap support). This clade corresponds to the previously described *Cryptosporidium* sp. yak genotype (Fig. 2). The phylogenetic tree of *G. intestinalis* displayed 7 well-supported clades corresponding to Assemblages A–G. The 2 *G. intestinalis* strains identified in this study (both from *V. ferrilata* and *V. vulpes* samples and belonging to a single haplotype CHSQ.G.13.9), were placed within the subclade AII of Assemblage A (98% support) (Fig. 3). A phylogenetic tree constructed using *Eimeria* sp. sequences from NCBI and haplotype sequences from this study resolved into 6 major clades, each associated with a specific group of host animals (e.g., birds, ungulates, and rodents). Among these, *E. banffensis* from this study (CHSQ.E.25.5) clustered with 2 other *E. banffensis* strains (both from pika hosts) with 93% support. Another strain, *E. falciformis* (CHSQ.E.23.8), clustered within a clade comprising other *Eimeria* species (such as *E. fluviatilis*, *E. vermiformis*, *E. falciformis*, and *E. apionodes*), all of which are known to infect voles (e.g., *Myocastor coypus*, *Apodemus flavicollis*, and *Myodes glareolus*). Additionally, CHSQ.E.25.4 clustered (84% support) with *E. magna*, *E. vejdovskyi*, *E.*

https://doi.org/10.3347/PHD.26037

Table 2. Eight protozoan haplotypes from wild carnivores in the eastern Tibetan Plateau matched with NCBI GenBank

Haplotype names	No. of samples	Host (no. of samples)	NCBI accession No.	Coverage and similarity of the most similar sequences in GenBank (%)	Species with the closest sequence in GenBank	Genotype of the closest sequence in GenBank
CHSQ.C.36.7	1	*Vulpes ferrilata* (1)	PX249759	KF971356 (100%, 100%)	*Cryptosporidium*	Yak genotype
CHSQ.G.13.9	2	*V. ferrilata* (1) *Vulpes vulpes* (1)	PX262650	MN844148 (100%, 99.09%)	*Giardia intestinalis*	Assemblage AII
CHSQ.E.25.5	25	*V. ferrilata* (23) *V. vulpes* (2)	PX249765	PP594267 (100%, 100%)	*Eimeria banffensis*	-
CHSQ.E.23.8	26	*V. ferrilata* (26)	PX249766	MH752019 (100%, 100%)	*Eimeria falciformis*	-
CHSQ.E.25.4	1	*V. ferrilata* (1)	PX249767	OP352330 (100%, 99.25%)	*Eimeria magna*	-
CHSQ.E.4.2	11	*V. ferrilata* (11)	PX262653	MN190621 (100%, 99.19%)	*Enterocytozoon bieneusi*	D genotype
CHSQ.E.4.8	1	*V. ferrilata* (1)	PX262654	MZ090559 (100%, 99.59%)	*E. bieneusi*	ST3
CHSQ.E.8.3	1	*V. ferrilata* (1)	PX262655	OL411937 (100%, 100%)	*E. bieneusi*	PigEBITS5

stiedai, *E. intestinalis*, and *E. coecicola*, species primarily reported in European rabbits (*Oryctolagus cuniculus*) (Fig. 4). The phylogenetic tree of *E. bieneusi* was divided into 15 genetic groups (Groups 1–15), with Group 1 further subdivided into 9 subgroups (a–i). All *E. bieneusi* haplotypes in this study belonged to Group 1: CHSQ.E.4.8 (99.59% similarity to ST3, MZ090559) formed subgroup 1i with genotypes from yak and sheep on the Tibetan Plateau; CHSQ.E.8.3 (100% identity to PigEBITS5, OL411937) clustered in subgroup 1e (hosts: pigs, sheep, humans); CHSQ.E.4.2 (99.19% similarity to genotype D, MN190621) fell within subgroup 1a, which includes known human-pathogenic genotypes, such as Henan V and Peru10 (Table 2; Fig. 5).

Intestinal protozoan prevalence

No protozoa were detected in *C. lupus*, *M. leucurus*, *M. altaica*, *U. arctos pruinosus* or *P. bengalensis*. Six protozoan species were identified exclusively in canids (*V. ferrilata* and *V. vulpes*), and the detection rate in fecal samples was 19.37% (68/351; 95% CI, 15.24%–23.51%) in foxes. Detection rates varied significantly among protozoan species ($\chi^2 = 64.31$, $P < 0.01$). *E. falciformis* (7.41%, 26/351; 95% CI, 4.67%–10.15%) and *E. banffensis* (7.12%, 25/351; 95% CI, 4.43%–9.81%) exhibited the highest rates, followed by *E. bieneusi* (3.70%, 13/351; 95% CI, 1.73%–5.68%). A single *Cryptosporidium* sp.-positive and one *G. intestinalis*-positive sample occurred in *V. ferrilata*, while one additional *G. intestinalis* was detected in *V. vulpes*. *V. ferrilata* was the only host for all identified protozoa, showing a significantly higher detection rate (21.17%, 65/307; 95% CI, 16.60%–25.74%) than *V. vulpes* (3/44; $\chi^2 = 5.08$, $P = 0.02$) (Table 3).

Discussion

The eastern Tibetan Plateau, situated at the convergence of Sichuan, Qinghai, and Xizang, features complex terrain shaped by dual monsoon systems from the Indian and Pacific Oceans. This creates a humid climate (400–800 mm annual precipitation) supporting the plateau's most complete vertical vegetation spectrum, which offers diverse microhabitats for wildlife [14]. Canids dominated the carnivore community (98.61%), with *V. ferrilata* representing 85.52% of identified samples. Compared to large carnivores (e.g., snow leopards, brown bears), small carnivores like foxes and weasels exhibit lower individual spatial requirements but higher population densities. While ecologically vital for ecosystem stability, they may act as reservoirs for zoonotic pathogens, amplifying disease circulation across wildlife-domestic-human interfaces and elevating regional public health risks [15].

Cryptosporidium, a major diarrheal pathogen second only to rotavirus, infects diverse vertebrates and persists in environmental matrices. Over 49 species and 120 genotypes exist, with 23 genotypes confirmed as human-infective, including *C. hominis*, *C. parvum*, *C. meleagridis*, *C. canis*, *C. felis*, *C. ubiquitum*, *C. cuniculus*, *C. viatorum*, *C. muris*, *C. andersoni*, *C. erinacei*, *C. tyzzeri*, *C. bovis*, *C. suis*, *C. scrofarum*, *C. occultus*, *C. xiaoi*, *C. fayeri*, *C. ditrichi*, *C. equi* (horse genotype), *C. wrairi*, *C. mortiferum* (chipmunk genotype I), *C. baileyi*, mink genotype, and skunk genotype [16]. To the best of our knowledge, there have been no reports of *Cryptosporidium* sp. yak genotype infecting the human populations within the study area. Although the plateau's harsh climate was historically considered unfavorable for *Cryptosporidium* spp. [17], we detected it in *V. ferrilata*, with the strain showing 100% identity to the *Cryptosporidium* sp. yak genotype previously reported

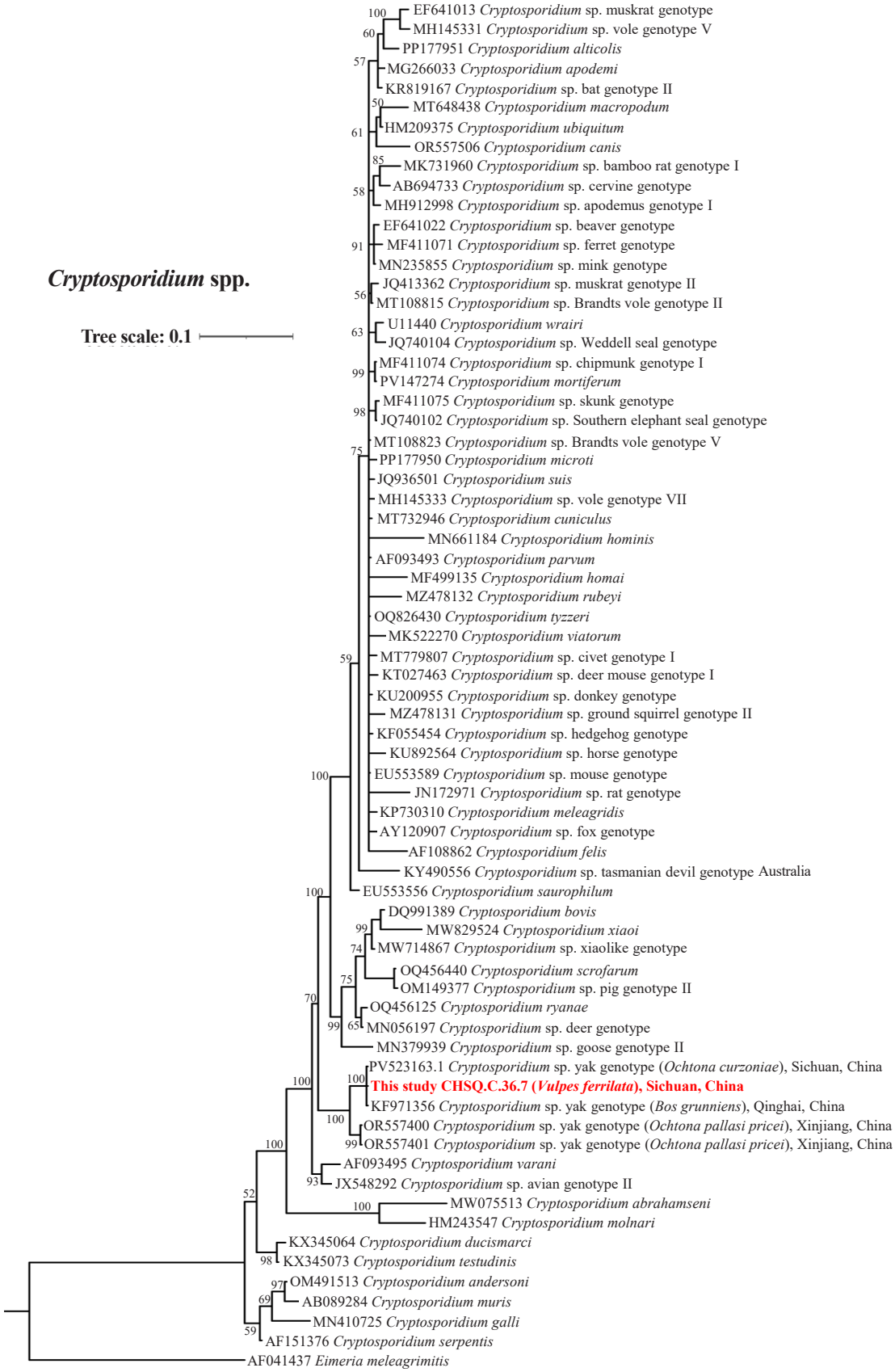


Fig. 2. Phylogenetic tree based on the *Cryptosporidium* spp. based on partial *SSU rRNA* gene sequences with the nucleotide substitution model of *TVM+I+G*.

https://doi.org/10.3347/PHD.26037

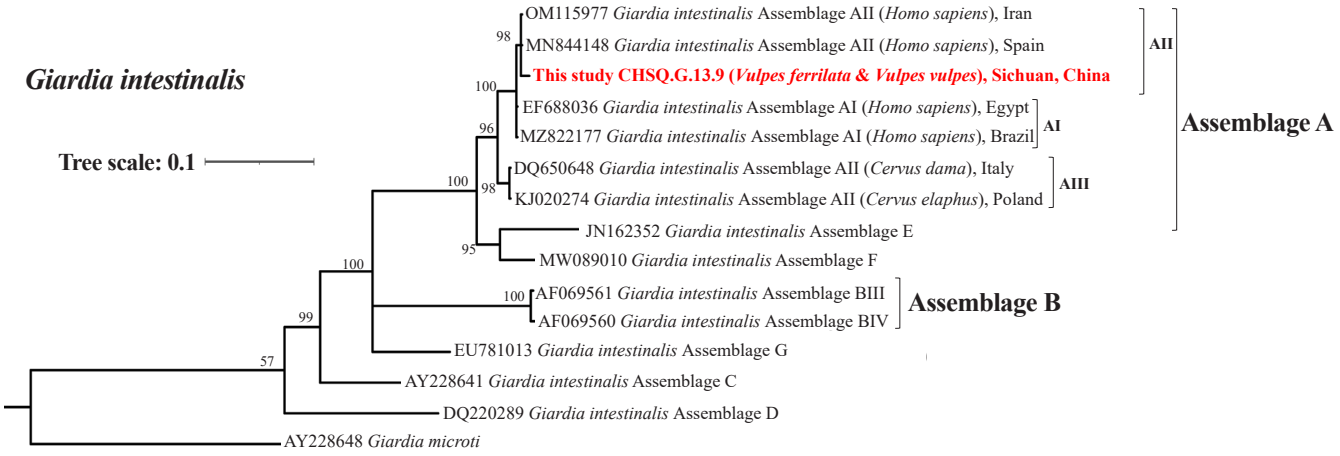


Fig. 3. Phylogenetic tree based on the *Giardia intestinalis*, based on partial *TPI* gene sequences with the nucleotide substitution model of *TIM3+I+G*.

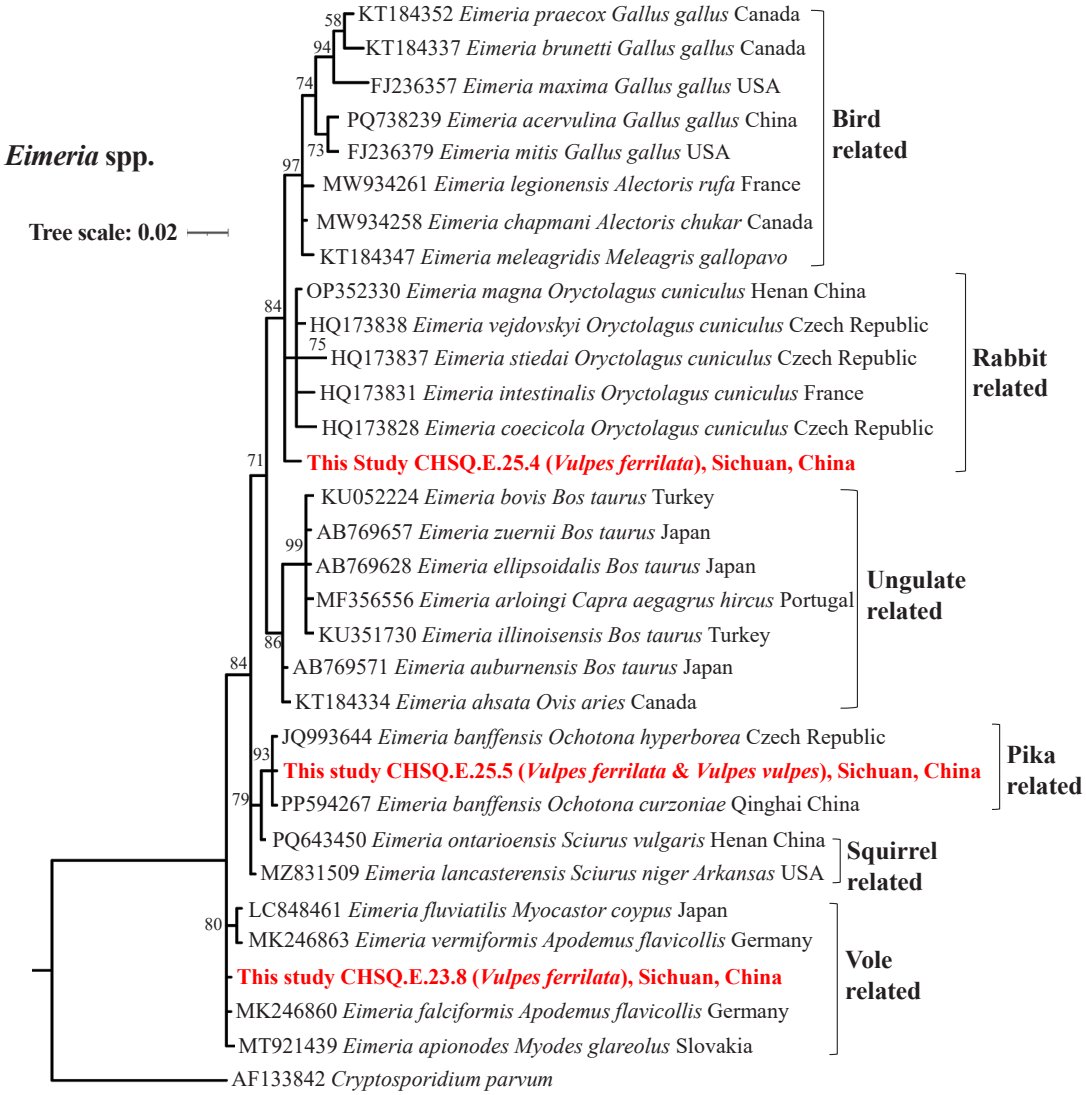


Fig. 4. Phylogenetic tree based on the *Eimeria* spp. based on partial *SSU rRNA* gene sequences with the nucleotide substitution model of *TrN+I+G*.

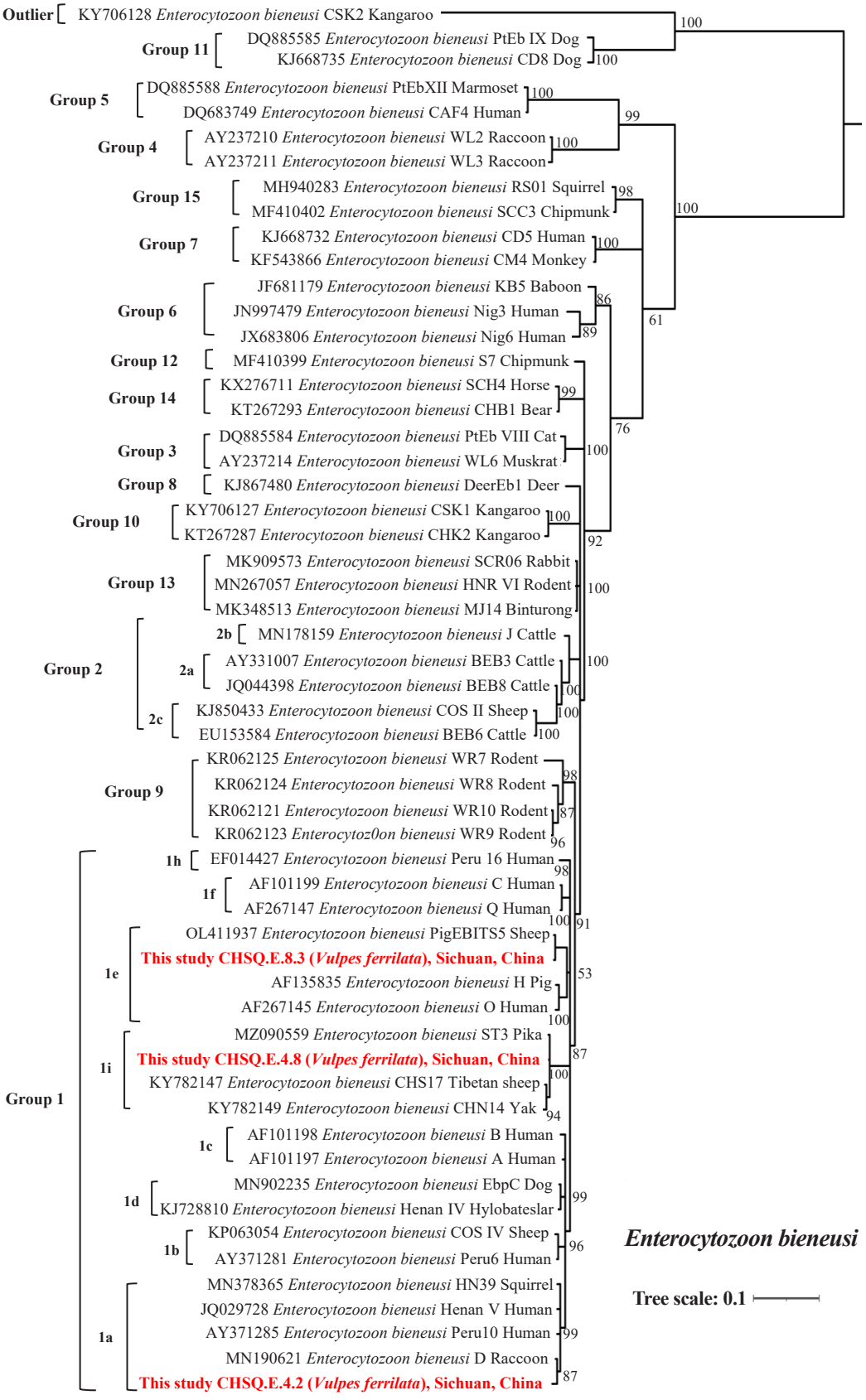


Fig. 5. Phylogenetic tree based on the *Enterocytozoon bieneusi* based on partial *ITS1* gene sequences with the nucleotide substitution model of *TPM1uf+G*.

https://doi.org/10.3347/PHD.26037

Table 3. Detection rate of protozoa parasites in main wild carnivores from Tibetan Plateau

Protozoan	Detection rate (%) in carnivores, with 95% CI		
	Vulpes ferrilata	*Vulpes vulpes*	Total
Cryptosporidium sp. yak genotype	0.33 (1/307, 0–0.96)	0 (0/44)	0.28[a] (1/351, 0–0.84)
Giardia intestinalis	0.33 (1/307, 0–0.96)	2 (1/44, 0–7)	0.57[a,b] (2/351, 0–1.36)
Eimeria banffensis	7.49 (23/307, 4.55–10.44)	5 (2/44, 0–11)	7.12[c] (25/351, 4.43–9.81)
Eimeria falciformis	8.47 (26/307, 5.35–11.58)	0 (0/44)	7.41[c] (26/351, 4.67–10.15)
Eimeria sp.	0.33 (1/307, 0.00–0.96)	0 (0/44)	0.28[a] (1/351, 0–0.84)
Enterocytozoon bieneusi	4.23 (13/307, 1.98–6.49)	0 (0/44)	3.70[b,c] (13/351, 1.73–5.68)
Total	21.17 (65/307, 16.60–25.74)	7 (3/44, 0–14)	19.37 (68/351, 15.24–23.51)

[a,b,c] represent results of the post-hoc tests of the chi-square tests for detection rates of protozoa in all wild carnivores; *P*-values were adjusted by Bonferroni correction and compared with 0.05 level, the same letter indicates that there is no statistical significance between the 2 protozoa species.

in *B. grunniens* from Qinghai Province [18]. Identical genotypes were also found in *O. curzoniae* (PV523163) in this region [19]. Phylogenetic analysis (Fig. 2) revealed this genotype forms a distinct clade closely related to strains from Pallas's pika (*Ochotona pallasi pricei*, OR557400 and OR557401) in Xinjiang, suggesting it may represent a novel plateau-adapted genotype circulating among sympatric foxes, pikas, and livestock via shared pastures and water. Its zoonotic potential warrants further investigation.

This study detected *G. intestinalis* in the feces of both *V. ferrilata* and *V. vulpes*. This flagellate is an intestinal parasitic protozoan with complex host specificity, featuring a life cycle that includes infectious cysts and pathogenic trophozoites [20]. In China, *G. intestinalis* and *Cryptosporidium* spp. are the only 2 parasites prioritized as microbial indicators explicitly listed in the Standards for Drinking Water Quality (GB 5749–2022), underscoring their public health significance [21]. Genetic analyses divide *G. intestinalis* into host-adapted assemblages: A and B infect humans and diverse mammals, while C/D (canids), E (livestock), F (felids), and G (rodents) show stricter host specificity [22]. The assemblage AII identified here (Fig. 3) matches dominant human-infective strains in China [23]. Environmental contamination by fox-derived cysts poses health risks, particularly for pastoral communities reliant on natural water sources.

For *E. bieneusi*, over 500 genotypes (including 52 zoonotic types) are recognized [24]. ITS-based phylogeny classifies genotypes into Groups 1–15, with Groups 1 and 2 demonstrating broad host ranges and zoonotic potential, while Groups 3–15 are typically host-specific (e.g., Group 3 in wild rodents, Group 4 in carnivores/rodents) [25]. In this study, CHSQ.E.4.2 (99.19% similarity to genotype D, MN190621) belongs to subgroup 1a, a major human-infective group; CHSQ.E.8.3 (identical to PigEBITS5, OL411937) clusters in subgroup 1e, confirmed to infect humans. In particular, CHSQ.E.4.8 (predominant genotype, 11/13) aligns with genotypes of ST3, CHS17, and CHN14 in subgroup 1i from pika, sheep, and yak, respectively, in Qinghai [26,27]. Therefore, it is suggested that subgroup 1i is a dominant genotype group circulating among wild and domestic animals in the eastern Tibetan Plateau, and further research is required to verify its human-infective capacity (Fig. 5).

The intestinal parasites common to these animals also pose a potential persistent threat to human health. *Cryptosporidium* infection is one of the most common causes of diarrhea in humans worldwide. As of 2021, incomplete statistics indicate that at least 29 provinces in China have reported human *Cryptosporidium* infections, involving 107 cities and a total of 4,975 clearly confirmed cases [28]. Although this disease is not a statutory infectious disease in China, it is easy ignored. With regard to *G. intestinalis*, an estimated 280 million people worldwide suffer from clinically diagnosable giardiasis. High infection rates of giardiasis have been documented in developing countries. In China, approximately 28.5 million human cases of giardiasis are estimated to occur annually. According to the limited genotyping studies available, both assemblage A (subtypes AI and AII) and assemblage B of *G. intestinalis* have been identified in China, with assemblage AII and assemblage B being the predominant genotypes [23]. It is worth noting that *E. bieneusi*, by far the most frequently reported microsporidian species causing human disease, is responsible for intestinal illness in both non- and immunocompromised patients. A recent meta-analysis estimated the overall prevalence of *E. bieneusi* infection in humans at 7.9% (95% CI, 6.9%–8.8%). Furthermore, in some low-income countries, nearly 10% of children presenting with diarrhea test positive for *E. bieneusi* [29].

On the other hand, it should be noted that the most frequently detected parasite in canid fecal samples was *Eimeria* spp. However, existing data indicate that the parasitism of

Eimeriidae in canids is a complex and controversial issue. Although oocysts of species such as *E. canis*, *E. aurei*, and *E. lomarii* have been found in canid feces or intestines, their endogenous developmental stages (e.g., schizonts, gametocytes) have not been confirmed within canid hosts. Thus, *Eimeria* are suspected to be spurious parasites in canids, with their presence likely due to the consumption of infected true hosts by canids [30]. Nonetheless, although these oocysts are likely not replicating in foxes, they remain intact and sporulation-competent, posing a potential transmission risk. In this study, *E. banffensis* (pika-associated) and *E. falciformis* (vole-associated) dominated in fox feces, aligning with dietary analyses showing pikas and voles as primary prey [31]. The rare detection of a rabbit-associated *Eimeria* sp. (CHSQ. E.25.4) (Table 3), which likely originated from the native plateau hare (*Lepus oiostolus*), and is distinctly separated from those derived from *O. cuniculus* in the phylogenetic tree, further supports prey-derived transmission. The findings indicate the presence of these *Eimeria* species in the environment or food chain of the eastern Tibetan Plateau, indirectly reflecting the complex flow of protozoan parasites within the local ecosystem.

Although this study detected multiple intestinal protozoans in carnivore fecal samples from the eastern Tibetan Plateau using molecular methods, the inherent limitations of fecal material make it difficult to confirm whether these parasites truly colonized the wildlife hosts or induced pathological effects. Detection of this pathogen in carnivore feces may suggest a potential food chain transmission risk, as exemplified by *Mastophorus muris*. This parasite utilizes insects (e.g., beetles, locusts, grasshoppers, cockroaches) as intermediate hosts and rodents as definitive hosts [7]. Although *M. muris* does not require *V. ferrilata* in its life cycle, ingestion of infected rodents by *V. ferrilata* results in excretion of parasite eggs in the carnivore's feces, thereby posing a potential transmission risk. These findings heighten concerns regarding carnivores as potential vectors of zoonotic protozoans. Given the relatively scarce baseline research and insufficient host investigations in the Tibetan Plateau, this study underscores significant public health concerns.

As an ecological hotspot on the Qinghai-Tibet Plateau, Shiqu County harbors abundant wildlife resources. Animal husbandry serves as the primary source of income for local residents, with nomadism representing a traditional way of life. The considerable overlap between grazing areas and wildlife habitats, coupled with the sharing of water sources, poses a potential risk for the transmission of zoonotic enteric protozoan parasites from wildlife to humans [7]. To improve the living conditions of pastoralists, the Chinese government-initiated settlement construction projects in 2001. However, smaller and more remote settlements often lack basic public facilities, leading to difficulties in accessing clean water [32]. The combination of inadequate clean water access and local herders' customs—such as not washing hands before meals and lying directly on the grass—in an area where water sources are shared with wildlife, may facilitate the spread of intestinal protozoa. Notably, the overlapping activity areas create opportunities for indirect contact between humans and wildlife, specifically through livestock. Previous studies have indicated that with the progression of human society, the boundaries between humans and wildlife are gradually blurring, and the living space of wildlife is increasingly compressed. Consequently, wildlife is forced to share resources and habitats with humans to a certain extent. Although wild animals tend to avoid direct human disturbance, they may occasionally come into contact with livestock for predation [33]. During such interactions, pathogen spillover can occur among humans, livestock, and wildlife.

Zoonotic parasites pose a serious challenge to global public health due to their cross-species transmission potential, complex life cycles, and diverse host range, which complicate control efforts [34]. These pathogens form intricate transmission networks through multi-host interactions within food webs, with their virulence and spread influenced by host ecology, behavior, and environmental factors [35]. As apex predators, carnivores accumulate a diversity of parasites through bioaccumulation, posing a considerable health risk to herders who frequently interact with natural environments. Of particular concern are traditional local practices (such as consuming untreated water, raw or undercooked meat), which may serve as key risk factors for acquiring these zoonotic infections.

This study not only provides the first regional assessment of potentially transmissible protozoans carried by wildlife in the eastern Tibetan Plateau, but also highlights how grazing activities may foster transmission chains among humans, livestock, and wildlife. It thus calls for sustained attention to the cross-species mechanisms and ecological risks of zoonotic protozoan diseases.

Canids, particularly *V. ferrilata*, dominated the wild carnivore assemblage in the eastern Tibetan Plateau and showed a notable detection rate of protozoan infections (all protozoan species detected in this study were identified in *V. ferrilata* samples). This research represents the first documentation of intestinal protozoa detected in wildlife in this region, reveal-

https://doi.org/10.3347/PHD.26037

ing the detection of 2 confirmed zoonotic pathogens: *G. intestinalis* assemblage AII (CHSQ.G.13.9) and *E. bieneusi* genotype CHSQ.E.8.3 (identical to PigEBITS5). Additionally, a potentially zoonotic genotype of *E. bieneusi* (CHSQ.E.4.2) was detected, underscoring the existence of wildlife-origin protozoan pathogens and their latent threat to human health. The discovery of the *Cryptosporidium* sp. yak genotype and *E. bieneusi* (CHSQ.E.4.8) in yaks, foxes, and rodents suggests that these genotypes are dominant locally and reveals potential pathogen transmission and spillover risks between wildlife and livestock. It is important to emphasize that protozoan infections in wildlife remain understudied across the Tibetan Plateau. Further investigation is needed to elucidate the transmission patterns of poorly characterized native protozoa (such as the *Eimeria* sp. reported here), and to clarify their life cycles and potential public health implications.

Data availability

All data generated or analyzed during this study are included in this published article.

Author contributions

Conceptualization: Deng X, Wang X. Data curation: Deng X. Formal analysis: Deng X. Funding acquisition: Wang X. Investigation: Deng X, Xue C, Chen Q, Zuo Q, Li M, Peng X, Wang X. Methodology: Deng X, Wang X. Project administration: Wang X. Resources: Wang X. Software: Deng X, Wang X. Supervision: Deng X, Wang X. Validation: Deng X, Wang X. Visualization: Deng X. Writing – original draft: Deng X. Writing – review & editing: Li P, Wang X.

Conflict of interest

The authors have no conflicts of interest to declare.

Funding

This work was supported by the Prevention and Control of Emerging and Major Infectious Diseases-National Science and Technology Major Project (grant No. 2025ZD01900100, 2025ZD01900112) and the National Natural Science Foundation of China (grant No. 82404325).

Acknowledgments

We gratefully acknowledge the Shiqu County Center of Disease Control for its support during the field study.

During the writing of this manuscript, we employed AI-based language tools (DeepSeek) solely for the purposes of language refinement, grammar correction, and stylistic improvement. These tools were not used to generate any scientific content, data, or conclusions. All AI-suggested changes were critically reviewed and either accepted or modified by the authors to ensure that the final manuscript accurately reflects our own findings and interpretations. The authors assume full responsibility for the originality, accuracy, and integrity of the content presented.

ORCID

Xueying Deng, https://orcid.org/0000-0002-6377-6290
Chuizhao Xue, https://orcid.org/0000-0001-9055-5779
Qilu Chen, https://orcid.org/0000-0002-2475-4259
Qingqiu Zuo, https://orcid.org/0009-0007-1344-6115
Mengqing Li, https://orcid.org/0009-0001-4940-9080
Xiaoxue Peng, https://orcid.org/0009-0003-8876-600X
Peng Li, https://orcid.org/0009-0004-6978-2482
Xu Wang, https://orcid.org/0000-0002-5193-9697

References

1. Lv S, Tian LG, Liu Q, et al. Water-related parasitic diseases in China. Int J Environ Res Public Health 2013;10:1977-2016. https://doi.org/10.3390/ijerph10051977
2. Thompson RCA, Smith A. Zoonotic enteric protozoa. Vet Parasitol 2011;182:70-8. https://doi.org/10.1016/j.vetpar.2011.07.016
3. Li SA, Lin YL, Bai YP, et al. Prevalence and molecular characterization of *Cryptosporidium* spp. and *Giardia duodenalis* in humans and dogs from Fujian Province, Southeast China. Food Waterborne Parasitol 2025;40:e00278. https://doi.org/10.1016/j.fawpar.2025.e00278
4. Robertson LJ, Clark CG, Debenham JJ, et al. Are molecular tools clarifying or confusing our understanding of the public health threat from zoonotic enteric protozoa in wildlife? Int J Parasitol Parasites Wildl 2019;9:323-41. https://doi.org/10.1016/j.ijppaw.2019.01.010
5. Trout JM, Santín M, Fayer R. *Giardia* and *Cryptosporidium* species and genotypes in coyotes (*Canis latrans*). J Zoo Wildl Med 2006;37:141-4. https://doi.org/10.1638/05-06TYM-123005.1
6. Leśniańska K, Perec-Matysiak A. Wildlife as an environmental reservoir of *Enterocytozoon bieneusi* (Microsporidia): analyses of data based on molecular methods. Ann Parasitol 2017;63:265-81. https://doi.org/10.17420/ap6304.113
7. Chen Q, Wang X, Li C, et al. Investigation of parasitic nematodes detected in the feces of wild carnivores in the eastern Qinghai-Tibet Plateau, China. Pathogens 2022;11:1520. https://doi.org/10.3390/pathogens11121520
8. Jenkins EJ, Simon A, Bachand N, Stephen C. Wildlife parasites in a

One Health world. Trends Parasitol 2015;31:174-80. https://doi.org/10.1016/j.pt.2015.01.002
9. Xiong M, Shao X, Long Y, et al. Molecular analysis of vertebrates and plants in scats of leopard cats (*Prionailurus bengalensis*) in southwest China. J Mammal 2016;97:1054-64. https://doi.org/10.1093/jmammal/gyw061
10. Khan A, Shaik JS, Grigg ME. Genomics and molecular epidemiology of *Cryptosporidium* species. Acta Trop 2018;184:1-14. https://doi.org/10.1016/j.actatropica.2017.10.023
11. Wang Y, Cao J, Chang Y, et al. Prevalence and molecular characterization of *Cryptosporidium* spp. and *Giardia duodenalis* in dairy cattle in Gansu, northwest China. Parasite 2020;27:62. https://doi.org/10.1051/parasite/2020058
12. Buckholt MA, Lee JH, Tzipori S. Prevalence of *Enterocytozoon bieneusi* in swine: an 18-month survey at a slaughterhouse in Massachusetts. Appl Environ Microbiol 2002;68:2595-9. https://doi.org/10.1128/AEM.68.5.2595-2599.2002
13. Orlandi PA, Carter L, Brinker AM, et al. Targeting single-nucleotide polymorphisms in the 18S rRNA gene to differentiate *Cyclospora* species from *Eimeria* species by multiplex PCR. Appl Environ Microbiol 2003;69:4806-13. https://doi.org/10.1128/AEM.69.8.4806-4813.2003
14. Zhuo G, Chen S, Zhou B. Spatio-temporal variation of vegetation coverage over the Tibetan Plateau and its responses to climatic factors. Acta Ecol Sin 2018;38:3208-18. https://doi.org/10.5846/stxb201705270985
15. Marneweck C, Butler AR, Gigliotti LC, et al. Shining the spotlight on small mammalian carnivores: global status and threats. Biol Conserv 2021;255:109005. https://doi.org/10.1016/j.biocon.2021.109005
16. Peng X, Wang X, Jian J, et al. Investigation of *Cryptosporidium* spp. and *Enterocytozoon bieneusi* in free-ranged livestock on the southeastern Qinghai-Xizang Plateau, China. BMC Infect Dis 2025;25:356. https://doi.org/10.1186/s12879-025-10737-5
17. Wang X, Jiang Y, Wu W, et al. Cryptosporidiosis threat under climate change in China: prediction and validation of habitat suitability and outbreak risk for human-derived *Cryptosporidium* based on ecological niche models. Infect Dis Poverty 2023;12:35. https://doi.org/10.1186/s40249-023-01085-0
18. Ma J, Cai J, Ma J, Feng Y, Xiao L. Occurrence and molecular characterization of *Cryptosporidium* spp. in yaks (*Bos grunniens*) in China. Vet Parasitol 2014;202:113-8. https://doi.org/10.1016/j.vetpar.2014.03.030
19. Zuo Q, Bianba Z, Xue C, et al. Infections and genetic diversity of *Cryptosporidium* spp. and *Giardia* spp. in small wild mammals on the Eastern Tibetan plateau: public health implications. BMC Microbiol 2025;25:616. https://doi.org/10.1186/s12866-025-04363-z
20. Einarsson E, Troell K, Hoeppner MP, et al. Coordinated changes in gene expression throughout encystation of *Giardia intestinalis*. PLoS Negl Trop Dis 2016;10:e0004571. https://doi.org/10.1371/journal.pntd.0004571
21. National Public Service Platform for Standards Information. GB 5749-2022 Standards for drinking water quality [Internet]. 2023 [cited 2026 Apr 10]. Available from: https://std.samr.gov.cn/gb/search/gbDetailed?id=DAB6B92C0764FC96E05397BE0A0A5F84
22. Sprong H, Cacciò SM, van der Giessen JW; ZOOPNET network and partners. Identification of zoonotic genotypes of *Giardia duodenalis*. PLoS Negl Trop Dis 2009;3:e558. https://doi.org/10.1371/journal.pntd.0000558
23. Li J, Wang H, Wang R, Zhang L. *Giardia duodenalis* infections in humans and other animals in China. Front Microbiol 2017;8:2004. https://doi.org/10.3389/fmicb.2017.02004
24. Zhang Y, Koehler AV, Wang T, Gasser RB. *Enterocytozoon bieneusi* of animals: with an 'Australian twist'. Adv Parasitol 2021;111:1-73. https://doi.org/10.1016/bs.apar.2020.10.001
25. Li W, Feng Y, Santin M. Host specificity of *Enterocytozoon bieneusi* and public health implications. Trends Parasitol 2019;35:436-51. https://doi.org/10.1016/j.pt.2019.04.004
26. Zhang Q, Cai J, Li P, et al. *Enterocytozoon bieneusi* genotypes in Tibetan sheep and yaks. Parasitol Res 2018;117:721-7. https://doi.org/10.1007/s00436-017-5742-1
27. Liu X, Du S, Yang X, et al. First genotyping of *Enterocytozoon bieneusi* in plateau pikas (*Ochotona curzoniae*) from the Qinghai Plateau, Northwest China. Vet Res Commun 2021;45:453-7. https://doi.org/10.1007/s11259-021-09824-0
28. Wang X, Shen Y, Cao J. Epidemic status and prevention and control progress of cryptosporidiosis in China. J Trop Dis Parasitol 2022;20:136-48. https://doi.org/10.3969/j.issn.1672-2302.2022.03.004
29. Nourrisson C, Lavergne RA, Moniot M, Morio F, Poirier P. *Enterocytozoon bieneusi*, a human pathogen. Emerg Microbes Infect 2024;13:2406276. https://doi.org/10.1080/22221751.2024.2406276
30. Gherman CM, Mihalca AD. A synoptic overview of golden jackal parasites reveals high diversity of species. Parasit Vectors 2017;10:419. https://doi.org/10.1186/s13071-017-2329-8
31. Wang X, Xue C, Deng X, et al. Seasonal population dynamics and dietary switching of *Vulpes* spp. amplify *Echinococcus* spp. transmission in the Eastern Tibetan plateau: implications for wildlife-mediated zoonotic risks. BMC Vet Res 2025;21:475. https://doi.org/10.1186/s12917-025-04907-5
32. Wang Q, Wang Y, Luo Z, et al. Settlement characteristics and transmission of echinococcosis: a cross-sectional study in nomadic communities on the Qinghai-Tibet Plateau, China. Infect Dis Poverty 2025;14:47. https://doi.org/10.1186/s40249-025-01316-6

https://doi.org/10.3347/PHD.26037

33. Mohan M, Sathyakumar S, Krishnamurthy R. Predator in proximity: how does a large carnivore respond to anthropogenic pressures at fine-scales? Implications for interface area management. PeerJ 2024;12:e17693. https://doi.org/10.7717/peerj.17693
34. Thompson RC. Parasite zoonoses and wildlife: One Health, spillover and human activity. Int J Parasitol 2013;43:1079-88. https://doi.org/10.1016/j.ijpara.2013.06.007
35. Han BA, Schmidt JP, Bowden SE, Drake JM. Rodent reservoirs of future zoonotic diseases. Proc Natl Acad Sci U S A 2015;112:7039-44. https://doi.org/10.1073/pnas.1501598112

Original Article

Parasites Hosts Dis 2026;64(4):350-359
https://doi.org/10.3347/PHD.26014

Parasites, Hosts and Diseases

pISSN 2982-5164 • eISSN 2982-6799

Morphological and molecular identification of hard ticks using mitochondrial 16S and 12S rDNA in Korea

Choon-Mee Kim[1,†], Seon Gyeong Kim[2,†], You Mi Lee[3], Jun-Won Seo[3], Da Young Kim[3], Na Ra Yun[3], Dong-Min Kim[3,*]

[1]Premedical Science, College of Medicine, Chosun University, Gwangju, Korea; [2]Division of Infectious Disease Investigation, Health and Environment Research Institute of Gwangju City, Gwangju, Korea; [3]Department of Internal Medicine, College of Medicine, Chosun University, Gwangju, Korea

Accurate identification of tick species is essential for understanding their role in pathogen transmission and guiding vector control strategies. Although morphological classification is widely used, it can be limited by specimen damage or immature developmental stages. In this study, we comparatively evaluated mitochondrial 16S and 12S ribosomal DNA (rDNA) markers for species-level identification and morphological verification of hard ticks and rodent-associated ectoparasites collected from vegetation, wild rodents, and patients in Gwangju, Republic of Korea. A total of 74 morphologically identified adult ticks—*Haemaphysalis longicornis*, *Haemaphysalis flava*, and *Ixodes nipponensis*—along with 3 damaged ticks removed from patients, were analyzed. PCR and sequencing success varied among species and markers. The 16S rDNA marker showed a higher amplification rate but lower sequencing success, whereas 12S rDNA showed more consistent performance. *I. nipponensis* showed the most balanced performance (89.5% for 16S and 78.9% for 12S), *H. flava* showed moderate variation, and *H. longicornis* demonstrated strong marker dependence, with low 16S but complete 12S success. Importantly, 16S rDNA identified 3 severely damaged ticks from patients—2 *I. nipponensis* and 1 *Amblyomma testudinarium*—demonstrating its diagnostic value when morphology was uninformative. Phylogenetic analyses of both markers yielded well-supported clades consistent with morphological identification. Additionally, 12S rDNA identified 3 flea specimens (*Ctenophthalmus* sp. and *Neopsylla specialis*) obtained during tick collection from wild rodents, indicating exploratory applicability to other rodent-associated ectoparasites. These findings support mitochondrial 16S and 12S rDNA markers as reliable tools for tick identification, especially when morphological assessment is limited by damage or developmental stage.

Keywords: Ticks, *Haemaphysalis flava*, *Haemaphysalis longicornis*, *Ixodes nipponensis*, mitochondrial DNA, polymerase chain reaction

Introduction

Vector-borne infectious diseases transmitted by mosquitoes, ticks, fleas, and other arthropod vectors account for over 17% of all infectious diseases worldwide [1]. In Korea, 5 genera and 27 species of ixodid ticks have been identified [2]. Among these, hard ticks play a critical role as vectors for various pathogens, including viruses, rickettsiae, and protozoa, which affect both humans and animals [3-5]. Interest in tick-borne diseases has increased significantly since *Haemaphysalis longicornis*, one of the most widespread tick species in East Asia, was identified as the primary vector of severe fever with thrombocytopenia syndrome virus in China, Japan, and Korea [6,7].

Accurate species-level identification of ticks is essential for understanding their role in pathogen transmission and developing effective control strategies [8,9]. However, morphological

Received: February 3, 2026 Accepted: June 12, 2026
*Correspondence: drongkim@chosun.ac.kr

[†]These authors contributed equally to this work.

Citation
Kim CM, Kim SG, Lee YM, Seo JW, Kim DY, Yun NR, Kim DM. Morphological and molecular identification of hard ticks using mitochondrial 16S and 12S rDNA in Korea. Parasites Hosts Dis 2026;64(4):350-359.

© 2026 The Korean Society for Parasitology and Tropical Medicine

This is an open-access article distributed under the terms of the Creative Commons Attribution Non-Commercial License (http://creativecommons.org/licenses/by-nc/4.0/) which permits unrestricted non-commercial use, distribution, and reproduction in any medium, provided the original work is properly cited.

identification is often hampered by intraspecific variation, cryptic species, specimen damage during collection or detachment from hosts, and the presence of immature developmental stages [10]. These limitations become particularly pronounced when closely related species exhibit similar morphological features, making it difficult to differentiate based solely on external traits. In such cases, molecular identification using DNA extracted from tick specimens provides a reliable and precise alternative for taxonomic classification [11].

Molecular approaches have proven useful in addressing species-level identification challenges in tick taxonomy. For example, in China, genetic analysis using partial 16S ribosomal DNA (rDNA) and the second internal transcribed spacer (ITS-2) sequences successfully distinguished *H. longicornis* from the morphologically similar *Haemaphysalis qinghaiensis* Teng, 1980, demonstrating clear interspecific divergence and supporting the utility of molecular tools in differentiating closely related tick species [12]. In addition, Lv et al. [13] reported the value of several genetic markers, including cytochrome oxidase I (COI), 16S rDNA, ITS-2, and 12S rDNA, for identifying hard tick species. Among these, mitochondrial 16S and 12S rDNA regions are particularly useful because of their species-specific variability and moderate evolutionary rates, making them suitable for identifying damaged, engorged, or immature specimens that are difficult to classify morphologically [12,14].

In Korea, direct comparisons between morphological identification and mitochondrial 16S and 12S rDNA-based molecular identification remain limited for ticks collected from diverse sources, particularly for damaged specimens removed from patients. In this study, hard ticks were collected from vegetation, wild rodents, and patients in Gwangju, Korea, and additional rodent-associated ectoparasites obtained during tick collection from wild rodents were included to evaluate the broader applicability of this molecular approach. Morphological identification was compared with molecular identification based on partial 16S and 12S rDNA sequences. Accordingly, this study aimed to compare morphological identification with mitochondrial 16S and 12S rDNA-based molecular identification in ticks collected from vegetation and wild rodents, as well as damaged tick specimens removed from patients.

Methods

Ethics statement

This study was approved by the Ethics in Human Research Committee of Chosun University Hospital under an institutional review board, which approved all the experiments that used ticks removed from tick-bitten humans (approval No. CHOSUN NON2019-001). The institutional review board approved the protocol with verbal consent for the use of ticks and not human participants. We read and explained the verbal version of the consent form to use samples for research purposes and obtained individual consent.

This study was also approved by the Institutional Animal Care and Use Committee of Chosun University. All animals were used in accordance with the approved animal use protocol issued by the Institutional Animal Care and Use Committee of Chosun University for the capture, handling, and sampling of wild rodents.

Tick collection

Tick collection from vegetation by flagging and dragging

From April to November 2014, hard ticks were collected from 5 forested and park-adjacent sites near urban areas in Gwangju, Korea, using standard flagging and dragging techniques. A piece of flannel was swept across the vegetation and any ticks attached to the fabric were carefully detached using forceps. Each specimen was placed in a labeled vial containing information on the collection site, date, and time. All collected specimens were preserved for subsequent morphological and molecular analyses.

Tick collection from wild rodents using Sherman live traps

In October and November 2014, to collect ticks parasitizing wild rodents, Sherman live traps were deployed in 2 forested areas of Gwangju [15]. Biscuit bait coated with peanut butter was used as the attractant. During the summer months, traps were set at dusk and retrieved the next morning; during winter, to prevent rodent hypothermia, traps were set at 16:00 and collected at 22:00 on the same day. After capture, the rodents were anesthetized in accordance with an approved animal use protocol, and biological samples, such as blood and internal organs, were harvested for parallel studies. Ectoparasitic ticks were collected by suspending rodents head-down above water-filled containers and allowing the detached ticks to fall naturally. Tick specimens obtained from rodents were processed following the same procedures as vegetation-derived samples.

Tick collection from tick-bitten patients

Between January 2015 and December 2018, 3 partially damaged ticks that had been removed from 3 patients after tick bites were collected at Chosun University Hospital, Korea. These patient-derived specimens were handled and examined using the

same identification and washing protocols described in the 'Imaging and washing procedures' section.

Tick processing, imaging, and DNA extraction

Imaging and washing procedures

Only adult ticks collected using the aforementioned methods were selected for morphological examination. Morphological identification was conducted under a stereomicroscope using standard taxonomic keys [16], and both dorsal and ventral surfaces of each specimen were photographed. Prior to DNA extraction, ticks were surface-sterilized by immersion in a 10% diluted bleaching solution containing 3%–8% sodium hypochlorite and 0.01%–0.05% sodium hydroxide for 1–2 min. This was followed by sequential rinsing with 70% ethanol (2–5 min) and sterile distilled water (3 min). Individual ticks (~3 mm in size) were then transferred to the wells of sterile U-bottom plates, and the washing solutions were replaced at each step.

Homogenization and DNA extraction

Washed ticks were dried on sterile absorbent paper and transferred into grinding tubes prefilled with 600 µl of lysis buffer and a 2.8-mm stainless steel bead. The buffer consisted of sterile phosphate-buffered saline supplemented with 10% fetal bovine serum and 5% penicillin-streptomycin. Homogenization was performed twice using a FastPrep-24 Classic instrument (MP Biomedicals) at 6,000 rpm for 25 sec. Genomic DNA was extracted from the homogenate using a QIAamp Tissue & Blood Mini Kit (Qiagen), following the manufacturer's protocol.

PCR amplification of 16S and 12S rDNA

Conventional PCR was performed to amplify the mitochondrial 16S and 12S rDNA fragments for species identification of ticks. For 16S rDNA amplification, the primer pair 16s+1F and 16S-1R was used, and for 12S rDNA amplification, the primer set T1B and T2A was used [12,14] (Table 1).

The 16S rDNA region was amplified using AmpliTaq Gold 360 Master Mix (Applied Biosystems) in a total volume of 20 µl. PCR cycling conditions were as follows: initial denaturation at 95°C for 5 min; 40 cycles of 95°C for 45 sec, 55°C for 1 min, and 72°C for 90 sec; followed by a final extension at 72°C for 5 min. PCR products were electrophoresed on a 1.2% agarose gel and visualized by ethidium bromide staining. Amplification of the 12S rDNA fragment was carried out using AccuPower PCR PreMix (Bioneer) in a 20 µl reaction volume. The PCR condition included an initial denaturation at 95°C for 5 min, followed by 30 cycles of 95°C for 15 sec and 53°C for 45 sec, with a final extension step at 72°C for 5 min. The PCR was performed using an AB thermal cycler (Applied Biosystems). Amplified products were similarly run on a 1.2% agarose gel and stained with ethidium bromide for visualization. The primer sequences are listed in Table 1.

Sequencing and phylogenetic analysis

PCR amplicons of 16S and 12S rDNA were excised from the agarose gels and purified using a QIAquick Gel Extraction Kit (Qiagen). Bidirectional sequencing was performed using specific PCR primers (Solgent). The resulting sequences were searched against the GenBank database using the Basic Local Alignment Search Tool (BLAST) available through the National Center for Biotechnology Information (NCBI), and sequence assembly and alignment were performed using Lasergene software version 8 (DNASTAR). Multiple sequence alignment was performed using ClustalX, the Windows-based interface of Clustal W, with default parameters. Phylogenetic analysis was conducted using the neighbor-joining method based on genetic distances. The robustness of the inferred tree was assessed by bootstrap analysis with 1,000 replicates using the Kimura 2-parameter model. This approach was used to evaluate species-level clustering and concordance with morphological identification based on partial mitochondrial 16S and 12S rDNA sequences.

Results

Morphological identification of tick species

H. longicornis and *Haemaphysalis flava* ticks were collected by flagging and dragging from forested areas, whereas *Ixodes nip-*

Table 1. Primer sequences used for amplification of 16S rDNA and 12S rDNA

Target gene	Primer name	Sequence (5′–3′)	Expected product size (bp)	References
16S rDNA	16s+1F	CTG CTC AAT GAA TAT TTA AAT TGC	450	[12]
	16S-1R	CGG TCT AAA CTC AGA TCA TGT AGG		
12S rDNA	T1B	AAA CTA GGA TTA GAT ACC CT	360	[14]
	T2A	AAT GAG AGC GAC GGG CGA TGT		

rDNA, ribosomal DNA.

https://doi.org/10.3347/PHD.26014

ponensis ticks were collected from wild rodents captured using Sherman live traps. Only adult ticks were selected for the morphological analysis.

The most frequently collected species was *H. longicornis*, comprising 30 adult specimens (No. 60–89), all of which were female; no males were detected. Among the 24 *H. flava* specimens (No. 1–24), 13 were male and 11 were female. All 20 *I. nipponensis* (No. 30–49) collected from wild rodents were female (Fig. 1A-J). In addition to ticks, various ectoparasites such as suspected fleas (No. 25–29), lice (No. 50–54), and mites (No. 55–59) were recovered from rodents.

In addition to the ticks collected from vegetation and rodents, 3 ticks were obtained from patients who had experienced recent tick bites. These specimens were partially damaged during removal, and could not be readily identified by morphological examination. Among them, 2 were tentatively classified under stereomicroscopy as *I. nipponensis* (Fig. 1Jb) and *Amblyomma testudinarium* (Fig. 1Jc), respectively; however, owing to specimen conditions, further confirmation via molecular analysis was deemed necessary. The third tick was too extensively damaged for morphological evaluation (Fig. 1Ja), and was directly subjected to molecular identification.

Molecular identification of ticks using 16S rDNA

Molecular identification based on 16S rDNA sequence analysis revealed species-dependent variation in the PCR amplification and sequencing success for molecular identification. Of the 74 morphologically identified tick specimens, 73 (98.6%) produced positive PCR amplicons. Sequencing was performed for all 73 PCR-positive samples, resulting in 38 (52.1%) high-quality sequences suitable for species-level identification (Table 2). All obtained sequences were verified

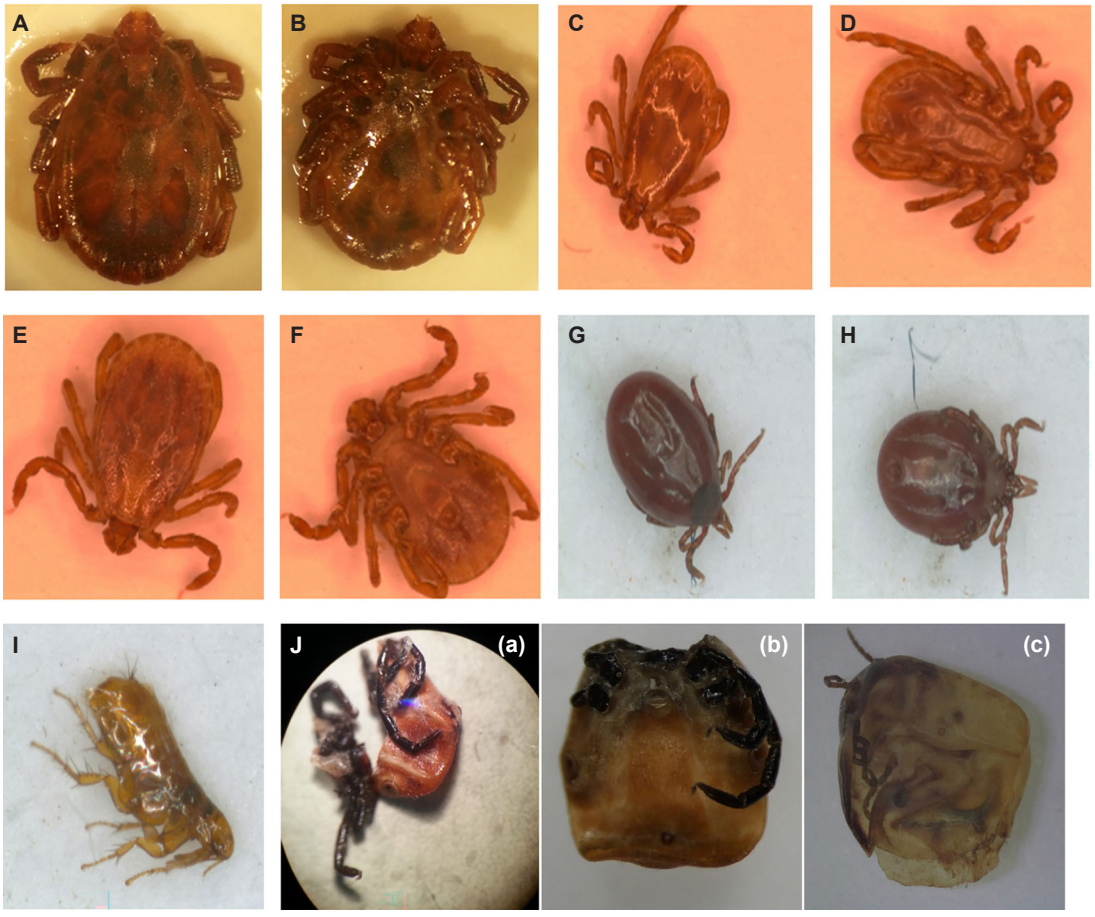


Fig. 1. Dorsal and ventral views of morphologically identified adult ticks (*Haemaphysalis longicornis*, *Haemaphysalis flava*, and *Ixodes nipponensis*), a *Ctenophthalmus* sp. flea collected from a wild rodent, and 3 damaged tick specimens removed from patients in this study. *H. longicornis* female, (A) dorsal and (B) ventral views; *H. flava* male, (C) dorsal and (D) ventral views; *H. flava* female, (E) dorsal and (F) ventral views; *I. nipponensis* female, (G) dorsal and (H) ventral views; (I) *Ctenophthalmus* sp. flea collected from a wild rodent; (J) Tick specimens removed from patients that were partially destroyed and unidentifiable by morphology: (a) severely damaged tick; (b) partially damaged tick tentatively identified as *I. nipponensis*; (c) partially damaged tick tentatively identified as *Amblyomma testudinarium*.

Table 2. PCR amplification and sequencing results for molecular identification of tick and rodent-associated ectoparasites based on 16S and 12S rDNA

Morphological identification[a]	PCR amplification		Sequencing success for identification	
	16S rDNA	12S rDNA	16S rDNA	12S rDNA
Haemaphysalis flava ($n=24$)	24/24 (100)	24/24 (100)	13/24 (54.2)	23/24 (95.8)
Haemaphysalis longicornis ($n=30$)	30/30 (100)	21/30 (70.0)	8/30 (26.7)	21/21 (100)
Ixodes nipponensis ($n=20$)	19/20 (95.0)	19/20 (95.0)	17/19 (89.5)	15/19 (78.9)
Suspect rat flea ($n=5$)	0/5 (0)	3/5 (60.0)	0/0 (0)	3/3 (100)
Suspect rat mite ($n=5$)	0/5 (0)	0/5 (0)	0/0 (0)	0/0 (0)
Suspect rat louse ($n=5$)	0/5 (0)	0/5 (0)	0/0 (0)	0/0 (0)

Values are presented as positive samples/total samples (%).
[a]*H. longicornis* and *H. flava* were collected by flagging and dragging, whereas *I. nipponensis*, as well as suspected fleas, mites, and lice were collected from wild rodents. Sequencing success indicates samples that yielded sequence data suitable for molecular identification.

using BLAST analysis against the NCBI nucleotide database.

H. flava sample (No. 1–24) exhibited a 100% PCR amplification rate (24/24), with 13 of 24 samples (54.2%) yielding sequence data suitable for molecular identification. The 16S rDNA sequences from 3 *H. flava* specimens (No. 11, 12, and 18) showed 98.6%–99.4% identity with the *H. flava* mitochondrial genome (GenBank accession No. NC_005292.1), originally isolated in Japan. The remaining ten 16S rDNA sequences showed 98.9%–100% identity with the *H. flava* isolate *H. flava*/HA2-16 large subunit ribosomal RNA gene, partial sequence (GenBank accession No. PP346283.1), which was originally isolated in China.

H. longicornis (No. 60–89) also showed 100% PCR amplification (30/30), but only 8 of 30 samples (26.7%) yielded sequence data suitable for molecular identification. These sequences shared 99.2%–99.7% identity with the *H. longicornis* mitochondrial genome (GenBank accession No. NC_037493.1), originally reported in China. In contrast, *I. nipponensis* (No. 30–49) showed a slightly lower PCR success rate (95.0%, 19/20) but the highest sequencing success for molecular identification (89.5%, 17/19). These sequences exhibited 93.7%–98.8% identity with the *I. nipponensis* isolate Liuyang mitochondrial genome (GenBank accession No. NC_058242.1), which was originally isolated in China. For concise presentation, identity values are shown here relative to a representative *I. nipponensis* reference genome sequence. However, species assignment was based on comparative similarity across multiple *I. nipponensis* 16S rDNA reference sequences, and some specimens showed higher similarity to other conspecific references, including PV602748, AB006022, and MF948173, than to NC_058242.1 (data not shown). All 38 sequences were consistent with their respective morphological identifications, supporting the overall reliability of 16S rDNA-based molecular identification of these tick species.

In addition, 16S rDNA sequence analysis enabled species-level identification of 3 severely damaged tick specimens that had been removed from patients and could not be classified morphologically (Fig. 1J). Two of the specimens (Fig. 1Ja, b) were identified as *I. nipponensis* and one (Fig. 1Jc) as *A. testudinarium*. The 16S rDNA sequences obtained from 2 *I. nipponensis* specimens (No. 2015-26, 2018-317) showed 99.4% and 97.6% identity, respectively, with the *I. nipponensis* isolate Liuyang mitochondrial genome (GenBank accession No. NC_058242.1) reported from China. The sequence from *A. testudinarium* specimen (No. 2018-433) showed 99.7% identity with the *A. testudinarium* isolate A59 mitochondrial genome (GenBank accession No. NC_062071.1), which was previously isolated from Gyeonggi province, Korea.

Molecular identification of ticks using 12S rDNA

Molecular identification based on 12S rDNA revealed species-dependent variations in PCR amplification and sequencing success for molecular identification. Of the 74 morphologically identified tick specimens, 64 (86.5%) produced positive PCR amplicons. Sequence analysis was performed for all 64 PCR products, and 59 (92.2%) yielded high-quality sequences suitable for species-level identification (Table 2). All obtained sequences were validated by BLAST analysis using the NCBI nucleotide database.

Sequencing success rates varied among the tick species. *H. flava* samples (No. 1–24) exhibited a 100% PCR amplification rate (24/24), with 23 of 24 samples (95.8%) yielding sequence data suitable for molecular identification. The resulting 12S rDNA sequences showed 98.5%–100% identity with the *H. flava* mitochondrial genome (GenBank accession No. NC_005292.1) isolated in Japan. *H. longicornis* (No. 60–89) exhibited the lowest PCR success rate, 70.0% (21/30); however, all 21 PCR-positive samples (100%) yielded sequence data

https://doi.org/10.3347/PHD.26014

suitable for molecular identification. These sequences showed 99.3%–99.7% identity with the *H. longicornis* mitochondrial genome (GenBank accession No. NC_037493.1) reported in China. *I. nipponensis* samples (No. 30–49) showed a PCR success rate of 95.0% (19/20) and 15 of the 19 PCR-positive samples (78.9%) yielded sequence data suitable for molecular identification. The resulting sequences exhibited 98.2%–99.4% identity with the *I. nipponensis* isolate Liuyang mitochondrial genome (GenBank accession No. NC_058242.1), which was originally isolated in China.

Molecular identification of rodent-associated ectoparasites

In addition to ticks, several ectoparasites presumed to be mites, lice, and fleas, were collected from wild rodents. PCR amplification targeting both 16S and 12S failed for the suspected mites and lice, thereby preventing molecular identification. However, 12S rDNA PCR was performed on 5 suspected flea specimens (No. 25–29), and 3 samples yielded positive amplicons. The resulting sequences were of high quality and suitable for species-level comparisons.

One flea specimen (No. 25) showed 94.1% identity to *Ctenophthalmus quadratus* Jordan & Rothschild, 1920 mitochondrial genome (GenBank accession No. NC_072692.1), suggesting that it belongs to the genus *Ctenophthalmus* (hereafter referred to as *Ctenophthalmus* sp.). Two other flea specimens (No. 25 and 29) showed 98.8% and 99.3% identity, respectively, with the *Neopsylla specialis* Smit, 1954 mitochondrial genome (GenBank accession No. NC_073019.1), which was also isolated in China.

Phylogenetic analysis

Phylogenetic analyses based on mitochondrial 16S and 12S rDNA sequences were performed to confirm species-level identification. The 16S rDNA phylogenetic tree was constructed using 41 sequences, including 38 tick specimens collected from vegetation and wild rodents and 3 damaged tick specimens removed from patients, together with reference sequences retrieved from the NCBI database. The resulting phylogenetic tree based on the 16S rDNA sequences clearly resolved *H. flava*, *H. longicornis*, *I. nipponensis*, and *A. testudinarium* into distinct and well-supported clades, with no outliers or unexpected placements (Fig. 2A). Similarly, the 12S rDNA phylogenetic tree, constructed from 59 tick and 3 flea sequences, showed well-defined and strongly supported clades corresponding to *H. flava*, *H. longicornis*, and *I. nipponensis*, without any anomalous branching. Additionally, sequences derived from flea specimens clustered with the reference sequences of *Ctenophthalmus* sp. (*C. quadratus* and *C. yunnanus* Liu, Wu & Wu, 1986) and *N. specialis* available in GenBank (Fig. 2B).

Discussion

Accurate identification of tick species is essential for understanding their ecological roles, assessing the risk of tick-borne disease transmission, and developing targeted control measures [8,9]. In this study, we evaluated the utility of mitochondrial 16S and 12S rDNA markers in identifying hard ticks and rodent-associated ectoparasites collected from diverse sources, including vegetation, wild rodents, and patients in Gwangju, Korea.

When the specimens were morphologically intact, molecular identification using both the 16S and 12S rDNA markers yielded results consistent with those of traditional taxonomy, supporting the reliability of both approaches under optimal conditions. However, morphology-based identification is often limited by physical damage, particularly in specimens removed from human patients. In such cases, molecular analysis proved essential and 3 morphologically unidentifiable specimens were successfully classified using 16S rDNA as *I. nipponensis* ($n=2$) and *A. testudinarium* ($n=1$), demonstrating the diagnostic utility of molecular methods in clinical or degraded samples. These findings further highlight the practical value of mitochondrial markers in identifying degraded or otherwise unidentifiable tick samples when morphological features are insufficient for taxonomic discrimination.

Although both mitochondrial markers were useful for species identification, their performances varied considerably among species. The 16S rDNA marker showed a high PCR amplification rate (98.6%) but a relatively low proportion of samples yielding sequence data suitable for molecular identification (52.1%). In contrast, 12S rDNA exhibited lower amplification efficiency (86.5%) but much higher sequencing success for molecular identification (92.2%). The relatively low sequencing success of 16S rDNA, despite PCR positivity, suggests that successful amplification did not always yield sequence data of sufficient quality for reliable analysis. This may have reflected variation in amplicon quality, reduced band resolution during preparative electrophoresis for gel extraction, purification-associated loss of sequence quality, or limited sequencing readability in some samples. These differences likely reflect interspecific variations in template DNA integrity, mitochondrial genome organization, and primer-binding affinity [12,13].

Among the 3 tick species, *I. nipponensis* showed the most

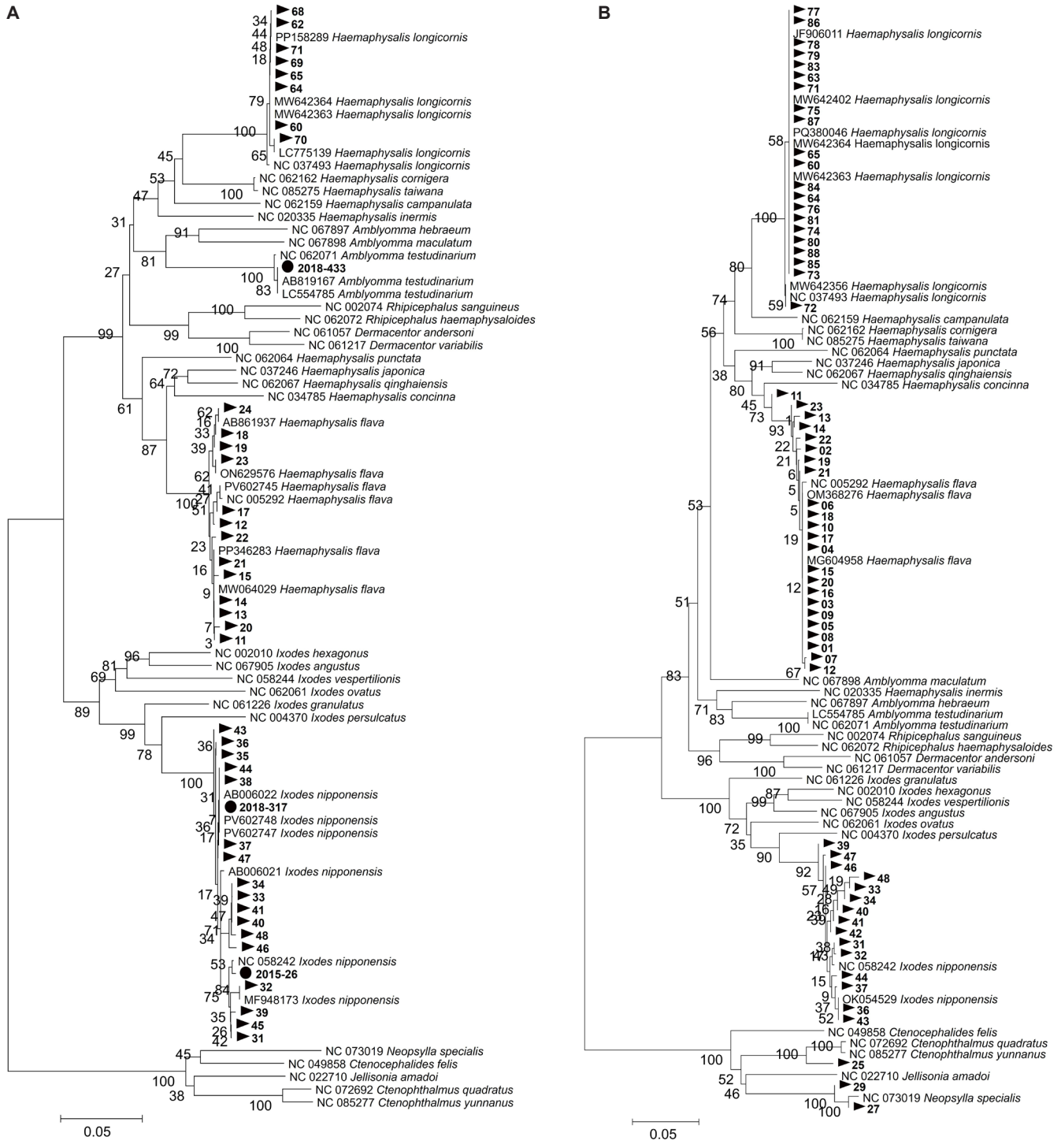


Fig. 2. Phylogenetic trees based on partial 16S and 12S ribosomal DNA (rDNA) sequences from ticks (*Haemaphysalis longicornis*, *Haemaphysalis flava*, *Ixodes nipponensis*, and *Amblyomma testudinarium*) and flea specimens (*Ctenophthalmus* sp. and *Neopsylla specialis*) collected in this study and reference sequences obtained from GenBank. Phylogenetic analyses were conducted using the neighbor-joining method based on aligned partial sequences of (A) 16S (354 bp) and (B) 12S (300 bp) rDNA. Bootstrap values (1,000 replicates) are shown at the nodes. Sequences generated in this study are marked with triangles (►), and sequences obtained from ticks removed from human patients (n=3) are indicated by filled circles (●). GenBank accession numbers are indicated for reference sequences.

https://doi.org/10.3347/PHD.26014

balanced performance across both markers, reflecting good primer compatibility and stable DNA integrity. In comparison, *H. flava* exhibited greater variation between the 2 loci, whereas *H. longicornis* showed a clear marker-dependent bias, with very low sequencing success for 16S but complete success for 12S. Together, these findings indicate that the performance of mitochondrial markers is influenced not only by marker type but also by species-specific sequence characteristics, and that marker choice may substantially affect identification outcomes. Therefore, species-specific optimization of molecular protocols is essential to enhance the accuracy and reproducibility of mitochondrial-based identification.

Previous studies have demonstrated that mitochondrial markers such as 16S and 12S rDNA are reliable tools for tick identification because of their moderate evolutionary rates, maternal inheritance, and lack of recombination [13,14]. The use of 12S rDNA sequences has been shown to effectively resolve phylogenetic relationships within *Rhipicephalus* and *Boophilus*, confirming their ability to distinguish closely related taxa [14]. Moreover, evaluations of multiple genetic loci have confirmed that both 16S and 12S rDNA markers are suitable for accurate species discrimination in ixodid ticks [13]. Additionally, the limitations of morphology-based identification for immature or damaged specimens have been highlighted, emphasizing the value of molecular approaches as complementary tools for species confirmation [4].

The phylogenetic analyses conducted in this study further validated the accuracy of molecular identification. Neighbor-joining phylogenetic trees based on 16S and 12S rDNA sequences reliably distinguished *H. flava*, *H. longicornis*, *I. nipponensis*, and *A. testudinarium*, with each species forming a distinct, well-supported clade. Moreover, 12S rDNA analysis successfully identified 3 flea specimens as *N. specialis* ($n=2$) and *Ctenophthalmus* sp. ($n=1$), indicating that this marker may be applicable beyond ticks and useful for detecting other arthropod ectoparasites in rodent surveillance. However, PCR amplification failed for all lice and mite specimens, indicating that the current primers are insufficient for broad ectoparasite detection. This finding suggests that, under the current assay conditions, the markers are more suitable for targeted tick identification than for broader ectoparasite screening. Taken together, these results support the exploratory utility of 12S rDNA for selected rodent-associated ectoparasites while also underscoring the limited taxonomic breadth of the present assay conditions. This limitation underscores the need to develop degenerate primers or adopt alternative molecular targets to improve the taxonomic coverage in future surveillance studies.

The ecological context also influenced the species composition of the ticks collected. Most *H. longicornis* and *H. flava* specimens were collected from vegetation in adjacent urban sites, whereas *I. nipponensis* was primarily associated with wild rodents, which is consistent with previous findings [17,18]. All *H. longicornis* and *I. nipponensis* specimens in this study were female, consistent with nationwide surveys reporting female dominance in field-collected ticks [19,20]. This female-biased pattern has also been documented in other ixodid tick populations and is thought to reflect behavioral and ecological differences between sexes. Adult females generally remain attached to hosts for extended feeding periods to complete engorgement and egg development, whereas males detach shortly after mating or exhibit limited feeding activity, resulting in their lower capture frequency during flagging or host-associated sampling [21,22]. Such biological differences likely contribute to the predominance of females observed in both vegetation-derived and rodent-derived samples. Importantly, this study demonstrated the presence of ticks capable of transmitting pathogens in commonly encountered environments, such as urban parks and nearby forested areas, supporting concerns regarding tick exposure risks during outdoor activities [23-25].

These findings also have practical implications for routine surveillance and clinical diagnostics. Mitochondrial 16S and 12S rDNA markers may complement morphological identification, particularly when tick specimens are damaged or difficult to classify, such as in field-collected or patient-derived specimens. In addition, the combined use of morphological and molecular methods may improve the accuracy of species-level data used in vector monitoring programs, thereby supporting more reliable epidemiological risk assessment and vector control planning.

Although this study focused on adult ticks, previous studies have demonstrated that the same molecular markers can be applied to larval and nymphal stages [8,13]. Several limitations of this study should also be considered. The number of tick specimens obtained directly from patients was small, which limits broader evaluation of the diagnostic utility of these markers in clinical specimens. Furthermore, because all specimens were collected in Gwangju, Korea, the results may not fully reflect tick diversity or marker performance in other geographic regions. The current primer sets also failed to amplify lice and mite specimens collected from wild rodents, suggesting that the current assay conditions are not yet suitable for broader ectoparasite detection without further optimization. Although the exact cause could not be determined

from the current data, limited primer compatibility is a plausible explanation, while reduced DNA quality in these specimens cannot be excluded. Future studies should extend molecular evaluations to immature stages, include larger numbers of patient-derived specimens from broader geographic areas, and assess additional markers, such as COI and ITS-2, after further optimization, to improve diagnostic resolution and taxonomic coverage.

In conclusion, mitochondrial 16S and 12S rDNA markers are effective tools for species-level identification of hard ticks, particularly when morphological identification is limited. Their combined use with morphological examination may improve species confirmation in routine surveillance and clinical settings, especially for damaged or morphologically ambiguous specimens. Continued efforts to refine molecular protocols, expand reference databases, and assess broader ectoparasite taxa across wider geographic regions and specimen types are essential to enhance tick surveillance and disease risk assessment.

Data availability

Sequence data and other study materials are available from the corresponding author upon reasonable request.

Author contributions

Conceptualization: Kim DM. Data curation: Kim SG, Lee YM. Formal analysis: Kim CM, Kim SG. Funding acquisition: Kim CM. Investigation: Lee YM, Kim SG. Methodology: Kim CM, Lee YM. Project administration: Kim DM. Resources: Kim SG, Seo JW, Kim DY, Yun NR. Supervision: Seo JW, Kim DY, Yun NR. Validation: Seo JW, Kim DY, Yun NR, Kim DM. Visualization: Kim SG, Lee YM. Writing – original draft: Kim CM, Kim SG. Writing – review & editing: Kim CM, Kim DM.

Conflict of interest

The authors have no conflicts of interest to declare.

Funding

This study was supported by a research fund from Chosun University, 2021.

ORCID

Choon-Mee Kim, https://orcid.org/0000-0003-4404-6214
You Mi Lee, https://orcid.org/0009-0002-4202-8282
Jun-Won Seo, https://orcid.org/0000-0002-2806-1863
Da Young Kim, https://orcid.org/0000-0002-1372-2286
Na Ra Yun, https://orcid.org/0000-0002-4219-0127
Dong-Min Kim, https://orcid.org/0000-0001-6373-0922

References

1. World Health Organization. Vector-borne diseases [Internet]. 2024 [cited 2026 Feb 1]. Available from: https://www.who.int/news-room/fact-sheets/detail/vector-borne-diseases
2. Song BG, Lee WG, Ju YR. Geographical distribution of Ixodid ticks in the Republic of Korea, 2015. Public Health Wkly Rep 2017;10:107-113.
3. Gai ZT, Zhang Y, Liang MF, et al. Clinical progress and risk factors for death in severe fever with thrombocytopenia syndrome patients. J Infect Dis 2012;206:1095-102. https://doi.org/10.1093/infdis/jis472
4. Walker AR, Bouattour A, Camicas JL, et al. Ticks of domestic animals in Africa: a guide to identification of species. University of Edinburgh; 2003.
5. Yu XJ, Liang MF, Zhang SY, et al. Fever with thrombocytopenia associated with a novel bunyavirus in China. N Engl J Med 2011;364:1523-32. https://doi.org/10.1056/NEJMoa1010095
6. Park SW, Song BG, Shin EH, et al. Prevalence of severe fever with thrombocytopenia syndrome virus in *Haemaphysalis longicornis* ticks in South Korea. Ticks Tick Borne Dis 2014;5:975-7. https://doi.org/10.1016/j.ttbdis.2014.07.020
7. Luo LM, Zhao L, Wen HL, et al. *Haemaphysalis longicornis* ticks as reservoir and vector of severe fever with thrombocytopenia syndrome virus in China. Emerg Infect Dis 2015;21:1770-6. https://doi.org/10.3201/eid2110.150126
8. Eisen RJ, Paddock CD. Tick and tickborne pathogen surveillance as a public health tool in the United States. J Med Entomol 2021;58:1490-502. https://doi.org/10.1093/jme/tjaa087
9. Makwarela TG, Seoraj-Pillai N, Nangammbi TC. Tick control strategies: critical insights into chemical, biological, physical, and integrated approaches for effective hard tick management. Vet Sci 2025;12:114. https://doi.org/10.3390/vetsci12020114
10. Intirach J, Lv X, Han Q, Lv ZY, Chen T. Morphological and molecular identification of hard ticks in Hainan Island, China. Genes (Basel) 2023;14:1592. https://doi.org/10.3390/genes14081592
11. Makwarela TG, Nyangiwe N, Masebe TM, et al. Morphological and molecular characterization of tick species infesting cattle in South Africa. Vet Sci 2024;11:638. https://doi.org/10.3390/vetsci11120638
12. Tian Z, Liu G, Xie J, et al. Discrimination between *Haemaphysalis longicornis* and *H. qinghaiensis* based on the partial 16S rDNA and the second internal transcribed spacer (ITS-2). Exp Appl Acarol 2011;54:165-72. https://doi.org/10.1007/s10493-010-9423-3
13. Lv J, Wu S, Zhang Y, et al. Assessment of four DNA fragments (COI, 16S rDNA, ITS2, 12S rDNA) for species identification of the Ixodida

(Acari: Ixodida). Parasit Vectors 2014;7:93. https://doi.org/10.1186/1756-3305-7-93
14. Beati L, Keirans JE. Analysis of the systematic relationships among ticks of the genera *Rhipicephalus* and *Boophilus* (Acari: Ixodidae) based on mitochondrial 12S ribosomal DNA gene sequences and morphological characters. J Parasitol 2001;87:32-48. https://doi.org/10.1645/0022-3395(2001)087[0032:AOTSRA]2.0.CO;2
15. Jalal S, Jha B, Kim CM, et al. Molecular detection of viruses causing hemorrhagic fevers in rodents in the south-west of Korea. J Neurovirol 2019;25:239-47. https://doi.org/10.1007/s13365-018-0708-3
16. Yamaguti N, Tipton VJ, Keegan HL, Toshioka S. Ticks of Japan, Korea, and the Ryukyu Islands. Brigh Young Univ Sci Bull Biol Ser 1971;15:1.
17. Kim CM, Yi YH, Yu DH, et al. Tick-borne rickettsial pathogens in ticks and small mammals in Korea. Appl Environ Microbiol 2006;72:5766-76. https://doi.org/10.1128/AEM.00431-06
18. Kim HC, Han SH, Chong ST, et al. Ticks collected from selected mammalian hosts surveyed in the Republic of Korea during 2008-2009. Korean J Parasitol 2011;49:331-5. https://doi.org/10.3347/kjp.2011.49.3.331
19. Kim-Jeon MD, Jegal S, Jun H, et al. Four year surveillance of the vector hard ticks for SFTS, Ganghwa-do, Republic of Korea. Korean J Parasitol 2019;57:691-8. https://doi.org/10.3347/kjp.2019.57.6.691
20. Kang SW, Doan HT, Choe SE, et al. Molecular investigation of tick-borne pathogens in ticks from grazing cattle in Korea. Parasitol Int 2013;62:276-82. https://doi.org/10.1016/j.parint.2013.02.002
21. Finney SK, Elston DA. Natural attachment duration of adult female ticks *Ixodes uriae* (Acari: Ixodidae) on free-living adult black-legged kittiwakes *Rissa tridactyla*. Exp appl acarol 1999;23:765-9. https://doi.org/10.1023/A:1006249309647
22. Richards SL, Langley R, Apperson CS, Watson E. Do tick attachment times vary between different tick-pathogen systems? Environments 2017;4:37. https://doi.org/10.3390/environments4020037
23. Niu G, Li J, Liang M, et al. Severe fever with thrombocytopenia syndrome virus among domesticated animals, China. Emerg Infect Dis 2013;19:756-63. https://doi.org/10.3201/eid1905.120245
24. Liang S, Bao C, Zhou M, et al. Seroprevalence and risk factors for severe fever with thrombocytopenia syndrome virus infection in Jiangsu Province, China, 2011. Am J Trop Med Hyg 2014;90:256-9. https://doi.org/10.4269/ajtmh.13-0423
25. Kato CY, Chung IH, Robinson LK, et al. Assessment of real-time PCR assay for detection of *Rickettsia* spp. and *Rickettsia rickettsii* in banked clinical samples. J Clin Microbiol 2013;51:314-7. https://doi.org/10.1128/JCM.01723-12

Brief Communication

Parasites Hosts Dis 2026;64(4):360-365
https://doi.org/10.3347/PHD.26011

Parasites, Hosts and Diseases

pISSN 2982-5164 • eISSN 2982-6799

Infection status of zoonotic intestinal helminths in striped field mice from Jeollabuk-do, Korea

Woon-Mok Sohn[1,*], Byoung-Kuk Na[1,2], Cheon-Hyeon Kim[3]

[1]Department of Parasitology and Tropical Medicine, Institute of Medical Science, Gyeongsang National University College of Medicine, Jinju, Korea; [2]Department of Convergence Medical Science, Gyeongsang National University, Jinju, Korea; [3]Department of Microbiology, Jeollabuk-do Institute of Health and Environment Research, Imsil, Korea

The present study was performed to investigate the infection status of zoonotic intestinal helminths in field mice captured from 7 local sites of Jeollabuk-do, Korea. A total of 78 *Apodemus agrarius* were collected in 7 survey sites, i.e., Sunchang-gun, Wanju-gun, Imsil-gun, Muju-gun, Gochang-gun, Jeonju-si, and Namwon-si, with Sherman live traps (Bioquip) for the surveillance of rodent-borne diseases through 2 times in 2019. The small intestine of each mouse was resected and longitudinally opened using scissors. The intestinal contents were washed with 0.85% saline until the supernatant became clear. The helminthic worms were collected with naked eyes and/or under a stereomicroscope from the sediment of the intestinal content. A total of 3 species of zoonotic intestinal helminths (1 trematode sp. and 2 cestode spp.) were collected. *Plagiorchis muris* were found in the small intestines of 7 (9.0%) mice (from Sunchang, Muju, Jeonju, and Namwon). Two species of tapeworm, *Hymenolepis nana* (from all survey sites except Wanju) and *Hymenolepis diminuta* (from Wanju, Imsil, and Namwon) were detected in 14 (17.9%) and 4 (5.1%) mice, respectively. The ventral view of *P. muris* was morphologically described. In this study, it was confirmed that 3 species of zoonotic intestinal helminths, *P. muris*, *H. nana*, and *H. diminuta*, are prevalent in striped field mice from Jeollabuk-do, Korea.

Keywords: Zoonotic intestinal helminth, *Plagiorchis muris*, *Hymenolepis nana*, *Hymenolepis diminuta*, *Apodemus agrarius*, Jeollabuk-do

Surveys on the rodent helminths of medical and veterinary importance have been performed to prevent disease transmission to human and domestic animals. A variety of rodent species were investigated in various regions of the world [1]. The striped field mouse, *Apodemus agrarius*, is the most dominant species and the agricultural pillager in Korea. This mouse species is widely and abundantly distributed in rural areas, especially forest in small mountains and agricultural fields, of Korea. It causes a great deal of economic loss in agricultural products and also acts as the natural transmitter for zoonotic parasites as well as pathogens like tularemia, leptospirosis, and hemorrhagic fever [2].

Since Nakamura and Kobayashi [3] first reported 2 species of helminths as the rodent parasites in Korea, many researchers have studied the helminthic infections of rodents. Ogura [4] reported 2 species of tapeworms, *Hymenolepis diminuta* and *Hymenolepis nana*, and Park [5] described *Isthmiophora hortensis* (syn. *Echinostoma hortense*) from the small intestine of brown rats, *Rattus norvegicus*. Seo et al. [6], Seo et al. [7], and Seo et al. [8] found and listed a variety of helminth species from the various species of rodent hosts in Korea. Seo et al. [9] detected 6 trematode species from 170 house rats, *Rattus* spp., collected from 13 localities of Korea. Lee et al. [10] also detected 6 trematode species in 2 brown rats from Yangyang-gun, Gangwon-do.

Received: January 24, 2026 Accepted: May 6, 2026
*Correspondence: wmsohn@gnu.ac.kr

© 2026 The Korean Society for Parasitology and Tropical Medicine

This is an open-access article distributed under the terms of the Creative Commons Attribution Non-Commercial License (http://creativecommons.org/licenses/by-nc/4.0/) which permits unrestricted non-commercial use, distribution, and reproduction in any medium, provided the original work is properly cited.

Citation
Sohn WM, Na BK, Kim CH. Infection status of zoonotic intestinal helminths in striped field mice from Jeollabuk-do, Korea. Parasites Hosts Dis 2026;64(4):360-365.

Yong et al. [11] reported the infections of 2 protozoa and 7 helminth species from 107 field mice examined. Seong et al. [12] found 3 helminth species in 43 brown rats from Chuncheon-si, Gangwon-do.

In the 2000s, Chai et al. [13], Chai et al. [14], and Chai et al. [15] described infections with *Plagiorchis muris*, *Neodiplostomum seoulense* (syn. *Fibricola seoulensis*), and echinostomes in field mice from northern Gyeonggi-do near the Demilitarized Zone in Korea. Lee et al. [16] reported the infections of intestinal helminths in 43 *A. agrarius* and 11 *Apodemus peninsulae* caught from 3 sites of Yanggu-gun and Inje-gun in northern Gangwon-do. Sohn et al. [17] described the infection status of intestinal helminths in striped field mice from 2 southern regions, Hapcheon-gun, Gyeongsangnam-do, and Gurye-gun, Jeollanam-do. Lee et al. [18] surveyed the infection status of intestinal helminths in 2 species of field mice, *A. agrarius* and *A. peninsulae*, captured in the mountainous areas and agricultural fields of Gangwon-do and Chungcheongnam-do. Kim et al. [19] reported a case of fascioliasis in a wild nutria, *Myocastor coypus*, in Korea. Recently, we performed a survey to know the infection status of zoonotic intestinal helminths (ZIH) in striped field mice, *A. agrarius*, captured in 7 local sites of Jeollabuk-do, Korea. Additionally, the ventral view of *P. muris* was described with the worm samples recovered in this study.

A total of 78 striped field mice, *A. agrarius*, were collected in 7 local sites of Jeollabuk-do, Korea in each 2 times, May–June and September–October, 2019. Shermen rodent live traps (3.0×3.5×9.0 inch; Bioquip) were set in these survey areas in the afternoon and were collected at the early morning of next day. The number of mice captured and survey localities are detailed in Table 1. The collected mice were anesthetized and killed after taking samples for preventive studies of febrile diseases in the laboratory of Jeollabuk-do Institutes of Health and Environment Research, in Imsil-gun, Korea. Intestines of each mouse were extracted from the abdominal cavity after dissection, contained in a specimen bottle with 0.85% saline, and transported to the laboratory in the Department of Parasitology and Tropical Medicine, Gyeongsang National University College of Medicine, in Jinju-si, Gyeongsangnam-do. The small intestines of each mouse were resected and longitudinally opened with scissors. The intestinal contents were washed with 0.85% saline until the supernatant became clear. The helminths were collected with naked eyes and/or under a stereomicroscope from the sediment of intestinal content. The collected helminths were counted to get hold of infection rates and intensities per mouse infected by the survey localities. Additionally, we observed the ventral morphologies of 10 *P. muris* adults recovered in this study with a light microscope (Olympus BH-22, Olympus) equipped with a micrometer. All measurements are given in μm, and length × width (average).

Three species of ZIH, i.e., *P. muris*, *H. nana*, and *H. diminuta*, were recovered. Adult worms of *P. muris* were found in 7 (9.0%) mice from 4 survey sites. *H. nana* was detected in 14 (17.9%) mice from 6 survey sites. *H. diminuta* was collected in 4 (5.1%) mice from 3 survey sites. The prevalence of 3 ZIH by survey sites was shown in Table 1. The infection intensity of *P. muris* was 3.3 on average. It was the highest in a mouse from Namwon-si (6.0), followed by 3 mice from Jeonju-si (3.7 on average), 2 mice from Sunchang-gun (2.5 on average) and a mouse from Muju-gun (1.0).

Adults of *P. muris* (Fig. 1) were dorsoventrally flattened and elongated, 1,050–1,750 (1,610) long and 450–650 (548) in maximum width, which is in the ventral sucker (VS) and/or ovary level. The ratio of body width to body length 1:2.94 on average. The oral sucker (OS) was round, 155–210 (186) × 170–220 (192) in size. Pharynx muscular, oval shape and 55–80 (68) × 75–105 (88) in size. Esophagus absent and intestinal ceca immediately bifurcated at the posterior end of pharynx and then terminated at the posterior region of the body. VS round, slightly smaller than the OS (the ratio of OS to VS 1:0.93 on average), 140–205 (172) × 155–200 (177) in size and situated on the anterior 1/3 of body. The cirrus sac was reverse C-shaped, 200–420 (327) long

Table 1. Results of the worm recovery in the small intestines of striped field mice from 7 localities of Jeollabuk-do, Korea

Helminth		No. (%) of mice infected with helminth by localities[a]							
		Sunchang (*n*=7)	Wanju (*n*=12)	Imsil (*n*=11)	Muju (*n*=21)	Jeonju (*n*=9)	Namwon (*n*=13)	Gochang (*n*=5)	Total (*n*=78)
Trematoda	*Plagiorchis muris*	2 (28.6)	0	0	1 (4.8)	3 (33.3)	1 (7.7)	0	7 (9.0)
Cestoda	*Hymenolepis nana*	1 (14.3)	0	3 (27.3)	1 (4.8)	3 (33.3)	5 (38.5)	1 (20.0)	14 (17.9)
	Hymenolepis diminuta	0	1 (8.3)	2 (18.2)	0	0	1 (7.7)	0	4 (5.1)

[a]Sunchang (Jisan-ri, Ingae-myeon, Sunchang-gun: 35°23'37.9"N 127°10'16.3"E), Wanju (Yongam-ri, Sanggwan-myeon, Wanju-gun: 35°43'36.0"N 127°13'47.5"E), Imsil (Shinan-ri, Imsil-eup, Imsil-gun: 35°35'34.4"N 127°14'32.7"E), Muju (Daeso-ri, Bunam-myeon, Muju-gun: 35°58'36.7"N 127°33'37.4"E), Jeonju (Daeseong-dong, Wansan-gu, Jeonju-si: 35°47'16.2"N 127°10'35.8"E), Namwon (Doryong-ri, Bojeol-myeon, Namwon-si: 35°31'52.8"N 127°26'04.9"E), Gochang (Yeonhwa-ri, Simwon-myeon, Gochang-gun: 35°29'58.6"N 126°33'29.5"E).

and 45–70 (54) maximum wide, obliquely passing between the left bottom side of VS and the right upper side of ovary. The ovary was round or elliptical, located at the left bottom side of cirrus sac and leftly deviated from the median line, 110–185 (144) × 125–160 (151) in size. Testes round or elliptical, big, located at the posterior region of ovary, obliquely located and separated from each other by uterine coils. Anterior testis mostly round, 195–330 (246) × 165–290 (230) in size. Posterior testis long elliptical, 210–360 (282) × 155–275 (199) in size. Seminal receptacle was absent. The vitellaria were follicular and numerous mostly distributed to both lateral fields from the mid-level of OS to posterior end of body, and confluently distributed at anterior body between the mid-level of OS and VS level. Uterus reverse S-shape or ?-shape, mostly occupying from the right 2/3-level side or bottom side of VS to the posterior end. Eggs yellowish with an operculum, numerous, 28–33 (31) × 18–20 (19) in size.

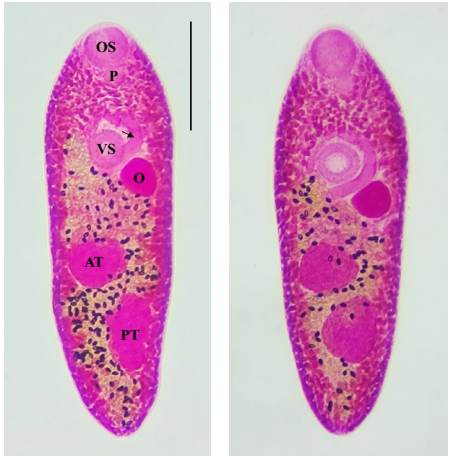


Fig. 1. Ventral views of 2 *Plagiorchis muris* detected in a striped field mouse, *Apodemus agrarius*, from a survey site of Namwon-si, Jeollabuk-do, Korea. OS, oral sucker; P, pharynx; VS, ventral sucker; O, ovary; AT, anterior testis; PT, posterior testis. Arrow indicates cirrus sac. Scale bar=500 μm.

This study was only performed with the intestines resected from individual field mouse transported from Department of Microbiology, Jeollabuk-do Institute of Health and Environment Research. The institutional animal care and use committee was not responsible in the institution of corresponding author, Gyeongsang National University, College of Medicine. However, the ethical approval in institutional animal care and use committee was obtained on the collection, euthanasia and necropsy of field mice individuals in the original project entitled "Study on the pathogenic characterization of rodent-borne diseases by climatic changes."

The striped field mouse, *A. agrarius*, is the most widely and abundantly distributed in rural areas of Korea. Therefore, the helminthic infections were most frequently examined with this mouse species (Tables 2, 3) [6,8,11,13,16-18]. Seo et al. [6] examined the helminthic infection with 221 *A. agrarius* from 5 local areas of Gangwon-do and Gyeonggi-do. Chai et al. [13], Chai et al. [14], and Chai et al. [15] examined a total of 1,366 striped field mice from 3 regions of northern Gyeonggi-do. A helminthic survey was performed with 43 *A. agrarius* (together with 11 *A. peninsulae*) from Yanggu-gun and Inje-gun in northern Gangwon-do [16]. A survey on the infection status of helminths was performed with 133 and 103 striped field mice from Hapcheon-gun, Gyeongsangnam-do and Gurye-gun, Jeollanam-do [17]. Lee et al. [18] surveyed the infections of intestinal helminths with 57 *A. agrarius* (together with 26 *A. peninsulae*), from mountainous regions and agricultural fields of Gangwon-do and Chungcheongnam-do. In this study, we examined 78 small intestines of striped field mice captured in 7 local areas of Jeollabuk-do. The number of mice examined were much different by the survey localities, from 5 (Gochang-gun) to 21 mice (Muju-gun). Therefore, the prevalence of ZIH is more or less meaningless by survey localities, but the overall trend of ZIH infections is obviously revealed in striped field mice from Jeollabuk-do by this study.

Table 2. Comparison of *Plagiorchis muris* recovery in the striped field mice, *Apodemus agrarius*, by authors in Korea

Items	Present study (2026)	Sohn et al. (2014) [17][a]	Lee et al. (2013) [16]	Chai et al. (2007) [13]	Seo et al. (1964) [6]
No. of mice examined	78	236	43	1,366	221
No. (%) of mice infected	7 (9.0)	35 (14.8)	2 (4.7)	72 (5.3)	5 (2.3)
No. (average) of worms recovered	1–6 (3.3)	1–71 (7.8)	- (1.0)	1–263 (22.9)	- (5.5)[b]
Survey localities	Seven local sites in Jeonbuk	Hapcheon in Gyeongnam, Gurye in Jeonnam	Yanggu-gun, Inje-gun in Gangwon	Paju-si, Yeoncheon-gun, Pocheon-si in Gyeonggi	Cheorwon-gun in Gangwon, Pocheon-si in Gyeonggi

[a]In 2 survey localities, Hapcheon-gun, Gyeongsangnam-do and Gurye-gun, Jeollanam-do, 133 and 103 striped field mice were examined; 26 (19.5%) and 9 (8.7%) mice infected; 1–71 (9.9) and 1–3 (1.9) infection intensities were showed, respectively; [b]A total of 33 *P. muris* were recovered from 5 *A. agrarius* and 1 *Rattus alexandrinus*.

https://doi.org/10.3347/PHD.26011

Table 3. Prevalence[a] of intestinal tapeworms in the striped field mice, *Apodemus agrarius*, by authors in Korea

Items	Present study (2026)	Lee et al. (2018) [18][b]	Sohn et al. (2014) [17]	Lee et al. (2013) [16][c]	Yong et al. (1991) [11][d]	Seo et al. (1968) [8][e]
Hymenolepis nana	14/78 (17.9)	-	79/236 (33.5)	4/43 (9.3)	16/85 (18.8)	10/219 (4.6)
Hymenolepis diminuta	4/78 (5.1)	9/57 (16.4)	21/236 (8.9)	12/43 (27.9)	13/85 (15.2)	7/219 (3.2)
Raillietina coreensis	-	-	-	-	-	2/219 (0.9)
Paranoplocephala sp.	-	-	-	-	-	1/219 (0.5)
Survey localities	Seven local sites in Jeonbuk	Wonju-si in Gangwon, Gongju-si in Chungnam	Hapcheon in Gyeongnam, Gurye in Jeonnam	Yanggu-gun, Inje-gun in Gangwon	Goyang-si in Gyeonggi, Iksan-si in Jeonbuk	Paju-si, Pocheon-si, Cheongpyeong-myeon in Gapyeong-gun, Gyeonggi, Cheorwon-gun in Gangwon

[a]No. of mice infected/No. of mice examined (%); [b]*H. diminuta* were detected in 5 (19.2%) out of 26 *Apodemus peninsulae* examined; [c]*H. diminuta* were found in 6 (54.5%) out of 11 *A. peninsulae* examined; [d]*H. nana* were found in 1 (16.7%) *Crocidura russula* and 1 (16.7%) *Micronys minutus*; [e]*H. diminuta* were detected in 2 (6.1%) out of 33 brown rats, *Rattus norvegicus*, examined. Seo et al. [7] reported the prevalence of 2 tapeworm species, i.e., *H. diminuta* and *H. nana*, in 52 (16.0%) and 4 (1.2%) out of 325 brown rats, *R. norvegicus*, captured in Seoul respectively.

Since Park [5] first reported *I. hortensis* as a rodent trematode in 1938, more than 11 trematode species were described and listed from rodent hosts in Korea [6-11,13-17,19]. Seo et al. [6] described the infections of 5 trematode species, i.e., *I. hortensis*, *Echinostoma cinetorchis*, *Euparyphium murinum*, *P. muris*, and *N. seoulense*, from rodent hosts. Seo et al. [9] found 6 trematode species, i.e., *Clonorchis sinensis*, *Metagonimus yokogawai*, *E. cinetorchis*, *I. hortensis*, *P. muris*, and *N. seoulense*, from 170 house rats. Lee et al. [10] also reported 6 trematode species, i.e., *I. hortensis*, *E. cinetorchis*, *Echinostoma revolutum*, *Echinoparyphium recurvatum*, *P. muris*, and *N. seoulense*, in 2 house rats from Yangyang-gun, Gangwon-do. Only 1 specimen of *Echinochasmus japonicus* was detected from a striped field mouse by Yong et al. [11]. Chai et al. [13], Chai et al. [14], and Chai et al. [15] detected *P. muris*, *N. seoulense*, and 4 species of echinostomes (*I. hortensis*, *E. cinetorchis*, *E. japonicus*, and *E. murinum*) in the field mice from the northern Gyeonggi-do. Sohn et al. [17] reported 4 species of trematodes, *I. hortensis*, *E. cinetorchis*, *P. muris*, and *Brachylaima* sp., recovered in the small intestines of *A. agrarius* from Hapcheon-gun, Gyeongsangnam-do and Gurye-gun, Jeollanam-do. Recently, Kim et al. [19] described a case of *Fasciola* sp. infection in a wild nutria from the wetland around Nakdong-gang (gang means river). From the previous studies, we can know that 3 trematode species, *I. hortensis*, *E. cinetorchis*, and *P. muris*, were commonly detected from rodent hosts in Korea.

In this study, only 1 trematode species, *P. muris*, was recovered in 7 (9.0%) out of 78 striped field mice examined, and the infection intensity was 1–6 (3.3 on average) per mouse infected. In Sohn et al. [17], the prevalence of this trematode was 19.5% and 8.7% in 133 and 103 striped field mice from Hapcheon-gun, Gyeongsangnam-do and Gurye-gun, Jeollanam-do, Korea. Their infection intensities were 1–71 (9.9) and 1–3 (1.9) in mice from Hapcheon-gun and Gurye-gun. Chai et al. [13] detected 1–263 (22.9 on average) *P. muris* from 72 (5.3%) out of 1,366 striped field mice from 3 regions, Paju-si, Yeoncheon-gun and Pocheon-si, of northern Gyeonggi-do. Lee et al. [16] recovered these trematodes from 2 (4.7%) out of 43 *A. agrarius* caught from Yanggu-gun and Inje-gun in northern Gangwon-do. Lee et al. [10] found 2 *P. muris* in a house rat from Yangyang-gun, Gangwon-do. Seo et al. [9] detected 2 *P. muris* from 2 (1.2%) out of 170 house rats, *Rattus* spp. caught in 13 localities of Korea. Seo et al. [6] collected a total of 33 *P. muris* from 5 (2.3%) out of 221 *A. agrarius* and 1 (12.5%) of 8 *Rattus alexandrinus* (Table 2) [6,13,16,17]. When we analyze the infection status of *P. muris* reported in previous studies and in the present study, we can presume that the striped field mouse, *A. agrarius*, is to be the most suitable rodent host of this trematode. Additionally, the prevalence of this trematode was more or less higher in mice from Hapcheon-gun, Gyeongsangnam-do, but the infection intensity was much higher in mice from northern Gyeonggi-do [13,17]. However, it is questionable that how the field mice get infected with these trematodes. The dragonflies have been commonly known as the second intermediate hosts and the infection source of this trematode in definitive hosts like bats [20]. How can field mice readily catch and consume dragonflies?

We found that the morphological descriptions of *P. muris* were made with the dorsal-side view in previous studies [6,16]. Therefore, we described the ventral-side view of *P. muris* adults recovered in this study. This species of trematode is morphologically characterized by a small and/or medium sized, an OS slightly larger than VS, a left-deviated ovary, 2

tandem testes, and follicular vitellaria mainly distributed to both lateral fields from the mid-level of OS to posterior end of body. This species distinctly differs from other 3 species, i.e., *P. koreanus*, *P. rhinolophi*, and *P. magnacotylus*, which were described from Korean bats, in the body size and distribution of vitellaria.

A total of 5 species of tapeworms, i.e., *Cysticercus fasciolaris* (metacestode of *Hydatigera taeniaeformis*), *H. diminuta*, *H. nana*, *Raillietina coreensis*, and *Paranoplocephala* sp., have been reported from rodent hosts in Korea [3,4,8]. Since Nakamura and Kobayashi [3] first reported *C. fasciolaris* as the rodent tapeworm in Korea, this larval cestode was frequently detected in the liver of rodent hosts [7,8,11,12]. Especially, Seo et al. [7] found *C. fasciolaris* in 65 (20.0%) out of 325 brown rats, *R. norvegicus*, captured in Seoul. Seo et al. [8] detected *C. fasciolaris* in 2 (6.1%) out of 33 brown rats. Yong et al. [11] and Seong et al. [12] also reported the infections of this larval cestode in Korea. Since Ogura [4] described *H. diminuta* and *H. nana* from rodent hosts of Korea, many Korean workers reported the infection status of intestinal rodent tapeworms in Korea (Table 3) [8,11,16-18]. In this study, 2 tapeworm species, *H. diminuta* and *H. nana*, were found in 4 (5.1%) and 14 (17.9%) out of 78 *A. agrarius* caught from 7 local sites of Jeollabuk-do. From the previous and present studies, we can know that 3 tapeworm species, *C. fasciolaris*, *H. diminuta*, and *H. nana*, are frequently found from the rodent hosts of Korea [3,4,8,11,12,16-18]. The larval tapeworm, *C. fasciolaris*, inhabited in the liver of rodent hosts was not found in recent surveys on the intestinal helminth infections including the present study [16-18]. Two species of tapeworm, *H. nana* and *H. diminuta*, were widely distributed and zoonotic intestinal cestodes of rodents in Korea. They can be distinguished by their unique morphologies, i.e., the size of whole strobila, scolex, mature and gravid proglottids, and eggs, even in mixed infections in the small intestines of field mouse.

Conclusively, the infection trend of ZIH is partly revealed with a survey of 78 striped field mice, *A. agrarius*, from 7 local sites of Jeollabuk-do, Korea by the present study. Some species of helminths belong to the nematode, trematode and cestode parasitic in the rodent hosts can be the zoonotic pathogens. Especially, 4 trematode species, *E. cinetorchis*, *I. hortensis*, *P. muris*, and *N. seoulense*, and 2 cestode species, *H. nana* and *H. diminuta*, also infect humans. Wild rodents can act as the reservoir hosts of these ZIH in Korea. Accordingly, the surveillance on the ZIH infections in wild rodents should be continued in the future.

Author contributions

Conceptualization: Sohn WM. Data curation: Sohn WM, Na BK, Kim CH. Formal analysis: Sohn WM, Na BK. Investigation: Sohn WM, Na BK, Kim CH. Methodology: Sohn WM, Na BK, Kim CH. Project administration: Sohn WM, Kim CH. Supervision: Sohn WM. Validation: Sohn WM, Na BK. Visualization: Sohn WM. Writing – original draft: Sohn WM. Writing – review & editing: Sohn WM, Na BK.

Conflict of interest

Woon-Mok Sohn and Byoung-Kuk Na serve as editors of Parasites, Hosts and Diseases but had no involvement in the decision to publish this article. No other potential conflicts of interest relevant to this study were reported.

ORCID

Woon-Mok Sohn, https://orcid.org/0000-0002-9795-9386
Byoung-Kuk Na, https://orcid.org/0000-0002-6734-1673
Cheon-Hyeon Kim, https://orcid.org/0009-0007-5026-6236

References

1. Chaisiri K, Chaeychomsri W, Siruntawineti J, et al. Diversity of gastrointestinal helminths among murid rodents from northern and northeastern Thailand. Southeast Asian J Trop Med Public Health 2012;43:21-8.
2. Rabiee MH, Mahmoudi A, Siahsarvie R, Kryštufek B, Mostafavi E. Rodent-borne diseases and their public health importance in Iran. PLoS Negl Trop Dis 2018;12:e0006256. https://doi.org/10.1371/journal.pntd.0006256
3. Nakamura K, Kobayashi S. Rat species in Chosen and their ecto- and endoparasites. J Chosen Med Assoc 1935;25:183-4.
4. Ogura K. Studies on the *Hymenolepis nana* in Korea. Chosen Igakkai Zasshi 1936;26:649-68.
5. Park JT. A rat trematode, *Echinostoma hortense* Asada, from Korea. Keijo J Med 1938;9:283-6.
6. Seo BS, Rim HJ, Lee CW. Studies on the parasitic helminths of Korea: I. Trematodes of rodents. Korean J Parasitol 1964;2:20-6. https://doi.org/10.3347/kjp.1964.2.1.20
7. Seo BS, Rim HJ, Lee CW, Yoon JS. Studies on the parasitic helminths of Korea: II. Parasites of the rat, *Rattus norvegicus* Erxl. in Seoul, with the description of *Capillaria hepatica* (Bancroft, 1893) Travassos, 1915. Korean J Parasitol 1964;2:55-62. https://doi.org/10.3347/kjp.1964.2.1.55
8. Seo BS, Rim HJ, Yoon JJ, Koo BY, Hong NT. Studies on the parasitic helminths of Korea: III. Nematodes and cestodes of rodents. Korean J Parasitol 1968;6:123-31. https://doi.org/10.3347/kjp.1968.6.3.123

https://doi.org/10.3347/PHD.26011

9. Seo BS, Cho SY, Hong ST, Hong SJ, Lee SH. Studies on parasitic helminths of Korea: V. Survey on intestinal trematodes of house rats. Korean J Parasitol 1981;19:131-6. https://doi.org/10.3347/kjp.1981.19.2.131
10. Lee SH, Sohn WM, Chai JY. *Echinostoma revolutum* and *Echinoparyphium recurvatum* recovered from house rats in Yangyang-gun, Kangwon-do. Korean J Parasitol 1990;28:235-40. https://doi.org/10.3347/kjp.1990.28.4.235
11. Yong TS, Chung KH, Ree HI. Infection status of parasites of field rodents in Korea. Yonsei Rep Trop Med 1991;22:55-9.
12. Seong JK, Huh S, Lee JS, Oh YS. Helminths in *Rattus norvegicus* captured in Chunchon, Korea. Korean J Parasitol 1995;33:235-7. https://doi.org/10.3347/kjp.1995.33.3.235
13. Chai JY, Park JH, Guk SM, et al. *Plagiorchis muris* infection in *Apodemus agrarius* from northern Gyeonggi-do (province) near the demilitarized zone. Korean J Parasitol 2007;45:153-6. https://doi.org/10.3347/kjp.2007.45.2.153
14. Chai JY, Park JH, Guk SM, et al. *Apodemus agrarius* as a new definitive host for *Neodiplostomum seoulense*. Korean J Parasitol 2007;45:157-61. https://doi.org/10.3347/kjp.2007.45.2.157
15. Chai JY, Park JH, Jung BK, et al. Echinostome infections in the striped-field mouse, *Apodemus agrarius*, and the Ussuri white-toothed shrew, *Crocidura lasiura*, caught near the demilitarized zone, Gyeonggi-do (Province), Republic of Korea. Korean J Parasitol 2009;47:311-4. https://doi.org/10.3347/kjp.2009.47.3.311
16. Lee YI, Pyeon HJ, Seo M. Intestinal parasites among wild rodents in northern Gangwon-do, Korea. Korean J Parasitol 2013;51:603-6. https://doi.org/10.3347/kjp.2013.51.5.603
17. Sohn WM, Na BK, Song HJ, Kim CM, Nam GJ. Intestinal helminthic infections in striped field mice, *Apodemus agrarius*, from two southern regions of Korea. Korean J Parasitol 2014;52:419-23. https://doi.org/10.3347/kjp.2014.52.4.419
18. Lee JH, Gong S, Park YC, et al. Infections of intestinal helminth at two species of field mice, *Apodemus agrarius* and *A. peninsulae*, in Gangwon-do and Chungcheongnam-do, Korea. Korean J Parasitol 2018;56:301-4. https://doi.org/10.3347/kjp.2018.56.3.301
19. Kim HS, Kong JY, Kim JH, Yeon SC, Hong IH. A case of fascioliasis in a wild nutria, *Myocastor coypus*, in Republic of Korea. Korean J Parasitol 2018;56:375-8. https://doi.org/10.3347/kjp.2018.56.4.375
20. Hong SJ, Woo HC, Lee SU, Huh S. Infection status of dragonflies with *Plagiorchis muris* metacercariae in Korea. Korean J Parasitol 1999;37:65-70. https://doi.org/10.3347/kjp.1999.37.2.65

Brief Communication

Parasites Hosts Dis 2026;64(4):366-373
https://doi.org/10.3347/PHD.26019

Parasites, Hosts and Diseases

pISSN 2982–5164 • eISSN 2982–6799

Toxoplasma gondii GRA16 enhances the inhibitory effects of standard DNA-damaging chemotherapeutics in liver, pancreatic, and colorectal cancer cells

Seung-Hwan Seo[1,2], Ji-Eun Lee[1], Eun-Ji Cho[1], Eun-Hee Shin[1,2,3,*]

[1]Department of Tropical Medicine and Parasitology, Seoul National University College of Medicine, Seoul, Korea; [2]Institute of Endemic Diseases, Medical Research Center, Seoul National University, Seoul, Korea; [3]Seoul National University Bundang Hospital, Seongnam, Korea

Dense granule protein 16 (GRA16), an effector protein from *Toxoplasma gondii*, has been reported to enhance antitumor responses in several malignancies. However, whether GRA16 can enhance the inhibitory effects of standard anticancer drugs across diverse cancer types remains unclear. Gemcitabine, oxaliplatin, and irinotecan continue to play a key role in clinical oncology; however, their efficacy is limited by persistent tumor survival-promoting pathways. In this study, we stably expressed GRA16 in HepG2, PANC-1, and HCT116 cells and evaluated their responses to gemcitabine, oxaliplatin, and irinotecan under 50% inhibitory concentration-normalized dosing conditions. In vector control cells, baseline drug sensitivity was quantified using the CCK-8 assay across 0–64 μM after 48 h of exposure, and 50% inhibitory concentration was determined for each drug and cell line. Time-dependent proliferation assays (0–72 h) demonstrated that GRA16 reduced the basal growth rate and enhanced the growth inhibitory effects of all 3 drugs in all 3 cell models. Representative microscopy images at 48 h were consistent with reduced cell density in GRA16-expressing cultures under each treatment condition. These in vitro data indicate that GRA16 enhances the inhibitory effects of standard chemotherapeutic agents in hepatic, pancreatic, and colorectal cancer cell lines. This study provides a cross-cancer, multi-drug evaluation of GRA16-associated enhancement of drug response and includes, to our knowledge, the first assessment in a pancreatic cancer model. The underlying mechanism may involve pathway modulation, as suggested by previous studies and supported by the pancreatic cancer model although it was not comprehensively examined across all cell lines.

Keywords: *Toxoplasma gondii*, GRA16, drug response, gemcitabine, oxaliplatin, irinotecan

Gemcitabine, oxaliplatin, and irinotecan are widely used chemotherapeutic agents in clinical oncology that exert cytotoxic effects primarily through DNA damage or topoisomerase I (Topo-I) inhibition [1-4]. However, their clinical activity is often constrained by persistent tumor cell survival signaling, which can drive the development of chemoresistance. Gemcitabine resistance has been associated with activation of the phosphoinositide 3-kinase/protein kinase B (PI3K/AKT) and dysregulation of extracellular signal-regulated kinase (ERK) signaling [1]. Oxaliplatin resistance has similarly been associated with PI3K/AKT signaling, and pharmacologic inhibition of this pathway can restore drug responsiveness [2]. Irinotecan resistance has been linked to pro-survival nuclear factor-κB (NF-κB) and ERK signaling, and targeting these pathways can enhance the efficacy of SN38/irinotecan [3,4]. Collectively, these findings highlight the need for agents that can inhibit survival pathways to enhance the inhibitory response to chemotherapeutic treatment. To explore this concept in a relevant in vitro setting, we

Received: March 10, 2026; Accepted: June 2, 2026
*Correspondence: ehshin@snu.ac.kr

© 2026 The Korean Society for Parasitology and Tropical Medicine

This is an open-access article distributed under the terms of the Creative Commons Attribution Non-Commercial License (http://creativecommons.org/licenses/by-nc/4.0/) which permits unrestricted non-commercial use, distribution, and reproduction in any medium, provided the original work is properly cited.

Citation
Seo SH, Lee JE, Cho EJ, Shin EH. *Toxoplasma gondii* GRA16 enhances the inhibitory effects of standard DNA-damaging chemotherapeutics in liver, pancreatic, and colorectal cancer cells. Parasites Hosts Dis 2026;64(4):366-373.

focused on liver (HepG2), pancreatic (PANC-1), and colorectal (HCT116) cancer cell lines, which are widely used in studies of anticancer drug responses [5-8].

Dense granule protein 16 (GRA16), an effector protein from *Toxoplasma gondii*, has demonstrated anticancer activity across multiple malignancies, including hepatocellular carcinoma, non-small cell lung cancer, and colorectal cancer, and has been shown to enhance chemotherapeutic response in some cancer cell types [9-12]. Importantly, GRA16 activates convergent mechanisms that inhibit critical pro-survival signaling pathways implicated in chemotherapy resistance [10,12]. In hepatocellular carcinoma models, GRA16 induces apoptosis by enhancing the nuclear localization of phosphatase and tensin homolog (PTEN) and suppressing AKT signaling [9]. In non-small cell lung cancer, GRA16 enhances irinotecan efficacy by upregulating protein phosphatase 2A, B55 regulatory subunit (PP2A-B55), suppressing AKT and ERK signaling, and inactivating NF-κB [10]. In colon cancer cells, GRA16 inhibits cell growth by suppressing the PTEN/AKT/telomerase reverse transcriptase (TERT) axis and downregulating c-Myc/TERT-induced glycolysis [11,12]. These pathways intersect with survival signaling linked to resistance against gemcitabine, oxaliplatin, and irinotecan, providing a rationale to test whether GRA16 can enhance inhibitory responses to chemotherapeutic agents across different tumor types. Accordingly, we hypothesized that GRA16 enhances the inhibitory response of hepatocellular, pancreatic, and colorectal cancer cells to standard chemotherapeutic agents (DNA-damaging drugs and a Topo-I inhibitor) and evaluated whether stable GRA16 expression amplifies the growth-inhibitory effects of gemcitabine, oxaliplatin, and irinotecan under 50% inhibitory concentration (IC_{50})-normalized dosing in HepG2, PANC-1, and HCT116 cells. In addition, this study was designed to determine whether GRA16-associated enhancement of inhibitory drug effects could be observed across multiple cancer types and multiple clinically relevant drugs, including a pancreatic cancer model that has not previously been evaluated in this context.

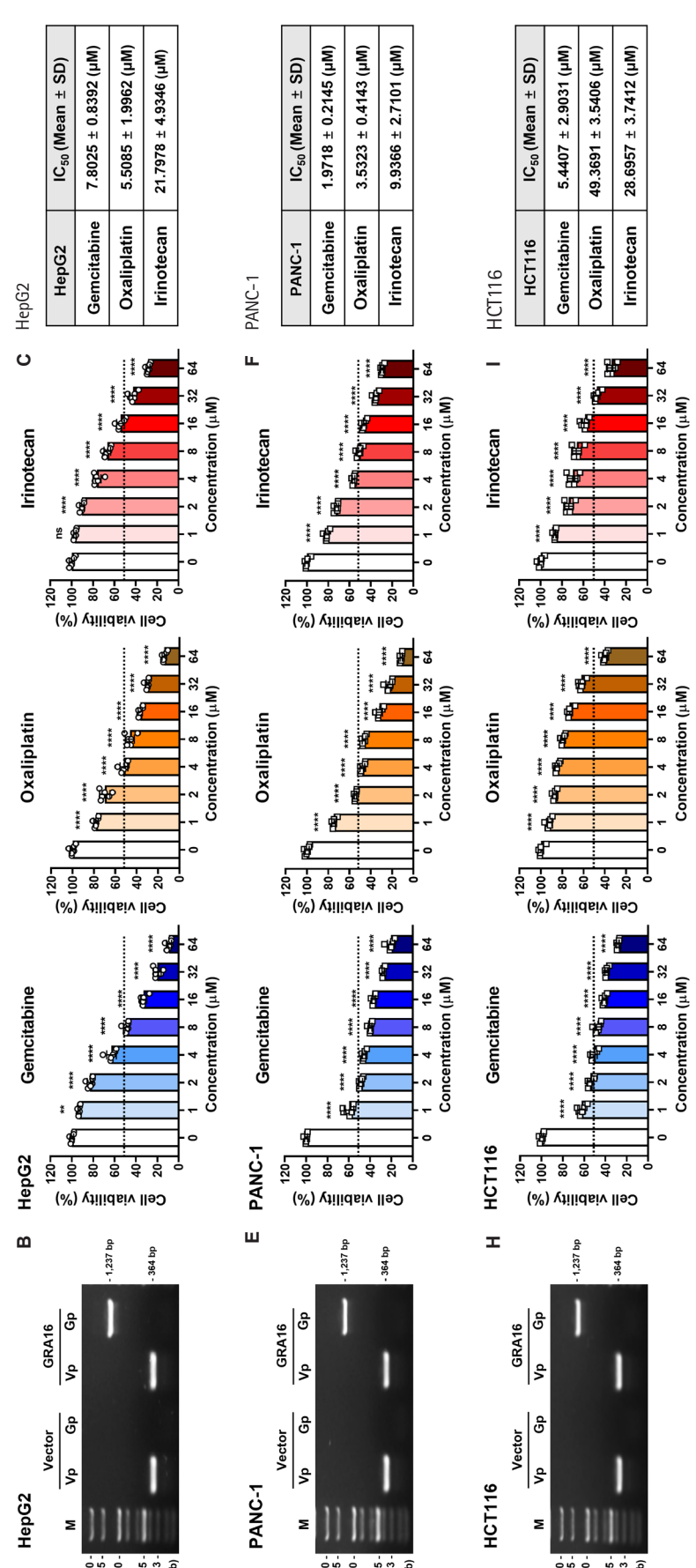
To test this hypothesis, GRA16 from the *T. gondii* RH strain (ATCC) was cloned into a lentiviral expression vector and introduced into HepG2 (KCLB), PANC-1 (KCLB), and HCT116 (KCLB) cells by lentiviral transduction to generate stable cell populations. Recombinant lentiviral particles were produced in Lenti-X 293T (Takara) cells using packaging and envelope plasmids, and target cells were transduced in the presence of polybrene (Santa Cruz Biotechnology). For both the empty vector and GRA16 constructs, GFP-positive transduced populations were enriched by flow-cytometric sorting based on GFP fluorescence using a SH800S cell sorter (Sony Biotechnology), and the sorted stable cell populations were used for subsequent assays. A lentiviral system was selected rather than transient transfection because this study required consistent construct expression across multiple downstream assays, extended incubation periods, and repeated drug-treatment conditions.

To validate construct expression at the mRNA level, total RNA was extracted from HepG2, PANC-1, and HCT116 vector and GRA16-expressing stable cell populations using the HiGene Total RNA Prep Kit (Biofact), and cDNA was synthesized using a Reverse-Transcription Premix (Elpis Biotech). PCR was performed using primers targeting vector-derived GFP (Vp) or GRA16 (Gp) under the following conditions: 95°C for 5 min; 35 cycles of 95°C for 30 sec, 58°C for 40 sec, and 72°C for 1.5 min; followed by 72°C for 3 min. The Vp primer sequences were 5′-AAG TTC ACC TTG ATG CCG TT-3′ (forward) and 5′-TGA AGT TCA TCT GCA CCA CC-3′ (reverse). The Gp primer sequences were 5′-GGG ATT GAG TGG AAC GAA GG-3′ (forward) and 5′-AAG TGC TAG AGT CGT CCA CA-3′ (reverse).

Cell viability was quantified using CCK-8 (Dojindo) after gemcitabine (Selleckchem), oxaliplatin (Selleckchem), and irinotecan (Selleckchem) treatment at concentrations ranging from 0 to 64 μM for 48 h.

The IC_{50} was subsequently determined by linear interpolation using the 2 adjacent drug concentrations that directly bracketed 50% cell viability, allowing assessment of baseline drug sensitivity in vector cells for each cancer type (Fig. 1). Specifically, if A and B represent the lower and higher concentrations bracketing 50% viability, and C and D represent the corresponding viability values at A and B, IC_{50} was calculated as: $IC_{50} = A + [(50 - C)/(D - C)] \times (B - A)$. This approach provided a transparent estimate of the concentration corresponding to 50% inhibition within the tested concentration range and was used to define normalized treatment concentrations for subsequent cross-cell-line comparisons. These IC_{50} values were then used as normalized treatment concentrations for subsequent time-course cell proliferation analyses at 0, 24, 48, and 72 h (Fig. 2). IC_{50}-based normalization adjusts drug exposure to reflect the distinct drug sensitivities of each cell line and allows comparison at a similar inhibition level.

For mechanistic validation, PANC-1 vector and GRA16-expressing cells were left untreated or treated with gemcitabine, oxaliplatin, or irinotecan for 24 h. Protein lysates were subjected to Western blot analysis to evaluate p-AKT/AKT, p-NF-κB/NF-κB, and p-ERK/ERK expression. Details of the primary and secondary antibodies used for Western blotting are provided in Supplementary Table S1. Relative band intensities were quanti-



HepG2	IC_{50} (Mean ± SD)
Gemcitabine	7.8025 ± 0.8392 (μM)
Oxaliplatin	5.5085 ± 1.9962 (μM)
Irinotecan	21.7978 ± 4.9346 (μM)

PANC-1	IC_{50} (Mean ± SD)
Gemcitabine	1.9718 ± 0.2145 (μM)
Oxaliplatin	3.5323 ± 0.4143 (μM)
Irinotecan	9.9366 ± 2.7101 (μM)

HCT116	IC_{50} (Mean ± SD)
Gemcitabine	5.4407 ± 2.9031 (μM)
Oxaliplatin	49.3691 ± 3.5406 (μM)
Irinotecan	28.6957 ± 3.7412 (μM)

Fig. 1. RT-PCR validation of GRA16 expression and 50% inhibitory concentration (IC_{50}) determination in vector control cells. (A) RT-PCR validation of construct expression in HepG2 stable cell populations. (B) Dose-response curves of HepG2 vector control cells treated with gemcitabine, oxaliplatin, or irinotecan at 0 to 64 μM for 48 h. Cell viability was measured by CCK-8 at 450 nm and normalized to 0 μM (100% viability). Dotted lines denote 50% viability, and asterisks indicate significant differences versus untreated cells (0 μM). (C) IC50 values estimated by linear interpolation from the corresponding HepG2 dose-response curves. (D) RT-PCR validation of construct expression in PANC-1 stable cell populations. (E) Dose-response curves of PANC-1 vector control cells treated as described above. (F) IC_{50} values estimated by linear interpolation from the corresponding PANC-1 dose-response curves. (G) RT-PCR validation of construct expression in HCT116 stable cell populations. (H) Dose-response curves of HCT116 vector control cells treated as described above. (I) IC_{50} values estimated by linear interpolation from the corresponding HCT116 dose-response curves. In the RT-PCR analyses, vector cells showed only the GFP-target band (Vp, 364 bp), whereas GRA16-expressing cells showed both the GFP-target band (Vp, 364 bp) and the GRA16-target band (Gp, 1,237 bp). Statistical analysis was performed using one-way ANOVA followed by Dunnett's multiple comparisons test in GraphPad Prism 8. Data are expressed as mean±SD for each group (n=6 independent biological replicates). Significance was defined as follows: $^{*}P<0.05$, $^{**}P<0.01$, $^{***}P<0.001$, $^{****}P<0.0001$ vs. untreated cells (0 μM).

https://doi.org/10.3347/PHD.26019

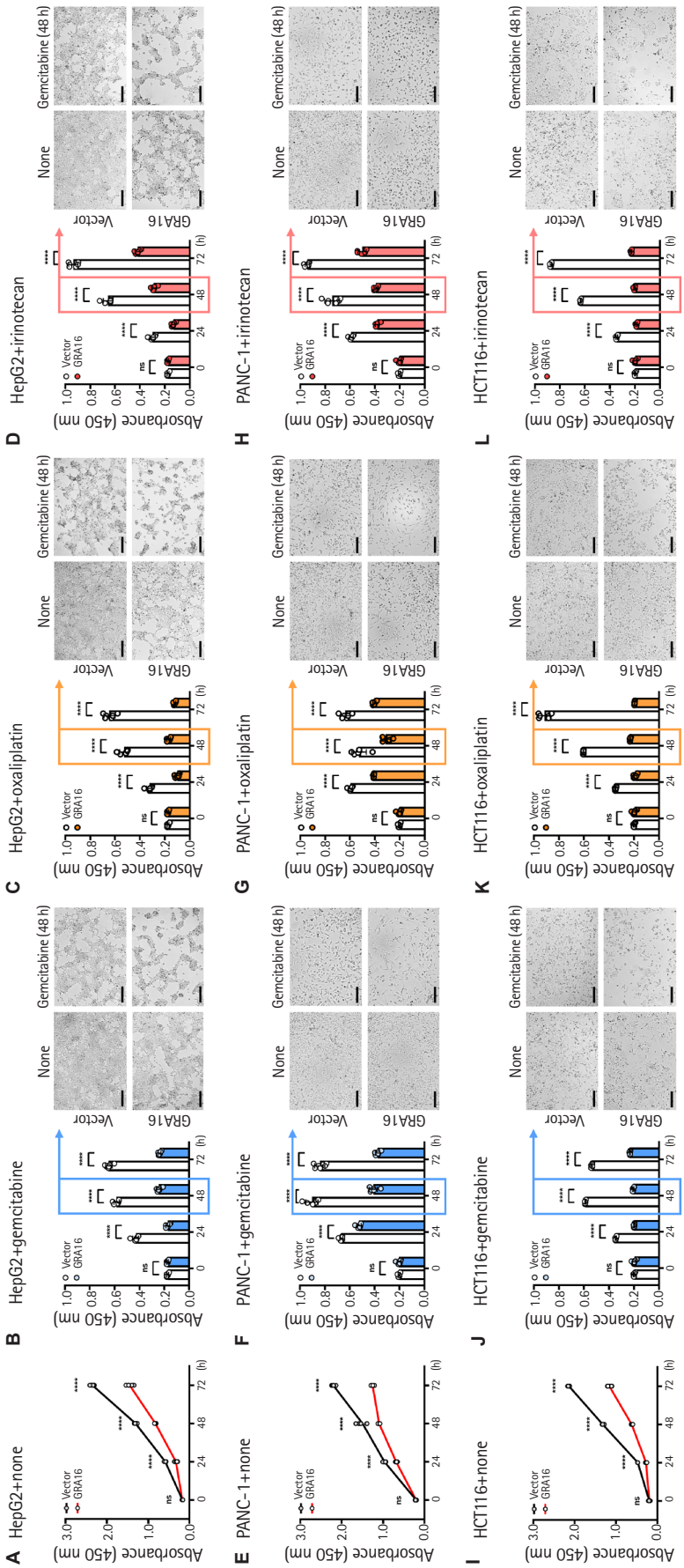


Fig. 2. GRA16 decreases basal proliferation and enhances inhibitory drug effects across 3 cell lines. (A-D) HepG2, (E-H) PANC-1, and (I-L) HCT116 vector control and GRA16-expressing cells were analyzed by CCK-8 over 0–72 h at 24 h intervals. (A, E, I) No drug (baseline proliferation); (B, F, J) gemcitabine; (C, G, K) oxaliplatin; (D, H, L) irinotecan, each administered at the 50% inhibitory concentration defined in Fig. 1. In each drug-treatment panel, the bar graphs show quantitative comparisons between the 2 experimental groups (Vector and GRA16) at each time point, whereas the accompanying microscopy panels show representative phase-contrast images of the same 2 groups under 2 conditions: untreated (None) and drug-treated at 48 h. The highlighted 48 h time point in the bar graphs corresponds to the representative microscopy images. Statistical analysis was performed using two-way ANOVA followed by Šidák's multiple comparisons test in GraphPad Prism 8, with comparisons made between the Vector and GRA16 groups at the same time point. Data are expressed as mean±SD for each group (n=6 independent biological replicates). Scale bar=250 μm. Significance was defined as follows: $^{*}P<0.05$, $^{**}P<0.01$, $^{***}P<0.001$, $^{****}P<0.0001$ vs. Vector at the same time point.

fied and compared between vector and GRA16 groups under each treatment condition.

For apoptosis analysis, PANC-1 vector and GRA16-expressing cells were left untreated or treated with gemcitabine, oxaliplatin, or irinotecan for 24 h, followed by staining with the Annexin V Apoptosis Detection Kit with 7-AAD (BioLegend). Stained cells were analyzed using a BD FACSCanto II flow cytometer (BD Biosciences). Total apoptotic cells were calculated as the sum of early and late apoptotic populations.

All statistical analyses were performed using GraphPad Prism 8 (GraphPad Software). For Fig. 1, concentration-dependent viability data were analyzed using one-way ANOVA followed by Dunnett's multiple comparisons test, with the untreated group (0 μM) used as the control. For Fig. 2, time-course proliferation and viability data were analyzed separately using two-way ANOVA followed by Šídák's multiple comparisons test, with comparisons made between the Vector and GRA16 groups at each corresponding time point. For Fig. 3, Western blot quantification data were analyzed using two-way ANOVA followed by Holm–Šídák's multiple comparisons test, whereas apoptosis/cell-death-associated population data were analyzed using two-way ANOVA followed by Šídák's multiple comparisons test. In both analyses, comparisons were made between the Vector and GRA16 groups within each treatment condition. A P-value <0.05 was considered statistically significant. Unless otherwise indicated, the reported n-values represent independent biological replicates derived from separately cultured dishes.

Prior to functional analyses, expression of the introduced constructs was verified at the mRNA level by RT-PCR in HepG2, PANC-1, and HCT116 stable cell populations (Fig. 1A, D, G). In vector cells, only the GFP-target band (364 bp) was detected, whereas GRA16-expressing cells showed both the GFP-target band (364 bp) and the GRA16-target band (1,237 bp). These results confirmed successful expression of the introduced constructs in the stable cell populations used for subsequent experiments. Using these validated cell populations, we next assessed baseline chemotherapy sensitivity profiles in the 3 cell lines. HepG2 vector cells displayed IC_{50} values of 7.8025 μM for gemcitabine, 5.5085 μM for oxaliplatin, and 21.7978 μM for irinotecan (Fig. 1B, C). PANC-1 cells were more sensitive to gemcitabine (IC_{50} = 1.9718 μM) and oxaliplatin (IC_{50} = 3.5323 μM), whereas the IC_{50} for irinotecan was 9.9366 μM (Fig. 1E, F). HCT116 cells exhibited comparatively high resistance to oxaliplatin and irinotecan, with IC_{50} values of 5.4407 μM for gemcitabine, 49.3691 μM for oxaliplatin, and 28.6957 μM for irinotecan (Fig. 1H, I).

In a drug-by-drug comparison within cell lines, HepG2 exhibited a high relative resistance to irinotecan, with oxaliplatin (5.5085 μM) < gemcitabine (7.8025 μM) < irinotecan (21.7978 μM) (Fig. 1C). PANC-1 cells were relatively sensitive to all 3 drugs, with gemcitabine (1.9718 μM) < oxaliplatin (3.5323 μM) < irinotecan (9.9366 μM), and demonstrated a notably strong response to gemcitabine (Fig. 1F). HCT116 exhibited selective resistance to oxaliplatin, with gemcitabine (5.4407 μM) < irinotecan (28.6957 μM) < oxaliplatin (49.3691 μM) (Fig. 1I). In a cross-drug comparison of cell lines, PANC-1 cells were most sensitive to both gemcitabine and irinotecan (Fig. 1C), whereas HCT116 cells were significantly resistant to oxaliplatin (Fig. 1I). These results quantitatively illustrate the significant heterogeneity in sensitivity across cell lines and drug combinations.

The previously identified IC_{50} values for each anticancer drug were used as normalized treatment concentrations for comparative inhibitory-response analysis. Using these IC_{50}-normalized concentrations, we compared proliferation over 72 h between vector-expressing and GRA16-expressing cells (Fig. 2). Under drug-free conditions, GRA16 expression decreased basal proliferation in all 3 cell lines, indicating an intrinsic growth inhibitory effect (Fig. 2A, E, I). When treated with gemcitabine (Fig. 2B, F, J), oxaliplatin (Fig. 2C, G, K), or irinotecan (Fig. 2D, H, L), GRA16-expressing cells consistently showed lower proliferation than vector controls at the corresponding time points under the same treatment conditions across all cell lines. Representative microscopic images, captured at the 48 h time point used for IC_{50} calculations, visually corroborate the 0–72 h CCK-8 results. The accompanying microscopy panels do not represent additional experimental groups, but instead provide representative images of the same Vector and GRA16 groups under untreated and drug-treated conditions at the 48 h time point corresponding to the highlighted bar graph data. In the 48 h images, cells in the GRA16 group exhibited lower cell density under each drug condition compared with the vector group (Fig. 2B-D, F-H, J-L). These results indicate that GRA16 further enhances the growth inhibitory effects of standard anticancer drugs in vitro, even when doses are normalized to reflect the distinct drug sensitivities of each cell line.

To determine whether the enhanced inhibitory phenotype observed in GRA16-expressing cells was associated with modulation of survival signaling pathways, Western blot analysis was performed in the newly introduced pancreatic cancer model (PANC-1) under untreated and chemotherapeutic treatment conditions (Fig. 3A, B). Compared with vector con-

https://doi.org/10.3347/PHD.26019

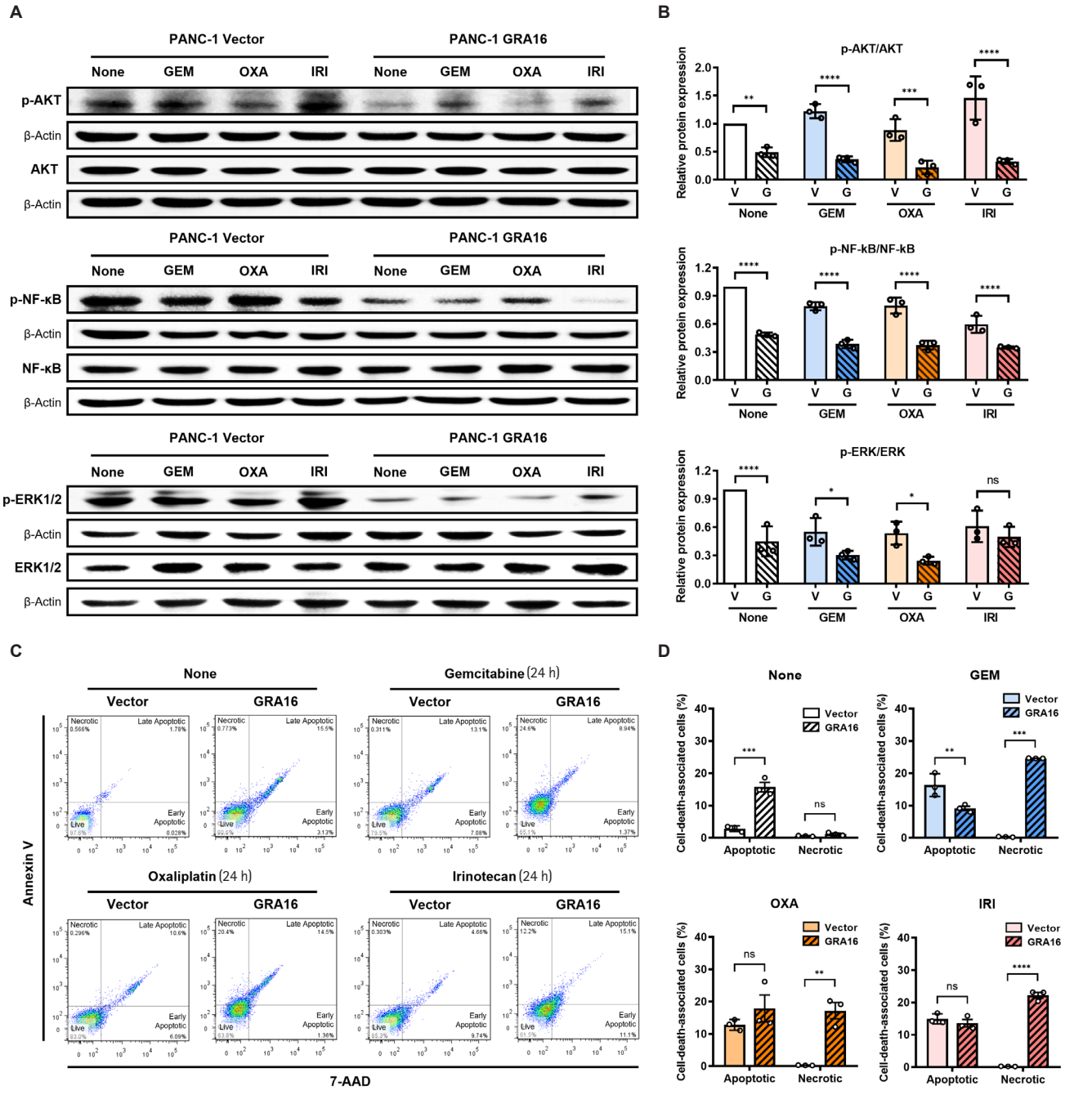


Fig. 3. Mechanistic and cell-death-associated validation in PANC-1 cells. (A) Representative Western blot images showing p-AKT, AKT, p-NF-κB, NF-κB, p-ERK1/2, and ERK1/2 expression in PANC-1 vector and GRA16-expressing cells under untreated conditions or after treatment with gemcitabine (GEM), oxaliplatin (OXA), or irinotecan (IRI) for 24 h. (B) Quantification of relative p-AKT/AKT, p-NF-κB/NF-κB, and p-ERK/ERK expression. (C) Representative Annexin V/7-AAD flow cytometry plots of PANC-1 vector and GRA16-expressing cells under untreated and drug-treated conditions. (D) Quantification of apoptotic cells, calculated as the sum of early and late apoptotic populations, and necrotic cells. Statistical analysis for Western blot quantification was performed using two-way ANOVA followed by Holm–Šídák's multiple comparisons test in GraphPad Prism 8, whereas apoptosis/cell-death-associated population data were analyzed using two-way ANOVA followed by Šídák's multiple comparisons test. In both analyses, comparisons were made between the Vector and GRA16 groups within each treatment condition. Data are expressed as mean±SD for each group (n=3 independent biological replicates). Significance was defined as follows: $^{*}P$<0.05, $^{**}P$<0.01, $^{***}P$<0.001, $^{****}P$<0.0001 vs. Vector within the same treatment condition. ns, not significant.

trols, GRA16-expressing PANC-1 cells showed reduced p-AKT/AKT and p-NF-κB/NF-κB expression under both untreated and drug-treated conditions. p-ERK/ERK expression was also reduced in GRA16-expressing cells, although the magnitude of this effect varied depending on the drug condition. These findings provide direct experimental support that the enhanced inhibitory phenotype associated with GRA16 is accompanied by attenuation of AKT-, NF-κB-, and ERK-related signaling in the pancreatic cancer model.

To further assess whether the reduced viability observed in GRA16-expressing cells was associated with cell death, Annexin V/7-AAD flow cytometry was performed in PANC-1 cells under untreated and chemotherapeutic treatment conditions (Fig. 3C, D). In untreated cells, GRA16 expression increased the apoptotic population compared with vector controls. Under gemcitabine, oxaliplatin, and irinotecan treatment, the relative proportions of apoptotic and necrotic populations varied by drug; however, GRA16-expressing cells showed increased cell-death-associated populations compared with vector controls. These findings support that the enhanced inhibitory phenotype observed in GRA16-expressing PANC-1 cells was not solely attributable to reduced basal proliferation.

Across HepG2, PANC-1, and HCT116 cells, GRA16 consistently enhanced the inhibitory response to chemotherapeutic treatment. This interpretation is supported not only by our previous studies, which showed that GRA16 can modulate PI3K/AKT, NF-κB, and ERK-related signaling in several cancer models [9-12], but also by the present Western blot analysis in the pancreatic cancer model. In PANC-1 cells, GRA16 expression was associated with reduced p-AKT/AKT, p-NF-κB/NF-κB, and p-ERK/ERK levels under untreated and chemotherapeutic treatment conditions. Because these signaling axes are also linked to gemcitabine, oxaliplatin, and irinotecan resistance [1-4], the present findings provide direct experimental support that the enhanced inhibitory phenotype is accompanied by attenuation of key pro-survival signaling pathways. A major strength of this study is that it is not limited to a single drug or tumor type, demonstrating enhanced inhibitory effects across 3 clinically relevant chemotherapeutic agents and 3 distinct tumor models. This design offers a practical framework for assessing chemotherapeutic agents in a mechanistically informed manner, reflecting drugs actually used in the treatment of pancreatic and colorectal cancers [5-8]. In addition, this is the first report evaluating GRA16-associated enhancement of chemotherapeutic inhibitory effects in a pancreatic cancer model, expanding the scope of previous studies focused on non-small cell lung cancer and colorectal cancer [10,12].

Collectively, our results support the possibility that GRA16 enhances the inhibitory effects of chemotherapeutic treatment in multiple cancer cell types. Together with previous reports [9-12], the present pancreatic cancer data further support pathway modulation as one plausible explanation for this effect. By extending our analysis across multiple tumor types and 3 clinically relevant agents, 2 DNA-damaging drugs and a Topo-I inhibitor, this study establishes a cross-cancer, multidrug framework for evaluating GRA16-associated enhancement of chemotherapeutic response. In addition, the inclusion of the pancreatic cancer model expands the scope of previous GRA16-related cancer studies [10-12]. Moreover, GRA16 decreased basal proliferation even in the absence of drug exposure, demonstrating a drug-independent antiproliferative effect that likely contributes to the overall growth-inhibitory phenotype.

In this study, HepG2 was primarily used as a comparative model to assess whether the GRA16-mediated inhibitory effect is consistent across different tumor backgrounds, rather than to recapitulate hepatocellular carcinoma-specific treatment indications. The 3 agents were chosen to represent DNA-damaging mechanisms and Topo-I inhibition rather than standard therapies for individual cancer types, with the analysis emphasizing mechanism-based alterations in drug response.

Although the present study now includes direct mechanistic validation in the pancreatic cancer model, pathway modulation was not comprehensively examined across all cell lines and treatment conditions. Therefore, broader interpretation regarding AKT, NF-κB, and ERK signaling should still be made with caution. Future studies should extend this validation to additional tumor models and further define how these pathways contribute to the observed inhibitory phenotype. Nevertheless, the consistent proliferation reduction across all 3 cell lines and drugs underscores the robustness of the inhibitory-response pattern and supports further evaluation of GRA16 in combination with standard chemotherapy in hepatocellular carcinoma, pancreatic cancer, and colorectal cancer models.

Data availability

The datasets used and/or analyzed in this study are available from the corresponding author and can be provided on reasonable request.

Author contributions

Conceptualization: Seo SH, Shin EH. Data curation: Seo SH, Shin EH. Funding acquisition: Shin EH, Seo SH. Investigation:

https://doi.org/10.3347/PHD.26019

Seo SH, Lee JE, Cho EJ. Methodology: Seo SH, Lee JE. Writing–original draft: Seo SH. Writing–review & editing: Seo SH, Shin EH.

Conflict of interest

Eun-Hee Shin serves as an editor of Parasites, Hosts and Diseases but had no involvement in the decision to publish this article. No other potential conflicts of interest relevant to this study were reported.

Funding

This work was supported by the National Research Foundation of Korea (NRF) grant funded by the Korea government (MSIT) (IRIS No. RS-2025-00516274 and RS-2025-00559259).

Supplementary information

Supplementary material is available with this article at https://doi.org/10.3347/PHD.26019.

ORCID

Seung-Hwan Seo, https://orcid.org/0000-0002-8645-1966
Ji-Eun Lee, https://orcid.org/0009-0008-4251-7442
Eun-Ji Cho, https://orcid.org/0009-0000-5946-9346
Eun-Hee Shin, https://orcid.org/0000-0003-1215-1079

References

1. Chiu CH, Lin YJ, Ramesh S, et al. Gemcitabine resistance in non-small cell lung cancer is mediated through activation of the PI3K/AKT/NF-κB pathway and suppression of ERK signaling by reactive oxygen species. J Biochem Mol Toxicol 2023;37:e23497. https://doi.org/10.1002/jbt.23497
2. Chen S, Chen A. Geniposide reverses oxaliplatin resistance in colorectal cancer via suppression of PI3K/AKT pathway. Rev Invest Clín 2025;77:100022. https://doi.org/10.1016/j.ric.2025.100022
3. Saurav S, Karfa S, Vu T, et al. Overcoming irinotecan resistance by targeting its downstream signaling pathways in colon cancer. Cancers (Basel) 2024;16:3491. https://doi.org/10.3390/cancers16203491
4. Jassi C, Kuo WW, Chang YC, et al. Aloin and CPT-11 combination activates miRNA-133b and downregulates IGF1R-PI3K/AKT/mTOR and MEK/ERK pathways to inhibit colorectal cancer progression. Biomed Pharmacother 2023;169:115911. https://doi.org/10.1016/j.biopha.2023.115911
5. Conroy T, Desseigne F, Ychou M, et al. FOLFIRINOX versus gemcitabine for metastatic pancreatic cancer. N Engl J Med 2011;364:1817-25. https://doi.org/10.1056/NEJMoa1011923
6. Goldberg RM, Sargent DJ, Morton RF, et al. A randomized controlled trial of fluorouracil plus leucovorin, irinotecan, and oxaliplatin combinations in patients with previously untreated metastatic colorectal cancer. J Clin Oncol 2004;22:23-30. https://doi.org/10.1200/JCO.2004.09.046
7. Sciortino C, Nichetti F, Bergamo F, et al. A phase III randomized clinical trial of gemcitabine and nab-paclitaxel as switch maintenance versus continuation of modified FOLFIRINOX as first-line chemotherapy in patients with advanced pancreatic cancer: the PANThEON Study. Dig Liver Dis 2025;57:2470-7. https://doi.org/10.1016/j.dld.2025.11.007
8. Zhang X, Duan R, Wang Y, et al. FOLFIRI (folinic acid, fluorouracil, and irinotecan) increases not efficacy but toxicity compared with single-agent irinotecan as a second-line treatment in metastatic colorectal cancer patients: a randomized clinical trial. Ther Adv Med Oncol 2022;14:17588359211068737. https://doi.org/10.1177/17588359211068737
9. Kim SG, Seo SH, Shin JH, et al. Increase in the nuclear localization of PTEN by the *Toxoplasma* GRA16 protein and subsequent induction of p53-dependent apoptosis and anticancer effect. J Cell Mol Med 2019;23:3234-45. https://doi.org/10.1111/jcmm.14207
10. Seo SH, Kim SG, Shin JH, Ham DW, Shin EH. *Toxoplasma* GRA16 inhibits NF-κB activation through PP2A-B55 upregulation in non-small-cell lung carcinoma cells. Int J Mol Sci 2020;21:6642. https://doi.org/10.3390/ijms21186642
11. Seo SH, Shin JH, Ham DW, Shin EH. PTEN/AKT signaling pathway related to hTERT downregulation and telomere shortening induced in *Toxoplasma* GRA16-expressing colorectal cancer cells. Biomed Pharmacother 2022;153:113366. https://doi.org/10.1016/j.biopha.2022.113366
12. Lee JE, Seo SH, Ham DW, Shin EH. *Toxoplasma gondii* GRA16 suppresses aerobic glycolysis by downregulating c-Myc and TERT expressions in colorectal cancer cells. Biomol Ther (Seoul) 2025;33:621-35. https://doi.org/10.4062/biomolther.2025.040

Brief Communication

Parasites Hosts Dis 2026;64(4):374-378
https://doi.org/10.3347/PHD.26041

Parasites, Hosts and Diseases

pISSN 2982-5164 • eISSN 2982-6799

Occurrence and preliminary molecular characterization of *Sarcocystis* spp. in wild Korean roe deer from Jeju Island, Korea

Da-Ye Nam[1], Sunmin Kim[1], Jinho Jang[1,2], YoungMin Yun[1,2], Jae-Hoon Kim[1], Ji-Youl Jung[1,*]

[1]College of Veterinary Medicine and Veterinary Medical Research Institute, Jeju National University, Jeju, Korea; [2]Jeju Wildlife Rescue Center, Jeju National University, Jeju, Korea

Sarcocystis spp. are common protozoan parasites infecting a wide range of intermediate hosts, including wild cervids. In this study, we investigated the occurrence and molecular characteristics of *Sarcocystis* infection in wild Korean roe deer (*Capreolus pygargus tianschanicus*) from Jeju Island, Korea. Sarcocysts were identified in the heart and skeletal muscle of 18 out of 40 examined animals (45.0%) based on histopathological examination. The cysts were oval to spherical in shape, measuring 42.41–340.29 μm in length and 31.62–129.76 μm in width, and were not associated with significant inflammatory responses. Molecular analysis targeting the 18S rRNA gene yielded 2 representative sequences, which showed 99.82% identity and high similarity to *Sarcocystis linearis*, as well as closely related species including *S. taeniata* and *S. grueneri*. Phylogenetic analysis placed these sequences within a clade of ungulate-associated *Sarcocystis* spp., although species-level resolution was not achieved due to the conserved nature of the marker. These findings provide baseline data on *Sarcocystis* infection in wild roe deer from Jeju Island and highlight the limitations of 18S rRNA-based identification for closely related *Sarcocystis* species.

Keywords: *Sarcocystis* spp., roe deer, molecular characterization, 18S rRNA, Korea

Sarcocystis spp. are obligate intracellular protozoan parasites with a 2-host life cycle involving carnivorous definitive hosts and herbivorous intermediate hosts [1,2]. These parasites are widely distributed and infect a variety of domestic and wild animals, including cervids, in which they form intramuscular cysts [1]. Although infections in intermediate hosts are typically subclinical, *Sarcocystis* spp. are of veterinary and ecological importance due to their high prevalence and complex host–parasite relationships [3,4].

Cervids, including roe deer (*Capreolus* spp.), are well-recognized intermediate hosts for multiple *Sarcocystis* species [4,5]. Previous studies have demonstrated a high diversity of *Sarcocystis* spp. in roe deer populations, particularly in Europe [3,6]. However, molecular identification of closely related species remains challenging due to the limited resolution of commonly used genetic markers such as the 18S rRNA gene.

In Korea, studies on *Sarcocystis* infection have primarily focused on domestic animals, and information on wildlife infections remains limited [7-10]. In particular, data on wild Korean roe deer (*Capreolus pygargus tianschanicus*) are lacking despite their ecological importance and high population density on Jeju Island. Therefore, the present study aimed to investigate the occurrence and histopathological characteristics of *Sarcocystis* infection in wild Korean roe deer from Jeju Island and to molecularly characterize the detected parasites using 18S rRNA gene sequences.

Between 2018 and 2025, a total of 40 wild Korean roe deer (*C. pygargus*) were submitted for postmortem examination.

Received: May 8, 2026 Accepted: June 20, 2026
*Correspondence: jungjy1982@jejunu.ac.kr

© 2026 The Korean Society for Parasitology and Tropical Medicine

This is an open-access article distributed under the terms of the Creative Commons Attribution Non-Commercial License (http://creativecommons.org/licenses/by-nc/4.0/) which permits unrestricted non-commercial use, distribution, and reproduction in any medium, provided the original work is properly cited.

Citation
Nam DY, Kim S, Jang J, Yun Y, Kim JH, Jung JY. Occurrence and preliminary molecular characterization of *Sarcocystis* spp. in wild Korean roe deer from Jeju Island, Korea. Parasites Hosts Dis 2026;64(4):374-378.

Among these, 18 animals were selected for the present study based on the histopathological identification of intramuscular sarcocysts in the heart and/or skeletal muscle tissues. These 18 cases were subsequently included for further histological and molecular analyses. Information regarding sex, estimated age, and body weight was collected from the necropsy records. The age of each animal was estimated using a combination of body weight, radiographic assessment of physeal closure, and antler development in males. Ethical approval for animal experimentation was not required for this study because all samples were obtained postmortem from wild roe deer that had died naturally or were found dead.

At necropsy, tissue samples including heart and skeletal muscle were collected and fixed in 10% neutral-buffered formalin. The samples were routinely processed, embedded in paraffin, sectioned at 3–4 μm, and stained with hematoxylin and eosin. Histological sections were examined for the presence, distribution, and morphological characteristics of sarcocysts. The location of cysts within muscle fibers, cyst shape, and associated inflammatory responses were evaluated. When present, cyst size was measured using a light microscope.

DNA was extracted from formalin-fixed, paraffin-embedded (FFPE) tissue sections of heart and skeletal muscle obtained from the 18 histologically positive roe deer using the Exgene FFPE Tissue DNA isolation kit (GeneAll), according to the manufacturer's instructions. The extracted DNA concentration ranged from 18.8 to 380 ng/μl.

Nested PCR targeting the 18S rRNA gene of *Sarcocystis* spp. was performed based on previously described methods [11]. Briefly, 2 rounds of amplification were carried out using the primer sets SarcoFext/SarcoRext and SarcoFint/SarcoRint, respectively, yielding an expected amplicon size of 639 bp. To improve species-level identification, additional PCR targeting the mitochondrial cytochrome c oxidase subunit 1 (*cox1*) gene was performed on selected samples that yielded high-quality 18S rRNA amplicons suitable for sequencing, as previously described [12]. Each PCR run included a negative control to monitor potential contamination.

PCR amplification targeting the 18S rRNA gene yielded positive bands in all 18 histologically positive samples. Based on amplification quality and DNA integrity, 2 PCR products were selected for Sanger sequencing. Sequencing was performed by Cosmogenetech. Forward and reverse reads were assembled to generate consensus sequences using Geneious Prime version 2025.2.2 [13], with low-quality regions trimmed prior to analysis.

For molecular identification, the obtained sequences were compared with reference sequences available in the GenBank database using BLAST [14]. For phylogenetic analysis, previously published *Sarcocystis* sequences were retrieved from GenBank and aligned with the sequences generated in this study based on the SSU rRNA gene. Sequence alignment was performed using Clustal W implemented in MEGA X version 10.1.7 [15]. Phylogenetic reconstruction was conducted using Bayesian inference (BI). The best-fit nucleotide substitution model was selected using jModelTest version 2.1.10 according to the Bayesian information criterion, and the HKY+I+G model was applied. Bayesian analysis was performed in MrBayes version 3.2.6 for 10,000,000 generations [16]. The resulting phylogenetic tree was visualized using FigTree version 1.4.4. Representative sequences from related taxa were included as outgroups.

A total of 18 wild Korean roe deer with histologically confirmed *Sarcocystis* infection were included in this study. Detailed case information is summarized in Supplementary Table S1. The study population consisted of 9 males and 9 females, with no apparent sex predilection. Age information was available for a subset of animals, with a mean estimated age of approximately 2.3 years. Body weights ranged from 2.14 to 27.3 kg (mean 18.59 kg).

Histopathological examination revealed multiple intramuscular sarcocysts in cardiac and skeletal muscle tissues (Fig. 1A, B). The cysts were located within the sarcoplasm of muscle fibers and were oval to spherical in shape. Cyst size ranged from 42.41 to 340.29 μm in length (mean 134.07 μm) and 31.62 to 129.76 μm in width (mean 59.65 μm). Each cyst contained numerous bradyzoites and was surrounded by a thin, smooth cyst wall, although the detailed cyst wall structure was not clearly discernible. No inflammatory response was observed in the surrounding muscle tissue. Based on these morphological features, the observed cysts were consistent with *Sarcocystis* spp., although species-level identification could not be determined by histological examination alone.

Nested PCR targeting the SSU rRNA gene yielded positive amplification in all 18 samples. Sequencing was attempted for all PCR products; however, high-quality sequences were obtained from only 2 samples. Additional PCR targeting the *cox1* gene was performed on these samples; however, no specific amplification products were obtained. Two PCR products yielded high-quality sequences and were deposited in GenBank under accession numbers PZ326468 and PZ326469, corresponding to cases 17 and 18, respectively. The 2 sequences showed high similarity, differing by a single nucleotide within an overlapping 568-bp region, corresponding to 99.82% identity. BLAST analy-

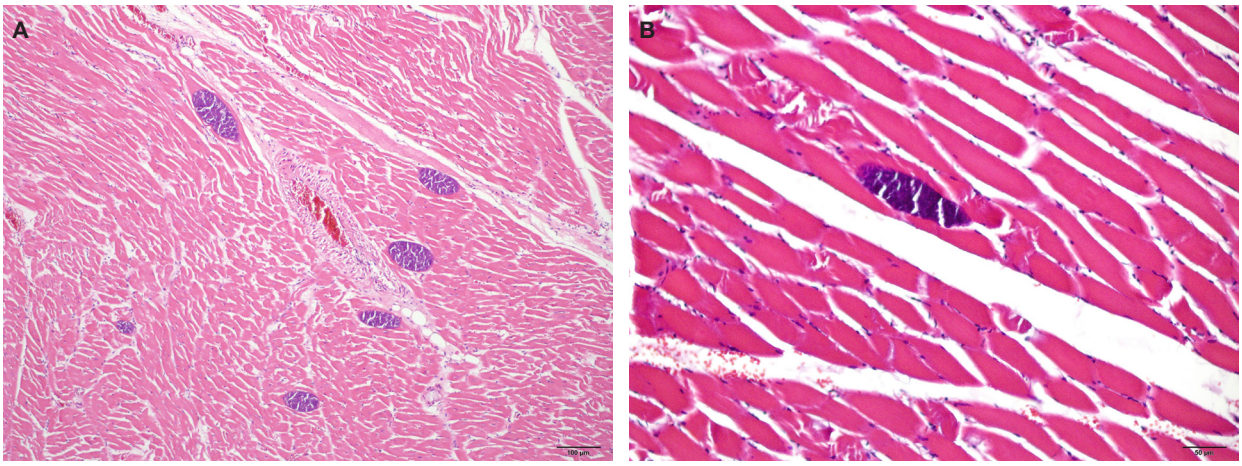


Fig. 1. Histopathologic findings. (A) Low-power view of multiple intramuscular sarcocysts distributed among myocardial fibers. Hematoxylin and eosin, scale bar=100 μm. (B) Longitudinal section of a sarcocyst within skeletal muscle. The cysts are located within the sarcoplasm of muscle fibers and contain numerous bradyzoites. No inflammatory response is present. Hematoxylin and eosin, scale bar=50 μm.

sis revealed that both sequences shared ≥99% identity with previously reported *Sarcocystis linearis* sequences and were also highly similar to closely related species, including *S. taeniata* and *S. grueneri*. Phylogenetic analysis based on the SSU rRNA gene placed the sequences within a clade of ungulate-associated *Sarcocystis* spp., including *S. linearis*, *S. taeniata*, and related taxa (Fig. 2). Within this clade, sequences assigned to different species were intermingled rather than forming distinct species-specific clades.

In the present study, *Sarcocystis* infection was identified in wild Korean roe deer from Jeju Island based on histopathological and molecular findings. Intramuscular sarcocysts were consistently observed within cardiac and skeletal muscle fibers, without any associated inflammatory response, indicating a subclinical infection pattern typical of intermediate hosts [1].

Molecular analysis targeting the 18S rRNA gene revealed that the obtained sequences were highly similar to *S. linearis* and closely related species, including *S. taeniata* and *S. grueneri*. However, species-level identification could not be achieved. This limitation is consistent with previous studies demonstrating that the SSU rRNA gene is highly conserved among closely related *Sarcocystis* species, particularly those infecting cervids, and therefore lacks sufficient discriminatory power for precise species differentiation [6].

In addition, the use of FFPE tissues may have further limited molecular resolution in this study. DNA extracted from FFPE samples is often fragmented and chemically modified, which can reduce amplification efficiency and restrict the length and quality of obtainable sequences [17]. This limitation may have contributed to the restricted number of sequences obtained and the difficulty in achieving species-level identification.

The phylogenetic analysis further supported this limitation, as sequences assigned to different *Sarcocystis* species were intermingled within the same clade rather than forming distinct species-specific groupings. This pattern highlights the difficulty of resolving taxonomic relationships within this group using SSU rRNA markers alone and underscores the need for additional genetic loci, such as mitochondrial loci (e.g., *cox1*), to improve species-level resolution.

Cervids are well-recognized intermediate hosts of diverse *Sarcocystis* species, and multiple species have been reported in roe deer in Europe [6,7]. However, information on *Sarcocystis* infection in wildlife in Korea remains limited. In particular, data on wild Korean roe deer are lacking despite their ecological importance. Previous studies in Korea have reported *Sarcocystis* infections in various domestic and wild animals, but investigations in wildlife remain scarce [7-10,18,19]. Therefore, the present study provides baseline data on the occurrence and molecular characteristics of *Sarcocystis* infection in this host species in Korea.

From an ecological perspective, the absence of inflammatory response observed in the present study suggests a well-adapted host–parasite relationship in wild roe deer. Such subclinical infections are characteristic of intermediate hosts and may facilitate the maintenance of *Sarcocystis* life cycles in natural ecosystems without causing overt disease [1]. Given the high population density of roe deer on Jeju Island, this host species may play an important role in sustaining parasite transmission dynamics in the region. However, completion of the *Sarcocystis* life cycle also depends on the presence of suitable definitive hosts. Although the definitive host of the *Sarcocystis* species detected in this study could not be determined, domestic dogs,

https://doi.org/10.3347/PHD.26041

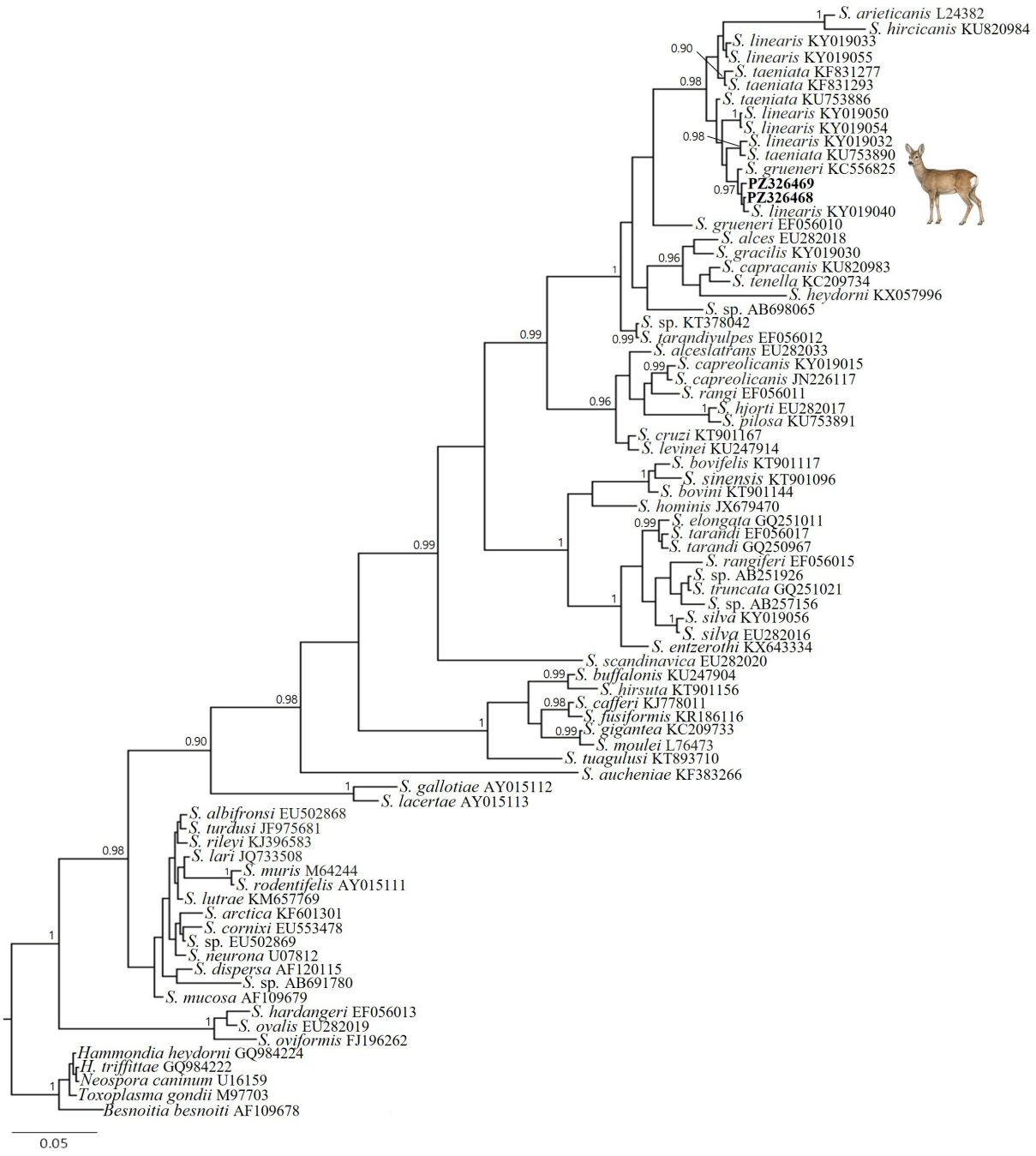


Fig. 2. Phylogenetic relationships within the genus *Sarcocystis* inferred from the small subunit rRNA dataset (639 bp) constructed under the HKY+I+G substitution model using Bayesian inference. The 2 newly generated sequences from the present study are shown in bold. Tree topology is based on the Bayesian all-compatible consensus tree. Posterior probabilities are shown at nodes only for values ≥0.90.

free-ranging dogs, and other carnivorous mammals present on Jeju Island may contribute to the maintenance of transmission cycles in the local ecosystem.

Although the number of sequences obtained in this study was limited, the combined histopathological and molecular findings provide preliminary evidence of *Sarcocystis* infection in wild roe deer. However, species-level identification was not possible based on the available 18S rRNA sequences alone. Future studies incorporating a larger number of samples and higher-resolution genetic markers will be necessary to further clarify species diversity and host–parasite relationships in this system.

Author contributions

Conceptualization: Jung JY. Data curation: Jang J, Yun Y. Formal analysis: Nam DY, Kim S. Investigation: Nam DY. Methodology: Nam DY, Jung JY. Resources: Jang J, Yun Y. Software: Kim S. Supervision: Jung JY. Validation: Kim JH. Writing – original draft: Nam DY. Writing – review & editing: Kim S, Kim JH, Jung JY.

Conflict of interest

The authors have no conflicts of interest to declare.

Funding

This work was supported by the National Institute of Wildlife Disease Control and Prevention as a "Special graduate school support project for wildlife disease specialists."

Supplementary information

Supplementary material is available with this article at https://doi.org/10.3347/PHD.26041.

ORCID

Da-Ye Nam, https://orcid.org/0000-0002-1575-6519
Sunmin Kim, https://orcid.org/0000-0002-3855-8785
Jinho Jang, https://orcid.org/0000-0002-7845-9028
YoungMin Yun, https://orcid.org/0000-0003-0695-0843
Jae-Hoon Kim, https://orcid.org/0000-0002-4410-9126
Ji-Youl Jung, https://orcid.org/0000-0002-5938-2029

References

1. Otranto D, Wall R. Veterinary protozoology. In: Otranto D, Wall R, Taylor MA, editors. Veterinary parasitology. Wiley-Blackwell; 2024. p. 138-215.
2. Dubey JP, Calero-Bernal R, Rosenthal BM, Speer CA, Fayer R. Sarcocystosis of animals and humans. CRC Press; 2015.
3. Pérez-Creo A, Panadero R, López C, et al. Prevalence and identity of *Sarcocystis* spp. in roe deer (*Capreolus capreolus*) in Spain: a morphological study. Res Vet Sci 2013;95:1036-40. https://doi.org/10.1016/j.rvsc.2013.08.003
4. Reissig EC, Helman E, Moré G. *Sarcocystis* spp. infection in South American deer huemul (*Hippocamelus bisulcus*) and pudu (*Pudu puda*) from Patagonian National Parks, Argentina. Parasitol Res 2020;119:3915-22. https://doi.org/10.1007/s00436-020-06889-9
5. Gjerde B, Luzón M, Alunda JM, de la Fuente C. Morphological and molecular characteristics of six *Sarcocystis* spp. from red deer (*Cervus elaphus*) in Spain, including *Sarcocystis cervicanis* and three new species. Parasitol Res 2017;116:2795-811. https://doi.org/10.1007/s00436-017-5590-z
6. Gjerde B, Giacomelli S, Bianchi A, et al. Morphological and molecular characterization of four *Sarcocystis* spp., including *Sarcocystis linearis* n. sp., from roe deer (*Capreolus capreolus*) in Italy. Parasitol Res 2017;116:1317-38. https://doi.org/10.1007/s00436-017-5410-5
7. Moon MH. *Sarcocystis* infection and identification of *Sarcocystis* species in pigs in Korea. Korean J Vet Res 1989;29:325-31.
8. Kang SS, Yi YJ, Cui XS, et al. *Sarcocystis* infestation in farmed elk (*Cervus canadensis*). J Vet Clin 1999;16:529-32.
9. Hong EJ, Sim C, Chae JS, et al. Ultrastructural and molecular identification of *Sarcocystis tenella* (Protozoa, Apicomplexa) in naturally infected Korean native goats. Vet Med 2016;61:374-81. https://doi.org/10.17221/93/2015-vetmed
10. Choi TI, Hong EJ, Ryu SY, et al. Detection and identification of *Sarcocystis cruzi* (Protozoa: Apicomplexa) by molecular and ultrastructural studies in naturally infected Korean cattle (*Bos taurus coreanae*) from Daejeon, Korea. Korean J Parasitol 2018;56:121-7. https://doi.org/10.3347/kjp.2018.56.2.121
11. Moré G, Schares S, Maksimov A, et al. Development of a multiplex real time PCR to differentiate *Sarcocystis* spp. affecting cattle. Vet Parasitol 2013;197:85-94. https://doi.org/10.1016/j.vetpar.2013.04.024
12. Gjerde B. Phylogenetic relationships among *Sarcocystis* species in cervids, cattle and sheep inferred from the mitochondrial cytochrome c oxidase subunit I gene. Int J Parasitol 2013;43:579-91. https://doi.org/10.1016/j.ijpara.2013.02.004
13. Kearse M, Moir R, Wilson A, et al. Geneious Basic: an integrated and extendable desktop software platform for the organization and analysis of sequence data. Bioinformatics 2012;28:1647-9. https://doi.org/10.1093/bioinformatics/bts199
14. Baker CS, Dalebout ML, Lavery S, Ross HA. www.DNA-surveillance: applied molecular taxonomy for species conservation and discovery. Trends Ecol Evol 2003;18:271-2. https://doi.org/10.1016/S0169-5347(03)00101-0
15. Larkin MA, Blackshields G, Brown NP, et al. Clustal W and Clustal X version 2.0. Bioinformatics 2007;23:2947-8. https://doi.org/10.1093/bioinformatics/btm404
16. Ronquist F, Teslenko M, van der Mark P, et al. MrBayes 3.2: efficient Bayesian phylogenetic inference and model choice across a large model space. Syst Biol 2012;61:539-42. https://doi.org/10.1093/sysbio/sys029
17. Srinivasan M, Sedmak D, Jewell S. Effect of fixatives and tissue processing on the content and integrity of nucleic acids. Am J Pathol 2002;161:1961-71. https://doi.org/10.1016/S0002-9440(10)64472-0
18. Kim TH, Han JH, Chang SN, et al. Detection of sarcocystic infection in a wild rodent (*Apodemus agrarius chejuensis*) captured on Jeju island. Lab Anim Res 2011;27:357-9. https://doi.org/10.5625/lar.2011.27.4.357
19. Kim HW, Kim HC, Ryu SY, et al. Molecular identification of *Sarcocystis grueneri* in wild Korean water deer (*Hydropotes inermis argyropus*). Korean J Parasitol 2018;56:129-34. https://doi.org/10.3347/kjp.2018.56.2.129

Case Report

Parasites Hosts Dis 2026;64(4):379-384
https://doi.org/10.3347/PHD.26030

Parasites, Hosts and Diseases

pISSN 2982-5164 • eISSN 2982-6799

Molecular and pathological characterization of a *Dirofilaria* sp. infection in a little egret (*Egretta garzetta*)

Eunjeong Go[1,†], You-Jeong Lee[2,†], Da-Ye Nam[1], Beoul Kim[2], Hyo-Min Woo[2], Min-Goo Seo[2], Dayoung Choi[1], Jae-Hoon Kim[1], Jinho Jang[1,3], YoungMin Yun[1,3], Ji-Youl Jung[1,*]

[1]College of Veterinary Medicine and Veterinary Medical Research Institute, Jeju National University, Jeju, Korea; [2]College of Veterinary Medicine, Kyungpook National University, Daegu, Korea; [3]Jeju Wildlife Rescue Center, Jeju National University, Jeju, Korea

Dirofilaria spp. are mosquito-borne filarial nematodes that primarily infect mammals. Here, we describe a filarial nematode infection in a female little egret (*Egretta garzetta*) from Jeju, Korea. Necropsy revealed multiple slender nematodes (4–6 cm) in the subcutaneous tissues of both legs. Histopathological examination demonstrated granulomatous inflammation with intralesional parasites. Morphologically, the nematodes exhibited a thick multilayered cuticle with prominent longitudinal ridges, consistent with members of the genus *Dirofilaria*. Molecular analysis based on 18S rRNA and mitochondrial c oxidase subunit I (*cox1*) gene sequences indicated that the parasite was most closely related to *D. repens*; however, the level of sequence divergence precluded definitive species-level identification. Phylogenetic analysis further demonstrated that the isolates clustered within the *Dirofilaria* clade and were clearly separated from avian-associated filarioid nematodes. This study provides molecular and histopathological evidence of a *Dirofilaria* sp. infection in an avian host and supports incidental infection under natural exposure conditions.

Keywords: Avian filariasis, *Dirofilaria* sp., granulomatous inflammation, little egret, subcutaneous tissue

Introduction

Dirofilaria spp. are mosquito-borne filarial nematodes that primarily infect mammals, particularly canines [1]. *Dirofilaria immitis* is the causative agent of heartworm disease and resides in the pulmonary artery and right ventricle of the host [2]. In contrast, *D. repens* typically inhabits the subcutaneous tissues and is associated with subcutaneous dirofilariasis [3].

In canines, *D. repens* infection is usually asymptomatic; however, it is of significant zoonotic importance because of its ability to infect humans. In humans, adult worms may localize to the periorbital region or form subcutaneous nodules [4].

To date, infections caused by *Dirofilaria* spp. have been primarily documented in mammalian hosts, including dogs, cats, and humans. In contrast, filarioid infections in avian species are typically associated with other genera, such as *Splendidofilaria*, *Eulimdana*, *Lemdana*, and *Diplotriaena*, which inhabit various tissues depending on the species [5]. Reports of *Dirofilaria* infection in birds are extremely limited, and species-level identification in such cases remains uncertain.

In this study, we describe a filarial nematode infection detected in the subcutaneous tissues of a female little egret (*Egret-*

Received: March 25, 2026 Accepted: June 13, 2026
*Correspondence: jungjy1982@jejunu.ac.kr

†These authors contributed equally to this work.

© 2026 The Korean Society for Parasitology and Tropical Medicine
This is an open-access article distributed under the terms of the Creative Commons Attribution Non-Commercial License (http://creativecommons.org/licenses/by-nc/4.0/) which permits unrestricted non-commercial use, distribution, and reproduction in any medium, provided the original work is properly cited.

Citation
Go E, Lee YJ, Nam DY, Kim B, Woo HM, Seo MG, Choi D, Kim JH, Jang J, Yun Y, Jung JY. Molecular and pathological characterization of a *Dirofilaria* sp. infection in a little egret (*Egretta garzetta*). Parasites Hosts Dis 2026; 64(4):379-384.

ta garzetta) from Jeju, Korea. Based on morphological characteristics and molecular analyses, the parasite was identified as a member of the genus *Dirofilaria* and was most closely related to *D. repens*. However, the available data did not allow definitive species-level identification. This case provides morphological and molecular evidence of a *Dirofilaria* sp. infection in an avian host and offers insight into host–parasite interactions in an unusual host under natural exposure conditions.

Case Report

On April 7, 2025, the Jeju Wildlife Rescue Center, Korea, rescued an adult female little egret of unknown age in an exhausted and ataxic state. At rescue, the bird was severely emaciated (body weight, 260 g; body condition score, 1/5) and exhibited moderate dehydration and hypothermia. No external trauma, fractures, dislocations, or respiratory distress were observed.

Hematological examination revealed anemia (packed cell volume, 24%; reference range, 40%–60%) and markedly decreased total protein (approximately 1 g/dl; reference range, 3.5–5.5 g/dl), indicating hypoproteinemia.

The prognosis of the bird was poor, and it died the following day. To determine the cause of death, a necropsy was performed at the Department of Veterinary Pathology, College of Veterinary Medicine, Jeju National University, Korea. Ethical approval was not required because the bird was rescued from the wild and died naturally.

Gross examination revealed a 2-cm hemorrhagic lesion in the right pectoral muscle and a perforating lesion in the upper region of the left pectoral muscle. Multiple pulmonary hemorrhages were observed in the lungs. No distinct nodular lesions were observed externally in the legs; however, upon incision, approximately 10 slender, thread-like nematodes (4–6 cm in length) were identified within the subcutaneous tissues of both legs (Fig. 1A, B).

Tissue samples were collected and immediately fixed in 10% neutral-buffered formalin, routinely processed, embedded in paraffin, sectioned at 3–4 μm, and stained with hematoxylin and eosin for histopathological examination. Recovered parasites were fixed in 70% ethanol and examined under a light microscope for morphological identification.

Histopathological examination revealed moderate-to-severe fibrous connective tissue proliferation and granulomatous inflammation in the subcutaneous tissues of the legs (Fig. 2A). The lesions were characterized by infiltration of numerous macrophages, lymphocytes, as well as multinucleated giant cells surrounding intralesional parasitic organisms in the affected subcutaneous areas (Fig. 2B). No microfilariae were observed in the examined tissue sections. Moderate-to-severe pulmonary hemorrhage was observed in the lungs.

Histological examination revealed transverse sections of a filarial nematode characterized by a thick, multilayered eosinophilic cuticle with prominent, regularly spaced external longitudinal ridges (Fig. 2C). Beneath the cuticle, a thin hypodermis and well-developed polymyarian–coelomyarian somatic musculature were observed. Within the pseudocoelomic cavity, reproductive structures containing numerous microfilariae were present, indicating a gravid female worm.

Gross morphological examination revealed a slender, elongated filarial nematode with a cylindrical body and tapering anterior and posterior ends. The worm was white-yellowish in color and measured approximately 6.0 cm in length and 0.5 mm in diameter. Microscopic examination of the worm surface further demonstrated distinct, parallel longitudinal ridges separated by shallow grooves.

For molecular identification, genomic DNA was extracted



Fig. 1. Gross findings. (A) Subcutaneous nodular lesion of the leg identified after incision, containing numerous nematodes. (B) Numerous white filarial nematodes observed in the subcutaneous tissues of the leg.

https://doi.org/10.3347/PHD.26030

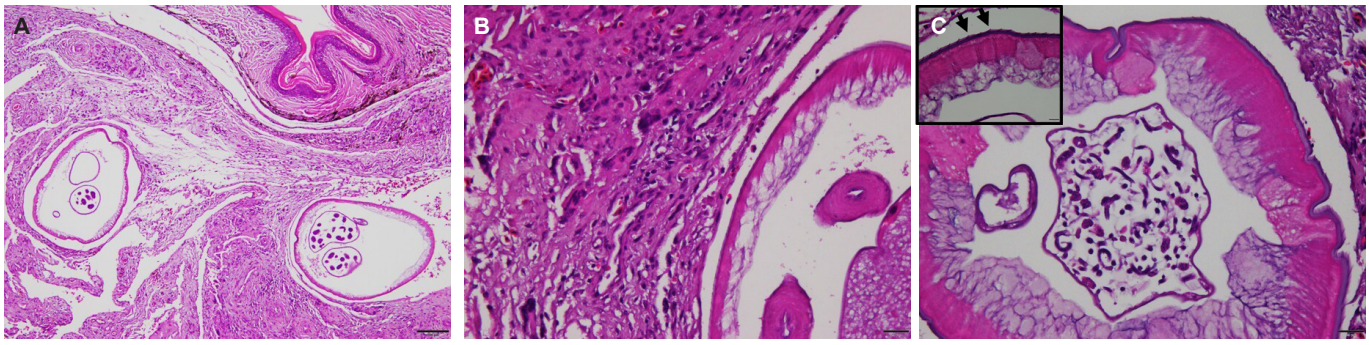


Fig. 2. Histopathological findings. All sections were stained with hematoxylin and eosin. (A) Subcutaneous lesion showing moderate to severe fibrous connective tissue proliferation with granulomatous inflammation and intralesional parasitic organisms. Scale bar=100 μm. (B) Multinucleated giant cells (arrows) with surrounding macrophages and lymphocytes forming a granulomatous reaction around the parasite. Scale bar=20 μm. (C) Transverse section of a filarial nematode showing a thick, multilayered eosinophilic cuticle. A thin hypodermis and well-developed polymyarian–coelomyarian somatic musculature are present. The inset highlights prominent external longitudinal ridges (arrows). Scale bar=20 μm.

from 4 parasite samples using the Clear-S Quick DNA Extraction Kit (Invirustech) according to the manufacturer's instructions. PCR amplification was performed using an AccuPower PCR Premix Kit (Bioneer). The 18S rRNA gene was amplified using the primer set 18S.631f/18S.1825r, yielding an amplicon of approximately 1,127–1,155 bp [6]. Additionally, the mitochondrial cytochrome c oxidase subunit I (*cox1*) gene was amplified using specific primers, resulting in an approximately 680-bp PCR product [7].

DNA sequencing was performed by Macrogen using the same primer sets. Sequence similarity was analyzed by comparison with reference sequences deposited in GenBank (National Center for Biotechnology Information). Multiple sequence alignments were performed using Clustal Omega version 1.2.1 and refined using BioEdit version 7.2.5. Phylogenetic analysis was conducted using MEGA software version 6.0 based on the maximum-likelihood method with the Kimura two-parameter model. Bootstrap analysis with 1,000 replicates was performed to assess the reliability of the resulting phylogenetic tree.

The 18S rRNA sequences obtained in this study shared the highest sequence identity (99.2%) with *D. repens* sequences deposited in GenBank. However, similarly high sequence identities were also observed with other filarial genera, including *Mansonella* spp. (99.0%–99.2%), *Dipetalonema* spp. (98.6%–99.1%), and *Loa loa* (99.0%), indicating that the 18S rRNA gene has limited discriminatory power for species-level identification. The sequences generated in this study have been deposited in GenBank under accession numbers PX279224 and PX981761–PX981763 (*Dirofilaria* sp. 18S rRNA) (Fig. 3).

The *cox1* gene sequences obtained in this study showed 95.1%–100% identity among themselves and 90.1%–94.7% identity with previously reported *D. repens cox1* sequences, representing the highest similarity among the compared taxa. Additional sequence similarity analyses revealed identities of 84.3%–86.9% with *Mansonella* spp., 88.0%–89.2% with *L. loa*, and 72.4%–90.2% with *Dipetalonema* spp. The sequences generated in this study have been deposited under accession numbers PX974591–PX974594 (*Dirofilaria* sp. *cox1*) (Fig. 4).

Discussion

To our knowledge, this study represents the first case of a filarial nematode infection most closely related to *D. repens* identified in an avian host. To date, reports of *Dirofilaria* infection in birds have been extremely limited, with only a single case of *D. immitis* infection in Humboldt penguins in Japan [8]. In the present case, filarial nematodes detected in a little egret from Jeju Island, Korea, exhibited prominent longitudinal ridges on their surface, which are suggestive of morphological features described for *D. repens* [9], although these findings are not sufficient for definitive species-level identification. The parasites were localized within the subcutaneous tissues and were associated with granulomatous inflammation, indicating an active host tissue response.

Although no distinct external nodular lesions were observed, subcutaneous nodular lesions were identified upon incision, corresponding to the location of the parasites. The cause of death was primarily attributed to traumatic injury, including pectoral muscle damage and pulmonary hemorrhage. Clinical findings such as severe emaciation, anemia, and hypoproteinemia may have been influenced, at least in part, by parasitism, and this possibility cannot be entirely excluded. Therefore, while trauma was considered the primary cause of death, it

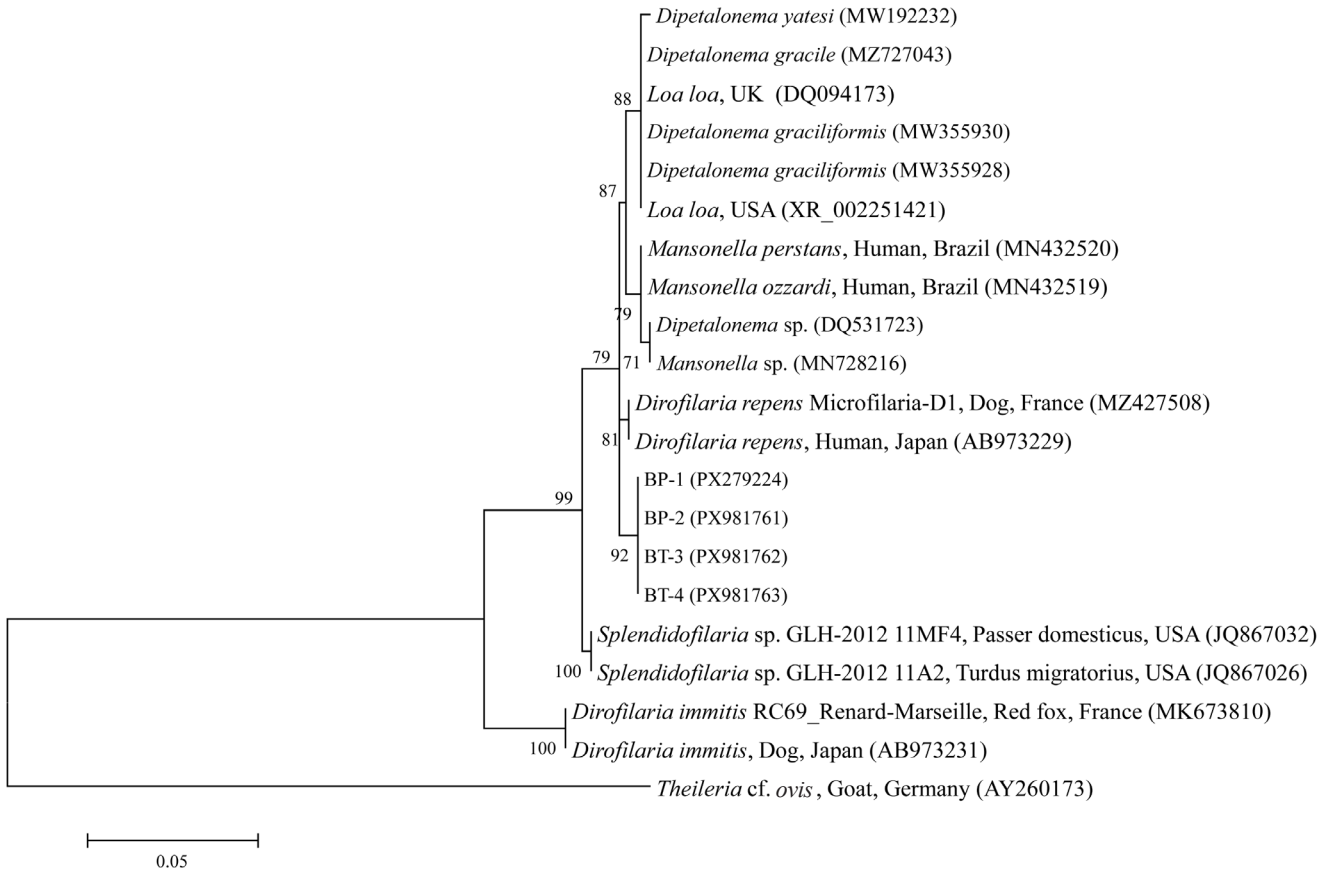


Fig. 3. Phylogenetic analysis of filarial nematodes based on 18S rRNA gene sequences. The maximum-likelihood tree shows that the sequences obtained in this study (BP-1–BP-4) cluster within the *Dirofilaria* clade and are most closely related to *Dirofilaria repens*, while clearly separated from other filarioid nematodes, including avian-associated species. Taxon labels indicate the species, host, geographic origin, and GenBank accession number; accession numbers are shown in parentheses. Statistical support was evaluated using 1,000 bootstrap replicates under the Kimura two-parameter model. The scale bar indicates 0.05 nucleotide substitutions per site. *Theileria* cf. *ovis* was used as the outgroup.

may have represented the final event in a multifactorial process. Accordingly, the filarial infection was considered incidental with respect to the immediate cause of death, although it may have contributed to the overall condition of the bird.

Molecular analyses provided additional insight into the taxonomic identity of the parasite. The 18S rRNA gene showed high sequence similarity not only with *D. repens* but also with other filarial genera, including *Mansonella*, *Dipetalonema*, and *Loa*, reflecting the highly conserved nature of this marker and its limited utility for species-level discrimination. In contrast, the mitochondrial *cox1* gene demonstrated that the sequences obtained in this study were most closely related to *D. repens* among the available reference sequences, although the observed sequence divergence (90.1%–94.7%) was relatively high. Taken together, these findings indicate that the parasite cannot be conclusively identified as *D. repens*, but rather represents a *Dirofilaria* sp. that is most closely related to *D. repens*. Furthermore, phylogenetic analyses based on both 18S rRNA and *cox1* genes consistently placed the sequences obtained in this study within the *Dirofilaria* clade and clearly separated them from other filarial genera, including *Mansonella*, *Dipetalonema*, and *Loa*. In addition, all 18S rRNA sequences were identical, and 3 out of 4 *cox1* sequences shared an identical haplotype, supporting the presence of a single parasite lineage rather than mixed infection or contamination.

Several genera of filarioid nematodes, including *Splendidofilaria*, *Eulimdana*, *Lemdana*, and *Diplotriaena* spp., are known to infect avian species, typically inhabiting subcutaneous, connective, muscular, vascular, or respiratory tissues [5]. Based on host range and tissue tropism, filarial infections in birds are generally attributed to avian-specific filarioids. However, in the present study, both morphological and molecular findings consistently support the classification of the parasite as belonging to the genus *Dirofilaria*, as the sequences were clearly placed within the *Dirofilaria* clade and distinctly separated from avian-associated filarioid nematodes. These find-

https://doi.org/10.3347/PHD.26030

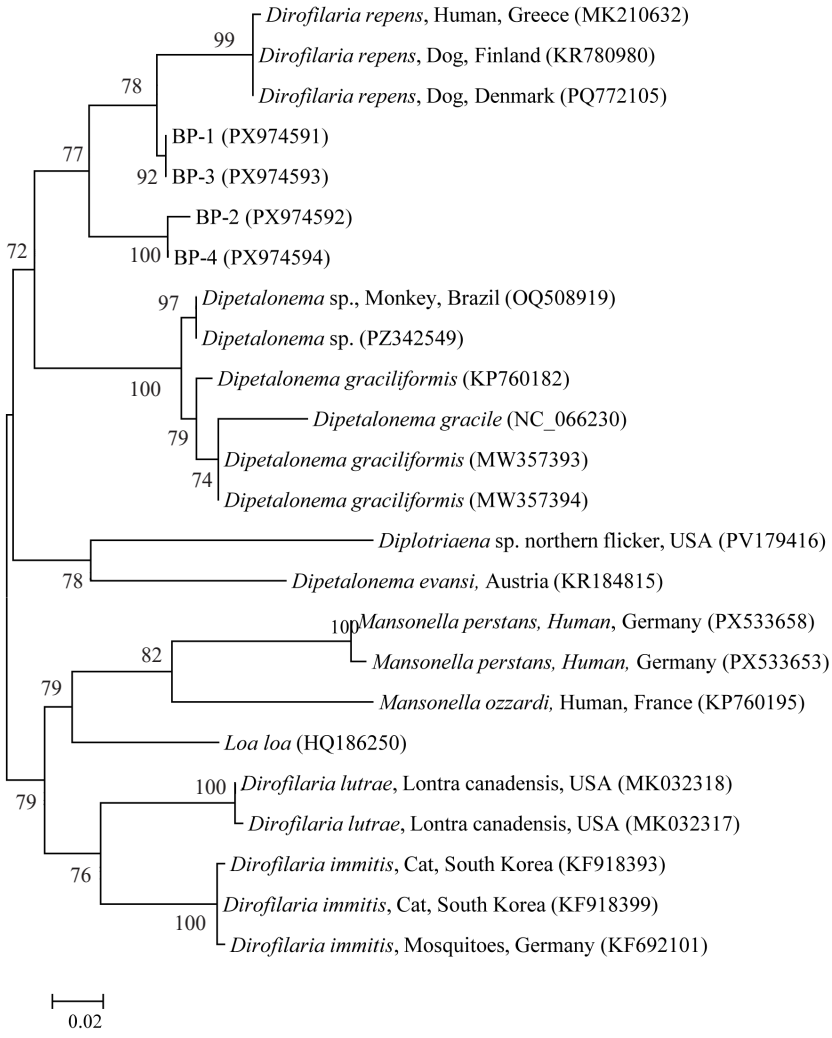


Fig. 4. Phylogenetic analysis of filarial nematodes based on mitochondrial cytochrome c oxidase subunit I (*cox1*) gene sequences. The maximum-likelihood tree shows that the sequences obtained in this study (BP-1–BP-4) cluster within the *Dirofilaria* clade and are most closely related to *Dirofilaria repens*, while clearly separated from other filarioid nematodes, including avian-associated species. Taxon labels indicate the species, host, geographic origin, and GenBank accession number; accession numbers are shown in parentheses. Statistical support was evaluated using 1,000 bootstrap replicates under the Kimura two-parameter model. The scale bar indicates 0.02 nucleotide substitutions per site. *Diplotriaena* sp. was used as the outgroup.

ings suggest that birds may be incidentally exposed to mammalian filarial parasites under natural ecological conditions.

The little egret is both a resident and migratory species in East Asia and is commonly observed on Jeju Island. Therefore, it is unclear whether the individual in this study was a local resident or a migratory bird. Considering the prepatent period of *Dirofilaria* spp., the geographic origin of infection cannot be determined. This uncertainty should be considered when interpreting the epidemiological context of this case.

Little egrets primarily inhabit wetland environments, such as rice paddies, rivers, fishponds, and intertidal mudflats [10], where exposure to mosquito vectors is common. As *Dirofilaria* spp. are transmitted by mosquitoes via infective third-stage larvae (L3), such ecological conditions may allow incidental exposure of birds. Although avian species are unlikely to support full parasite development, natural exposure followed by limited tissue invasion can occur, as demonstrated in this case.

This study has several limitations. Because the parasitic infection was initially considered an incidental finding during necropsy, detailed parasitological characterization, including sex and developmental stage, was not systematically performed. Furthermore, although a gravid female worm was identified, microfilariae were not observed in tissue sections, and no blood-based examination was performed. Therefore, the host competence of this species could not be determined. Additional morphological examinations and analyses using supplementary molecular markers will be required to further clarify the taxonomic status of this parasite.

Data availability

Data supporting the findings of this study are available from the corresponding author upon reasonable request.

Author contributions

Conceptualization: Jung JY. Formal analysis: Go E, Lee YJ. Investigation: Go E, Lee YJ, Nam DY, Kim B, Woo HM, Choi D. Methodology: Go E, Lee YJ. Resources: Jang J, Yun Y. Supervision: Jung JY. Writing - original draft: Go E, Lee YJ. Writing - review & editing: Kim JH, Jung JY, Seo MG.

Conflict of interest

Min-Goo Seo serves as an editor of Parasites, Hosts and Diseases but had no involvement in the decision to publish this article. No other potential conflicts of interest relevant to this study were reported.

Funding

This work was supported by a grant from the National Institute of Wildlife Disease Control and Prevention, funded by the Ministry of Environment of the Republic of Korea (NIWDC-2024-SP-02).

ORCID

Eunjeong Go, https://orcid.org/0009-0003-8895-2945
You-Jeong Lee, https://orcid.org/0009-0009-8058-570X
Da-Ye Nam, https://orcid.org/0000-0002-1575-6519
Beoul Kim, https://orcid.org/0009-0001-5159-4801
Hyo-Min Woo, https://orcid.org/0009-0009-5637-5681
Min-Goo Seo, https://orcid.org/0000-0003-1752-5105
Dayoung Choi, https://orcid.org/0009-0007-7956-6400
Jae-Hoon Kim, https://orcid.org/0000-0002-4410-9126
Jinho Jang, https://orcid.org/0000-0002-7845-9028
YoungMin Yun, https://orcid.org/0000-0003-0695-0843
Ji-Youl Jung, https://orcid.org/0000-0002-5938-2029

References

1. Lee SE, Kim HC, Chong ST, Klein TA, Lee WJ. Molecular survey of *Dirofilaria immitis* and *Dirofilaria repens* by direct PCR for wild caught mosquitoes in the Republic of Korea. Vet Parasitol 2007;148:149-55. https://doi.org/10.1016/j.vetpar.2007.04.015
2. McCall JW, Genchi C, Kramer LH, Guerrero J, Venco L. Heartworm disease in animals and humans. Adv Parasitol 2008;66:193-285. https://doi.org/10.1016/S0065-308X(08)00204-2
3. Albanese F, Abramo F, Braglia C, et al. Nodular lesions due to infestation by *Dirofilaria repens* in dogs from Italy. Vet Dermatol 2013;24:255-e56. https://doi.org/10.1111/vde.12009
4. Simón F, Siles-Lucas M, Morchón R, et al. Human and animal dirofilariasis: the emergence of a zoonotic mosaic. Clin Microbiol Rev 2012;25:507-44. https://doi.org/10.1128/CMR.00012-12
5. Bartlett CM. Filarioid nematodes. In: Atkinson CT, Thomas NJ, Hunter DB, editors. Parasitic diseases of wild birds. Wiley-Blackwell; 2008. p. 439-62.
6. Laidoudi Y, Ringot D, Watier-Grillot S, Davoust B, Mediannikov O. A cardiac and subcutaneous canine dirofilariosis outbreak in a kennel in central France. Parasite 2019;26:72. https://doi.org/10.1051/parasite/2019073
7. Folmer O, Black M, Hoeh W, Lutz R, Vrijenhoek R. DNA primers for amplification of mitochondrial cytochrome c oxidase subunit 1 from diverse metazoan invertebrates. Mol Mar Biol Biotechnol 1994;3:294-9.
8. Sano Y, Aoki M, Takahashi H, et al. The first record of *Dirofilaria immitis* infection in a Humboldt penguin, *Spheniscus humboldti*. J Parasitol 2005;91:1235-7. https://doi.org/10.1645/GE-3492-RN.1
9. Suzuki J, Kobayashi S, Okata U, et al. Molecular analysis of *Dirofilaria repens* removed from a subcutaneous nodule in a Japanese woman after a tour to Europe. Parasite 2015;22:2. https://doi.org/10.1051/parasite/2015002
10. Pang CC, Sung YH, Chung YT, et al. Spatial ecology of little egret (*Egretta garzetta*) in Hong Kong uncovers preference for commercial fishponds. PeerJ 2020;8:e9893. https://doi.org/10.7717/peerj.9893

https://doi.org/10.3347/PHD.26030

Case Report

Parasites Hosts Dis 2026;64(4):385-390
https://doi.org/10.3347/PHD.26005

Parasites, Hosts and Diseases

pISSN 2982-5164 • eISSN 2982-6799

Isolation and whole-genome characterization of *Coxiella burnetii* from an acute Q fever patient in Korea

Yejin Choi[1,2,†], Dayoung Kim[3,†], Yeon-Joo Choi[4,5,†], Sun-Woo Choi[1,2], Da-Eun Jeong[1,2], Jeong Yoon Lee[1,2], Nam-Hyuk Cho[6,7], Kwang-Jun Lee[8], Dong-Min Kim[3,*], Won-Jong Jang[4,5,*], Jun-Gu Kang[1,2,*]

[1]Korea Zoonosis Research Institute, Jeonbuk National University, Iksan, Korea; [2]Department of Veterinary and Animal Science, College of Veterinary Medicine, Jeonbuk National University, Iksan, Korea; [3]Division of Infectious Disease, Department of Internal Medicine, College of Medicine, Chosun University, Gwangju, Korea; [4]Department of Microbiology, College of Medicine, Konkuk University, Seoul, Korea; [5]Institute of Glocal Disease Control, College of Medicine, Konkuk University, Chungju, Korea; [6]Department of Microbiology and Immunology, College of Medicine, Seoul National University, Seoul, Korea; [7]Department of Biomedical Sciences, College of Medicine, Seoul National University, Seoul, Korea; [8]Division of Zoonotic and Vector Borne Diseases Research, Center for Infectious Diseases Research, Korea National Institute of Health, Osong, Korea

Coxiella burnetii is an environmentally stable intracellular bacterium responsible for severe global outbreaks of the zoonotic disease, Q fever. Q fever is transmitted by the inhalation of aerosols contaminated with the birth products and excretions of infected animals, mainly of sheep and goats. A 28-year-old cattle raiser presented with headache and fever without a significant medical history, although his cattle herd had previously been diagnosed with brucellosis. He spent time outdoors but reported no tick bites or eschar. Initial evaluation revealed mild thrombocytopenia and elevated aspartate aminotransferase, alanine aminotransferase, and C-reactive protein levels. On day 2 after disease onset, his blood tested positive for the IS1111 gene of *C. burnetii* by nested PCR. After amplifying *C. burnetii* in severe combined immunodeficient mice, the pathogen was isolated using a cell culture system. The isolated CH12 strain was confirmed via PCR, nucleotide sequence analysis, and whole-genome sequencing. This study reports a case of acute Q fever in Korea, in which *C. burnetii* was isolated and characterized using whole-genome sequencing.

Keywords: *Coxiella burnetii*, Q fever, Korea, isolation, whole genome sequencing

Introduction

Coxiella burnetii is an obligate intracellular, gram-negative bacterium belonging to the family *Coxiellaceae*, and it is recognized as the etiological agent of Q fever in humans and coxiellosis in animals [1]. With a broad host range that encompasses mammals, birds, reptiles, and arthropods, *C. burnetii* is globally distributed and notable for its high environmental stability and extremely low infectious dose, which are factors that contribute to its classification as an emerging zoonotic pathogen [2]. Human infection typically occurs through the inhalation of aerosolized particles contaminated with the birth products or bodily fluids derived from infected animals, which consequently leads to Q fever. This condition is often asymptomatic or pres-

Received: January 12, 2026 Accepted: June 1, 2026
*Correspondence: dmk, drongkim@hanmail.net; wjj, wjjang@kku.ac.kr; jgk, herculess@jbnu.ac.kr

†These authors contributed equally to this work.

© 2026 The Korean Society for Parasitology and Tropical Medicine
This is an open-access article distributed under the terms of the Creative Commons Attribution Non-Commercial License (http://creativecommons.org/licenses/by-nc/4.0/) which permits unrestricted non-commercial use, distribution, and reproduction in any medium, provided the original work is properly cited.

Citation
Choi Y, Kim D, Choi YJ, Choi SW, Jeong DE, Lee JY, Cho NH, Lee KJ, Kim DM, Jang WJ, Kang JG. Isolation and whole-genome characterization of *Coxiella burnetii* from an acute Q fever patient in Korea. Parasites Hosts Dis 2026;64(4):385-390.

ents as a nonspecific influenza-like illness, although severe and occasionally fatal cases have been documented [2]. In animals, *C. burnetii* infection is frequently subclinical, although it can result in reproductive complications, such as abortion, stillbirth, low birth weight, and weakened offspring [3].

In Korea, the first case of Q fever was reported in 1992 [4]. Over the past decade (2014–2024), 814 Q fever cases have been reported, with a peak of 163 cases in 2018, followed by a decline to approximately 50–60 cases annually. Among the cases with known occupations, 19.0% comprised individuals in high-risk animal-related professions, such as livestock farmers, slaughterhouse workers, and veterinary quarantine officers [5]. In 2020, the first isolation of *C. burnetii* was reported from nonspecific febrile patients in Korea [6]. Here, we report the isolation and characterization of *C. burnetii* from the organs of severe combined immunodeficient (SCID) mice that died of hepatosplenomegaly after being injected with Q fever–confirmed patient blood.

Case Report

A 28-year-old man who worked as a cattle raiser presented to the emergency department on December 3, 2022, for further evaluation of his elevated liver function test results. Two days prior, he presented to a local clinic with a headache and fever; he had no other relevant medical history. Two years before presentation, his herd of approximately 100 cattle had been diagnosed with brucellosis. He reported spending time outdoors but had no history of tick bites or eschar. At presentation (on day 2), the patient had a platelet count of 116,000/μl (normal range, 150,000–450,000/μl), C-reactive protein (CRP) level of 8.95 mg/dl (normal range, 0–0.3 mg/dl), aspartate aminotransferase (AST) level of 90 U/L (normal range, 5–40 U/L), alanine aminotransferase level of 106 U/L (normal range, 5–40 U/L), and D-dimer concentration of 1,700 ng/ml FEU (normal range, 0–560 ng/ml FEU). The white blood cell count, procalcitonin, creatine phosphokinase, and total bilirubin levels of the patient were normal. Moreover, the patient exhibited a blood pressure of 110/70 mmHg, pulse of 86 beats/min, respiratory rate of 15 breaths/min, and body temperature of 36.3°C. No abnormal findings on thoracic or abdominopelvic computed tomography were observed. The patient was tested for tick-borne infectious diseases, including Q fever, anaplasmosis, and brucellosis, among others, and serological testing performed at the Gwangju Institute of Health and Environment (Gwangju, Korea). The *Brucella* microagglutination test showed a titer of < 1:20 (negative), and the *C. burnetii* indirect immunofluorescence antibody (IFA) assay revealed phases I and II IgG and IgM titers < 1:16, which were interpreted as negative. However, nested PCR assays targeting *IS1111* repeat elements in the blood sample tested positive on day 2 (Table 1). As the patient refused hospitalization, an outpatient follow-up was scheduled, and 7 days of doxycycline prescribed. At the follow-up visit (on day 6), the patient's headache had improved, although the AST and alanine aminotransferase levels were 86 and 93 U/L, respectively. Additionally, his platelet count was 181,000/μl. Most of the clinical data suggested that the bacterial infection did not progress. Nevertheless, the patient was asked to return for further evaluation, but his condition declined; thus, long-term evaluation for chronic Q fever and the assessment of delayed seroconversion could not be conducted.

Occasionally, SCID mice, which lack functional B cells, T cells, and adaptive immunity, have been used to isolate and study bacterial pathogens, including *C. burnetii* [7,8]. Therefore, pathogen isolation was performed using SCID mice. To amplify the bacteria, patient-derived blood was inoculated into SCID mice via the intraperitoneal route [9]. On day 90 post-infection, the infected mice died and developed severe splenomegaly and hepatomegaly. After autopsy, mouse spleens were collected and homogenized for cell culture and DNA extraction. Considering the slow replication kinetics of *C. burnetii* and its ability to establish persistent infections, particularly in

Table 1. Laboratory findings and antibody titers

Symptom onset date	Period between symptom onset and sampling	Antibiotic administration day from symptom onset	Laboratory finding						Nested PCR	IFA			
			WBC (10^3/μl) (neutrophil/lymphocyte, %)	Platelet (10^3/μl)	AST (U/L)	ALT (U/L)	CRP (mg/dl)	Procalcitonin (ng/ml)	Coxiella IS1111	Phase 1 IgG	Phase 1 IgM	Phase 2 IgG	Phase 2 IgM
1	1	0	4.39 (NA)	130	78	81	8.1	NA	NA	NA	NA	NA	NA
2	2	1	4.24 (65.8/25.0)	116	90	106	8.95	0.35	+	< 1:16	< 1:16	< 1:16	< 1:16
6	6	5	6.47 (40.8/40.2)	181	86	93	NA	NA	NA	NA	NA	NA	NA

IFA, indirect immunofluorescence antibody assay; AST, aspartate aminotransferase; ALT, alanine aminotransferase; CRP, C-reactive protein; NA, not available.

https://doi.org/10.3347/PHD.26005

immunocompromised hosts, extended infection periods are often necessary. In SCID mice, the lack of adaptive immunity permits long-term bacterial maintenance; thus, a long duration was selected to allow for adequate bacterial expansion and infection.

Cultures of the Vero E6 cell line (ATCC CRL-1586), which was maintained in RPMI-1640 medium (Welgene) supplemented with 2% fetal bovine serum (Welgene) and 1% amphotericin B (Welgene), were infected using the homogenized spleen material. The cultures were maintained in an incubator set at 34°C with 5% CO_2. The positive isolation cultures were maintained in the original cell culture dishes, with the medium refreshed weekly, and PCR testing conducted on the supernatant. The detection of *C. burnetii* in cell culture dishes was performed using *IS1111*-targeting quantitative PCR [10]. Nested PCR was also used to screen *C. burnetii* targeting the *omp1* gene: for the primary PCR, the outer primer set, WJ147 (forward, 5′-AGTAGAAGCATCCCAAGCATTG-3′) and WJ148 (reverse, 5′-TGCCTGCTAGCTGTAACGATTG-3′), was used, producing a 501-bp fragment; for the secondary PCR, the inner primer set, WJ149 (forward, 5′-GAAGCGCAACAAGAAGAACAC-3′) and WJ150 (reverse, 5′-TTGGAAGTTATCACGCAGTTG-3′), was used, generating a 334-bp amplicon [11]. To confirm the identity of *C. burnetii*, Sanger sequencing was performed for both the 16S rRNA and *com1* genes [12,13]. The 16S rRNA gene was amplified using primers WJ124 (forward, 5′-AGGAGGTGATCCANCCRCA-3′) and WJ195 (reverse, 5′-AGAGTTTGATCCTGGCTCAG-3′), and the *com1* gene amplified with primers WJ958 (forward, 5′-ACAAACGTTACAACCCAGCCCTG-3′) and WJ959 (reverse, 5′-GCGGAAGAGGTCGTATCAGTGAG-3′). The obtained sequences were identical to that of the *C. burnetii* MSU Goat Q177 strain. For whole-genome sequencing (WGS), genomic DNA was extracted from the homogenized spleens of inoculated mice using the FavorPrep Blood/Cultured Cell Genomic DNA Extraction Mini Kit (Favorgen Biotech). Subsequently, DNA libraries were prepared using a TruSeq Nano DNA kit (Illumina), and a quality check then conducted using FastQC version 0.11.5 (Babraham Bioinformatics). Using Trimmomatic version 0.36 (Usadellab), the raw data were trimmed to eliminate low-quality reads and then indexed. Information that can be used in many DNA sequence analyses, such as genome size prediction, genome coverage confirmation, and repeat sequence ratio calculations, was assembled using Jellyfish version 2.2.10. For annotation of the *C. burnetii* CH12 genome, the WG annotation pipeline (Macrogen) was used with strain CH12 as a reference (accession No. JBQPHR000000000).

WGS was performed to determine the genomic characteristics and phylogenetic position of the isolate. In the WGS analysis, 1,986,754 reads were obtained (299,383,989 bp in total), and the N50 was 55,499. Results showed that the CH12 genome (accession No. SAMN50566325) was 2,040,512 bp long, with 2,009 coding sequences, 56 contigs, 3 rRNA genes, 43 tRNA genes, and a GC ratio of 42.35%. The whole-genome sequences, including 24 reference strains, were aligned using BioEdit version 7.7.1, and a phylogenetic tree constructed using the maximum-likelihood method. Bootstrap analysis was performed with 1,000 pseudo-replicates. Results of the phylogenetic analysis showed that strain CH12 was closely related to the MSU-GoatQ177 and CbuKQ154 strains (Fig. 1).

The study protocol was approved by the Institutional Review Board of the Jeonbuk National University Hospital (approval No. 2022-10-012-004). All protocols involving the use of live animals were reviewed and approved by the Institutional Animal Care and Use Committee (approval No. NON2022-042) and the Institutional Biosafety Committee (approval No. JBNU 2022-09-001). Experiments involving the *C. burnetii* CH12 strain, patient blood, and SCID mice were performed in biosafety level 3 or animal biosafety level 3 facilities at the Korea Zoonosis Research Institute, Jeonbuk National University (Iksan, Korea).

Discussion

Diagnosing Q fever is generally challenging because the disease often exhibits a self-limiting proliferative phase that spontaneously resolves within approximately 2 weeks. In the first 2 cases of Q fever reported in Korea, both IFA and PCR were performed during the initial diagnostic phase; however, the results were negative [6]. Moreover, the laboratory analyses showed elevated alkaline phosphatase, AST, and CRP levels, and 1 of the 2 patients had mild thrombocytopenia. As detectable antibody levels typically develop only several weeks after infection, diagnosis is often retrospectively confirmed through the serological testing of convalescent-phase samples, which poses a significant diagnostic challenge for Q fever [6,14]. Cases of Q fever have also been reported in China and Vietnam [14,15], where hepatomegaly and elevated alkaline phosphatase, AST, CRP, and procalcitonin levels have been observed. Moreover, in the case specifically reported in Vietnam, leukocytopenia and thrombocytopenia were observed [15].

In the present case, *C. burnetii* DNA and specific antibodies were simultaneously detected at an early stage of infection (Table 1). This finding markedly differs from those of previously reported Korean cases, in which PCR failed to confirm infection, and a definitive diagnosis was achieved only 9–14 weeks

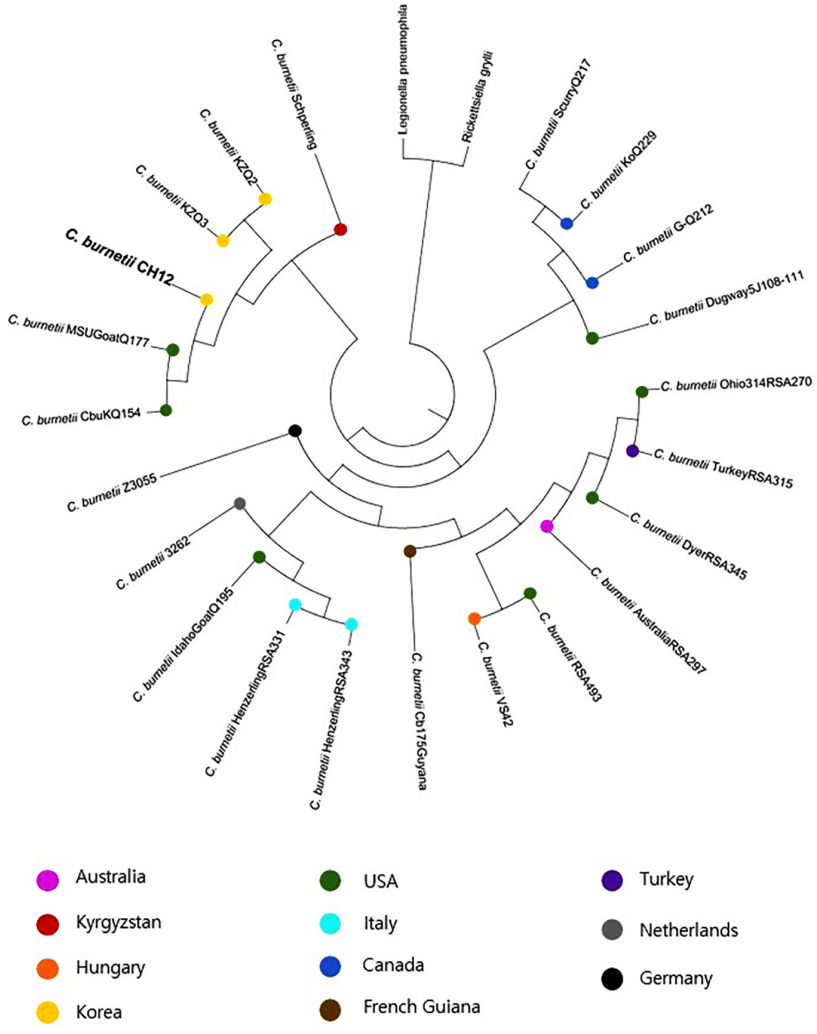


Fig. 1. Phylogenetic tree of *Coxiella burnetii* based on complete genome sequences. Bold letters indicate the *C. burnetii* sequences obtained from a patient in this study.

later via IFA positivity in convalescent-phase serum. In contrast, in the current case, both the pathogen and antibodies were identified only 2 days after the onset of fever, a distinct and noteworthy feature. Given that *C. burnetii* typically replicates slowly and elicits a delayed antibody response, this clinical case was unusual. Several hypotheses could explain this phenomenon. First, given the patient's occupational exposure—raising livestock and having daily contact with animals—continuous or repeated exposure to the pathogen might have triggered the unusually rapid onset of acute Q fever. Although speculative, exposure to highly infectious materials, such as placentas or birth products containing high concentrations of *C. burnetii*, might have resulted in infection despite the presence of pre-existing antibodies. Second, the patient might have already developed Q fever antibodies before the febrile episode. Although the exact time at which the patient began livestock farming could not be determined due to loss to follow-up, medical records indicated a previous diagnosis of brucellosis 2 years earlier, suggesting that the patient had likely been engaged in livestock work for several years. Although the present report presents a diagnosis of acute Q fever, intermittent prior exposure to *C. burnetii* cannot be ruled out. Furthermore, a limitation of this study is that no follow-up was conducted, which prevented the assessment of seroconversion or further analyses, such as those performed in previous studies, consequently leading to inherently limited interpretations. However, the early detection of *C. burnetii* DNA and IFA may provide a basis for the diagnosis of acute Q fever. Compared to previously reported Q fever cases, the present patient similarly showed elevated liver enzyme, CRP,

https://doi.org/10.3347/PHD.26005

and procalcitonin levels. Thrombocytopenia was also observed in the present study and in a Chinese case; however, the occurrence of thrombocytopenia in bacterial infections rather than in viral infections is uncommon. Although the limited number of clinical cases makes the establishment of a definitive link between Q fever and thrombocytopenia difficult, this case could serve as a reference that indicates a potential connection. Therefore, additional serological and molecular testing would be helpful for a more thorough assessment and precise differential diagnosis.

Recent epidemiological studies suggest that human Q fever transmitted by cattle is relatively uncommon compared with that transmitted by sheep or goats [16]. For example, a systematic review analyzing 81 unique human Q fever outbreaks worldwide found that exposure to ruminants and their products was the leading risk factor. Sheep were implicated in approximately 34.6% of outbreaks (28/81), goats in 14.8% (12/81), and cattle in 8.6% (7/81), indicating that human Q fever is far less frequently associated with cattle than with sheep or goats [17]. In this context, the present case offers an opportunity to investigate the epidemiological role of livestock in Q fever transmission.

The morphology of the isolated *C. burnetii* in Vero cells was similar to that of previously reported Korean isolates [6]. Based on the WGS results, the CH12 isolate showed the highest sequence homology with the Korean isolates, KZQ2 and KZQ3, exhibiting 99.94% nucleotide identity. Phylogenetic analysis revealed that the most closely related strains were MSUGoatQ177 and CbuKQ154, with 99.93% sequence similarity (Fig. 1). The Schperling, CH12, KZQ2, KZQ3, MSUGoatQ177, and CbuKQ154 isolates formed a distinct, small clade that was separated from the other *C. burnetii* isolates in the phylogenetic tree. As only a limited number of *C. burnetii* isolates have been obtained and characterized in Korea and other Asian regions, a comprehensive analysis of the genetic diversity and regional distribution patterns remains challenging. Therefore, continuous efforts are necessary to isolate and characterize the genome of *C. burnetii* to better understand its molecular epidemiology and strain-specific features. Moreover, further studies are required to better understand the pathogenicity and transmission mechanisms of *C. burnetii*.

Author contributions

Conceptualization: Choi Y, Kim D, Choi YJ, Kim DM, Jang WJ, Kang JG. Data curation: Choi Y, Choi SW, Jeong DE. Formal analysis: Choi Y, Kim D, Choi YJ. Funding acquisition: Kang JG. Investigation: Choi Y, Kim D, Choi YJ, Choi SW, Jeong DE, Cho NH. Methodology: Choi Y, Kim D, Choi YJ. Project administration: Kim DM, Jang WJ, Kang JG. Resources: Lee KJ, Kim DM, Jang WJ, Kang JG. Software: Lee JY, Choi SW, Jeong DE. Supervision: Lee KJ, Kim DM, Jang WJ, Kang JG. Validation: Cho NH, Lee JY, Choi Y, Kim D, Choi YJ. Visualization: Choi Y, Kim D, Choi YJ, Lee JY. Writing – original draft: Choi Y, Kim D, Choi YJ. Writing – review & editing: Kim DM, Jang WJ, Kang JG.

Conflict of interest

The authors have no conflicts of interest to declare.

Funding

This research was supported by the National Institute of Health research project (project No. 2022ER210801).

ORCID

Yejin Choi, https://orcid.org/0009-0003-9379-2034
Dayoung Kim, https://orcid.org/0000-0002-1372-2286
Yeon-Joo Choi, https://orcid.org/0009-0000-0788-5049
Sun-Woo Choi, https://orcid.org/0009-0006-6521-0852
Da-Eun Jeong, https://orcid.org/0009-0006-6780-0434
Jeong Yoon Lee, https://orcid.org/0000-0002-4207-9779
Nam-Hyuk Cho, https://orcid.org/0000-0003-3673-6397
Kwang-Jun Lee, https://orcid.org/0000-0002-7831-5905
Dong-Min Kim, https://orcid.org/0000-0001-6373-0922
Won-Jong Jang, https://orcid.org/0000-0003-2866-4370
Jun-Gu Kang, https://orcid.org/0000-0002-9083-8098

References

1. Maurin M, Raoult D. Q fever. Clin Microbiol Rev 1999;12:518-53. https://doi.org/10.1128/CMR.12.4.518
2. Parker NR, Barralet JH, Bell AM. Q fever. Lancet 2006;367:679-88. https://doi.org/10.1016/S0140-6736(06)68266-4
3. Agerholm JS. *Coxiella burnetii* associated reproductive disorders in domestic animals: a critical review. Acta Vet Scand 2013;55:13. https://doi.org/10.1186/1751-0147-55-13
4. Park HS, Lee EG, Lee SY, et al. A case of Q fever: associated with pancytopenia, hepatitis, and myocarditis. Korean J Infect Dis 1992;24:45-54.
5. Korea Disease Control and Prevention Agency. Infectious disease portal (in Korean) [Internet]. 2025 [cited 2025 Jun 26]. Available from: https://www.kdca.go.kr/kdca/2877/subview.do
6. Lee SH, Lee JH, Park S, et al. Isolation of *Coxiella burnetii* in patients with nonspecific febrile illness in South Korea. BMC Infect Dis

2020;20:421. https://doi.org/10.1186/s12879-020-05130-3

7. Andoh M, Zhang G, Russell-Lodrigue KE, et al. T cells are essential for bacterial clearance, and gamma interferon, tumor necrosis factor alpha, and B cells are crucial for disease development in *Coxiella burnetii* infection in mice. Infect Immun 2007;75:3245-55. https://doi.org/10.1128/IAI.01767-06
8. Custer RP, Bosma GC, Bosma MJ. Severe combined immunodeficiency (SCID) in the mouse. Pathology, reconstitution, neoplasms. Am J Pathol 1985;120:464-77.
9. Andoh M, Naganawa T, Hotta A, et al. SCID mouse model for lethal Q fever. Infect Immun 2003;71:4717-23. https://doi.org/10.1128/IAI.71.8.4717-4723.2003
10. Mathews KO, Phalen D, Sheehy PA, et al. Molecular detection and characterisation of *Coxiella burnetii* in Koala (*Phascolarctos cinereus*) urogenital tract swabs. Pathogens 2024;13:873. https://doi.org/10.3390/pathogens13100873
11. Zhang GQ, Nguyen SV, To H, et al. Clinical evaluation of a new PCR assay for detection of *Coxiella burnetii* in human serum samples. J Clin Microbiol 1998;36:77-80. https://doi.org/10.1128/JCM.36.1.77-80.1998
12. Baker GC, Smith JJ, Cowan DA. Review and re-analysis of domain-specific 16S primers. J Microbiol Methods 2003;55:541-55. https://doi.org/10.1016/j.mimet.2003.08.009
13. Zhang GQ, To H, Yamaguchi T, Fukushi H, Hirai K. Differentiation of *Coxiella burnetii* by sequence analysis of the gene (com1) encoding a 27-kDa outer membrane protein. Microbiol Immunol 1997;41:871-7. https://doi.org/10.1111/j.1348-0421.1997.tb01943.x
14. Lai CH, Lin JN, Chang LL, Chen YH, Lin HH. Circulating cytokines and procalcitonin in acute Q fever granulomatous hepatitis with poor response to antibiotic and short-course steroid therapy: a case report. BMC Infect Dis 2010;10:193. https://doi.org/10.1186/1471-2334-10-193
15. Thi Vinh An D, Thi Viet Ha B, Xuan Co D, et al. The first case of *Coxiella burnetti* infection detected through bone marrow biopsy in Vietnam. Clin Pathol 2022;15:2632010X221096397. https://doi.org/10.1177/2632010X221096397
16. Clark NJ, Soares Magalhães RJ. Airborne geographical dispersal of Q fever from livestock holdings to human communities: a systematic review and critical appraisal of evidence. BMC Infect Dis 2018;18:218. https://doi.org/10.1186/s12879-018-3135-4
17. Tan T, Heller J, Firestone S, Stevenson M, Wiethoelter A. A systematic review of global Q fever outbreaks. One Health 2023;18:100667. https://doi.org/10.1016/j.onehlt.2023.100667

https://doi.org/10.3347/PHD.26005

Case Report

Parasites Hosts Dis 2026;64(4):391-397
https://doi.org/10.3347/PHD.26045

Parasites, Hosts and Diseases

pISSN 2982-5164 • eISSN 2982-6799

Wound myiasis caused by *Lucilia* spp. (Diptera: Calliphoridae) in a dog and a cat in Korea

Subin Lee[1], Joohyung Kim[2], Kihwan Yang[2], Seongjun Choe[3], Seung-Hun Lee[1,*]

[1]Laboratory of Veterinary Parasitology, College of Veterinary Medicine, Chungbuk National University, Cheongju, Korea; [2]Shinsegae Animal Medical Center, Yangsan, Korea; [3]Department of Parasitology, School of Medicine, Chungbuk National University, Cheongju, Korea

This study presents 2 cases of wound myiasis in a dog and a cat involving morphological and molecular identification in Korea. A 7-year-old male Jindo mix dog, *Canis familiaris*, was admitted to a veterinary clinic in Yangsan-si, Gyeongsangnam-do, Korea, in July 2024. The bite wound near the right rib was infected with maggots. We carefully removed the 5 maggots using forceps. The wound healed without any subsequent complications. A Korean Shorthair stray cat, *Felis catus*, was brought to the same clinic in October 2024 after being hit by a car. The maggot-infected wounds were found in the anus and perianal regions. We removed all 10 maggots from the wounds. After treatment, no living maggots were observed; however, the cat was euthanized due to trauma-related complications. The maggots from the dog and the cat were third instars with 12 body segments and posterior spiracles containing 3 distinct slits. Compared with the dog-derived larvae, the cat-derived larvae had a more dorsally positioned posterior process of the mouth hook, reduced dorsal papillae distances, and distinctly sclerotized ventral cornua. Complete *cox1* gene analysis confirmed the dog- and cat-derived larvae as *Lucilia sericata* (Meigen, 1826) and *Lucilia illustris* (Meigen, 1826), respectively, whereas 18S rRNA gene analysis showed limited species-level resolution. In the present study, wound myiasis caused by *L. sericata* and *L. illustris* is described in a dog and a cat in Korea based on morphological and molecular findings.

Keywords: Myiasis, larva, Calliphoridae, dogs, cats

Introduction

Myiasis is the infection of vertebrates, including humans and animals, by larvae of flies that feed on living or dead tissue of their hosts [1]. Anatomically, myiasis is classified based on the site of infection, including auricular, cutaneous, gastrointestinal, ophthalmic, oral, and urogenital forms [2]. Ecologically, myiasis is categorized as specific (obligatory), semi-specific (facultative), or accidental (pseudomyiasis), depending on the degree to which the larvae rely on the host for survival and development [3].

The most commonly observed form is cutaneous myiasis, which is generally subdivided into furuncular, migratory, and wound myiasis [4]. Wound myiasis occurs when dipteran larvae infect open wounds in a living host. The most common flies that cause obligatory wound myiasis globally are *Cochliomyia hominivorax* (Coquerel, 1858), *Chrysomya bezziana* Villeneuve, 1914, and *Wohlfahrtia magnifica* (Schiner, 1862) [3], while facultative wound myiasis has been associated with the Muscidae, Calliphoridae, and Sarcophagidae families [4]. Wound myiasis can cause tissue damage, delayed wound healing, and secondary infections, particularly in debilitated, injured, or outdoor

Received: May 27, 2026 Accepted: July 14, 2026
*Correspondence: dvmshlee@chungbuk.ac.kr

© 2026 The Korean Society for Parasitology and Tropical Medicine
This is an open-access article distributed under the terms of the Creative Commons Attribution Non-Commercial License (http://creativecommons.org/licenses/by-nc/4.0/) which permits unrestricted non-commercial use, distribution, and reproduction in any medium, provided the original work is properly cited.

Citation
Lee S, Kim J, Yang K, Choe S, Lee SH. Wound myiasis caused by *Lucilia* spp. (Diptera: Calliphoridae) in a dog and a cat in Korea. Parasites Hosts Dis 2026;64(4):391-397.

animals, highlighting its clinical relevance in veterinary medicine [3,5].

Several cases of human myiasis have been reported in Korea, including nasal, submandibular, internal, and oral myiasis [6-9]. In contrast, myiasis in companion animals has rarely been documented, with only 2 canine cases reported to date, including cutaneous myiasis associated with tick infestation and wound myiasis caused by *Lucilia sericata* (Meigen, 1826) [10,11]. Therefore, species-level information on companion animal myiasis remains limited in Korea, and feline wound myiasis has not been well documented. The present study aimed to report wound myiasis in a domestic dog and a stray cat and to identify the causative fly species using morphological and molecular analyses.

Case Report

Case 1

A 7-year-old male Jindo mix dog, *Canis familiaris*, raised outdoors, was bitten by a stray dog in July 2024. This study was approved by the Institutional Animal Care and Use Committee of Chungbuk National University (CBNUA-26-0064-03). The dog was brought to a veterinary clinic in Yangsan-si (si means city), Gyeongsangnam-do (do means province), Korea, and the veterinarians found a wound near the right rib infected with dipteran larvae, leading to a diagnosis of wound myiasis (Fig. 1A, B). The dog showed lameness at presentation. Five maggots were carefully removed using forceps. A drain was inserted into the wound site to facilitate the drainage of exudates and inflammatory substances. At the 1-week follow-up, the drain was removed, and the wound healed completely without any subsequent complications.

Case 2

In October 2024, a Korean shorthair stray cat, *Felis catus*, was brought to the same veterinary clinic 4 days after being hit by a car. A physical examination revealed a wound in the anus and perianal region (Fig. 1C, D). The wound was filled with 10 maggots, which were removed using forceps. Necrotic tissue was removed and the wound was washed with 0.9% normal saline. Topical 1% ivermectin was applied to target maggots within necrotic tissue or inaccessible areas. Additionally, antibiotic treatment was administered. Although no maggots were observed after treatment, euthanasia was performed because of hind limb paralysis and complete loss of urination and defecation functions associated with a fractured fifth lumbar vertebra (L5).

Morphological identification of maggots

All maggots collected from the domestic dog and stray cat were preserved in 70% ethanol and transferred to the Veterinary Par-

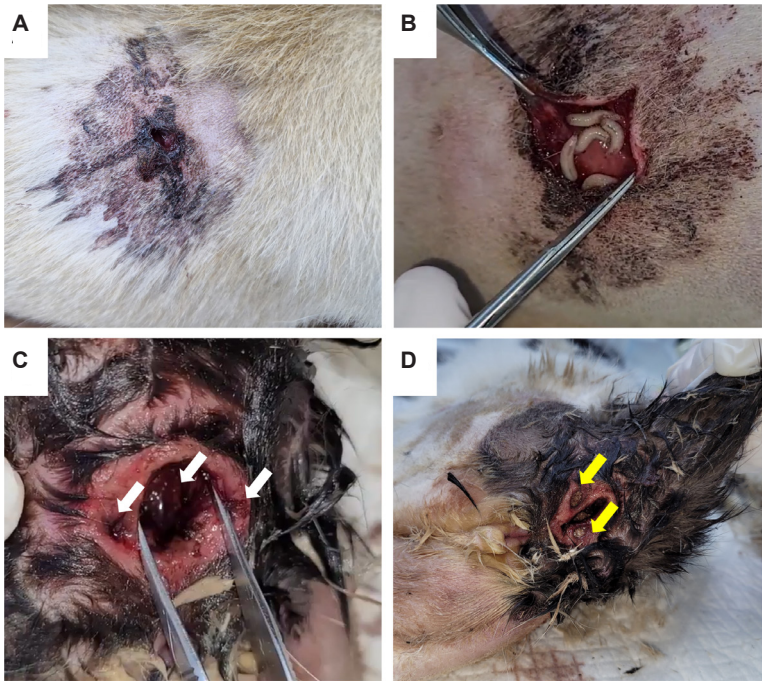


Fig. 1. Gross findings of wound myiasis in a domestic dog and a stray cat. A bitten scar (A) on the right rib area of a dog and maggots (B) in the opened wound. A wound (C) in the anal and perianal regions of a stray cat, indicated by white arrows, and dipteran larvae (D) on the affected region, indicated by yellow arrows.

https://doi.org/10.3347/PHD.26045

asitology Laboratory, College of Veterinary Medicine, Chungbuk National University, Korea, for species identification. The remaining larvae were preserved and retained as specimens in the same laboratory. For morphological examination, representative well-preserved larvae appropriate for microscopic observation were selected from each case.

Two larvae from the dog and 3 larvae from the cat were examined under a light microscope. The examined larvae were consistent with third-instar larvae based on posterior spiracular morphology, with 3 distinct slits observed in each spiracle [12]. The larvae from the dog measured approximately 13 mm in length and 2 mm in width, whereas those from the cat measured approximately 12 mm in length and 2 mm in width. In both hosts, the larval body was whitish-beige, and reddish internal contents were visible through the cuticle. The larvae were subcylindrical, slightly tapered anteriorly, composed of 12 segments, and the posterior margins of each segment were covered with numerous single-pointed spines. General external morphology appeared similar between the 2 groups.

Species identification was based on cephaloskeletal and posterior papillae characteristics described in published diagnostic keys for third-instar *Lucilia* larvae [12,13]. The posterior process of the mouth hook was positioned more dorsally in the cat-derived larvae than in the dog-derived larvae. The distance between the median dorsal papillae (p1–p1) and between adjacent dorsal papillae (p1–p2 and p2–p3) was almost uniform around the posterior spiracle in the dog-derived larvae. In contrast, these distances were noticeably reduced in the cat-derived larvae. Additionally, the posterior tip of the ventral cornua was poorly sclerotized or indistinct in the dog-derived larvae but distinctly sclerotized in the cat-derived larvae. These morphological differences supported the identification of the dog-derived larvae as *L. sericata* and the cat-derived larvae as *Lucilia illustris* (Meigen, 1826) (Fig. 2A-F). However, because

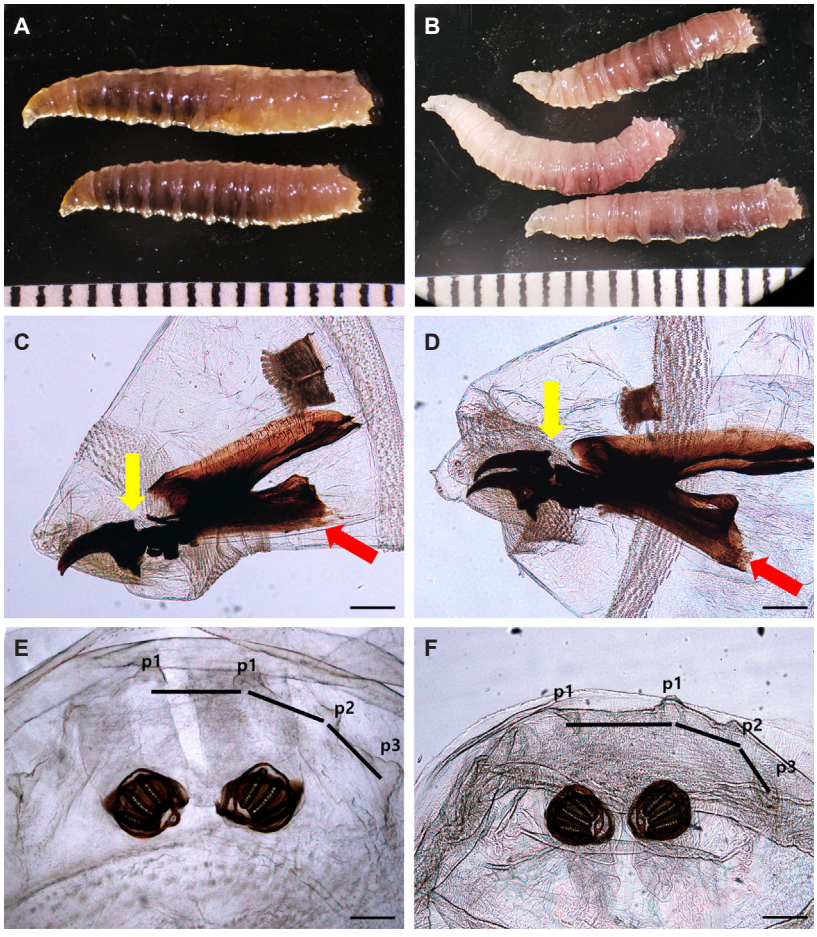


Fig. 2. Maggots of (A) *Lucilia sericata* and (B) *Lucilia illustris* were recovered from the wounds in the respective cases. The cephaloskeletons of (C) *L. sericata* and (D) *L. illustris*: the posterior process of the mouth hook (yellow arrow) was more dorsally positioned in *L. illustris* than in *L. sericata*, and the posterior tip of the ventral cornua (red arrow) was indistinct in *L. sericata* but distinctly sclerotized in *L. illustris*. The spiracular openings (posterior spiracles) of the 2 fly larvae species showed similar distances between papillae in (E) *L. sericata*, whereas the distances were unequal in (F) *L. illustris*. Scale bars: (A, B) 1 mm; (C-F) 200 μm.

the number of diagnostic characters available in larval specimens is limited and closely related *Lucilia* species can be difficult to distinguish morphologically, representative larvae from each case were further subjected to molecular analysis for species confirmation.

Molecular identification of maggots

For molecular identification, DNA was extracted from a single maggot from a domestic dog and a stray cat, respectively. Genomic DNA was extracted using the DNeasy Blood & Tissue Kit (Qiagen), following the manufacturer's instructions. DNA concentrations were confirmed using a spectrophotometer (DeNovix). PCR was conducted to amplify the complete cytochrome c oxidase subunit 1 (*cox1*) gene of each species of maggot using 2 primer sets (Table 1) [14-16]. Since amplifying the full-length *cox1* gene in a single PCR was unsuccessful, 2 partially overlapping fragments were amplified and assembled to obtain the complete sequence. The PCR products were sent to Macrogen for direct sequencing. Additionally, the complete 18S rRNA gene was amplified using a primer set common to eukaryotes (Table 1) [14-16]. The PCR products were subsequently cloned into *Escherichia coli* DH5α using the pGEM-T easy vector (Promega). For each sample, at least 3 colonies were selected and sequenced using a universal primer set (M13F and M13R) by Macrogen.

The obtained sequences were aligned using MEGA version 11, and species identification was performed through the BLAST (https://blast.ncbi.nlm.nih.gov/Blast.cgi), and phylogenetic analysis using MEGA version 11 with the maximum likelihood method. The bootstrap method with 500 replicates was used to assess the reliability of the tree.

The complete *cox1* gene (1,539 bp) of each maggot species was successfully sequenced and served as the primary marker for species-level confirmation. The sequences obtained from the maggots collected from the domestic dog and those from the stray cat showed 94.5% interspecies identity. The *L. sericata* sequence showed 99.9% identity with GenBank sequences from New Zealand (AJ417713) and Australia (MW255540). The *L. illustris* sequence, obtained from a maggot collected from the stray cat, showed 99.8% identity with *L. illustris* (FJ650565 and NC028056) deposited in the GenBank database. The phylogenetic analysis of *cox1* revealed a clear separation of *L. sericata* and *L. illustris* (Fig. 3A).

The complete 18S rRNA gene (1,984 bp) was also sequenced to provide additional molecular data for species identification. However, 18S rRNA analysis showed limited resolution for species-level differentiation. The 18S rRNA sequences of *L. sericata* and *L. illustris* showed 99.8% interspecies identity. The *L. sericata* sequence obtained in this study showed 99.9% identity with *L. sericata* (KP954339) deposited in the GenBank database. However, the identity of the *L. illustris* sequence could not be confirmed due to the absence of a reference sequence in the GenBank database. Unlike the *cox1* analysis, the 18S rRNA gene phylogenetic analysis could not determine the precise species due to the lack of a *Lucilia* reference database (Fig. 3B).

All sequences obtained in this study were deposited in the GenBank database (18S rRNA gene, PX566124-PX566125; *cox1*, PX566129-PX566130).

Discussion

Although both *L. sericata* and *L. illustris* are commonly found in Korea, maggot infections caused by these species, referred to as myiasis, have rarely been reported in companion animals [11]. This may be because veterinary clinicians primarily focus on wound treatment and may not fully recognize the importance of case reporting and species identification. Unfortunately, maggot samples recovered from clinical cases are often discarded without being transferred from clinical settings to a parasitology laboratory. Nevertheless, accurately identifying the species of fly is crucial because myiasis caused by certain species can lead to severe or malignant cases. Traditionally, fly species identification relied on morphological

Table 1. Primers used to identify the maggot species from a domestic dog and a stray cat in Korea

Target gene	Primers (5' to 3')	PCR condition	Expected size (bp)	Reference
cox1	CTGCTACTTTATGAGCTTTAGG CCATTGCACTAATCTGCCA	94°C/5 min; 30 cycles: 94°C/30 sec, 55°C/30 sec, 72°C/1 min; 72°C/15 min	560	[14,15][a]
	CCTTTAGAATTGCAGTCTAATGTCA CAAGTTGTGTAAGCATC	95°C/11 min; 35 cycles: 95°C/30 sec, 55°C/30 sec, 72°C/1 min 30 sec; 72°C 15 min	1,400	[15]
18S rRNA	AACCTGGTTGATCCTGCCAGT TGATCCTTCTGCAGGTTCACCTAC	95°C/2 min; 35 cycles: 92°C/30 sec, 55°C/30 sec, 72°C/45 sec, 72°C 7 min	1,900	[16]

[a]The forward and reverse primers were used based on previously described *cox1* primers in references [14] and [15], respectively.

https://doi.org/10.3347/PHD.26045

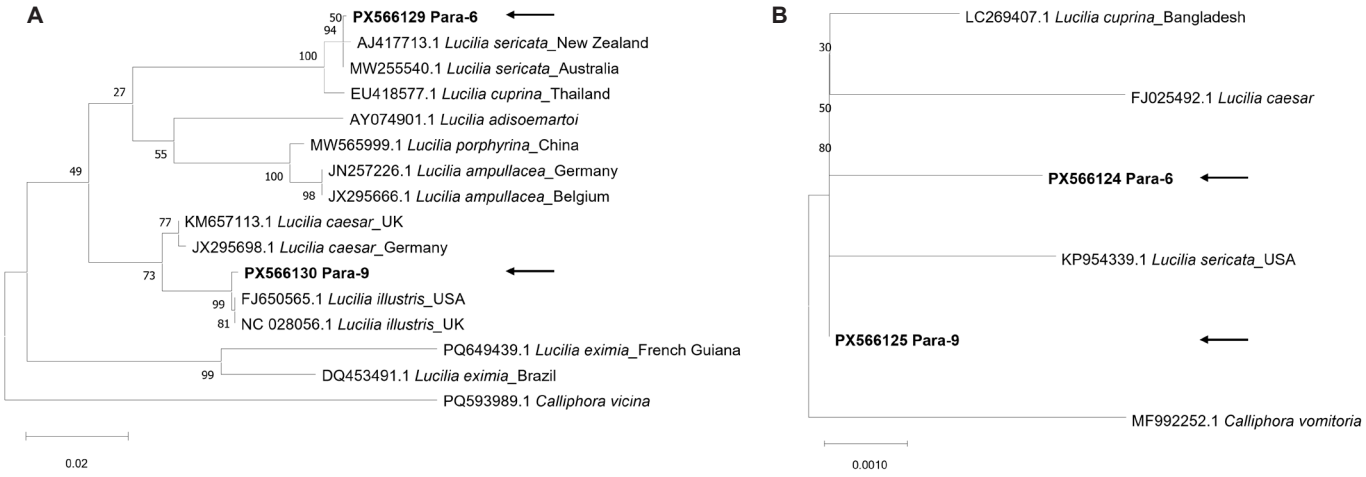


Fig. 3. Phylogenetic trees of *Lucilia* spp. Based on (A) *cox1*, (B) 18S rRNA gene. To construct the phylogenetic tree, the maximum likelihood method was used with 500 bootstrap replications. The sequences analyzed in this tree were obtained from the GenBank databases. The sequences identified in this study are indicated in bold and with arrows.

analysis under a microscope. However, identifying morphologically similar species can be challenging. For instance, *L. illustris* and *Lucilia caesar* (Linnaeus, 1758) are nearly identical, and males are the only stage that can be reliably distinguished. Additionally, species identification can be achieved by rearing the larvae to the adult stage and examining their morphological characteristics. However, this approach is time-consuming and requires expertise and optimal environmental conditions [11].

To address these challenges, molecular methods have become more common. These approaches offer faster, more reliable results, even with immature or dead specimens. Recent studies have focused on various molecular markers, including mitochondrial and nuclear genes, to differentiate between closely related species and improve the accuracy of identification in the forensic, medical, and veterinary fields [11]. In the present study, a molecular analysis of the complete *cox1* gene revealed that the maggots from a domestic dog and a stray cat were *L. sericata* and *L. illustris*, respectively. However, the species could not be determined using the 18S rRNA gene due to the limited reference sequences for the *Lucilia* genus in the database.

L. sericata, commonly known as the green bottle fly, lays eggs on necrotic tissue, wounded skin, or diseased areas, where the larvae primarily feed [2]. This species is one of the most widespread causative agents of myiasis worldwide and has been reported to infect various hosts, including cats, dogs, and humans [11]. Canine myiasis caused by *L. sericata* has been reported in Italy [1], Turkiye [17], Iran [18], Israel [19], and Korea [10,11]. In the present case, species identification of canine myiasis was confirmed to be *L. sericata*.

L. illustris is an important agent of wound myiasis in humans and livestock. It is often found in association with wounds, feces, and carcasses. This species is considered one of the primary contributors to sheep blowfly strike. Previous studies have reported *L. illustris* in association with cat carcasses; however, to our knowledge, no published clinical case of wound myiasis caused by this species in a living cat has been reported [20]. Therefore, the present case may represent the first report of feline wound myiasis caused by *L. illustris*.

These *Lucilia* species have been reported as causative agents of human myiasis. Therefore, the identification of these species in a dog and a cat suggests the public health relevance of *Lucilia*-associated myiasis in environments shared by humans and animals, where both may be exposed to the same flies. These findings highlight the importance of monitoring myiasis in stray and outdoor animals.

Both cases exhibited predisposing conditions that likely facilitated fly infection. Various predisposing factors increase the risk of myiasis in animals, including poor hygiene, traumatic injuries, dermatological conditions, and physical impairments that limit mobility or grooming behavior [5]. In particular, wounded or debilitated animals raised outdoors are at substantially higher risk of fly infection [10]. In case 1, the dog was raised outdoors and had an open wound, conditions that likely increased its exposure to flies and facilitated larval infection. Furthermore, this occurred during the summer when fly activity is high. The stray cat reported in case 2 was a free-roaming animal, a lifestyle that makes it susceptible to wounds from fights, car accidents, animal bites, or falls [1]. These environmental and behavioral factors can make animals more vulnerable to myiasis.

This study has several limitations. Only 2 clinical cases were examined, and the larvae were not reared to adult flies for adult-stage morphological confirmation. In addition, molecular analysis was performed on one representative larva from each case rather than on all recovered larvae; therefore, mixed-species infection cannot be completely excluded. However, the *cox1*-based molecular identification was consistent with the morphological analysis of the examined representative larvae. Furthermore, 18S rRNA gene analysis had limited resolution for species-level differentiation because of the limited availability of *Lucilia* reference sequences in GenBank. Therefore, additional case reports and expanded reference sequence data are needed to better understand companion animal myiasis caused by *Lucilia* spp. in Korea.

This study provides the case-based evidences of canine and feline wound myiasis caused by *Lucilia* spp. in Korea. To our knowledge, this is the first reported case of wound myiasis associated with *L. illustris* in a living cat. The causative fly species were identified through both larval morphological examination and complete *cox1* gene analysis, highlighting the importance of combining these approaches for accurate identification of *Lucilia* species. This report may serve as a reference for the diagnosis and species-level identification of *Lucilia*-associated wound myiasis in dogs and cats.

Data availability

The sequence data were deposited in the NCBI GenBank database (18S rRNA gene, PX566124–PX566125; *cox1*, PX566129–PX566130). Specimens collected during this study will be made available to qualified researchers upon reasonable request.

Author contributions

Conceptualization: Lee SH. Data curation: Lee S, Lee SH. Investigation: Lee S, Kim J, Yang K, Choe S. Methodology: Lee S, Lee SH. Resources: Kim J, Yang K. Supervision: Lee SH. Validation: Lee S, Choe S, Lee SH. Visualization: Lee S. Writing – original draft: Lee S. Writing – review & editing: Lee S, Kim J, Yang K, Choe S, Lee SH.

Conflict of interest

Seung-Hun Lee serves as an editor of Parasites, Hosts and Diseases but had no involvement in the decision to publish this article. No other potential conflicts of interest relevant to this study were reported.

ORCID

Subin Lee, https://orcid.org/0000-0002-4691-3994
Joohyung Kim, http://orcid.org/0009-0005-4386-943X
Kihwan Yang, http://orcid.org/0009-0005-4478-8973
Seongjun Choe, https://orcid.org/0000-0002-9204-2173
Seung-Hun Lee, https://orcid.org/0000-0002-6244-0381

References

1. Pezzi M, Scapoli C, Chicca M, et al. Cutaneous myiasis in cats and dogs: cases, predisposing conditions and risk factors. Vet Med Sci 2021;7:378-84. https://doi.org/10.1002/vms3.370
2. Pezzi M, Bonacci T, Leis M, et al. Myiasis in domestic cats: a global review. Parasit Vectors 2019;12:372. https://doi.org/10.1186/s13071-019-3618-1
3. Francesconi F, Lupi O. Myiasis. Clin Microbiol Rev 2012;25:79-105. https://doi.org/10.1128/CMR.00010-11
4. McGraw TA, Turiansky GW. Cutaneous myiasis. J Am Acad Dermatol 2008;58:907-26. https://doi.org/10.1016/j.jaad.2008.03.014
5. Pezzi M, Whitmore D, Chicca M, Lanfredi M, Leis M. Traumatic myiasis caused by an association of *Sarcophaga tibialis* (Diptera: Sarcophagidae) and *Lucilia sericata* (Diptera: Calliphoridae) in a domestic cat in Italy. Korean J Parasitol 2015;53:471-5. https://doi.org/10.3347/kjp.2015.53.4.471
6. Kim JS, Seo PW, Kim JW, et al. A nasal myiasis in a 76-year-old female in Korea. Korean J Parasitol 2009;47:405-7. https://doi.org/10.3347/kjp.2009.47.4.405
7. Joo CY, Kim JB. Nosocomial submandibular infections with dipterous fly larvae. Korean J Parasitol 2001;39:255-60. https://doi.org/10.3347/kjp.2001.39.3.255
8. Chung PR, Jung Y, Kim KS, et al. A human case of internal myiasis in Korea. Korean J Parasitol 1996;34:151-4. https://doi.org/10.3347/kjp.1996.34.2.151
9. Jang M, Ryu SM, Kwon SC, et al. A case of oral myiasis caused by *Lucilia sericata* (Diptera: Calliphoridae) in Korea. Korean J Parasitol 2013;51:119-23. https://doi.org/10.3347/kjp.2013.51.1.119
10. Choi J, Kim H, Na J, Kim S, Park C. Cutaneous myiasis associated with tick infestations in a dog. J Vet Clin 2015;32:473-5. https://doi.org/10.17555/jvc.2015.10.32.5.473
11. Choe S, Lee D, Park H, et al. Canine wound myiasis caused by *Lucilia sericata* (Diptera: Calliphoridae) in Korea. Korean J Parasitol 2016;54:667-71. https://doi.org/10.3347/kjp.2016.54.5.667
12. Szpila K. Key for the identification of third instars of European blowflies (Diptera: Calliphoridae) of forensic importance. In: Amendt J, Goff ML, Campobasso CP, Grassberger M, editors. Current concepts in forensic entomology. Springer; 2009. p. 43-56.
13. Velásquez Y, Magaña C, Martínez-Sánchez A, Rojo S. Diptera of forensic importance in the Iberian Peninsula: larval identification key. Med Vet Entomol 2010;24:293-308. https://doi.org/10.1111/

https://doi.org/10.3347/PHD.26045

j.1365-2915.2010.00879.x

14. Chen WY, Hung TH, Shiao SF. Molecular identification of forensically important blow fly species (Diptera: Calliphoridae) in Taiwan. J Med Entomol 2004;41:47-57. https://doi.org/10.1603/0022-2585-41.1.47
15. Park SH, Zhang Y, Piao H, et al. Use of cytochrome c oxidase subunit I (COI) nucleotide sequences for identification of the Korean Luciliinae fly species (Diptera: Calliphoridae) in forensic investigations. J Korean Med Sci 2009;24:1058-63. https://doi.org/10.3346/jkms.2009.24.6.1058
16. Mangold AJ, Bargues MD, Mas-Coma S. 18S rRNA gene sequences and phylogenetic relationships of European hard-tick species (Acari: Ixodidae). Parasitol Res 1998;84:31-7. https://doi.org/10.1007/s004360050352
17. Gökpinar S, Karsli B. Traumatic myiasis associated with *Wohlfahrtia magnifica* and *Lucilia sericata* larvae in dog. Van Vet J 2018;29:55-7.
18. Moshaverinia A, Mehrjerdi HK. Canine myiasis and its causal agents in Northeastern Iran. Iran J Parasitol 2016;11:91-7.
19. Schnur HJ, Zivotofsky D, Wilamowski A. Myiasis in domestic animals in Israel. Vet Parasitol 2009;161:352-5. https://doi.org/10.1016/j.vetpar.2009.01.026
20. Bagsby K, Hans K. *Lucilia silvarum* Meigen (Diptera: Calliphoridae) is a primary colonizer of domestic cats (*Felis catus*). Insects 2024;15:32. https://doi.org/10.3390/insects15010032

Instructions for authors

Parasites, Hosts and Diseases

Enacted: June 1963
Revised: February 2023
Last revision: January 1, 2026

Parasites, Hosts and Diseases (PHD) is an open access, peer-reviewed, online journal published quarterly on the last day of January, April, July, and October (beginning in 2026, the publication dates were changed from the last day of February, May, August, and November, which had been in effect through 2025). As the official journal of The Korean Society for Parasitology and Tropical Medicine, PHD aims to generate new knowledge on parasites infecting humans and animals, disease vectors, host-parasite relationships, zoonotic diseases, and tropical medicine.

Manuscripts should adhere to the Recommendations for the Conduct, Reporting, Editing, and Publication of Scholarly Work in Medical Journals, issued by the International Committee of Medical Journal Editors (ICMJE; http://www.icmje.org/recommendations/), unless otherwise specified.

1. Article Processing Charge

Accepted manuscripts are published with the understanding that the author(s) will cover the associated publication costs, including page charges. The standard page charge is 700,000 KRW for Korean authors and 700 USD for others, covering up to 10 pages. An additional 100,000 KRW (for Korean authors) or 100 USD per page applies from the 11th page onward. The page charge for Letters to the Editor is 350 USD.

2. Research and Publication Ethics

It is available at: https://parahostdis.org/policy/ethics.php

3. Submission and Peer Review Process

A. Submission

Authors should submit their manuscripts online through the PHD submission system at https://submit.parahostdis.org/. Once logged in, the system will guide you through the submission process step-by-step. Detailed submission instructions are available on the website, and all manuscripts must comply with these guidelines. Failure to do so may result in the return of the manuscript and potential delays in publication.

B. Peer review process

PHD reviews all submitted manuscripts. Each manuscript is first assessed for format and relevance to the journal's aims and scope. If it meets these criteria, it is sent to two experts in the relevant field for review. PHD uses a single-blind process, where reviewer identities are concealed from the author, but both are visible to the decision-making editor. Reviewers make one of four recommendations: accept, minor revision, major revision, or reject. A first decision is typically made within an average of 4 weeks after the reviewers have agreed to evaluate the manuscript. In cases of review discrepancies, the editorial board will conduct an additional review to make a final determination. Authors are expected to revise their manuscripts based on reviewer feedback and provide explanations for any feedback they choose not to implement. The editorial board makes the final publication decision and may request further changes.

C. Cover Letter

The cover letter should confirm that the submitted material, in whole or in part, has neither been published previously nor is under consideration for publication elsewhere. Additionally, it should disclose any potential conflicts of interest that could influence the authors' interpretation of the data, such as financial support, affiliations with pharmaceutical companies, political pressures from interest groups, or academically related conflicts. The cover letter should also specify that all authors have approved the manuscript for submission and confirm that the manuscript complies with ethical guidelines, including IRB approval and informed consent where applicable.

4. Manuscript Preparation

A. Article types

- Original articles: Original articles present results of research investigations on parasites, parasitic diseases, host-parasite relationships and tropical medicine. They should be organized in the following sequence: Title page, Abstract (≤250 words) and Keywords, Main text (Introduction, Methods, Results, and Discussion), References, Tables, Figure legends, and Figures. Original articles should not include more than a total of 35 references.
- Reviews or mini reviews: Reviews provide a comprehensive analysis of specific topics. The text should be organized in the following sequence: Title page, Abstract (≤250

words) and Keywords, Main text (Introduction, Body text, and Conclusion), References, Tables, Figure legends, and Figures. Unsolicited reviews are also welcome. A mini-review is a shorter version of a full review article. Systematic reviews and meta-analyses should be submitted as review articles but require a structured abstract and should follow the PRISMA guidelines (http://www.prisma-statement.org/).

- Case reports: Case reports are accepted only when they present clinically important information about unique cases. Reports should describe cases not previously observed or reported. If a case involves a common condition but is deemed significant, the editorial board will review it to determine acceptance. They should be organized in the following sequence: Title page, Abstract (≤250 words) and Keywords, Introduction, Case Report, Discussion, References, Tables, Figure legends, and Figures. The number of references should not exceed 20.
- Brief communications: Brief communication is a short article detailing clinically or experimentally significant findings or major advancements. It should adhere to the guidelines for original articles, but the text should be formatted as a single section without headings or section divisions. Additionally, the number of references should be no more than 20.
- Letters to the editor: Letters offer rapid publication of new findings of unique clinical importance, recent perspectives on articles, or topics of interest published in the journal. They may also include opinions on specific topics of academic relevance. The text should be organized in the following sequence: Title page, Main text, References, Tables, Figure legends, and Figures (if applicable). The text should be formatted as a single section without headings or section divisions with no more than 10 references.
- Book reviews: Invited book reviews are eligible for publication. Submissions should provide a critical evaluation of the book's arguments and content. The text should include the title of the book reviewed, the author(s) and editor(s), and publisher, the total number of pages, and the ISBN number, followed by the main text, with no more than 10 references.

B. General requirements

- Manuscripts should be prepared using Microsoft Word (doc or docx format). They should be formatted on A4 (21.0×29.7 cm), with margins of at least 2.54 cm on all sides.
- Texts should be double-spaced with the same normal, plain font throughout, preferably 11-point Times New Roman.
- Genera and species names of parasites and living organisms should be written in italic.
- Other Latin origin words, such as "et al.", "in situ", "in vitro", and "in vivo" should not be italicized.
- Provide the names of manufacturers.
- When quoting from other sources, give a reference number after the author's surname or at the end of the quotation.
- Authors should express all measurements in conventional units, using International System of Units (SI units).
- Authors should follow International Rules for Nomenclature and, if new names are introduced, the International Code for Zoological Nomenclature. All strains and sources of hosts and parasites should be stated.
- Abbreviations should be used sparingly and unambiguously.

C. Key features

Key features and limits of articles are summarized in Table 1 below. However, the limits are negotiable with the editor.

Table 1. Key features and limits of articles

Type of article	Abstract	Text structure	References
Original Article	≤250 words	Introduction, Methods, Results, Discussion	35
Review and Mini Review	≤250 words	Introduction, Body text, Conclusion	No limit
Case Report	≤250 words	Introduction, Case report, Discussion	20
Brief Communication	≤250 words	Single section with no headings	20
Letters to the Editor	Not required	Single section with no headings	10
Book reviews	Not required	Free-form style	10

D. Reporting guidelines

For specific study designs, such as randomized controlled trials, diagnostic accuracy studies, meta-analyses, observational studies, and non-randomized studies, authors should follow the relevant reporting guidelines. Recommended sources include the EQUATOR Network (https://www.equator-network.org/) and the National Library of Medicine (https://www.nlm.nih.gov/services/research_report_guide.html).

E. Manuscript structure and format

Organize your manuscript file as follows:

Manuscript file: (1) Title page (2) Abstract & keywords, (3) Body text, (4) References list, (5) Notes (author contributions,

conflict of interest, funding, acknowledgments) (6) Tables (each beginning on a new page), (7) Figure legends (upload figures in separate files)

Supplementary materials (upload separately)

• **Title page**

The title page should include the following items:

- **Title:** The article title should be concise and precise. The title should also indicate the study design. If the study involved human participants, the country where the study was conducted should be included.
- **Running title:** Less than 50 characters
- **Authors and affiliations:** Each author's given name and surname should be provided. For authors with different affiliations, use superscripted Arabic numerals (e.g., [1], [2], [3]) placed at the top-right of each author's name and before each corresponding affiliation. If an author is associated with multiple departments or institutions, arrange affiliations in the order of the authors and indicate them with superscript numbers. The corresponding author should be marked with an asterisk (*) as a superscript.
- **ORCID:** All authors are required to provide their ORCIDs. If an author does not have an ORCID, they can register for one at the ORCID website (https://orcid.org/). Registration is free to all researchers.
- **Corresponding author:** The corresponding author's email address should be provided. If no corresponding author is specified, the editorial board will assume the first author holds this role.

• **Abstract and keywords**

- **Abstract:** For original articles, reviews and mini reviews, case reports, and brief communications, provide an unstructured abstract of less than 250 words. Ensure all data in the abstract appear in the manuscript text or tables.
- **Keywords:** Up to 6 keywords should be listed at the bottom of the abstract to be used as index terms. PHD strongly recommends using Medical Subject Headings (MeSH; https://meshb.nlm.nih.gov/) keywords.

• **Main text**

The main text of an original article must be prepared under the following subheadings: Introduction, Methods, Results, and Discussion. Case report should be organized with Introduction, Case Report, and Discussion. In addition to these types, manuscripts that fall under specific reporting guidelines must be prepared accordingly.

- **Introduction:** Provide the background and purpose of the article, emphasizing its significance. Summarize the rationale with only relevant references, avoiding diffuse listing of related topics. Do not include data or conclusions from the study itself.
- **Methods:** Authors must provide sufficient details to enable an independent researcher to reproduce the work. Previously published methods should be summarized and cited appropriately, without unnecessary repetition. If directly quoting a published method, cite the source. Any major modifications to existing methods must be clearly described. The number of experiments, replicates, and statistical tests used should be specified. An ethics statement must be included when studies involve clinical samples, human data, or animals. This statement should appear as the first subheading in the Methods section. Examples are shown in the following: "We conducted this study in compliance with the principles of the Declaration of Helsinki. The study's protocol was reviewed and approved by the Institutional Review Board of OO (No. OO). Written informed consents were obtained from the patients. The requirement for informed consent was waived."
- **Results:** Present the results in a logical sequence across the text, tables, and figures. Avoid repeating data in the text that is already provided in tables or figures; instead, highlight and summarize key findings and insights.
- **Discussion:** Emphasize the novel and important aspects of the study, along with the conclusions drawn from them. Avoid detailed repetition of data or material already presented in the Introduction or Results sections. Discuss the implications and limitations of the findings, including potential impacts on future research. Connect the conclusions to the study's objectives by comparing and discussing relevant findings from other research. Avoid unqualified statements and conclusions not fully supported by the data. Where applicable, propose new hypotheses and include recommendations as appropriate.

• **References**

In the text, references should be cited with Arabic numerals in square brackets, numbered in the order of appearance. In the References, the references should be numbered and listed in the order of appearance in the text. List all authors when there are 5 or fewer. For sources with 6 or more authors, list the first 3 authors followed by "et al." If an article has been published online, but not yet assigned an issue or page numbers, the DOI should be supplied. journals should be abbreviated according to the style used in the list of journals indexed in the NLM Journal Catalog (https://www.ncbi.nlm.nih.gov/nlmcatalog/journals). For journal titles not list-

ed in the Catalog, they should follow the ISO abbreviation as described in "ISO 4:1997 Information and documentation—Rules for the abbreviation of title words and titles of publications" (https://www.iso.org/iso/home/store/catalogue_tc/catalogue_detail.htm?csnumber=3569).

Journal articles:

1. Aung JM, Joo SY, Na BK, et al. Establishing a Cre/loxP-based genetic manipulation system for *Acanthamoeba*: targeted genome editing and stable reporter expression. Parasites Hosts Dis 2025;63:25-36. https://doi.org/10.3347/PHD.24078
2. Kim MJ, Moon EK, Jo HJ, Quan FS, Kong HH. Identifying the function of genes involved in excreted vesicle formation in *Acanthamoeba castellanii* containing *Legionella pneumophila*. Parasit Vectors 2023;16:215. https://doi.org/10.1186/s13071-023-05824-y
3. Poncet AF, Blanchard N, Marion S. Toxoplasma and dendritic cells: an intimate relationship that deserves further scrutiny. Trends Parasitol 2019;35:870-86. https://doi.org/10.1016/j.pt.2019.08.001

Book & book chapter:

4. Khan NA. *Acanthamoeba*: biology and pathogenesis. 2nd ed. Caister Academic Press; 2015.
5. Nesheim MC. Ascariasis and human nutrition. In: Crompton DW, Nesheim MC, Pawlowski ZS, editors. Ascariasis and its prevention and control. Taylor and Francis; 1989. p. 87-100.

• **Notes**

- **Conflict of interest:** Authors should disclose any potential conflict of interest. If there are no conflicts of interest to declare, authors should include the following sentence: "The authors have no conflicts of interest to declare."
- **Author contributions:** Describe contributions using the Contributor Roles Taxonomy (CRediT; https://credit.niso.org/). Contributors must meet at least one core role (conceptualization, data curation, formal analysis, investigation, methodology, software, and validation) and one writing role (original draft preparation, review, and editing). Authors who do not meet these requirements will not qualify for authorship.
- **Funding:** Funding for the research should be detailed here. Provision of a FundRef ID is recommended, including the name of the funding agency, country, and (if available) the number of the grant provided by the funding agency. If the funding agency lacks a FundRef ID, please ask that agency to contact the FundRef registry (e-mail: fundref.registry@crossref.org).
- **Data availability:** Include a statement indicating where the data supporting the article's results can be found, with hyperlinks to publicly archived datasets if applicable.
- **Acknowledgments:** All persons who have made substantial contributions, but do not meet the criteria for authorship, should be acknowledged here.

• **Tables**

Table titles and content should be concise, clear, and self-explanatory, so readers do not need to refer to the main text. The table title should be placed at the top-left corner, formatted as "Table [Arabic numeral]." Tables should not contain vertical lines.

Include abbreviations or necessary descriptions in footnotes below the table, using superscript letters (a, b, c) to indicate each footnote, ensuring each note has a corresponding marker. List abbreviations in the footnote section, explaining any empty cells. Where possible, place units directly within the table, avoiding separate listing, and use lowercase symbols for units. In the main text, the term "Table" should appear as "Table" followed by an Arabic numeral.

• **Figures**

Number figures in the order they are cited in the text, using Arabic numerals. Upload each figure as a single image file with a resolution of at least 300 dpi. For figures depicting averages or proportions, use bar or line graphs. Specify the statistical methods used in a footnote for each figure. For multiple panels within the same figure number, use English letters after the numeral to indicate order (e.g., Fig. 1A, Fig. 2B, C).

• **Permission**

If any tables or figures are taken or modified from other papers, authors should obtain permission through the Copyright Clearance Center (https://www.copyright.com/) or from the individual publisher, unless the materials are from an open access journal under the Creative Commons license. For open access journal materials, simply verify the source in the accompanying footnote. Note the distinction between free-access and open access journals: permission from the publisher is required for using tables or figures from free-access journals.

Examples:

Reprinted (Modified) from Tanaka et al. [48], with permission of Elsevier.

Reprinted (Modified) from Weiss et al. [2], according to the Creative Commons License.

• **Supplementary materials**

Supplemental material includes files provided by the au-

thors to accompany their article, typically featuring additional content not included in the print version, such as appendices or extra tables. All supplemental materials will be published online with the full-text article. List the supplemental materials at the end of the manuscript file, and ensure they are cited consecutively within the manuscript text.

5. Processing After Acceptance

Once a paper is accepted for publication, the corresponding author must submit a signed copyright transfer agreement form via email to the editorial office. The paper will not be published until the copyright transfer is complete. Around this time, the invoice for the article processing charge (APC) will also be issued. Please note that publication will proceed only after the APC has been paid in full. Failure to complete payment may result in a delay in publication or, in some cases, withdrawal of the manuscript.

After the APC has been confirmed, the manuscript editor will format the paper to meet the journal's publication standards. Authors are required to respond within 3 working days to any revision requests from the manuscript editor. Please note that delays in response may result in the publication being postponed to the next issue.

A. Galley proofs

Once all corrections have been completed, the corresponding author will receive the final version of the manuscript in PDF format.

Within 5 working days of receipt, authors must reply to the printing office of any errors found in the file. The proof may be revised more than once by the corresponding author, if needed. Authors should double-check for corrections in the content, title, affiliation, capitalization, locations of figures, and references.

6. Post-Publication Corrections

To correct errors in published articles, the corresponding author should contact the journal's editorial office with a detailed description of the proposed correction. Corrections that profoundly affect the interpretation or conclusions of the article will be reviewed by the editors. Corrections will be published as author correction or publisher correction in a later issue of the journal.

Minor errors will be corrected directly in the online version of the article. An indication of the correction, along with the date it was made, will be added to the article information in both the HTML and PDF versions. A separate correction note will not be published.

Contact Us
Editor-in-Chief: Myeong Heon Shin, MD, PhD
Email: myeong@yuhs.ac

Editorial Office
Department of Tropical Medicine, Yonsei University College of Medicine, Yonsei-ro 50-1, Seodaemun-gu, Seoul 03722 Korea
Tel: +82-2-2228-1844 Email: support@parahostdis.org

NOTICE: These instructions to authors will be effective from the January 2026 issue.